中国科学院上海应用物理研究所

年 报

2011–2012

（第 25 卷）

《中国科学院上海应用物理研究所年报》
编辑委员会

内 容 简 介

本书为2011–2012年度中国科学院上海应用物理研究所年报，主要由全所各科研机构负责人以中英文介绍该部门或研究组于2011–2012年在相关研究领域中的工作进展，内容包括三大学科片的科研进展等。附录记载了2011–2012年度本所的学术活动、国际交流、人才培养等情况。

本年报供本所上级主管中国科学院和上海市各有关部门的领导与各类管理人员阅读，供各科研院所相关领域的科研人员、高等院校师生，以及本所科研人员和研究生阅读参考。

前　言

布局启动研究所“一三五”规划，深入实施“创新 2020”

2011–2012 年，根据中科院实施“创新 2020”规划的要求和“十二五”发展战略重点，在全面分析国家战略需求、世界科技前沿发展趋势和我所核心竞争力的基础之上，制定了我所“一三五”规划，对四大学科领域的重大科学问题、重要研究方向、科技先导项目凝练，以及科学研究、关键核心技术研发、系统集成技术发展等方面进行了所级项目部署，同时全面展开、稳步推进人才队伍建设、技术支撑与科技条件规划、产业化与科技企业发展、园区建设、国际交流合作、组织管理等研究所各项工作, 加速推进研究所实现跨越发展。

一、制定发展战略，全面推进“一三五”规划

2011 年，我所进入中国科学院研究所整体择优，迎来了新的发展机遇。根据中科院实施“创新 2020”规划的要求和“十二五”发展战略重点，我所制定了“一三五”规划，目标是将我所建设成独具特色、不可替代和具有国际竞争力的研究机构；建设国际先进的“光子科学研究基地”和“核能与核科学技术综合研究基地”。按此战略规划，在 2009–2014 年，我所将以“上海光源大科学装置集群”建设和“钍基熔盐堆核能系统”战略性先导专项两个重大科技任务以及“核科学与前沿交叉研究”为我所发展的三大战略重点，带动核能科学技术、光子科学、加速器科学技术、核科技与前沿交叉科学四大学科领域的发展，提高我所的核心竞争力，建设世界级的高水平研究机构。两年来，上海应用物理研究所“一三五”规划由布局启动转入全面攻坚，进入了开拓创新、实现跨越发展的新阶段。

2011–2012 年，全所新争取到各类科研项目 178 项。新增 973 项目课题 7 个，其中项目首席科学家 1 个。发表论文 407 篇，其中影响因子大于 5 的高水平论文 51 篇。共申请专利 132 个，专利授权 81 个。骨干队伍中中科院“百人计划”15 人、中国青年科技奖 1 人。

二、实施“一三五”规划，着力实现跨越发展

两年间，上海光源大科学装置实验能力和服务水平持续提升，主要运行技术指标处于国际先进水平，充分发挥了支撑科技发展的平台作用，持续产出重要和重大成果，荣获“中国科学院综合运行成果奖励”。上海光源于 2012 年 12 月 6 日正式开始恒流模式用户运行。后续建设正在按照计划实施、推进。完成了 X 射线自由电子激光试验装置可研报告的中咨公司组织的评审，完成了上海光源线站工程项建书的科学院评审并将正式上报发改委；上海光源蛋白质设施光束线与梦之线建设进展顺利，2013 年底全面建成向用户开放。光源相关的新原理实验验证、关键技术和实验方法研究取得了长足发展，在国际上率先实现了 EEHG-FEL 受激放大和 HGHG-FEL 大范围调谐，在上海光源微聚焦束线上获得了百纳米量级的硬 X 射线聚焦光束并用于用户实验。积极推进基础交叉与上海光源 In-house 研究布局优化、努力攻关突破、产出了重大和重要成果。上海光源团队荣获“2011 年中国科学院杰出科技成就奖”。

中国科学院先导专项——钍基熔盐堆核能系统(TMSR)按计划顺利实施和推进。2011 年，“钍基熔盐堆核能系统”战略性先导科技专项(TMSR)正式立项。两年来，TMSR 总体部充分利用现有资源，建立了基础研究的前期基本条件，构建了较完备的专项管理机制，组建了基本研究队伍，形成了国际合作框架，启动了 TMSR 核能系统相关核心科学与工程技术研究，进一步明确了专项科技目标、技术路线和实施方案，专项科研攻关全面启动，建成首个硝酸盐实验回路、反应堆设计平台、堆材料测试平台、熔盐实验室，完成熔盐泵及控制棒首个样机等的研制；完成了 2 MW 钍基熔盐实验堆(液态和固态)预概念设计与国际评审；初步形成一支年轻、有活力和成规模的专项基本科技队伍。

核科学与前沿交叉研究逐步形成特色，不断取得新进展。在核物理研究室在中高能重离子碰撞研究和反物质探测上取得了突破性进展，发现了反氦 4 核；依托上海光源等先进装置，物理生物学研究室在单分子操纵、纳米生物传感器、纳米材料的细胞应激效应、生物系统与微观水的关系等方面做出了出色的成绩。在我所传统优势学科核物理学的理论与模拟计算的基础上，与纳米科学交叉融合，开展了新兴交叉学科——水科学领域的研究。积极响应中科院在水科学研究领域的布局，于 2011 年 5 月成立了“水科学与技术研究室”，正式启动了水科学领域研究，并已显现出独特优势。

三、加快人才队伍建设，培育和凝聚国际一流水平的科研团队。

围绕研究所“一三五”规划，以凝聚和造就创新人才队伍为重点，以优化人才队伍结构为目标，保障重大科技任务实施，继续深化“谁用人谁负责”的用人联动机制，采取多种方式，利用多渠道补充各类人力资源。充分发挥科研骨干的人才引荐作用，2011–2012 年引进与招收各类人员 360 名，其中博士 143 名，高级岗位 34 名。“引才”与“引智”并举，凝聚吸引科技领军人才。启动实施了我所首位国家“千人计划”长期项目候选人的引进与申报工作，开拓用人新模式，吸引境外、所外智力实职到所开展长期工作。“使用”与“选拔”并重，全力推进青年科技创新人才培养。围绕人才队伍建设需求和科技任务要求，加强继续教育工作。

努力提高生源，继续扩大办学渠道，与中科大合作建立的“科技英才班”。完成了自审增列核科学与技术、物理学一级学科博士培养点及化学一级学科硕士培养点的申报工作并获中国科学院大学审批通过。加强与兰州大学核学院及复旦大学核科学与技术系的合作，与复旦大学合作的“联合培养本科生计划”项目获得国科大批准并正式启动。2011–2012 年共招收硕士生 160 名、博士生 99 名，毕业硕士 84 名、博士 81 名。

四、加强特色实验室建设与技术支撑，广泛开展国际国内合作

加强与发展重点实验室建设，2011 年上海市低温超导高频腔技术重点实验室首次通过上海市科委评估并获得择优支持；同时积极筹备建设中国科学院微观界面物理与探测重点实验室。通过中科院修购专项、所级公用技术支撑中心建设及仪器研制项目，提升我所整体装备能力。向院推选的“纳弧度长程面形仪”项目获得院批准；“新一代多功能核探针信号探测和数据获取系统研制”项目按期完成并通过院计财局验收；“基于饱和荧光共振能量转移原理的超分辨细胞显微成像系统”项目按期完成并通过院计财局验收；在研项目“新型核辐射成像检测系统样机研制”和“纳弧度长程面形仪”进展顺利。积极推动所级公共技术服务中心建设，加强大型仪器设备和公用实验平台运行管理。积极推动所级公共技术服务中心建设，规范大型仪器设备及公用实验平台运行管理，编制上报所级公共技术服务中心建设方案，编制印发“所级中心运行管理办法”，建设“所级公共技术服务中心”网页。完成“X 射线自由电子激光试验装置建设项目环境影响报告书”和“X 射线自由电子激光试验装置建设项目职业病危害预评价”报批。

完成科学院 CNGI 项目子任务——中国科学院上海应用物理研究所 IPv6 网络环境建设。上海光源工程档案获得国家档案局首批“全国建设项目档案管理示范工程”称号。联合编辑部顺利完成 3 刊两年出版任务

围绕研究所重点工作和中心任务，积极开展国际交流与合作，提升研究所国际影响力和竞争力。同时，根据学科方向的调整，积极谋划国际合作与交流新布局。深化大科学装置研究领域和前沿交叉学科领域的原有合作，努力开拓核能领域的合作与交流。我所分别与英国的 DLS、日本 Spring-8、NIRS、加拿大光源(CLS)、斯洛文尼亚的 COSYLAB 实验室、亚美尼亚的 CANDLE 光源、巴西同步辐射实验室的巴西光源(LNLS)、等著名的科研机构就同步辐射装置相关研究签署了合作协议，与美国橡树岭国家实验室、西北太平洋国家实验室、爱达荷国家实验室和法国原子能总署、澳大利亚核科学与技术组织(ANSTO)等研究机构达成了核能领域的合作意向，国际合作伙伴队伍范围进一步扩大。学术交流非常活跃，2011–2012 年人员出访 689 人次、来访 980 余人次。共举办大小国际学术会议 13 个，国际会议呈现专题化的趋势。

积极推进科技产业化与科技企业建设，提升研究所的竞争能力和社会影响力。积极推进科研成果的产业化，大力加强横向项目的争取与管理，加强所投资控股企业产权管理、经营管理和继续推进实验工厂发展工

作相结合。上海先进质子治疗装置、美国 ALS 六极磁铁研制、定时系统研发、超导高频腔技术应用等技术转移转化工作取得了显著成效。2011–2012 年共签订科技成果“四技”及销售合同 120 余项。

五、加强创新文化建设与研究所综合管理，营建和谐稳定的研究所氛围。

围绕研究所“一三五”规划，不断深化体制机制改革，加强研究所综合管理。为了更好地推进中科院战略性先导科技专项“未来先进核裂变能”——钍基熔盐堆核能系统的发展，对所研究机构的设置与学科方向进行适当的调整，成立了 TMSR 研究中心(筹)，下设 5 个技术部；根据核能发展需求进行所学科布局调整，将原核分析室、辐化辐照室、放药中心整体转入 TMSR 研究中心进行统一整合；调整了上海光源国家科学中心(筹)的功能及相关机构和人员，新建“水科学研究室”。持续强化内部预算管理，成立了预算执行联席会议领导小组及由科研处、财务处等相关职能部门负责人组成的预算执行联席会议小组。根据国家、上海市、中科院有关安全保卫保密工作精神与要求，制定了《开展部门实验室安全互查评比活动》的方案、《危化品专项整治方案》、《清剿火患活动的通知》，修订了《上海应用物理研究所危险化学物品管理规定》，构建长效机制。

按照中科院部署，积极推进财政部房屋修购专项的申请立项及调整工作，综合 TMSR 专项、SSRF 后续工程等基本建设需求，编制“钍基熔盐堆核能系统基础研究保障条件”建设项目建议书。完成了创新三期基建项目嘉定园区改造部分的局部整改和验收。

紧密围绕中科院“创新 2020”战略，以庆祝建党 90 周年为抓手，继续开展以“解放思想，开拓进取，实现创新 2020 跨越发展”为主题的创先争优活动。学习贯彻十八大精神，加强班子和干部队伍建设。注重发挥党办和工青妇学等群众组织的作用，营造积极向上、和谐奋进的研究所氛围。2011 年，我所首次获得“上海市文明单位”称号。抓好课题经费管理、基建项目管理、科研道德等几个反腐倡廉重点领域的监督工作。为进一步加强监察审计工作，成立了所监察审计室。积极承担传播科学知识的社会责任，开展科普工作。通过中国科学院“第八届公众科学日”、上海“城市新印象”科普展等主题活动以及上海光源接待社会各界参观的形式，向公众传播科学知识，弘扬科学精神。继续开展城乡结对帮扶工作，筹资帮助崇明庙镇鸽龙村基础建设。

2011–2012 年，我所在科研项目争取、人才队伍建设、学术交流与技术转移转化、体制机制改革等方面都取得了可惜的成绩。展望未来，机遇与挑战并存。我所正处于历史上最好的发展时期和关键的转型期，我们要抓住这难得的历史机遇，积极实施推进“创新 2020”和研究所“一三五”规划，攻坚克难、团结奋进、只争朝夕、不断实现跨越发展，努力把我所建设成为我国独具特色、不可替代和具有国际竞争力的研究机构，为国家科技进步做出重大贡献！

目 录

上海光源大科学装置集群(SSRF Large-Scale Scientific Facilities Complex)

钍基熔盐核能系统(Thorium Molten Salt Reactor System(TMSR))

核科技与前沿交叉研究(Nuclear Science and Frontier Interdiscipline Research(NSFI))

附录

上海光源
大科学装置集群
SSRF Large-Scal Scientific Facilities Complex

X 射线小角散射组研究进展

生命科学研究部　X 射线小角散射组

小角散射组 2011–2012 年主要致力于小角散射(SAXS)线站升级改造、生物小角(Bio-SAXS)线站建设、线站原位装置研制、小角散射实验方法及应用研究。

SAXS 线站 2 年间，运行 10653 h，故障率仅为 0.4%，提供用户机时 7892 h，用户发表 SCI 论文 59 篇。其中，一区论文 26 篇。

实验站改造方面，完成了光束线光学系统和实验站支撑平台的升级改造，更换了 CCD 探测器，提高了小角线站的光子通量，方便了管道更换、光路调试和实验操作。申请发明专利一项“一种光强探测电离室”，受理号：201210058796。

新线站建设方面，完成了 Bio-SAXS 线站的物理设计和工程设计。

实验方法方面，发展了亚秒级快速采集 SAXS 实验方法，蛋白质 SAXS 研究方法，GISAXS 实验方法，开展了合金反常小角散射和纤维体系小角散射方法学研究[1]。

为满足用户需求，完成了上海光源 SAXS 线站设计、研制流动样品装置(见图 1)、原位高分子在线拉伸装置(见图 2)的安装调试。申请发明专利一项“同步辐射原位在线纤维纺丝设备”(见图3)(已授权，专利号：ZL201110173600.4)

图 1　流动样品装置

除承担 SAXS 线站运行和用户支持之外，小角散射组还承担了以下科研项目：3 个科技部“973”项目；2 个国家自然科学基金青年项目；3 个中国科学院知识创新工程领域前沿项目；1 个教育部留学回国人员科研启动基金项目。组内人员在聚合物辐照、合金、聚合物掺杂，以及光学相干性等多个领域都开展了 in-house 研究[2-4]。

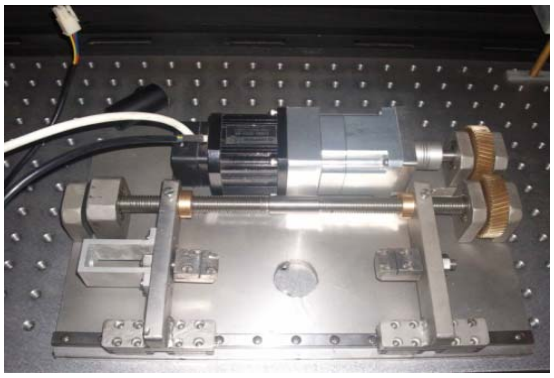

图 2　高分子拉伸装置

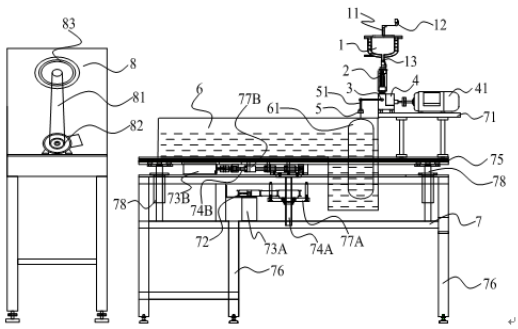

图 3　同步辐射原位在线纤维纺丝设备结构示意图

参考文献

1. Li Xiaoyun, Li Xiuhong, Wang Yuzhu, Wang Jie. Study of microstructure in polyethylene terephthalate(PET) fiberusing SAXS, Advanced Materials Research, 2011, 332-334, 1171-1175
2. Tian Feng, Tang Zhongfeng, Xu Hongjie, Wang Jie, Wu Guozhong, Li Xiuhong. SAXS Studies on the Structure Behaviors of Crosslinked PTFE Irradiated by Gamma Ray, Polymers & Polymer Composites, 2011, **19**: 4-5
3. 田丰, 唐忠锋, 李秀宏, 吴国忠, 徐洪杰, 王劼. 同步 X 射线散射技术研究 γ 射线辐照后 PTFE 的结构变化, 核技术, 2011, **34**: 7
4. LiXiuhong, Bernd Kretzschmar, Andreas Janke, Liane-Hassler, Konrad Schneider and Manfred Stamm, Investigation of structure and mechanical behavior of polyamide 6/ZnO and polyamide 6/Al2O3 nanocomposites. Advanced Materials Research,2012, 557-559, 272-276

Progresses in Research of X-ray Scattering Group

Department of Life Science X-ray Scattering Group

In 2011–2012, X-ray Scattering Group operated SAXS beamline (BL16B) and upgradedthe optics of the beamline and endstation. Some R&Ds of in-situ instruments and experimental methodology for SAXS were executed as well. On the other hand, a new SAXS beamline-BioSAXS beamline dedicated to protein solution was under construction.

BL16B status

BL16B provided total beamtime about 10653 hours for two years, of which 7892 hours were allocated to users, and the failure time of the beamline and endstation accounted for 0.4%. 59 users' journal articles were published.

Upgrading

BL16B changed its monochromator as flat double crystals instead of sagittally focusing double crystals. To compensate the absence of horizontally focusing, the toroidal profile of the focusing mirror was adopted. The upgrading gives users the same photon flux as that of the sagittally bent mono but much lower background noise. Another improvement of realization of new motorized optical table achieved, which was more convenient and quicker to change the sample-to-detector distance.

New beamline-BioSAXS

The physical design and engineering design of Bio-SAXSbeamline completed by X-ray scattering group in 2012.

Instrumentation and methodology

About the new SAXS methodology and technology, the sub-second SAXS experiment, Bio-SAXS and grazing incidence small angle X-ray scattering (GISAXS) were developed at BL16B. The anomalous SAXS study of alloy and SAXS study of fiber system were also open to users [1].

A new peristaltic device for solution SAXS measurement(Fig.1) and an in-situ stretching device (Fig.2) weredesigned.

Fig.1 Peristaltic device.

Fig.2 In-situ stretching device.

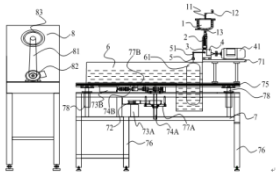

Fig.3 In-situ fiber spinning and stretching devices.

Scientificactivities

In-house researches are of importance. The Group involved in studies of polymer radiation effects, fusion, solidification and crystallization processes of alloy, nano-fibrilla-doped polymer and characteristics of coherent X rays[2-4], which supported respectively by three projects of the Major State Basic Research Development Program of China, two projects of National Natural Science Foundation of China, three projects of Knowledge Innovation Program of Chinese Academy of Sciences, and one project of Start Fund for Chinese Overseas Returnees.

We applied for a Patent for Invention of "An ion chamber for photon flux detection" (Patent application No. 201210058796). A Patent for Invention of "in-situ fiber spinning and stretching devices" was licensed. (Patent No.ZL201110173600.4).

References

1. Li Xiaoyun,Li Xiuhong, Wang Yuzhu,Wang Jie. Study of microstructure in polyethylene terephthalate(PET) fiberusing SAXS, Advanced Materials Research, 2011, 332-334, 1171-1175
2. Tian Feng, Tang Zhongfeng, Xu Hongjie, Wang Jie, Wu Guozhong, Li Xiuhong. SAXS Studies on the Structure Behaviors of Crosslinked PTFE Irradiated by Gamma Ray, Polymers & Polymer Composites, 2011,**19**: 4-5
3. Tian Feng, Tang Zhongfeng, Li Xiuhong, Wu Guozhong,Xu Hongjie, Wang Jie. Structural changes of irradiated PTFE studied by synchrotron X ray scattering, nuclear technology, 2011, **34**: 7
4. LiXiuhong, Bernd Kretzschmar, Andreas Janke, LianeHassler, Konrad Schneider and Manfred Stamm, Investigation of structure and mechanical behavior of polyamide 6/ZnO and polyamide 6/Al2O3 nanocomposites. Advanced Materials Research, 2012, 557-559, 272-276

生物大分子晶体学光束线 BL17U1 运行状态与用户成果

生命科学研究部　汪启胜　郁 峰　刘 科　徐春艳 张坤浩 潘强岩 杨利峰
王志军　孙 波　黄 胜　王思胜　　李 良　何建华

生物大分子晶体学一组专注于晶体学光束线 BL17U1 的运行开放，以及束线性能提高相关的技术研究。保持高性能、低故障率的运行是用户开放的前提，用户管理与培训工作保证用户有效地使用机时开展学术研究。在 2011–2012 年内，BL17U1 的运行状态与开放成果如下。

2011、2012 年度，BL17U1 光束线站均完成了运行开放任务，其相关统计如下表所示，累计对用户供光时间为 8655 h。2011 年度因设备升级改造，新设备调试导致该年度束线故障率为 1.91%，2012 年度系统更加稳定，该年度故障率降至 0.2%。在运行期间，束线各项指标均优于设计指标。

	计 划 供光	实际 供光	用户 时间	束线 研究	束线故 障
2011	5688	5318.6	4273	944.15	101.45
2012	5458	5347.05	4382.03	954.26	10.76

2 年内，用户在该光束线取得了丰硕的研究成果。2011 年 PDB 公开收录新结构 204 个，发表 SCI 文章 123 篇；2012 年 PDB 公开收录新结构 330 个，位居全球 130 多条晶体学光束线站之首，发表 SCI 文章 158 篇。其中发表在 CNS 上的论文累计 21 篇。

2011 年度，BL17U1 利用并不宽裕的束线研究机时，高效地执行了院线站升级改造项目“生物大分子晶体衍射高分辨结构测定和自动化筛选系统项目”。在 2012 年 1 月，该项目圆满的通过了验收，验收意见认为，该项目各项研究内容全部达到了项目任务书所要求的考核指标，可以实现高效率、高质量的生物大分子晶体衍射数据收集及结构解析；验收工作报告中的相关内容完整准确，设备和部件全部就位、运行正常，设备各项支出合理、资产管理规范。通过该项目的完成，提高了实验站设备的稳定性与效率。同时进行了软件系统的升级，软件 BluIce 的成功移植，提供给用户一个方便操作的集成软件界面，整个项目极大地提高了束线的稳定性和使用效率。

课题组开展了一系列的光束线性能提高的相关研究。结合加速器的针对改变插入件 Gap 值对轨道的影响的研究，控制程序的自动优化使得用户可以在光束线 5–18 keV 能量范围内快速、方便的选择波长。开展了通过复合折射透镜(CRL)获得微细光束的前期研究，使用气泡型 CRL 获得了 5 倍压缩比的聚焦光斑。控制系统的不断完善为用户远程实验提供了足够的准备。

在高性能低故障率的运行状态下，我们把上海光源生物大分子晶体学线站打造成了结构生物学研究的重要平台。同时，开展了多项光束线技术的研究，从而进一步提高光束线性能，探索新的技术手段及实验方法。

Operation Status of MX Beamline BL17U1

WANG Qisheng YU Feng LIU Ke XU Chunyan ZHANG Kunhao PAN Qiangyan
YANG Lifeng WANG Zhijun SUN Bo HUANG Sheng WANG Sisheng LI liang HH Jianhua
Department of the Life Sciences

Macromolecular crystallography group focus on the beamline BL17U1 operation and research the related technology to improve the beamline performance. During last two years, we made effort to operate the beamline high efficiently. Rational maintenance, relative flexible user management and the training program also contributed to the high productive yield. In the 2011-2012 year, the operation status and the output from user community as follow.

Both 2011 and 2012 year, BL17U1 beamline accomplished the operation plan and offered beam to users more than 4000 hours every year. The statistics data are shown in the table below. Due to the equipment upgrade project in 2011 year, we need more time to assemble the system and commissioning, the ratio of the failure to offer the beam as planed the 1.191%. In 2012 year the system works very well and the ratio number dropped to 0.2%. During the operation, the technical parameters of the beamline is better than the designed specifications.

	Planed Beamtime	Offered Beamtime	Users Beamtime	Beam Study	Ratio of Unavailable
2011	5688	5318.6	4273	944.15	101.45
2012	5458	5347.05	4382.03	954.26	10.76

Within two years, the users of the beamline achieved fruitful results. In 2011 there are 204 new structure determined from the beamline deposited to Protein Data Bank (PDB), and more than 123 papers published on SCI journal. The number increased to 330 new structures in 2012 year, and the number of the paper increase to 158 also. There are many highlights research results published on the top magazine, the total number is 21 which published on Science, Nature and Cell.

Year 2011, Bl17U1 use the limited beam study time to execute the upgrade project which help the beamline achieve to collect higher resolution dataset and automate screening crystal. In January 2012, the project successfully passed the review from CAS. The hardware is upgraded entirely, including the ADSC CCD detector, high precision goniometer system and the auto robotics. Besides the hardware the software also upgrade to integrated BluIce which is adapted to the hardware.

Our group also carried out a series of studies to improve the performance of the beamline. Research on the undulator Gap let users can change the wavelength as their wish in the energy range 5–18 keV. We also pursued minibeam by compound refractive lens (CRL), the bubbles type CRL can obtain the smaller beam with intensity gain. We will keep this research to put the CRL in beamline as a routine device. The consecutive improve on the software make the user experience feel better, the automation of the beamline make the remote access is realized.

We operated the beamline with high performance and low failure rate, now this beamline is the important platform for structure biological research to help users carry out various projects. At the same time we also explored the new techniques and experimental methods to further improve the performance of the beamline.

晶体结构揭示人源热休克蛋白 Hsp90 的 ATP 水解和激活机制

生命科学研究部

何建华　李 健　孙丽华　徐春艳　郁 峰　唐 琳　周 欢

热休克蛋白 Hsp90 主要作为分子伴侣负责帮助多种底物蛋白正确折叠，当细胞受到外界压力刺激时，其表达水平会进一步提高。Hsp90 客户蛋白与信号转导、细胞周期调控和凋亡路径有着密切的关系，HSP 对这些蛋白的折叠、成熟、稳定和定位至关重要。Hsp90 主要以同形二聚体的形式存在，全长的 Hsp90 分为三个结构域。高度保守的 N 末端含有一个 ATP 结合口袋，具有 ATP 酶活性。中段结构域有大的疏水表面，与客户蛋白的正确折叠有关，C 末端负责 Hsp90 的二聚体化。Hsp90 功能的实现依赖于 ATP 与 Hsp90 的结合及 N 末端对 ATP 的水解。ATP 与 Hsp90 结合后引发 Hsp90 的构象变化，这些构象变化导致 Hsp90 表面疏水性的改变，使客户蛋白与 Hsp90 亲和力增强并与 Hsp90 结合，关闭核苷酸结合口袋，N 端结构域与中段结构域相对运动并形成 N 端的二聚体化，同时水解中心形成，在此过程中 Hsp90 帮助客户蛋白质正确折叠。随后 ATP 水解为 ADP，γ 磷酸被释放，Hsp90 转变为更紧密的构象，折叠成熟的客户蛋白与 Hsp90 的亲和力下降，从分子伴侣释放，Hsp90 完成功能的执行。

通过解析 Hsp90N 端结构域及其与 ATP 或 ATP 类似物的复合物晶体结构提供了一个清晰的 Hsp90 水解 ATP 的机制。ATP 的 γ 磷酸基团与 Mg^{2+}形成配位。Gly132，Gly137，Glu47 和 Arg400 可与 ATP 发生直接或间接的接触，而 Arg46 和 Glu47 是 ATP 水解的关键性残基。首先，Arg46 与 Glu47 的羧基形成强的氢键，使 Glu47 极化成为碱。然后极化的 Glu47 亲核攻击水分子并夺取水分子中的质子，从而使水分子带负电。最终带负电的水分子亲核攻击 γ-磷酸基团的磷原子，导致 β 和 γ-磷酸基团之间的共价键断裂，形成 ADP 和磷酸根离子。

Structure Insights Into Mechanisms of ATP Hydrolysis and the Activation of Human Heat-shock Protein 90

HE Jianhua LI Jian SUN Lihua XU Chunyan YU Feng TANG Lin ZHOU Huan

Department of Life Science

The molecular chaperone heat-shock protein 90 (Hsp90), which is up regulated in response to stress, is essential for folding, maturation, stabilization, and localization events of the chaperone's client proteins that are involved in cell cycle regulation, signal transduction, and cell growth regulation. Hsp90 can be divided into three domains. The highly conserved N-terminal domain contains an unusually shaped ATP-binding cleft and is thus responsible for the catalytic activity of Hsp90. The middle domain containing a large hydrophobic surface helps the folding of its client proteins, while the C-terminal domain is critical for the formation of Hsp90 homodimer. The function of Hsp90 is tightly associated with the binding and hydrolysis of ATP as well as the dimerization of the chaperone. ATP binding in the N-terminal domain of Hsp90 drives a structural rearrangement and changes the surface properties of the N-terminal domain, which induces the dimerization of the N-terminal domains and influences the affinity of Hsp90 for client proteins. ATP-mediated closing of the inter protomer space drives client proteins remodeling. Once ATP hydrolysis occurs, a conversion of Hsp90 to its ADP bound state leads to the release of client proteins.

We have determined three crystal structures of the N-terminal domain of human Hsp90 in native and in complex with ATP and ATP analog, providing a clear view of the catalytic mechanism of ATP hydrolysis by Hsp90. The γ-phosphate oxygen atoms form coordination bonds with Mg^{2+}. Gly132, Gly137, Glu47 and Arg400 are binding with ATP directly or indirectly, while Arg46 and Glu47 are key residues for ATP hydrolysis. Firstly, Arg46 forms strong hydrogen bonds with the carboxyl group of Glu47, which polarizes Glu47 and makes it as a general base. Then, the polarized Glu47 nucleophilic attacks the water molecule and absorbs the proton from the water molecule, providing the electron to the water molecule and make it more negatively charged. Finally, the negative-charged water molecule nucleophilic attacks the phosphorus atom of the γ-phosphate, the covalent bond between β- and γ-phosphate is broken, and the products, a hydrogen phosphate and ADP, are formed.

BL14W1 XAFS 线站开放运行情况

物理与环境科学研究部　硬 X 射线谱学组

1　开放运行

2011–2012 年度，BL14W1 线站共为用户提供机时约 7896 h，束线研究机时约 1957 h。共完成了 400 余个研究课题，用户发表文章 130 篇，其中 SCI-I 区文章 40 篇，占文章总数的 30%。

2　实验技术和方法发展

2011–2012 年度，BL14W1 线站在原有基础上，开展新实验技术和方法的研究，利用多元固体探测器和自动配气系统等，有效提高了实验的信噪比和数据质量。此外，还发展了原位变温冷热台等多种原位实验装置，丰富了 XAFS 实验条件，拓展了研究范围。

(1) 多元固体探测器　BL14W1 线站原有的 4 元 Si 漂移探测器，由于其探测效率较低，尤其对于高能波段的光子计数率下降，因此，对于低浓度样品采集数据质量较差。通过对 32 元 Ge 探测器的性能调试优化，并改进采集程序，探测器表现出了较好的性能，使得荧光 XAFS 数据的采集质量大大提高(见图 1)。通过对液氮罐电磁阀更换，实现了液氮自动补充功能，大大提高了实验效率和使用安全性。

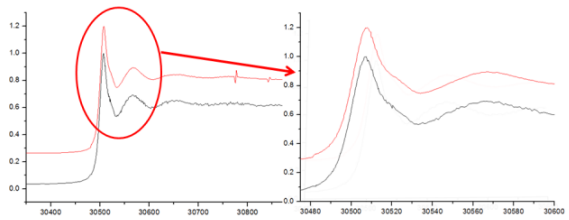

图 1　32 元 Ge 探测器与 4 元 Si 漂移探测器的对比

(2) 自动配气系统　为了达到最佳的信噪比要求，XAFS 实验需要对电离室的气体进行精确配比，而 BL14W1 线站原来使用的是手动配气方式，在配气精度上存在较大的误差。BL14W1 线站搭建了自动配气系统，能方便的将几种常用气体根据所需测量元素的要求按照一定比例混合，配合比例较为精确，能够满足 XAFS 实验最佳信噪比的要求(见图 2)。

(3) 原位变温冷热台　原位实验条件是获取真实反应过程结构信息的必要条件。BL14W1 线站搭建了 Linkam 冷热台装置，实现了从−195℃–400℃范围内的温度可调，并能通入各种气氛，能够适用于透射和荧光 2 种采集模式，满足了 XAFS 变温原位实验的要求(图 3)。

图 2　自动配气系统

图 3　原位冷热台

3　用户工作

2011–2012 年度，BL14W1 线站共接待了用户近千人次，课题数超过 400 个，涵盖了催化、材料、环境、化学、物理、生物等多个学科领域。共发表文章 130 篇，包含 Nature Chemistry、PRL、JACS 等 SCI-I 区高质量文章 40 篇。

中科院大连化学物理研究所张涛课题组，利用 X 射线吸收谱技术分析氧化铁负载铂催化剂，证实了“单原子”铂的存在和配位结构，该单原子催化剂的催化活性是传统纳米催化剂的 2–3 倍。此项研究成果可极大的降低催化材料在工业应用中的成本。

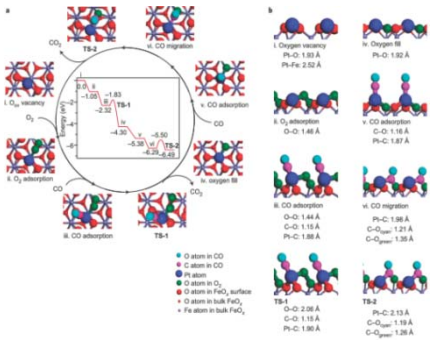

图 4　CO 在 Pt_1/FeO_x 催化剂上的反应路径

中科院国家纳米科学中心的聂广军课题组开发出一种高稳定性，低活性的纳米结构，可广泛应用于医学成像中。他们利用 XAFS 技术研究了该纳米结构与靶标蛋白结合时的结构状态，为理解该材料的活性机制提供了重要帮助。

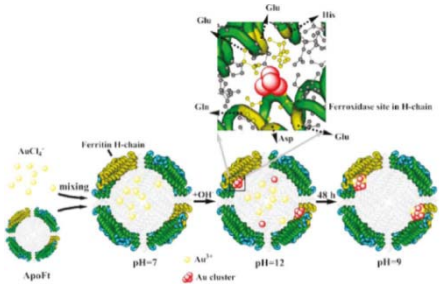

图 5　Au-Ft 蛋白合成路径示意图

南京航空航天大学的杨亮课题组利用 XAFS 及高能衍射实验数据结果，结合 RMC 模拟，对非晶结构解析的各种团簇内部的原子堆积效率进行计算，最终发现在非晶形成能力出现极值的成分点，其对应的原子堆积效率也相应出现极值。该工作表明，虽然在合金体系近邻成分的非晶样品中，其微观结构的主体特征(团簇类型和分布)比较相似，团簇内部的原子随成分变化不断调整其堆积效率，从而影响团簇的结构稳定性。

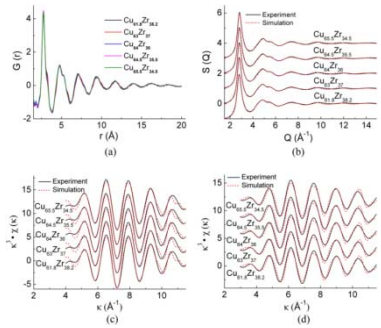

图 6　CuZr 样品 EXAFS、XRD 实验谱与 RMC 法计算谱的对比

中科院化学研究所朱道本课题组利用 EXAFS 方法研究基于聚乙烯的有机热电材料中 Ni 原子周围的配位情况，解决了该材料形成中的初态、中间态以及末态的分子构型，为理解该材料的热导率、Seebeck 系数等关键性能参数提供了结构信息。

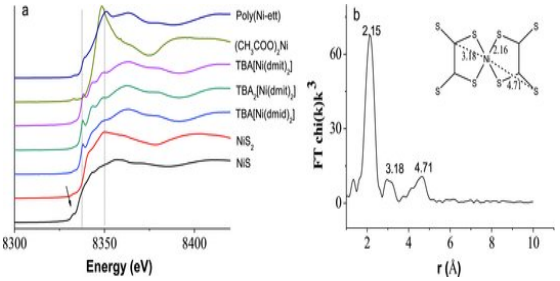

图 7　四巯基乙烯的镍配位聚合物 Ni K 边近边谱及分子构型

参考文献

1. Qiao Botao, Wang Aiqin, Yang Xiaofeng, Lawrence F Allard, Jiang Zheng, Cui Yitao, Liu Jingyue, Li Jun, Zhang Tao. Single-atom catalysis of CO oxidation using Pt1/FeOx, Nature Chemistry, 2011, **3**(8): 634–641
2. Sun Cuiji, Yang Hui, Yuan Yi, Tian Xin, Wang Liming, Guo Yi, XU Li, Lei Jianlini, Gao Ning, Gregory J Anderson, Liang Xingjie, Chen Chunying, Zhao Yuliang, Nie Guangjun. Controlling assembly of paired gold clusters within apoferritinnanoreactor for in vivo kidney targeting and biomedical imaging, J Am Chem Soc, 2011, **133**(22): 8617–8624
3. Yang L, Guo G Q, Chen L Y, Huang C L, Ge T, Chen D, Liaw P K, Saksl K, Ren Y, Zeng Q S, LaQua B, Chen F G, Jiang J Z. Atomic-Scale Mechanisms of the Glass-Forming Ability in Metallic Glasses, Phys Rew Lett, 2012, **109**: 105502
4. Sun Yimeng, Sheng Peng, Di Chongan, Jiao Fei, Xu Wei, Qiu Dong, Zhu Daoben. Organic Thermoelectric Materials and Devices Based on p- and n-Type Poly(metal 1,1,2,2- ethenetetrathiolate)s, Advanced Materials, 2012, **24**(7): 932-937

Opening and Operation of BL14W1 XAFS Beamline

Department of Physics and Environment　Hard X-Ray spectroscopy Group

1　Overall operation

From 2011 to 2012，BL14W1 XAFS beamline has totally provided 7275 hours of beam time to the users, as well as 1957 hours for beamline research. Over 400 projects have been completed, and 130 papers are published.

2　Development of experimental technique

The main purpose of the beamline study is to improve the stability of the beamline, to improve the data quality, and to develop various in-situ experimental techniques. All these studies would improve the performance of the beamline.

Solid state detector　The XAFS data quality of samples with low concentrations largely depend on the performance of the detector. A new 32-element germanium detector (SSD) was used at BL14W1, and the performance was fully optimized for the XAFS experiment. The data quality, especially for the detection of high energy element, was significantly improved compared to the four element silicon drift detector (SDD).

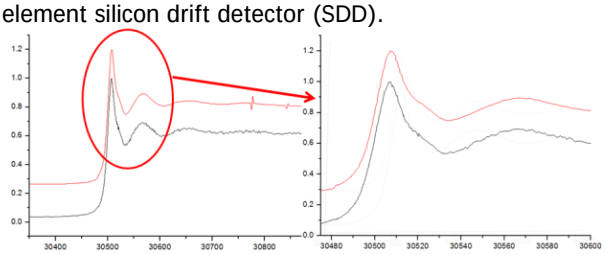

Fig.1　Comparison of 4-element SDD and 32-element SSD.

Automatic distribution system　To obtain the best XAFS data quality, precise gas proportion of the ion chamber is necessary. Instead of the long-used manual operation, a new automatic distribution system is developed at BL14W1. The accuracy of the gas proportion is largely increased, and thus improved the data quality.

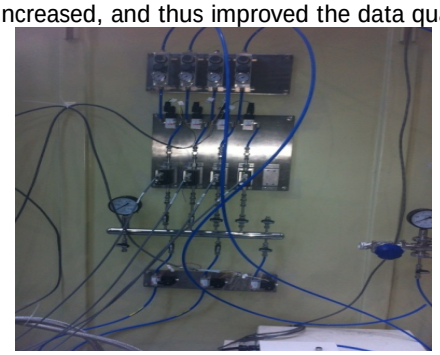

Fig.2　Automatic gas distribution system.

In-situ device　To obtain the real structures during the reaction process, the in-situ experimental devices are needed. For this reason, a Linkam-type variable temperature apparatus is set up at BL14W1. The variation range of temperature could be from -195°– 400°, with various gas atmospheres. Both transmission and fluorescence mode could be used.

Fig.3　In-situ sample chamber.

3　Research production of beamline users

Between the years of 2011-2012, nearly 1000 users have carried out their experiments at BL14W1 beamline, and implemented more than 400 projects including many subjects such as catalysis, material, environment, chemistry, physics, and biology. During the 2 years, users published 130 papers in total, including 40 high quality ones appeared in Nature Chemistry, PRL, JACS, etc.

Zhang's group in Dalian Institute of Chemical Physics, CAS, synthesized a novel catalyst that consist of only single Pt atoms uniformly dispersed on a FeOx support of high surface area, and characterized it by XAFS method. Its catalytic reactivity is 2-3 times of traditional nano-catalyst. And this researching result has a great potential to reduce the high cost of commercial noble-metal catalysts in industry.

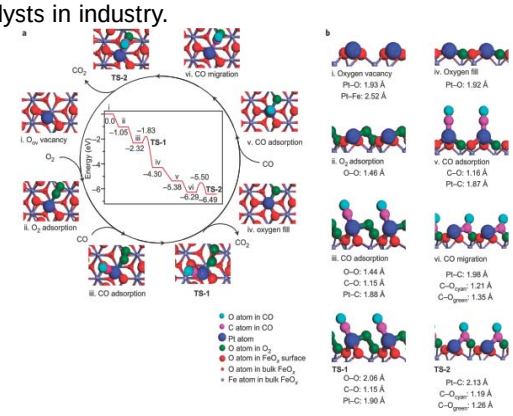

Fig.4　The reaction pathways for CO oxidation on Pt1/FeOx.

Nie's group of National Center for Nanoscience and Technology synthesized a kind of nanostructure with high biocompatibility and low cytotoxicity which has a great potential for biomedical applications. They studied the

bonding form between this nanostructure and target protein using XAFS, that provided valuable support to understanding the activity mechanism of this material.

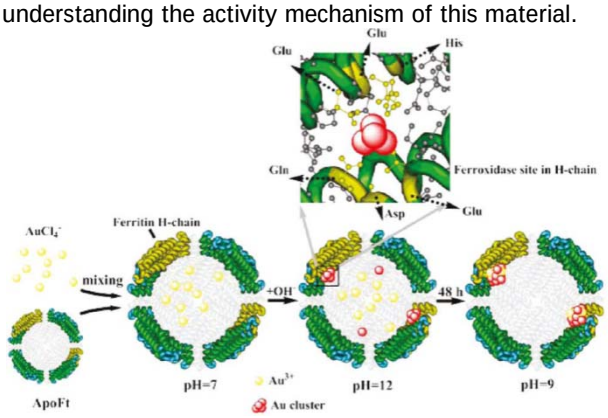

Fig.5 Schematic illustration of the synthesis of Au-Ft.

Yang's group form Nanjing University of Aeronautics and Astronautics investigated the microstructure of CuZr alloys by calculations based on the data from synchrotron radiation-based XRD and EXAFS experiments. They presented that the atomic-level packing efficiency strongly relates to their glass-forming ability (GFA). The best GFA is located at the largest difference in the packing efficiency of the solute-centered clusters between the glassy and crystal alloys in both metallic glasses systems.

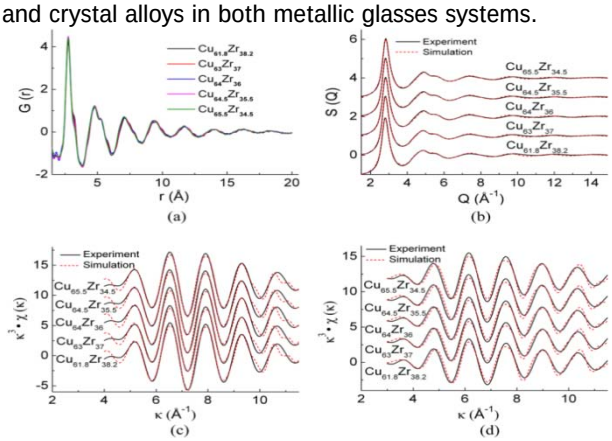

Fig.6 EXAFS data in the CuZr alloys compared with simulated curves.

Academician Zhu's group in the Institute of Chemistry, CAS, have studied the coordination conditions surrounding the Ni atom in organic thermoelectric materials. By EXAFS analysis, they obtained the molecular configuration of different stage in the formation process of this kind of material, that provided important information to understand their key performance parameters, such as thermal conductivity and the Seebeck coefficient.

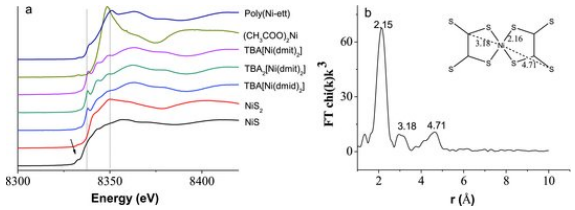

Fig.7 Normalized Ni K-edge XANES and EXAFS radial distribution curve of poly[Nax(Ni-ett)].

References

1. Qiao Botao, Wang Aiqin, Yang Xiaofeng, Lawrence F Allard, Jiang Zheng, Cui Yitao, Liu Jingyue, Li Jun, Zhang Tao. Single-atom catalysis of CO oxidation using Pt1/FeOx, Nature Chemistry, 2011, **3**(8): 634–641
2. Sun Cuiji, Yang Hui, Yuan Yi, Tian Xin, Wang Liming, Guo Yi, XU Li, Lei Jianlini, Gao Ning, Gregory J Anderson, Liang Xingjie, Chen Chunying, Zhao Yuliang, Nie Guangjun. Controlling assembly of paired gold clusters within apoferritinnanoreactor for in vivo kidney targeting and biomedical imaging, J Am Chem Soc, 2011, **133**(22): 8617–8624
3. Yang L, Guo G Q, Chen L Y, Huang C L, Ge T, Chen D, Liaw P K, Saksl K, Ren Y, Zeng Q S, LaQua B, Chen F G, Jiang J Z. Atomic-Scale Mechanisms of the Glass-Forming Ability in Metallic Glasses, Phys Rew Lett, 2012, **109**: 105502
4. Sun Yimeng, Sheng Peng, Di Chongan, Jiao Fei, Xu Wei, Qiu Dong, Zhu Daoben. Organic Thermoelectric Materials and Devices Based on p- and n-Type Poly(metal 1,1,2,2-ethenetetrathiolate)s, Advanced Materials, 2012, **24**(7): 932-937

束流测量与控制技术控制系统

束流测量与控制技术　沈立人

2011–2012 运行年度，上海光源控制系统主要专注于系统的维护与优化，并根据新的要求及新技术的发展，开展控制系统升级改造工作，主要包括控制系统环境虚拟化研究、插入件前馈校正、Top-up 运行模式及光源历史数据库、加速器远程监控研发等方面工作。取得的主要成果如下。

1　虚拟服务器系统运行环境的建立

控制系统虚拟化是指一种控制系统环境的虚拟化方法，其特点在于控制系统环境的虚拟化应用，包括控制系统服务器系统虚拟化、应用服务器模板、虚拟交换机的网络配置、控制系统应用网关的虚拟化及控制系统应用的自动故障迁移。特别是针对整个控制系统子网的虚拟交换机配置，其特征在于针对所有物理机对应的虚拟交换机的跨 VLAN 的设置，使得在其之上属于不同设备子网的虚拟机可以在不同的物理机之间迁移，实现了全部控制系统子网设备的高可用性。

通过构建基于 SAN 存储系统虚拟服务器系统，实现控制系统服务进程的在线可迁移，避免因某台服务器故障致控制系统故障。整个虚拟服务系统包括 16 台 Dell 2950 机架式服务器和 1 台 EMC CX-320 SAN 存储系统。在前期作了充分的系统测试和大量的准备工作基础上，整个工作于 2010 年暑期维护期间完成。全部工作包括服务器系统到虚拟机系统的迁移和 OPI 控制台到虚拟机系统的迁移。同时对全部服务器的操作系统由 fedora Core 7 更新至 Cent OS 5.4。实现了新系统与原有系统的无缝对接，EPICS 应用程序的稳定性得到提高。

2 年来的运行证明，通过虚拟化技术，使得控制系统环境所需的硬件资源得到了很好的整合，并通过虚拟机系统具有的高可用性特性，实现了控制系统环境的自动故障迁移，保证了 100%的可用性，并通过虚拟交换机设置，实现了不同控制系统子网的应用的无缝迁移。

2　控制系统 Top-up 运行模式实施

SSRF 在建造完成后稳定运行的前两年这一期间的运行模式为 Decay 模式。为了实现 Top-up 运行模式，控制系统建立了运行模式控制中心，对 MPS 子系统进行了升级改造，根据物理设计要求完成了 Top-up 运行模式下控制系统与 PPS、束测、电源等系统的协同设计与接口实施，实现了 Top-up 运行模式下的辐射剂量、能量、注入效率、束流流强和束流寿命的联锁。Top-up 运行安全联锁的核心基于硬件控制系统，并提供了作为辅助的软件联锁，在提高软件联锁可靠性方面开展了研究。

根据物理要求建立了 Top-up 运行模式控制系统，具体在机器保护系统(MPS 内实施。MPS 专门设置了运行模式控制机箱，将 Top-up 模式控制相关的联锁信号引入到控制机箱，通过由 PLC 控制器构成的逻辑控制系统和 OPI 操作面板，实现 Top-up 运行模式的联锁控制和手动操作。Top-up 运行模式控制的总体联锁逻辑即储存环注入允许的联锁逻辑。装置允许两种模式的储存环注入：Decay 模式和 Top-up 模式。图 1 为 Top-up 运行模式的总体实施结构图。

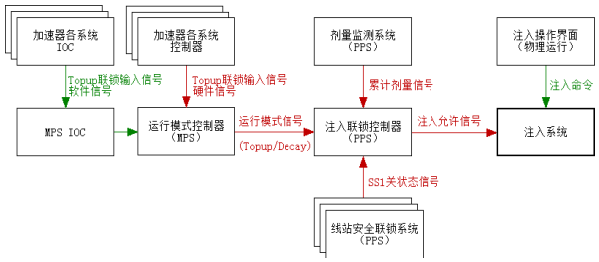

图 1　Top-up 运行模式实施结构

3　插入件自动前馈系统

插入件是现代光源重要组成设备之一，其质量直接影响上海光源整体性能。由于建造和安装工艺的限制，插入件的磁场会对束流轨道稳定性产生影响。为降低对束流的扰动，在插入件电子束流入口和出口位置增加校正线圈实现自动补偿功能。因此我们设计了基于 EPICS 的插入件前端反馈系统，经测试，该前馈系统用户界面简洁，反馈控制功能完整可靠，实时性高，提高了束流的稳定性，为给实验站稳定供光提供了保证。

前馈控制系统结构的核心部分由三个功能独立的 IOC (Input Output Controller)构成，驻留在一台嵌入式控制器中并通过以太网和 CA (Channel Access)协议进行互联。其中最主要的是设计了独

立的 IOC 专门用于前馈逻辑的实现，通过 CA 协议实时检测 PLC 控制 IOC 反馈的 GAP 和 SHIFT 读数，比对预先存储在 IOC 中的查找表来获取对应的校正线圈电源值并立即通过电源监控 IOC 设置校正线圈电源电流值。整个前馈系统通过 3 个 EPICS IOC 的协同实现了闭环控制的同时，通过 IOC 的协议转换将原本只能本地控制的 PLC 和电源控制器接入到光源的整个 EPICS 控制系统中。

在 EPICS 框架下，成功实现了上海光源插入件的前端反馈功能且无缝接入到光源 EPICS 控制环境中。根据不同设备和需求，精巧地设计了三个独立的 IOC，完成对各个设备的控制和简单明了的上层用户界面。在 IOC 驱动程序及运行数据库中通过中断和 FLNK 激励方式，有效地减少了查询方式带来的系统资源消耗并提高了系统运行速度。物理实验结果证实了该前馈系统结构完整，可靠性高，降低了插入件一二次积分磁场对束流的影响，增强了轨道的稳定性。图 2 为前馈打开与关闭后的束流轨道稳定性测试结果。

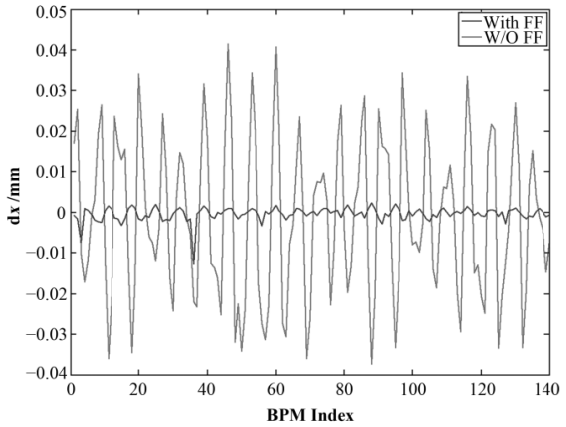

图 2 前馈 ON/OFF 的轨道稳定性变化结果

4 基于 Oracle RAC 的报警系统与历史数据数据库建设

开展了基于 CSS(Control System Studio)软件的 Alarm System 和 Channel Archive System 的数据库开发应用取得进展，主要工作包括基于 Oracle RAC(Real application clusters，实时应用集群)的历史数据库性能研究。其中 Alarm 系统自 2010 年 8 月开始运行，包括报警记录，消息订阅发送等。2011 年 5 月起，Channel Archive 系统开始记录数据，所记录的通道数与原 ChannelArchiver 完全相同，约 9000 个通道，日数据量约 2.5 GB，为基于 RDB 的存档和报警系统运行奠定了基础。

整个系统采用 4 台 HP 580G3 PC 服务器作为数据库服务器，SAN 的储存网络系统作为数据储存设备，每台服务器使用两块 SAN 的光纤卡与光纤交换机连接，系统架构(见图 3)。

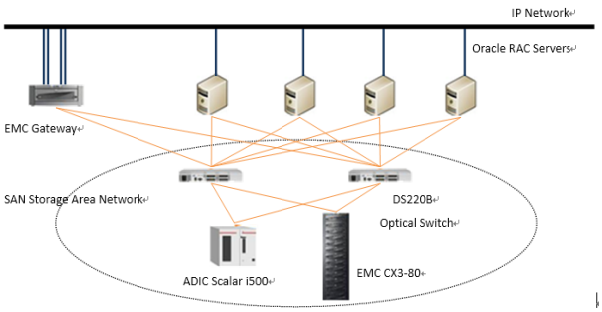

图 3 Oracle RAC 集群结构

5 辐射剂量固定监测控制系统（RMS）

辐射剂量固定监测系统，是独立的控制子系统。该系统分为实时监控部分和历史数据存储部分。RMS 系统目前共监控 109 台固定监测仪—58 台 G(伽马)监测仪，51 台 N(中子)监测仪，分布于直线、增强器、储存环、线站、大厅门、环境站。

RMS 实时监控系统采用 EPICS 控制系统的架构，采用 Modbus/TCP 通讯协议，目前各项功能都已实现并从 2010 年起开始投入运行。

6 基于下一代互联网的远程操作平台的研究

目前国际上大科学装置越来越依赖于国际合作，近年来加速器装置的远程协作与应用平台开发在国际上越来越得到重视。自 2011 年起我们在上海光源上开展了远程操作平台的研究项目，主要包括加速器远程协同调束平台，加速器设备远程诊断维护平台及加速器远程应用示范平台。目前已研发并建成的系统如下：

提供的故障及事件分析系统可供光源运行人员通过 IPV6 网络实时查看机器运行的事件及查询历史故障事件，给光源运行人员提供了一个有效的远程加速器故障诊断平台；基于 IPV6 的控制系统 EPICS 通道网关提供了远程控制及调试的基础服务，为基于 IPV6 的光源远程控制系统建立了基础；实时数据查询系统提供了实时控制系统通道数据访问，可通过 IPV6 提供加速器的各项参数的实时监控，并可对外提供基于 IPV6 的光源运行状态及参数查询。加速器历史数据访问，运行人员可在远程对加速器的历史数据进行查询及下载分析，为远程数据分析提供了有效的技术手段。在此基础之上为光源用户提供了基于 IPV6 的远程数据访问系统，用户可通过基于 IPV6 的 FTP 下载其实验数据。图

4 为加速器参数实时数据访问的网页。

图 4　加速器实时参数访问

参考文献

1. VIRTUALIZATION IN CONTROL SYSTEM ENVIRONMENT, ICALEPCS2011, WEPMU031
2. Safety Interlock Implementation of Top-up Operation in the SSRF Control System, IPAC12, THPPR034
3. 嵌入式上海光源 EPICS 插入件控制系统，强激光与粒子束, 2012, **25**(4)
4. 一个基于 EPICS 框架的 EPU 前端反馈系统, 核技术, 2012, **35**(8)
5. 上海光源远程实验与数据传输应用示范初步设计及概算实施方案,基于 CNGI 的科研信息基础设施建设和应用示范工程项目

Control Group Beam Instrument and Control Department

SHEN Liren Department of Beam Instrumentation and Control

During the annual operation of 2011–2012, the control group of Shanghai Light Source mainly focus on the system maintenance and optimization and according to the new requirements and the development of new technology, we start the control system upgrade work. The development of the control system mainly including control system virtualization environment research, feed-forward correction system of insertion devices, Top - up operation mode and the light source run time database, the research and development work of accelerator remote monitoring, etc. The main results are as follows.

1 VIRTUALIZATION IN CONTROL SYSTEM ENVIRONMENT

The virtualization of control system is a virtualization of the control system application environment, the characteristic is used for application virtualization for control system environment, including control system server virtualization, application server template, network configuration of virtual switches, application gateway virtualization and automatic fault migration of control system application. Especially for the configuration of virtual switch in entire control system subnet, its characteristic is that all the across the VLAN Settings of physical machine corresponding virtual switch can made virtual machine on the different device subnets migration between the different physical machine, that can realizes the high availability of whole equipment control system subnet of.

By constructing a virtual server system based on SAN storage system, the control system service process can migrate online and avoid fault cause by the failure of a server in control system. The virtual machine system including 16 Dell 2950 racks of servers and 1 CX-320 EMC SAN storage system. In the early stage of the system test and a lot of preparation work, the system completed during the 2010 summer maintenance stage. All the work include the migration of server and OPI console system to the virtual machine system and all the server operating system update from fedora Core 7 to the Cent OS 5.4 7 at the same time. It implemented the seamless docking of new system and old system and the EPICS application stability was improved.

Through the running of past two years, it proves that the hardware resources needed for the control system environment are well integrated by virtualization technology. The high availability features got by the virtual machine system realizes the automatic fault migration of control system environment and ensures 100% availability. Through the virtual switch Settings, it realize the seamless migration of the application in different control system subnet.

2 Safety Interlock Implementation of Top-up Operation in the SSRF Control System

The SSRF has performed two years stable operation on decay mode. In order to realize the top-up operation, the upgrade of control system has been carried out for top-up trial run. Control system sets up the operation mode control center and accomplishes the upgrading of the MPS system. According to the requirements of the physical design, control system accomplished the design and implementation of the interface for interoperate with PPS system, beam diagnosis system and power supply system and set up the interlocks of the radiation dose, energy, injection efficiency, beam current and beam life in top-up mode. The kernel of top-up operation safety interlock system is based on hardware interlock system and also provides software interlocking as auxiliary. In the meantime, the reliability of software interlock has been improved.

According to the physical requirements, we establish the Top-up operating mode control system and is embody particular in the machine protection system (MPS). The MPS set up a special operation mode controller and the interlock signals that Top-up mode control relevant are connected into this controller. The interlock control and manual operation of Top-up operation mode are realized by a set of logic control system constituted by the PLC system and OPI operator panel. Overall interlock logic of Top-up operation mode control is that the injection allowed interlocking logic of the storage ring. That allows two modes of the storage ring injection: Decay modes and Top-up mode. Fig.1 is a block diagram for the overall implementation of Top-up operation mode.

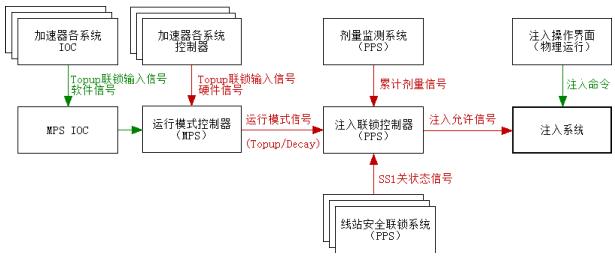

Fig.1 The diagram of structure of Top-up running mode.

3 Feedforward control system of the insertion devices

The insertion device is one of the important equipment of modern light source, its quality directly affects the overall performance of the Shanghai light source. Due to limitations of the construction and installation process, the magnetic field of insertion device will affect the sta-

bility of the beam orbit. To reduce the disturbance of the beam, we add the correction coils at the beam position of the inlet and outlet of insertion device to get the automatic compensation function. So we designed and tested a feedforwardsystem based on EPICS. The feedforward system has a simple kindly user interface and complete and reliable real-time feedback control that canimprove the stability of the beam and provides guaranteeof the stable supply light for experiment station.

The Core part of the feedforward control system structure consists of three function independent of the IOC (Input Output Controller), residing on an embedded Controller and through the Ethernet and CA (Channel Access protocol for interconnection. One of the most important is to design a independent of the IOC to realize the feedforward logic in dedicated, through CA protocol to real-time detection of the GAP and SHIFT reading value of IOC for the PLC control, then lookup the table that stored in the IOC to obtain the corresponding correction coil power value and set the correction coil current immediately by the IOC of power supply monitor. The feedforward system achieve the closed-loop control through three EPICS IOC coordination and at the same time, connect thelocal PLC and power supply controller to the whole EPICS control system of light source through the IOC protocol conversion.

Under the framework of EPICS, we successfulimplemented a feedforwardsystem for insertion deveice of Shanghai light source and connect to the EPICS control environment of light sourceseamlessly. According to the demandof different equipment, we exquisitely designed three separate IOC to complete the control of various equipment and the simple and clearupper layer user interface. Through the interrupt and FLNK incentives in the IOC driver and run time database, effectively reduce the system resource consumption cause by the query method of and improve the system running speed. Physics experimental results confirmed that the feedforward system structure is complete and high reliability that can reduce the effect of primary and quadratic integralmagnetic field of insertion device to the beam and enhanced the stability of the beam orbit. Fig.2 show the results ofbeam orbit stability after opening and closing the feedforward system.

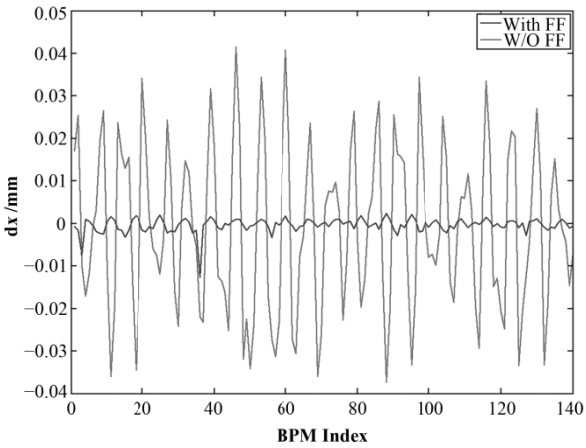

Fig.2 The beam orbit result at the feedforward ON/OFF.

4 The construction of alarm and archive system based on Oracle RAC

The development work for alarm and RDB archive system based on CSS (Control System Studio) software ware carried out and got some progress. The main work includes performance study of RDB archive system based on Oracle RAC (real application clusters, real-time application clusters). The alarm system run since August 2010, including Alarm record, message subscription sent, etc. From May 2011, RDB Channel Archive system began to record data, it record the same number of channels as the original Channel Archiver about 9000 channels and 2.5 GB of data volume per day, this laid a foundation for archive and alarm system based on RDB system.

The whole system consists of 4HP 580 g 3 PC server as the database server, SAN storage network system as a data storage device, each server use two pieces of SAN fiber card connected to the optical fiber switches, the system architecture as shown in Fig.3.

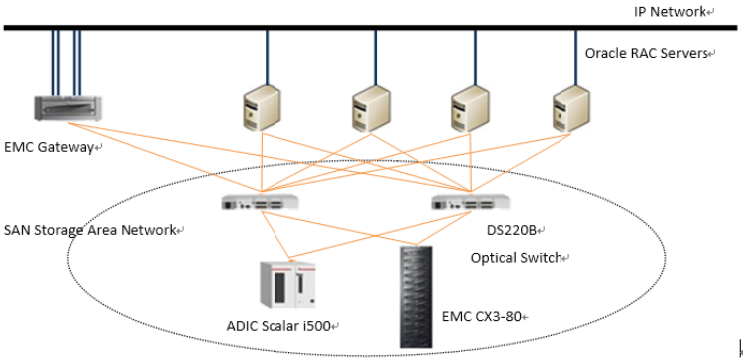

Fig.3 The Oracle RAC structure.

5 Fixed radiation dose monitor system (RMS)

Fixed radiation dose monitoring system is an independent control subsystem. The system is divided into real-time monitoring and historical data storage sections. The RMS system now include 109 fixed monitor, 58 m G (gamma) monitor and 51 N (neutron) monitor which distribution in linac, booster, storage ring, beam line, the hall door and environment station.

The RMS real-time monitoring system adopts the

EPICS control system architecture and use the Modbus/TCP communication protocol. Now all the functions have been implemented and put into operation since 2010.

6 The research of remote operation platform based on next generation internet

So far big science facility on the world are more and more dependent on international cooperation, the remote collaboration and application platform development of accelerator is increasingly attention in world recently. Since 2011, we carried out the research projects of remote operation platform in Shanghai light source, it mainly including remote accelerator beam study platform, remote diagnosis and maintenance platform and remote application demonstration platform. Has now we have developed and built the system are as follows:

Built a fault and event analysis system for the light source operator to check the machine running events-real-time and query historical fault events with the IPV6 network that provides an effective platform to diagnose accelerator fault remotely. In the Control system, EPICS gateway based on IPV6 provide the foundation of the remote control and debugging services, and build the foundation of the remote control system based on IPV6 for the light source. The real-time data query system provides real-time channel data access of control system, provides real-time monitoring of various accelerator-parameters through the IPV6 and can provide running state and parameter query for light source from outside. The Accelerator historical data access make the operation personnel remote query, download and analysis the accelerator historical data and provides effective technical means for remote data analysis. Furthermore we built a remote data access system based on IPV6 for the light source user, the user can through IPV6FTP to download their experimental data. Fig.4 for the accelerator parameters real-time data access page.

Fig.4 The real-time arguments access for the accelerator.

References

1. VIRTUALIZATION IN CONTROL SYSTEM ENVIRONMENT，ICALEPCS2011，WEPMU031
2. Safety Interlock Implementation of Top-up Operation in the SSRF Control System, IPAC12, THPPR034
3. Embedded EPICS insertion device control system of Shanghai light source, High Power Laser and Particle Beams, 2012, **25**(4)
4. AnEPU feedforward system based on EPICS framework, Nuclear Techniques, 2012, **35**(8)
5. The preliminary design and implementation planof remote experiment and data transfer demonstrate application of Shanghai light source,The scientific research information infrastructure construction and demonstration application based on CNGIprojects

硬 X 射线微聚焦及应用光束线站用户研究成果在《自然》上发表

材料与能源科学研究部　硬 X 射线微聚焦及应用光束线站　李爱国

上海光源硬 X 射线微聚焦及应用光束线站(BL15U1)利用上海光源高亮度的波荡器 X 射线辐射，结合先进的 X 射线光学系统，在实验站得到高通量、能量可调的单色 X 射线微束，配备先进的探测系统，使之成为高性能的 X 射线微探针装置。本光束线站目前可开展如下的实验研究：微束 X 射线荧光分析(μ-XRF)，分析样品中的元素组分；微束 X 射线吸收精细结构(μ-XAFS)，分析原子的紧邻环境和化学态；微束 X 射线衍射(μ-XRD)，主要分析粉末样品的晶体结构。2011–2012 年，BL15U1 线站用户共计在国际及国内期刊上发表文章 60 篇，其中新型铁基硫族化合物超导体在高压下的相变特性研究发表在《自然》上。

2010 年发现的新型铁基硫族化合物超导体 $A_{1-x}Fe_{2-y}Se_2$ (其中 A = K，Rb 或 Cs，及部分替代的 Tl) 为非常规超导体的研究探索开辟了新的研究方向和提供了新的机遇。这类超导体在常压下的超导转变温度约为 32 K，中子散射研究结果表明，这类超导样品具有很强的反铁磁磁距并在铁离子的正方型格子中存在铁离子有规律的缺位。为何这样高 Tc 的超导电性能够在如此强的磁背景中存在，以及反铁磁和铁离子有规律的空位如何对超导电性产生影响等问题倍受关注。大量的理论和实验研究结果表明，对于关联电子系统中的超导电性是由其晶体结构、电荷、轨道和自旋的状态及其相互作用所决定的，而这些因素对超导电性的影响可以通过外部参数的改变，如施加压力、磁场等进行调控。其中，压力是一种“干净”和有效的调控方法，它的独特之处在于不用改变研究系统的化学构成就能实现对系统的电子结构和晶体结构及其相关合作现象的有效调控，从而揭示其内在的物理机制。比如，利用压力手段可以改变电子密度、电子轨道的杂化和磁性能等，由此导致许多重要物理现象，如金属——绝缘体相变、价态变化、超导相的出现等。

其中，中国科学院物理研究所国家超导实验室赵忠贤院士小组的孙力玲研究员及其合作者与美国卡内基研究院地球物理实验室毛和光院士、陈晓嘉博士等合作，利用自行研制的高压—低温—磁场联合测试系统对这类新型铁基硫族化合物超导体进行了系统的高压原位输运性能和磁性能的研究。他们发现这类超导体的超导转变温度在压力小于 10 GPa (1GPa＝1 万大气压)时随着压力的升高而逐渐降低，直至消失；而当压力高于 10 GPa 以后，系统出乎意料地进入了一个新的超导态，超导电性再次出现。这个由压力诱发的第二个超导相的超导转变温度高达 48 K，远远高于第一个超导相的最高超导转变温度，是已有报导的铁基硫族化合物超导体家族中的最高超导转变温度。为了澄清压力驱动的超导再现是否与压致晶体结构的变化有关，在与上海光源硬 X 射线微聚焦线站 (BL15U1)工作人员的紧密合作下，在高压下对这种材料的晶体结构进行了 X 射线微区衍射测量和分析，得到了晶体结构与压力间的直接实验证据。该研究不仅对理解这类新型铁基硫族化合物超导体的超导机制和探索新的超导体提供了启迪，同时，也为进一步开展高温超导体超导机理的研究提出了新的研究课题。该项研究结果发表在(Nature, 2012, **483**: 67–69)。

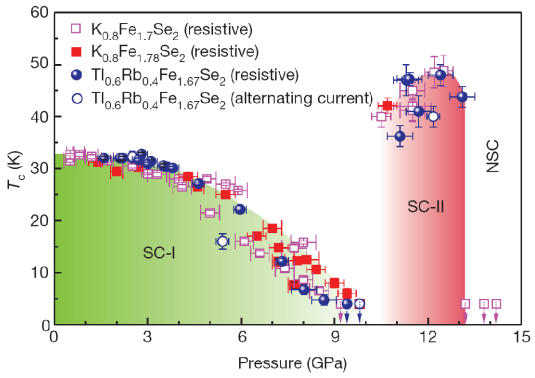

压力下新型铁基硫族化合物超导体 $Tl_{0.6}Rb_{0.4}Fe_{1.6}7Se_2$、$K_{0.8}Fe_{1.7}Se_2$ 和 $K_{0.8}Fe_{1.78}Se_2$ 的超导相图

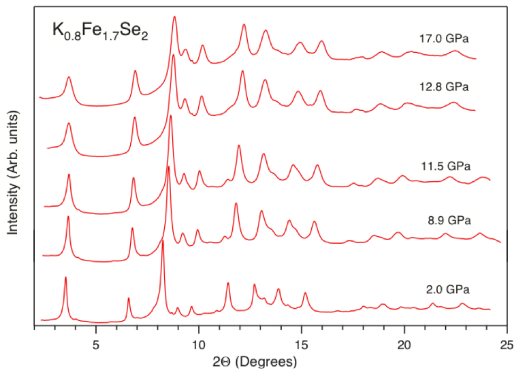

不同压力下 $K_{0.8}Fe_{1.7}Se_2$ 的 X 射线 微束衍射图谱

The Users of Hard X-ray Micro-Focusing in Shanghai Synchrotron Radiation Facility Published Their Research in Nature

LI Aiguo Hard X-Ray Micro-Focusing Beamline (BL15U1)
Department of Materials and Energy Science

By utilizing the high brightness undulator X-ray radiation light source and combining advanced X-ray optics system, the hard X-ray micro-focusing beamline (BL15U1) in Shanghai Synchrotron Radiation Facility (SSRF) gets a high-throughput and energy tunable monochromatic X-ray micro sized beam. In addition, this beamline equipped with advanced detection system and became a high-performance X-ray microprobe device. The experimental methods in BL15U1 include micro beam X-ray fluorescence analysis (μ-XRF), micro beam X-ray absorption fine structure (μ-XAFS) and micro beam X-ray diffraction (μ-XRD). In 2011–2012, the users of BL15U1 published 60 articles in international and domestic journals. Among them, the research of the new family of iron-based chalcogenide superconductors' phage transition under high pressure was published in Nature.

The recent discoveries of superconductivity at 30 K to 32 K in a new family of iron-based chalcogenide superconductors $A_{1-x}Fe_{2-y}Se_2$ (where A=K, Rb or Cs, with possible Tl substitution) bring new excitement to the field of superconductivity. These superconductors have unusually large magnetic moments up to 3.3 μB per Fe atom and a Fe-vacancy ordering in the Fe square lattice. How superconductivity with such a high Tc can exist on such a strong magnetic background remains perplexing. It has been established that superconductivity in strongly correlated electronic systems can be dictated by their crystallographic structure, electronic charge, and orbital and spin degrees of freedom, which can all be manipulated by controlling parameters such as pressure, magnetic field and chemical composition. Pressure is a 'clean' way to tune basic electronic and structural properties without changing the chemistry. High-pressure studies are thus very useful in elucidating mechanisms of superconductivity as well as in searching for new high-Tc superconducting materials.

The scientists from Institute of Physics, Chinese Academy of Sciences and Geophysical Laboratory of the Carnegie Institution of Washington used their self-developed combining high pressure - low temperature - magnetic field test system to study this new type of iron-based chalcogenide superconductors' transport and magnetic properties in situ under high-pressure. They found that such superconducting transition temperature gradually decreased with increasing pressure at less than 10 GPa until the superconductivity disappeared. However, when the pressure was higher than 10 GPa, the system entered a new superconducting state unexpectedly and the superconductivity reappeared. The pressure-induced superconducting phase (SC-II) has a Tc of 48 K, which is much higher than the maximum in SC-I. This temperature was the highest Tc of the family of iron-based chalcogenide superconductors' phage transition which has been reported. To clarify whether the reappeared superconductivity driven by pressure related to the changes in the crystal structure, they measured the crystal structure of this material under high pressure by synchrotron radiation μ-XRD technique with the great help of BL15U1 staff and obtained direct experimental evidence between the crystal structure and pressure. Their study not only provided inspiration for understanding the superconductivity mechanism of the new family of iron-based chalcogenide superconductorsin and exploring new superconductors, but also proposed a new research topic on the mechanism of high-temperature superconductors superconducting. The study was published in Nature 483, 67–69 (01 March 2012).

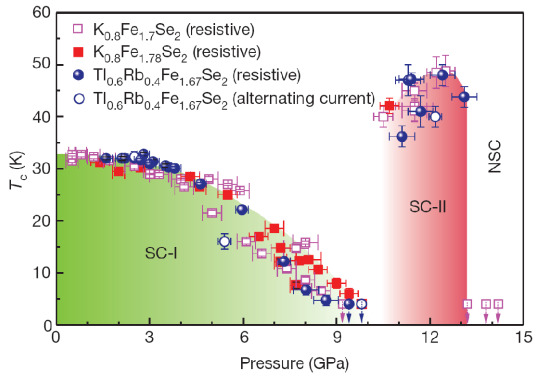

Pressure dependence of the Tc for $Tl_{0.6}Rb_{0.4}Fe_{1.67}Se_2$, $K_{0.8}Fe_{1.7}Se_2$ and $K_{0.8}Fe_{1.78}Se_2$.

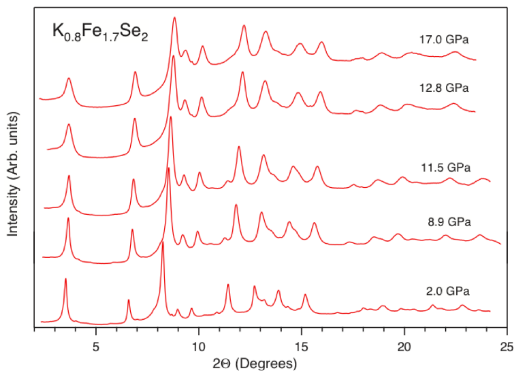

X-ray powder diffraction patterns of $K_{0.8}Fe_{1.7}Se_2$ at various pressures up to 17.0 GPa.

纳米探针测试系统及利用同步辐射微区分析技术系统研究纳米材料生物效应

材料与能源科学研究部

2011 年初，线站进行纳米聚焦装置首次带光调试，利用 8 nm 厚的 Fe 膜激发荧光测量光斑尺寸，得到了约 400 nm 的聚焦光斑。根据首次测试结果的数据分析，2011 年 3 月起，进一步改进机械设计和测试方案。改进后的设计方案增加了波带片和样品台的调节方便性，改进了运动平台的机械稳定性，以及增加了波带片和 OSA 支撑部件的刚性。2011 年 8 月再次完成系统的加工和安装。最终纳米探针设计图和照片如图 1 所示。为了检测光斑尺寸，在国内首次采用自行制作厚度为 70 nm 的 Ni 薄膜刀口进行荧光检测，刀口平直度好于 10 nm，检测光斑尺寸最小可达 119 nm×129 nm(@10 keV)。

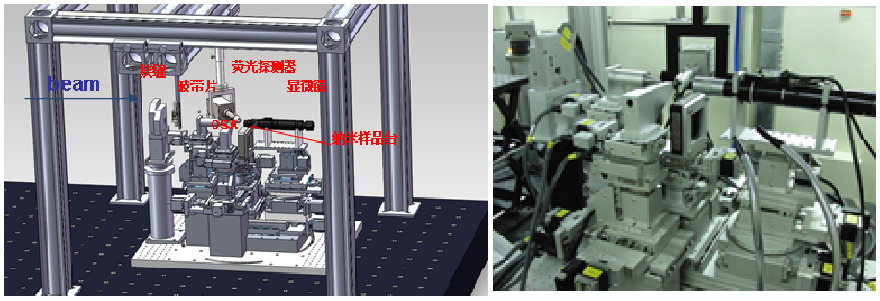

图 1 硬 X 射线纳米探针机械设计图和实物照片

基于同步辐射先进光源发展起来的多种元素高灵敏分析技术近年来已开始应用于纳米材料的表征、化学结构分析等领域，但用于生物体系内原位的研究尚无报道。国家纳米科学中心中国科学院纳米生物效应与安全重点实验室陈春英研究组和纳米材料研究室唐智勇研究组合作，利用上海光源 BL-15U1 线站，创新性地将多种同步辐射技术如 X 射线原位微区元素成像与化学结构分析技术应用于量子点材料在体内代谢与降解过程的研究，揭示了量子点在线虫消化系统微环境内降解、氧化和代谢的过程，并指出了利用纳米材料光学特性进行分布研究的不可靠性，提出集成光学成像、原位元素成像与结构分析、细胞生物学、毒理学等多种方法来研究纳米材料在生物体系内分布代谢等重要问题的系统研究方法。该研究方法对于建立以秀丽线虫为模式生物评价纳米材料生物效应的研究平台具有重要意义，并有望在后续研究中推广应用于多种重要纳米材料的研究，在不同层次阐明纳米材料与生物体系相互作用的机制。

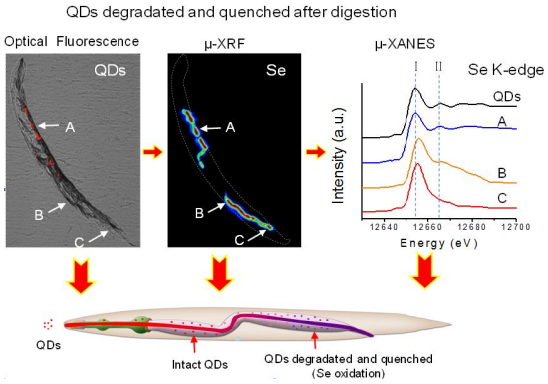

量子点在秀丽线虫消化道内的降解过程

参考文献

1. Ying Qu, Wei Li, Yunlong Zhou, Xuefeng Liu, Lili Zhang, Liming Wang, Yu-feng Li, Atsuo Iida, Zhiyong Tang, Yuliang Zhao, Zhifang Chai, Chunying Chen. Nano Lett, 2011, **11**: 3174–318

Nano-Probe System and the Research of Biological Effects of Nanomaterials Using Synchrotron Radiation Ttechnology

Hard X-Ray Micro-Focusing Beamline　Department of Materials and Energy Science

In early 2011, during the first nano-probe system test, about 400 nm spot size is obtained using Fe film with thickness of 8 nm by X ray fluorescence method. According to the test results, in Mar. 2011, an improved mechanical design and testing program is designed. The adjustment of zone plate and the sample stage is much more convenient and the mechanical stability of platform is improved, as well as the rigidity of the zone plate and OSA support. The processing and installation of the system is finished in Aug. 2011. The final design drawings and photographs of the nanoprobes is shown in Fig.1. We used Ni films with thickness of 70 nm to detect the spot size of the system by X ray fluorescence technique. The spot size is 119 nm×129 nm (@10keV).

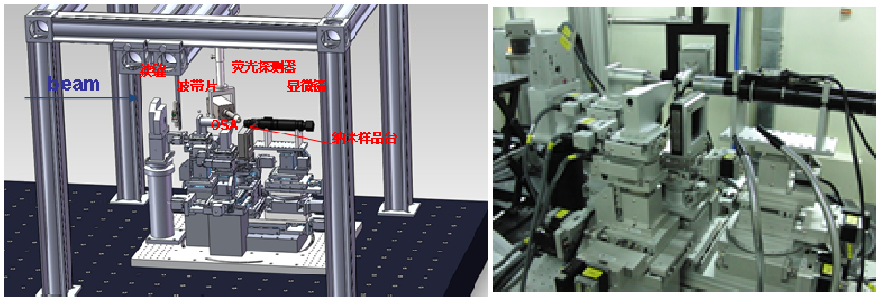

Fig.1　Hard X-ray nanoprobe mechanical designs drawings and photographs.

Water-soluble quantum dots (QDs) is a type of semiconductor nanoparticle exhibiting quantum confinement effect, it have been considered as alternatives of conventional fluorescent dyes for biomedical imaging due to their significant advantages, e.g. broad optical absorption, bright and tunable fluorescence, remarkable stability against light and chemicals, and easy conjugation with biomolecules.

In this study, Caenorhabditis elegans (C. elegans) is used as a model organism for thorough investigation of the fate and physiological behavior of QDs in bioentity. The model is useful for toxicological studies of QDs from whole-animal level down to single cell level. The researcher evaluated the in vivo fate and physiological behavior of quantum dots (QDs) in Caenorhabditis elegans by GFP transfection, fluorescent imaging, synchrotron radiation based elemental imaging, and speciation techniques. The in situ metabolism and degradation of QDs in the alimentary system and long-term toxicity on reproduction are fully assessed.

This work highlights the utility of the C. elegans model as a multi flexible platform to allow noninvasively imaging and monitoringin vivo consequences of engineered nanomaterials.

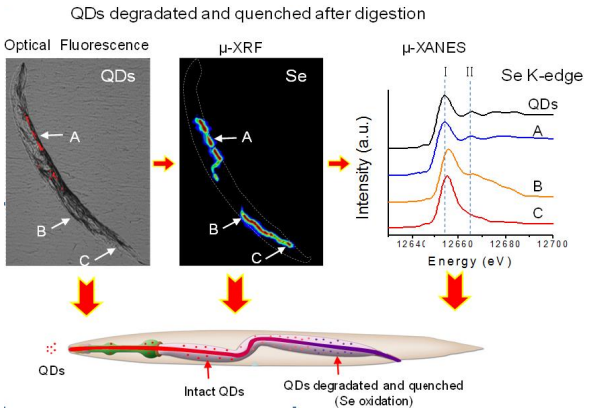

In situ elemental analysis and degradation of QDs.

References

1. Ying Qu, Wei Li, Yunlong Zhou, Xuefeng Liu, Lili Zhang, Liming Wang, Yu-feng Li, Atsuo Iida, Zhiyong Tang, Yuliang Zhao, Zhifang Chai, Chunying Chen. Nano Lett, 2011, **11**: 3174–3183

X 射线衍射组原位设备研制及应用

材料与能源科学研究部　X 射线衍射组

1　原位设备以及有机光伏器件研制

研制出应用于原位 X 射线衍射、吸收光谱研究锂电池电极材料构效关系的原位池，测试了 $BiFeO_3$ 电池电极材料电化学循环性能，在衍射站/吸收谱站分别实现了原位的测试，相应成果获得发表。

本年度还研制出了用于测试纳米材料原位生长的设备，并进行了系列前期实验，取得了一定的成果，为进一步实验室合成指明方向。

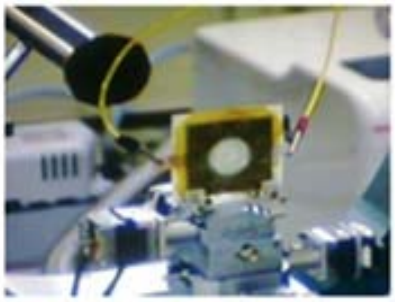

原位锂离子测试设备

制备了基于聚合物材料 P3HT 和 PCBM 等一系列有机薄膜太阳能电池，原位和非原位地表征了薄膜的自组装微结构，并用光伏测试系统研究了器件的光电转换性能。同时，采用本课题组合成的有机配体金纳米颗粒用于有机薄膜太阳能电池制备，系统研究了金纳米颗粒的自组装对薄膜微结构调控和器件性能增强作用。

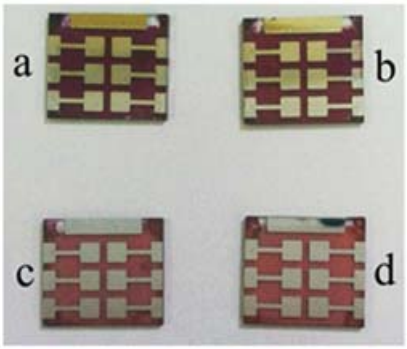

不同优化条件下制备的有机太阳能电池

此外，还研制了可以进行常压 CVD 薄膜生长、电场下薄膜结构研究、低温下薄膜电荷有序研究等原位设备，并成功应用于衍射线站多个用户的研究工作中。

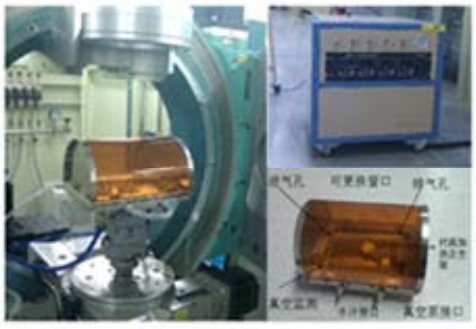

常压 CVD 石墨烯生长平台

2　原位设备应用

2.1 原位锂离子电池测试设备应用

研究了 $BiFeO_3$ *vs* Li 锂电池电化学性能，应用原位衍射谱对于 $BiFeO_3$ 材料在充放电过程中的相变情况进行了详尽的研究。研究发现，$BiFeO_3$ 材料放电时，Li+离子首先嵌入到 $BiFeO_3$ 晶格内部，在一定的 Li+嵌入后，嵌 Li^+ $BiFeO_3$ 中的 Bi 以 Li_2Bi 合金的形式脱出。 第二次循环中的 Li+ 进一步分别从 Li_2Bi 以及嵌 Li $BiFeO_3$ 中脱出，循环多次后，Li_2Bi 对于 Li 的 嵌入/脱嵌不完全可逆，在多次循环后，分解为金属 Bi。

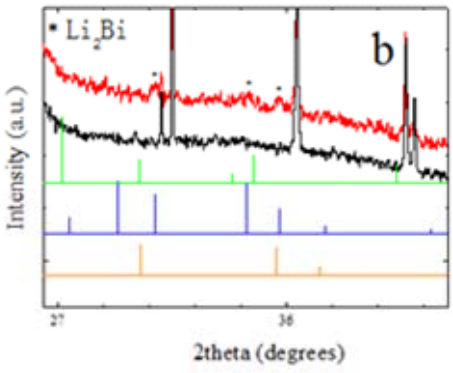

原位观测 Li_2Bi 生成

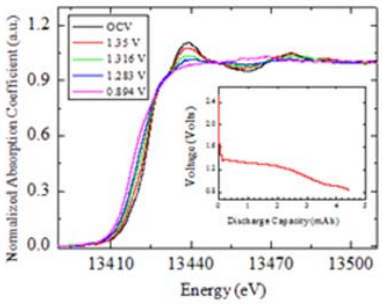

原位观测放电过程中 Bi^{3+}还原过程

在吸收谱站应用 Bi L_{III} 吸收边，进一步对于放电过程中的 Bi 离子价态进行了研究，研究发现，放电时 Bi 离子价态逐渐由 3 价减少到 0 价，而 Fe 离子的价态并没有发生变化，证明在放电过程中，Bi 离子是电化学活性位点。综合原位衍射谱以及吸收谱，我们对于 $BiFeO_3$ 与 Li 锂离子电池的放电机理给出了详尽的阐释。

2.2 原位气相纳米生长设备应用

研究了掺杂 Ce $BiFeO_3$ 材料在变温过程中的相变情况，观测到加热过程中样品前驱体(共沉淀法合成的 Fe、Bi、Ce、O 的混合物)在加热过程中向 $BiFeO_3$ 相的转变过程、温度。进一步分析衍射峰的 FWHM, 可以计算出样品晶粒尺寸的大小。发现 Ce 掺杂升高了 $BiFeO_3$ 相的生成温度， 但是减少了晶粒的尺寸， 在 600 ºC 时在 20 nm 左右。

2.3 其它原位设备应用

应用其它原位设备，比如气相纳米原位生长设备、原位加电场设备以及原位高温设备等与相关单位展开了一系列的合作研究，相关研究成果发表在 Angew. Chem. Inter. Ed.、Appl. Phys. Lett. 以及 Adv. Mater. 上。

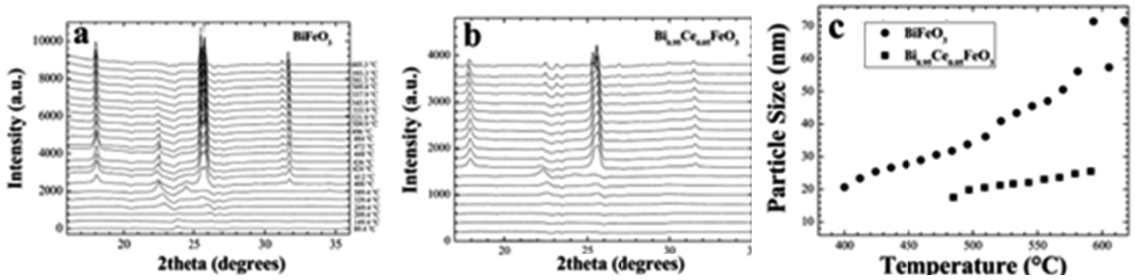

原位观测加热过程中 $BiFeO_3$ 相的生长过程

3 实验室建立

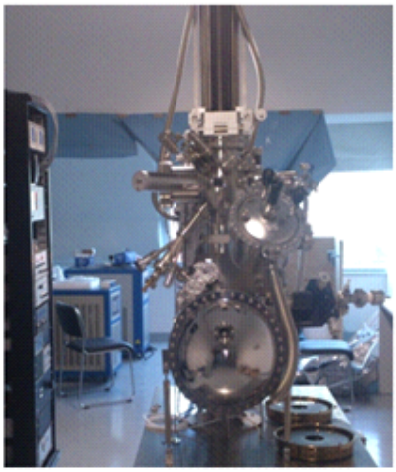

超高真空光电子能谱系统

物理实验室配备了超高真空光电子能谱系统，包括 X 射线和真空紫外光电子能谱，具备物质电子结构、元素化学成分测量以及部分薄膜原位蒸发沉积功能。光电子能谱设备所有硬件搭建已经完毕，正在进一步调试。

参考文献

1. Luo S H, Gao M, Chen J, Xing X R, Li Z, Zhou X T, Wen W. J New Mater Electrochem Sys, 2011, **14**: 141
2. Zhang X M, Gao M, Gu Y L, Bao H L, Li X L, Zhou X T, Wen W. J Phys Chem C, 2012, **116**: 20230
3. 文闻, 张兴民, 高梅, 杨铁莹, 何庆, 周兴泰. 基于同步辐射的纳米材料原位气相生长装置, 申请号: 201120538631.0
4. 文闻, 高梅, 顾月良, 何庆, 黎忠, 周兴泰. 一种基于同步辐射的锂离子电池原位测试装置, 申请号: 201120537974.5

X-ray Diffraction Group- *in-situ* Cells Developments and Applications

X-ray Diffraction Group Department of Materials and Energy Science

1 *In-situ* Measurements Cells And Organic Solar Cells Developments

In-situ cell, which is designed for both X-ray diffraction and absorption spectroscopy measurements, was invented for lithium battery electrodes' structure-property relationship studies. *In-situ* measurements have been successfully carried out at both X-ray diffraction and absorption beamlines and some of the results were published. Gas-flow cell for *in-situ* nano-material growth was invented and preliminary work therein was accomplished, which can guide future efforts.

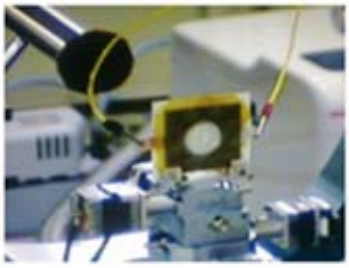

In situ Lithium battery measurements cell.

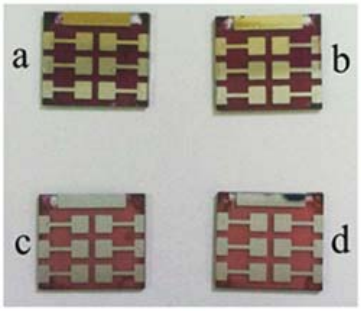

Organic solar cells optimized at various conditions.

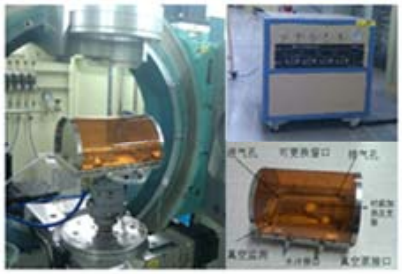

Ambient pressure CDV graphene growth cell.

Besides, a series of P3HT/PCBM organic thin film solar cells were fabricated. These thin films' self-assembled microstructures were characterized using *in-situ* and *ex-situ* synchrotron techniques and their photoelectric conversion efficiency was investigated using photovoltaic test system. In addition, ligated Au nano-particles were prepared and blended into the solar cells. The microstructures of the active layer can be greatly influenced by the gold nano-particle self-assembly leading to enhanced photovoltaic performances.

In addition, many other *in-situ* cells were invented, such as one with electric field, one for heating in a gas environment, one at high temperature, and one at high/low temperature.

2 The Applications of *In-situ* Cells

2.1 *In-situ* cell for lithium battery electrodes studies

Our group studied the electrochemical performance of $BiFeO_3$ *vs* Li battery. Its structural transformations during the cycling were investigated by *in-situ* X-ray diffraction. The results show that Li^+ ions were firstly inserted into $BiFeO_3$ during the discharge. After certain amount of Li^+ inserted, Bi was separated out of $BiFeO_3$ crystal lattice with Li_2Bi alloy formed. During the 2nd charge process, Li^+ ions were extracted out of Li_2Bi and Li doped $BiFeO_3$. During the subsequent cycles, due to the irreversible Li^+ insertion/extraction, Li_2Bi was decomposed into metallic Bi.

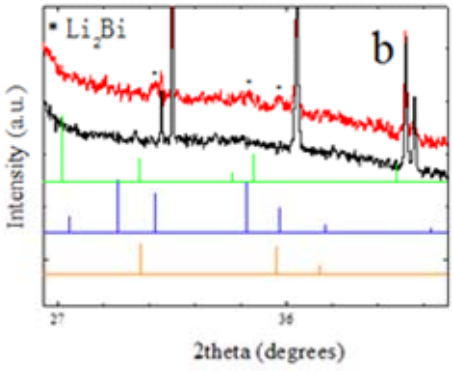

In situ observation of Li_2Bi formation.

Using Bi L_{III}-edge X-ray absorption spectroscopy, we further investigated Bi ions valence state change during the discharge process. It was observed that Bi valence state gradually decreased from +3 to 0 during the discharge process, while Fe valence state remained unchanged. This proves that Bi ions are active sites for electrochemical activity. Combined *in-situ* X-ray diffraction and absorption spectroscopy, $BiFeO_3$ *vs* Li battery discharge mechanism was successfully revealed.

2.2 *In-situ* Gas Phase Nano-materials Growth Cell

Our group investigated Ce doped $BiFeO_3$ phase transitions at different temperatures and found that the precursor (Mixture of Fe, Bi and Ce Oxides synthesized using co-precipitation technique) was transformed into $BiFeO_3$ phase during heating. After further analyzing the diffraction peaks FWHM, $BiFeO_3$ particle sizes can be calculated during the heating. It is observed that Ce

doping increases $BiFeO_3$ formation temperature with their particle size decreased. Actually, the particle size is only ~20 nm at 600 ℃.

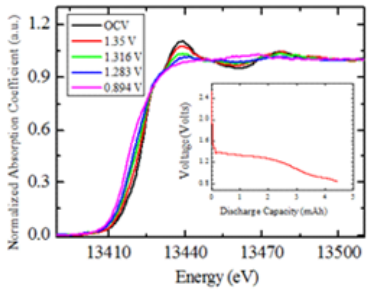

In situ observation of Bi^{3+} ions reduction during discharge.

2.3 Other In-situ Cells

Using other *in-situ* cells, such as the one for gas phase *in-situ* growth, the one with electric field, the one with high temperature, we collaborated with several other groups on different projects and some of the joint works have been published in *Angew. Chem. Inter. Ed.*, *Appl. Phys. Lett.* and *Adv. Mater.*, etc.

3 Physics Laboratory

Physics Laboratory is equipped with ultra-high vacuum system for X-ray photoemission spectrometry, which includes both X- ray tube and UV lamp sources. In this system *in-situ* thin film growth can be preceded. The system has just been set up and further adjustments and testing are underway.

Ultra high vacuum photo-electron spectrometry.

Reference

1. Luo S H, Gao M, Chen J, Xing X R, Li Z, Zhou X T, Wen W. J New Mater Electrochem Sys, 2011, **14**: 141
2. Zhang X M, Gao M, Gu Y L, Bao H L, Li X L, Zhou X T, Wen W. J Phys Chem C, 2012, **116**: 20230
3. 文闻, 张兴民, 高梅, 杨铁莹, 何庆, 周兴泰. 基于同步辐射的纳米材料原位气相生长装置,申请号: 201120538631.0
4. 文闻, 高梅, 顾月良, 何庆, 黎忠, 周兴泰. 一种基于同步辐射的锂离子电池原位测试装置,申请号: 201120537974.5

X 射线成像组研究进展

先进成像与工业应用研究部　X 射线成像光学组

X 射线成像组主要承担“上海光源”首批线站“X 射线成像及生物医学应用光束线站”的运行维护与用户实验支持工作。该线站在 2011–2012 年度高效低故障率运行，总供光机时 10585.7 h，总故障率为 1%。累计提供用户机时 9026 h，接待用户实验人员 1179 人次，执行用户课题 317 个，用户研究涵盖生物医学、材料科学、地质考古学等众多学科领域，共发表用户成果 86 篇，其中二区及以上文章 24 篇。线站维护方面，完成了光束线准直复测、滤波器维护、单色器水冷管的更换、白光狭缝横向刀口平行度调节、实验站不同实验方法的布局调整、荧光快速扫描装置改进、大开口毫秒快门研制等。

除负责上海光源一期 X 射线成像及生物医学应用线站的日常运行维护及用户实验支持外，本组还负责上海光源线站工程 2 条新建线站“快速 X 光成像线站”和“纳米三维成像线站”及中石化拟建显微 CT 线站、上海交通大学拟建医学影像分支线站的设计工作，2011–2012 年度本组负责完成了上述相关线站物理设计及项目建议书的撰写。

为满足不同学科领域用户研究的需求，本组在 X 射线成像方法学研究及相关应用研究方面进行了不断的研究和探索，共发表论文 23 篇，其中 SCI 收录 16 篇，获授权专利一项，在同轴相位衬度成像相位恢复算法研究[1-5]、快速 X 射线荧光 CT[6-8]、相干 X 射线衍射成像[9,10]、X 射线螺旋显微 CT[11]、多重能量吸收衬度 CT 结合数据约束模型(DCM)算法实现材料的三维结构定量分析[12-13]、CT 重构伪影消除算法研究[14]、远程 CT 快速重构软硬件实现[15]、劳厄弯晶聚焦特性研究[16]等方法学研究方面取得了一系列的成果。此外，还建立了光栅微分相衬成像实验方法并开展了初步实验研究。应用研究方面，开展了中药材显微特征结构研究、木竹材无损检测研究、新型骨修复支架成骨作用的定量评价、和材料的定量结构表征研究[17]等。

在研项目主要有：国家重点基础研究发展计划(973 课题)“同步辐射 X 射线医学影像新型成像方法及关键技术研究”、中国科学院对外合作重点项目“依托上海光源的 X 射线医学成像新方法及其应用国际合作计划”、国家自然科学基金“基于同步辐射的三维 X 射线荧光 CT 研究”、“中药材特征结构的 X 射线相衬显微 CT 研究”和“硅酸钙/玉米蛋白多孔活性支架及其在体骨修复评价中的研究”；新申请获批项目有：CAS-CSIRO 合作研究项目“基于同步辐射显微 CT 的肿瘤血管三维结构定量分析”、国家自然科学基金面上项目“基于“飞行”扫描与 OSEM 加速 X 射线荧光 CT 成像”等。

2013 年度本组除了进行成像线站的运行维护和用户实验支持、新建相关线站的设计以及执行上述科研项目外，还将在快速荧光 CT、小动物原位活体动态研究、螺旋 CT、定量 CT、光栅微分成像、快速 CT 重建算法研究以及中药材显微鉴别、木材无损检测等方法学和相关应用领域继续进行深入研究。

参考文献

1. Chen R C, Xie H L, Rigon L, *et al*. Opt Lett, 2011, **36**(9): 1719-1721
2. Chen R C, Dreossi D, Mancini L, *et al*. J Synchrotron Rad, 2012, **19**(5): 836-845
3. Ren Y Q, Chen C, Chen R C, *et al*. Opt Express, 2011, **19**(5): 4170-418
4. 刘慧强，任玉琦,周光照等. 物理学报，2012, **61**(7): 078701
5. Liu H Q, Ren Y Q, Guo H, *et al.* Chin Opt Lett, 2012, **10**(12):
6. Deng B A, Yang Q, Xie H L, *et al.* Chinese Phys C, 2011, **35**(4): 402-404
7. 杨群，邓彪，吕巍巍，等. 光谱学与光谱分析，2011, **31**(10): 2753-2757
8. Yang Q, Deng B, Lv W W, *et al.* J Synchrotron Radiat, 2012, **19**: 210-215
9. 周光照，佟亚军，陈灿，等. 物理学报，2011, **60**(2): 028701
10. 周光照，王玉丹，任玉琦，等. 物理学报，2012, **61**(1): 018701
11. 王玉丹，彭冠云，佟亚军，等. 物理学报，2012, **61**(5): 054205
12. Wang Y D, Stevenson A, Yang Y S, *et al.* J Synchrotron Rad., 2012, **19**: 827-830
13. Wang Y D, Yang Y S, Cole I, *et al.* Materials and Corrosion, DOI: 10.1002/maco.201106341
14. 张国强，周虎，和友，等. 光学学报, 2012, **32**: 534001
15. 沈飞，陈荣昌，肖体乔. 核技术, 2011, **34**(6): 401-405
16. 陈灿，佟亚军，谢红兰，等. 物理学报，2012, **61**(10): 104102
17. Guo Han, Wei Jie, Song Wenhua, *et al*. International Journal of Nanomedicine, 2012, **7**: 3613-3624

Research Development of X-ray Imaging Group

X-ray Imaging Group Department of Advanced Imaging and Industrial Applications

X-ray imaging group is mainly in charge of operation and user support of X-ray imaging and biomedical applications beamline. During 2011–2012, this beamline has supported beam time of 10,585.7hwith a low fault rate of 1%. There are 9026 hours provided for 1179 users from the 317 proposals, whose research fields covering biomedicine, material science, archeology paleontology and son on. And 86 papers have been published by users during this time. The completed work about beamline maintenance includes: maintenance of the filters, replacement of water-cooling tubes of monochromator, adjustment of the layout of experimental station for different experimental methods; devices improvement of the fast fluorescence mapping, development of the large opening millisecond shutter and so on.

In addition, the physical design and project proposals of four new beamlines have been completed: two new beamlines of SSRF phase-II project named as “Fast X-ray imaging beamline” and “Nano 3D imaging beamline”, “micro-CT beamline” proposed by Sinopec, “medical imaging beamline branch” proposed by Shanghai Jiaotong University.

In order to meet the demands of users for different samples, many X-ray imaging methodologies have also been developed and explored with 23 papers (16 SCI-cited papers) and one patent, including phase retrieval algorithm of in-line X-ray phase-contrast imaging[1-5], fast X-ray fluorescence micro-CT[6-8], coherent X-ray diffraction imaging[9,10], X-ray spiral micro-CT[11], Multi-energy absorption micro-CT combined with data constrain model for quantitative analysis of materials[12-13], Ring Artifacts Correction algorithm in CT image[14], hardware and software setup for fast and remote CT reconstruction[15], research on the focusing characteristics of Laue bent Crystals[16]and so on. Moreover, the grating-based differential phase-contrast imaging (GDPC) method has been built.

Some application researches have also been carried out, including microscopic identification of Chinese herbal medicine, nondestructive testing of bamboo structure, quantitative evaluation on effect of osteogenesis of new scaffolds for bone repair[17] and so on.

The ongoing projects include the National Basic Research Program of China (973 Program) “The Novel X-ray Medical Imaging Methodology and Key technology based Synchrotron Radiation”, External Cooperation Program of Chinese Academy of Sciences “The International Cooperation Program on the Novel X-ray Medical Imaging Methodology and its Applications at Shanghai Synchrotron Radiation Facility”; the National Natural Science Foundation of China “3D X-ray fluorescence CT based SR” ,“The X-ray phase contrast microscope CT research on structure of traditional Chinese medicine” and “Study of porous scaffolds made by Calcium silicate/corn protein in bone repair” and so on.

In 2012, there are some new projects including the CAS-CSIRO cooperative research project “Automated Quantitative Analysis of 3D Angiogenesis for Early Diagnosis of Tumors using Synchrotron Radiation X-Ray Microtomography”, the National Natural Science Foundation of China “Accelerating X-ray fluorescence CT based fast scanning and OSEM”.

In 2013，besides the beamline operation and user experiments support, design of new beamlines and perform theabove research projects, the group will focus on the following research aspects including fast fluorescence CT, spiral CT, quantitative CT, GDPC, fast CT reconstruction algorithm and further study on methodology and related applications.

Reference

1. Chen R C, Xie H L, Rigon L, *et al.* Opt Lett, 2011, **36**(9):1719-1721
2. Chen R C, Dreossi D, Mancini L, *et al.* J Synchrotron Radiat, 2012, **19**(5): 836-845
3. Ren Y Q, Chen C, Chen R C, *et al.* Opt Express, 2011, **19**(5): 4170-4181
4. Liu H Q, Wang Y D, Ren Y Q, *et al.* ACTA Physica SINICA. 2012, **61**(7): 078701
5. Liu H Q, Ren Y Q, Guo H, *et al.* Chin Opt Lett, 2012, **10**: 121101
6. Deng B A, Yang Q, Xie H L, *et al.* Chinese Phys C, 2011, **35**(4): 402-404
7. Yang Q, Deng B, Lv W W, *et al.* Spectroscopy and Spectral Analysis, 2011, **31**(10): 2753-2757
8. Yang Q, Deng B, Lv W W, *et al.* J Synchrotron Radiat, 2012, **19**: 210-215
9. Zhou G Z, Tong Y J,Chen C, *et al.* ActaPhysicaSinica, 2011, **60**(2): 028701
10. Zhou G Z, Wang Y D, Ren Y Q, *et al.* ActaPhysicaSinica, 2012, **61**(1): 018701
11. Wang Y D, Peng G Y,Tong Y J, *et al.* ActaPhysicaSinica, 2012, **61**(5): 054205
12. Wang Y D, Stevenson A, Yang Y S, *et al.* J Synchrotron Rad, 2012, **19**, 827-830
13. Wang Y D, Yang Y S, Cole I, *et al.* Materials and Corrosion, DOI: 10.1002/maco. 201106341
14. Zhang G Q, Zhou H, He Y, *et al.* ACTA OPTICASINICA. 2012, **32**: 534001
15. Shen F, Chen C C, Xiao T Q. Nuclear Science and Techniques, 2011, **34** (6): 401-405
16. Chen C, Tong Y J, Xie H L, *et al.* ActaPhysicaSinica, 2012, **61** (10): 104102
17. Guo Han, Wei Jie, Song Wenhua, *et al.* International Journal of Nanomedicine, 2012, **7**: 3613-3624

上海光源“梦之线”DEPU 波荡器研制进展

机械工程技术部

上海光源在建 ARPES 和 PEEM 软 X 射线光束线站将采用 1 台覆盖光子能量 20–2000 eV 且极化可变的双 EPU 插入件。由机械工程部和大装置管理部等部门技术骨干组成的“梦之线”DEPU 波荡器项目组承担该插入件的磁铁、机械、控制、真空等研制工作。

该双 EPU 插入件包含低能波荡器 LEID 和高能波荡器 HEID 2 台长度约 5 m、周期长度分别为 148 mm，58 mm 的 APPLE-II 型纯永磁可变椭圆极化波荡器，可分别提供基波光子能量的范围 20–200 eV，200–2000 eV。这条指标、要求都堪称世界顶级的“梦之线”，在波荡器研制上具有结构复杂、运动精度高、总装精度高、整体尺寸大、空间极度受限等特点。“梦之线”DEPU 波荡器项目组在上海光源加速器设备研制技术和条件基础上，在国际上首次创新性地采用了高、低能波荡器并列放置共用一个 H 型机架设计，该机架可横向移动实现高、低能波荡器的切换，2011 年 3 月通过了初步设计国际评审并进行了改进设计。随后紧锣密鼓地开展了各部件加工制造、标准件采购、设备总装、磁场测量和垫补等工作，2012 年底完成了整个设备研制，并成功解决了远距离连接臂滑动梁纵向传动稳定性、磁场测量空间受限等问题，为 2013 年初 DEPU 隧道就位安装做好了充分准备，并且为整个“梦之线”工程节点的可控提供了重要保证。

磁场测量空间受限等问题，为 2013 年初 DEPU 隧道就位安装做好了充分准备，并且为整个“梦之线”工程节点的可控提供了重要保证。

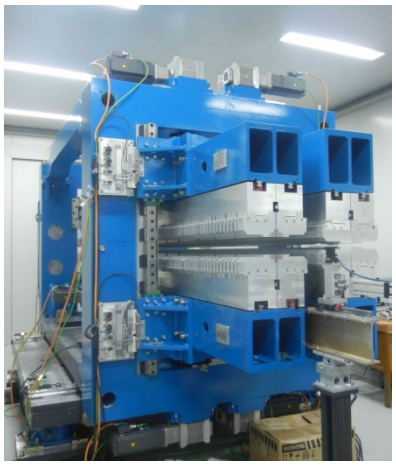

磁测间的 DEPU

Progresses in Development of DEPU for Dreamline at SSRF

Department of Mechanical Engineering

A soft X-ray beamline for ARPES and PEEM is being built at SSRF. The source will be a pair of EPUs covering the energy ranges from 20 eV to 2000 eV of arbitrary polarized light with the first and third harmonics. DEPU Project Group consists of staff from division of mechanical engineering and SSRF administrative department, which takes charge of development of magnet, mechanical system, control system, vacuum, and so on.

DEPU consists of a low energy EPU (LEID) and a high energy EPU (HEID). Period length of LEID is 148mm while that of HEID is 58mm. The two EPUs have the different period lengths but the roughly same magnet array lengths, 5 m, and cover the energy ranges from 20 to 200 eV and from 200 to 2000 eV, individually. The development of DEPU for Dreamline has the characteristics of complex structure, high precision, assembly of high precision, large size and constraint of space. Based on experience of equipment design and development for SSRF accelerator, DEPU Project Group first designs a common support system with H-type in DEPU, with the whole structure seating on a base with linear guides, which enables transverse movement for selecting the working EPU. Conceptual design of DEPU was passed in March, 2011. In the following days, parts manufacture, standard parts procurement, equipment assembly, magnetic field measurement and shimming have been carried out. The development of DEPU was finished by the end of 2012. The shift driving systems for polarization adjustment, which are set on top of the backing beams for the constraint of space, are sophisticated designed to assure position stability under longitudinal magnet force change. The difficulty of magnetic field measurement because of limited space is also solved successfully. The work has prepared enough for tunnel installation and guarantees the whole Dreamline project.

DEPU for Dreamline.

超导波荡器热负载测试装置的研制

机械工程技术部　许皆平　崔 剑　李明　张正臣　季现凯　樊 勇

介绍

与传统插入件相比，超导插入件可显著的提高磁场强度，以进一步提高光子能量和亮度。因此，世界各大同步辐射光源在超导插入件领域纷纷开展研究。束流热负载、低温下的磁场测量、以及磁场相位垫补是超导插入件研制过程中遇到的几大挑战。束流热负载是超导波荡器在低温下的动态热负载，其主要包括镜像电流、来自于上游的同步辐射光，电子云以及 RF 效应等。

为优化超导波荡器磁体设计，美国劳伦斯伯克利国家实验室与我所在超导波荡器领域开展合作，合作建设一台超导波荡器热负载测试装置。超导波荡器热负载测试装置用于测量储存环束流热负载。该国际合作项目由 LBNL 科学家提供最初的设计理念，由所机械部低温组实施建造，并与 2012 年安装在上海光源储存环 C04 单元开始在线实验。图 1 所示是按在隧道 C04 单元内的热负载测试装置。

图 1　C04 单元热负载测试装置

低温系统

超导波荡器热负载测试装置采用无液氦冷却系统，无液氦冷却系统具有结构简单以及维护方便等优点。其低温系统使用 2 台脉冲管式小型液氦制冷机为低温部件进行冷却。一台是日本住友公司的 SPR-082B 冷头，另一台是美国 CRYOMECH 公司的 PT415。脉冲管式小型制冷机比 GM 制冷机的震动小，更加有利于满足束流稳定性的要求。制冷机的二级换热器通过铜编织带冷却束流平板，二级换热器用于冷却 50 K 冷屏。在无束流的情况下，束流平板可以降温到 15 K 以下。

主要结构

超导波荡器热负载测试装置主要包括 2 块平行的束流平板、2 台脉冲管液氦制冷机、1 套 50 K 冷屏、2 套超高真空袖套结构、超高真空真空室以及测控系统。

束流平板采用铝合金材料，长度 1 m，并在其表面上附有无氧铜铜膜。当电子束在两块束流板中间通过时，束流热负载就会沉积在铜膜上并发热。上下束流平板上均安装了 5 个高精度低温传感器，用于实验温度数据的测量。

真空室是绝热真空与束流真空共享同一个超高真空。真空室直径 400 mm，长度为 1.4 m。真空室使用 1 台 400 $L\cdot s^{-1}$ 离子泵和 2 台 400 $L\cdot s^{-1}$ 的 NEG 吸气泵，以满足储存环真空度的要求。采用超高真空袖套结构隔开束流真空和制冷机的绝热真空。该结构的优点是，可在未安装制冷机的情况下，进行超高真空的烘烤调试；并且，该结构方便制冷机例行维护。

首次在线实验

超导波荡器热负载测试装置在 2012 年 9 月开始在线实验。装置的经过 24 h 的降温，一级和二级冷头均达到工作温度。在没有束流的情况下，冷屏的温度可以降到 55 K，束流板的可以降到 1 5 K。在储存环束流 200 mA 和 20 mm gap 情况下，束流板温度升高到 25 K。

总结

超导波荡器热负载测试装置采用两台制冷机可以使得束流板和冷屏达到预期的工作温度。后续实验将会给出在不同束流工况和不同 gap 下的束流热负载数据，以指导超导波荡器磁体和低温系统的设计和建造。

Development of Cryogenic Calorimeter for Investigating the Heat Load of Superconducting Undulators

XU Jieping CUI Jian LI Wei LI Ming ZHANG Zhengchen

Department of Mechanical Engineering

Introduction

Comparing to conventional permanent insertion devices (IDs), superconducting insertion devices can enhance magnetic field strength signally. Therefore, superconducting IDs have been widespread applied in synchrotron light sources to increase the brilliance and photon energy. Beam-based heating, magnet measurement system working with cold magnet, and phase correction, are three key remaining issues to be resolved in the R&D of superconducting undulators. Beam-based heat loads are dynamic heat loads which include image current, synchrotron radiation from upstream bending magnet, E-cloud and RF effects.

To optimize the design of cryogenic system and undulator magnet, LBNL and SSRF collaborate to build a cryogenic calorimeter to quantify beam-based heat load. The scientists of LBNL propose the original concept of cryogenic calorimeter. SSRF is tasked with implementing the cryogenic calorimeter, and first installation and experiments on SR of SSRF.

Cryogenic system

The calorimeter is a cryogen free system which has simplicity and flexibility for the design of cryostat, and has easy maintenance. It uses two sets of Pluse Tube cryocooler which has lower vibration comparing to Gifford-McMahon cryocooler. One model SPR-082B of Sumitomo cold head and one model PT415 of CRYOMECH cold head cool the thermal shield and beam plates. The first stages of two cryocoolers cool the 50 K thermal radiation shield. Two paralleled beam plates are connected to the second stages of those cryocoolers via the measurement blocks. Beam plates should work below 15 K without beam.

Mechanical structures

The calorimeter has been installed in the straight section of storage ring of SSRF. It mainly consists of two beam plates, two UHV sleeves, two Pulse Tube cryocoolers, one 50 K thermal shield and one UHV chamber.

Two paralleled beam plates which is 1 meter length and coated by 80 μm film of copper. When the electron beam goes through them, beam-based heat load will deposit on the copper films.

UHV chamber is 1.4 meter length and 400 mm diameter. Its vacuum system uses one 400 $L \cdot s^{-1}$ ion pump and two 400 $L \cdot s^{-1}$ NEG pumps to meet the requirement of SR. UHV sleeve is a part of vacuum chamber. The goal of using UHV sleeve is to separate the UHV of beam chamber and HV of cryocooler. That means we can bakeout this system without cryocooler. Also it's convenient to maintenance of cryocooler.

First online experiment

Since September of 2012, this calorimeter started to perform online experiment. After 24 hours cooling down, the temperature of 1st stage and 2nd stage reached stable condition. Without beam, thermal shield reached at 55 K, beam plates reached at 15 K and 2nd stage reached at 4.4 K. Temperature rising of beam plates could be as high as 25 K while 200 mA beam with decay pattern and 20 mm gap.

Summary

With two cryocoolers of cooling system, the beam plates and thermal shield of this calorimeter can reach expected temperature. The first online experiment shows that beam-based heat load is higher than we expected. Further measurement and analysis will show the amount of beam-based heat load in following several months. That will help the design of cooling system and undulator magnet.

蛋白设施 Canted 光束线建设

束线工程技术部　机械组　赵 雁　秦宏亮

国家蛋白设施(上海)中心基于上海光源(SSRF)建设了 2 条共直线节的插入件 undulator 光束线，简称 canted 光束线—复合物晶体结构光束线(BL19U1)和生物小角散射光束线(BL19U2)。canted 光束线最大的挑战就在于 2 条光束线距离很近，空间布局非常紧张。为了使 2 条光束线能分开足够的距离，在单色器下游加入了 1 台水平双偏转镜。BL19U1 光束线基本光学设置：液氮冷却双晶单色器位于距光源点 22.5 m 处，水平偏转镜位于 25.75 m，超环面镜位于 33.1 m，样品点位于 40.8 m。BL19U2 光束线基本光学设置：液氮冷却双晶单色器位于距光源点 23.6 m，水平偏转镜位于 28.2 m，水平聚焦镜位于 31.2 m，垂直聚焦镜位于 34 m，样品点位于 56 m。

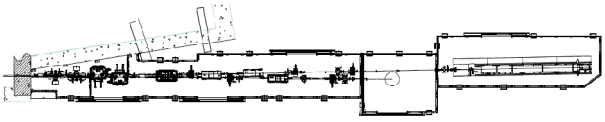

图 1　蛋白设施 canted 光束线总图

BL19U1 和 BL19U2 的单色器布局如图 2 所示，在 BL19U2、BL19U1 的第一晶体处的间距分别为 134 mm 和 143 mm。2 台单色器均使用 Si(111)晶体无色散排列，能量范围 5–18 keV，其光学性能和各技术参数一致。单色器的调节机构参数如表 1 所示。

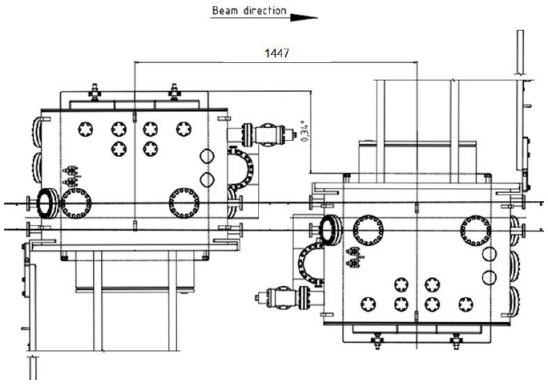

图 2　蛋白设施 canted 光束线单色器布局图

表 2　单色器调节机构主要参数

运动	范围	精度	分辨率
Bragg 角	-5°–40°	0.36”(全步)	<1”
带编码器		0.05”	<0.2”
Roll 1st	±1°	<0.5”	<1”
T2	10–30 mm	<0.5μm	<1 μm
Pitch 2nd	±1°	<1”	<2”
Piezo	100”	<0.05”	<0.2”

双线共用的偏转镜系统要求在超高真空环境中工作。偏转镜系统主要由平面镜、镜子底座、镜体调节机构、镜箱支撑调节机构、真空系统、控制系统等组成。镜体运动调节机构包括投角及 X 方向运动，但是要求滚角安装精度要好于 0.1°。偏转镜镜体调节机构如图 3，调节机构主要参数如表 2 所示。

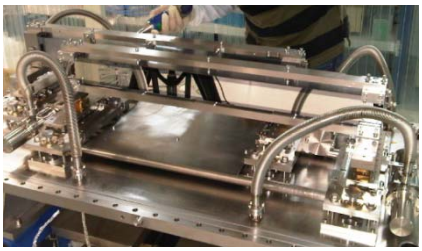

图 3　偏转镜镜体表 2 偏转镜调节机构参数要求

表 2　偏转镜调节机构参数要求

运　动	参数	生物小角散射	复合物
	调节范围	±0.5°	±0.5°
投角	步长	0.2″	0.2″
	重复性	≤±1″	≤±1″
滚角	安装精度	≤± 0.1°	
	调节范围	±5 mm	±5 mm
X 方向	步长	5 μm	2 μm
	重复性	≤±10 μm	≤±10 μm

复合物晶体结构光束线(BL19U1)和生物小角散射光束线(BL19U2)目前已完成调光及指标优化，即将面向用户开放。上海光源二期规划中将建设多条 canted 光束线，蛋白设施 canted 双光束线的建成为二期 canted 光束线的设计、布局、调试等方面积累了丰富的实践。.

Construction of Canted Beamlines for Protein Science at SSRF

ZHAO Yan QIN Hongliang Mechanical Group Department of Beamline Engineering

Two beamlines for protein science have been constructed at Shanghai Synchrotron Radiation Facility (SSRF) which are funded by National Facility for Protein Science. They are named canted beamlines, which are complex crystallographybeamline (BL19U1) and biology X-ray small angel scattering beamline (BL19U2), because they are originating from the same undulator source. The greatest challenge for designing the canted beamlines is setting up optical components at very limited space between two beamlines. To separate sufficient space between two beamlines, two reflecting mirrors which are mounted in one chamber are set up downstream of double crystal monochromator (DCM) respectively. The layout for BL19U1 beamline is, DCM, horizontal reflecting mirror, toroidal mirror and sample point are located 22.5 m, 22.75 m, 33.1 m and 40.8 m from the center of the 2ndundulator source respectively. The layout for BL19U2 beamline is, DCM, horizontal reflecting mirror, horizontal focusing mirror, vertical focusing mirror and sample point are located 23.6 m, 28.2 m, 31.2 m, 34 m and 56 m from the center of the 1stundulator source respectively. This is illustratedin Fig.1.

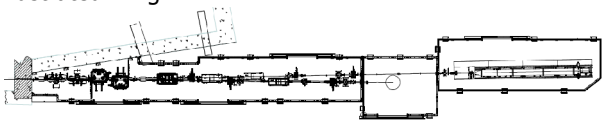

Fig.1 Layout of the canted beamlines.

The layout of two DCMs for canted beamlines are illustrated in Fig.2. The distance between two beams is 134mm at the center of the first crystal of the DCM (left) and 143 mm for the DCM (right) respectively. A pair of Si(111) are adapted for both DCMs which energy range are the same, from 5 keV to 18 keV. Specifications of DCM adjustments are shown in Table 1.

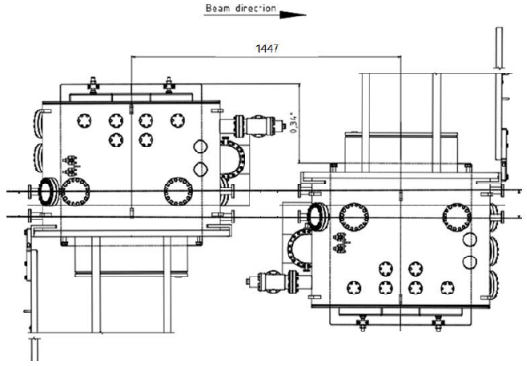

Fig.2 Layout of the two DCMs for canted beamlines.

The Deflection Mirror system shared of two beam-lines works in the ultra high vacuum. Deflection Mirror system consists of plane mirror, mirror set, adjustment mechanism of mirror, support system, vacuum system, control system, etc. Adjustment Mechanism of Mirror contains the motion of pitch and X direction, and the installment accuracy of roll is less than 0.1°.

Table1 Adjustment specifications for DCMs

Adjustment	Range	Accuracy	Resolution
Bragg With encoder	-5°–40°	0.36″(per full step) 0.05″	<1″ <0.2″
Roll 1st	±1°	<0.5″	<1″
T2	10-30mm	<0.5 μm	<1 μm
Pitch 2nd	±1°	<1″	<2″
Piezo	100″	<0.05″	<0.2″

The deflection mirror adjustment mechanism as shown in Fig.3. Parameters of deflection mirror adjustment are specified in Table3.

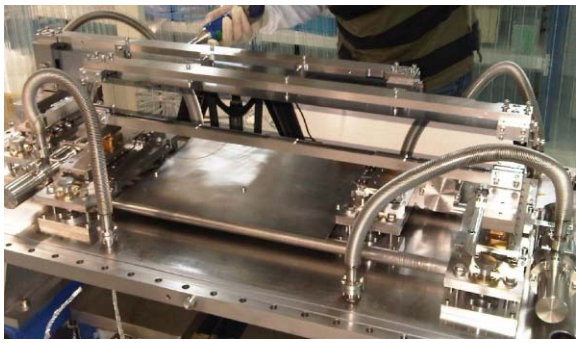

Fig.3 Adjustment Mechanism of Mirrors.

Table3 Parameters of Deflection Mirror Adjustment

Motion	Parameter	BioSAXS	Complex Crystallography
Pitch	Range	±0.5°	±0.5°
	Step	0.2′′	0.2′′
	Repeatability	≤±1″	≤±1″
Roll	Installation Accuracy	≤±0.1°	
Horizontal (X)	Range	±5 mm	±5 mm
	Step	5 μm	2 μm
	Repeatability	≤±10 μm	≤±10 μm

Complex Crystallography beamline (BL19U1) and BioSAXS (BL19U2) has been completed beam tuning and parameter optimization, and it will be opened to users. Multiple canted beamlines will be built in the two phase of SSRF. We have accumulated a wealth experience from the achievement of the canted beamlines for protein science which will contribute to the design and commissioning for canted beamlines during SSRF II.

红外光束线引出镜系统

束线工程技术部　前端真空组　李勇军　张 敏

蛋白质设施红外光束线 BL01B 是上海光源第一条红外光束线，目前已完成光束线站的建设和测试，将于 2014 年正式向用户开放。该光束线采用弯铁边缘引出，引出的红外辐射同时包含边缘辐射和弯铁辐射。

图 1 是红外光束线的布局示意图，其中，引出镜 M1 是最为关键的设备之一，其光束入射角为 45°。它用来分离高能 X 射线和紫外线，使光束中仅存可见光和红外线，并将光束偏转 90°后引出到反射镜 M2。

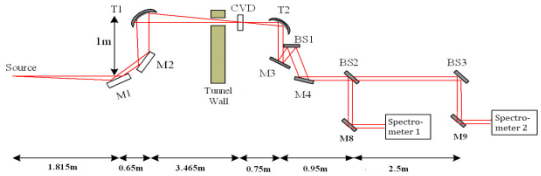

图 1　红外光束线布局示意图

从储存环引出的同步光张角为40 mrad(H) ×20 mrad(V)，到达 M1 的总热功率约为 2904 W，最高功率密度达到了 205 W·mm^{-2}，图 2 是 M1 处同步光的功率密度分布图。为减轻 M1 的热负载，在 M1 镜子中心处开一条宽度为 2.6 mm 的狭缝，此时，超过 99.5%的热功率被释放，而 10 μm 处的通量损失仅为 13.28%。

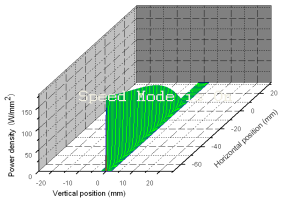

图 2　M1 处同步光的功率密度分布图

M1 镜子面型为平面镜，基底选用 Glidcop，表面镀 Al，镜架和水管材料选用无氧铜，采用底面冷却方式对 M1 进行间接冷却，镜架和水管通过钎焊连接以提高传热效率。图 3 是 M1 的有限元分析结果，可以看出镜子的最高温度仅为 19.3 ℃，最大应力仅为 78.7 Mpa。

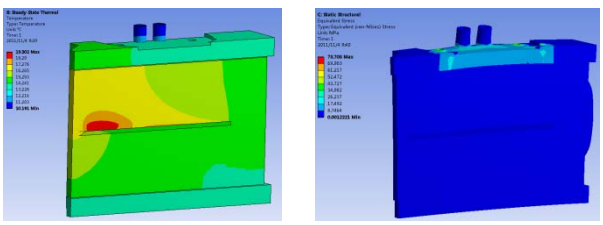

(a)　温度分布云图　　(b)　等效应力分布云图

图 3　M1 有限元分析结果

引出镜系统通过阀门与储存环真空室连接，静态真空度要求≤5×10^{-10} Torr。M1 有三个位置：工作位置、待机位置和维护位置。受空间的限制，M1 在垂直方向的运动行程要求≥435 mm，在工作位置的重复精度要求≤0.01 mm。同时，在镜子狭缝的边缘安装 6 个温度传感器，用于监控镜子的温度变化及热负载状况，通过联锁控制确保设备的安全。

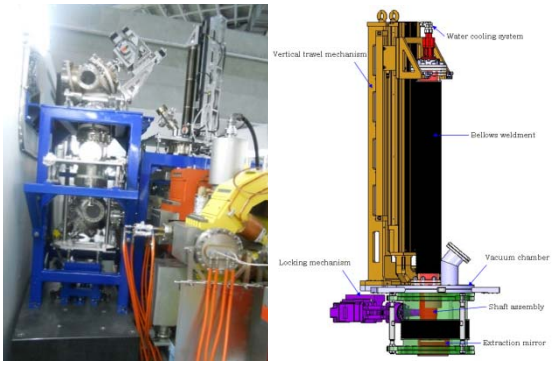

(a)　温度分布云图　　(b)　等效应力分布云图

图 4　引出镜系统

M1 固定在运动长轴上，由步进电机驱动、沿导轨作上下运动。当 M1 处于工作位置时，夹持机构会锁定长轴以增加 M1 的稳定性；当 M1 需要离开工作位置时，夹持机构会自动松开长轴。图 4 为引出镜系统的模型和安装到现场后的照片，表 1 是引出镜系统主要参数的测试结果。

表 1　引出镜系统的测试结果

M1 主要参数	设计指标	实测结果
行程/ mm	≥435	447.7
重复精度/μm	≤10	2.5

表 2 是红外光束线红外时间分辨谱学实验站的设计指标和自测结果。从表 2 可以看出，该光束线的实测结果全部达到或优于设计指标，总体性能位居世界先进行列。

表 2 红外光束线的设计指标和自测结果

测试项目	设计目标	实测结果
光谱范围/cm^{-1}	10–10000	10–10000
光谱分辨率/cm^{-1}	0.1	0.087
最小时间分辨/ns	10	10
谱仪入口处光通量	1×10^{13}	1.3×10^{13}

Extraction Mirror System for SSRF Infrared Beamline

LI Yongjun ZHANG Mi Department of Beamline Engineering

Infrared beamline BL01B for National Facility for Protein Sciences(NFPS) is the first infrared beamline at SSRF. It has been successfully constructed and measured, and will be open to users in 2014. The design of the IR beamline utilizes infrared synchrotron radiation from both bending magnet radiation and edge radiation.

Fig.1 is the layout of Infrared beamline. M1, which is the first mirror called extraction mirror, is one of the key components for the beamline. With an incident angle of 45°, M1 is used to collect infrared radiation, exclude X-rays and UV beam, redirect infrared beam toward M2.

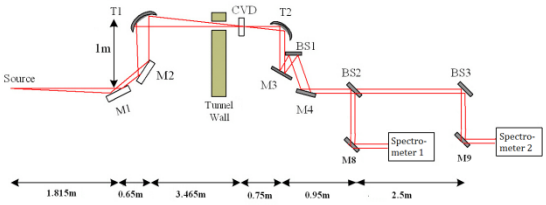

Fig.1 Layout of Infrared beamline.

The divergence angles of incident beam from storage ring are 40mrad in horizontal and 20mrad in vertical. M1 is located at 1815mm from the source, where the total power is about 2904 W and peak power density is 205W/mm2. The power density map is shown in Fig.2. To avoid overheating by the X-ray beam, M1 is designed to have a central slot of 2.6 mm, thus the excluded energy will be more than 99.5% while the flux at 10 μm will decrease only 13.28%.

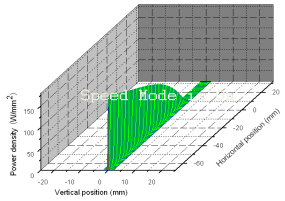

Fig.2 Power density map at M1.

The extraction mirror M1 is indirectly back cooled by water. With a coating of Aluminum, its substrate material is Glidcop. Materials of the mirror support and water pipes are both OFHC, and they are brazed to maintain a higher thermal conductivity. Finite element analysis shows that the highest temperature is less than 19.3℃ and maximum equivalent stress is only 78.7 Mpa.

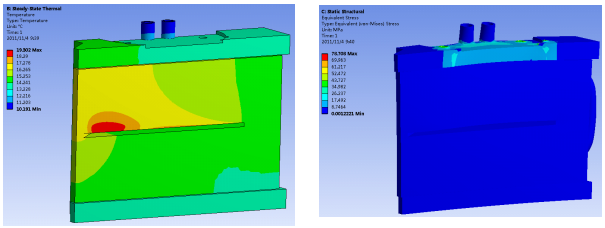

(a) Temperature distributing (b) Equivalent stress

Fig.3 Finite element analysis of M1.

An all-metal CF200 valve is mounted between the chamber of storage ring and M1 system to fully isolate the two parts in the event of maintenance. Therefore, degree of static vacuum for M1 system is required to be better than 5×10^{-10} Torr。M1 has three positions: working position, stand-by position and maintenance position. As strictly constrained by space, M1 need a long vertical travel range of 435 mm, and repeatability of the long travel is required to be better than 0.01 mm. Six thermal sensors close to the edges of the slot of M1 are mounted symmetrically to monitor its temperature to protect M1.

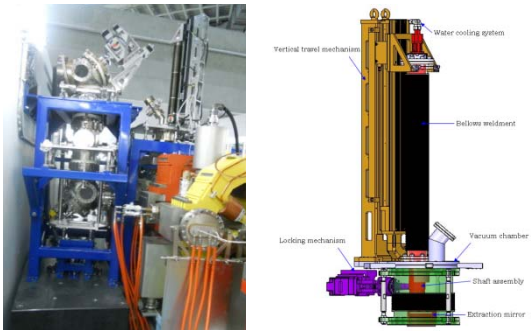

Fig.4 The extraction mirror system.

The vertical travel mechanism is actuated by a stepper motor and an out-vacuum linear encoder is mounted to read the real location of the mirror. When M1 is in the working position, the locking mechanism will lock the shaft to decrease vibrations. Contrarily, the locking mechanism will loose the shaft firstly if M1 need to leave the working position. Fig.4 shows a model and a picture of M1 system. Table 1 is the test results of several main parameters.

Table 1 Test results of extraction mirror system

Main parameters of M1	Requirements	Results
Travel range /mm	≥435	447.7
Repeatability /μm	≤10	2.5

As shown in Table 2, all test results of infrared beamline have met or are better than specifications, which is at the advanced world levels.

Table 2 Test results of Infrared beamline

Items	Specifications	Results
Energy range /cm^{-1}	10–10000	10–10000
Spectral resolution/cm^{-1}	0.1	0.087
Time resolution/ns	10	10
Flux at the sample (phs/sec/0.1% b.w.) at 1 μm @ 300 mA	1×10^{13}	1.3×10^{13}

准直镜的一种优化边冷方案

束线工程技术部　光学组　徐中民　王纳秀

通常在同步光源束线中的第一准直镜要从光源接收较高的热负载，它引起的反射镜表面变形对其性能有不利的影响。采用的评价标准就是反射镜中心的子午面形误差。一般来说，希望它尽可能的小。对于边冷来说，反射镜和冷却块之间接触区域的长度应该小于光斑的长度。通过优化接触区域的长度和宽度，就可以得到面型误差的最小值。

如图 1 所示，硅准直镜和无氧铜冷却块。反射镜的尺寸为 30 mm (X) ×250mm (Y) ×25 mm (Z). 对于 250 eV 的 X 光，它吸收的最大功率和功率密度分别为 85.7 W 和 0.13 W•mm^{-2}。光斑大小为 3 mm (X) ×230 mm (Y)，位于反射镜的中心; 采用水冷，膜系数为 3.0×10^{-3} W/(mm^2·℃)，参考温度为 30°C.

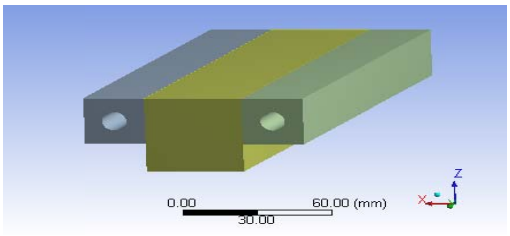

图 1　反射镜和冷却铜块的三维图

为了进行优化设计，接触区域的长度和宽度，DS_LENGTH 和 DS_HEIGHT，作为设计变量。最大面形误差 MaxYSlopeError 作为目标变量. 优化设计采用 AnsysDesignXplorer 模块.经过优化，可以得到响应表面图 (如图 2 所示) . 它对于评价目标函数对于设计变量的变化灵敏度很有用。从图中可以看出，当高度从 2 mm 增加到 10 mm 的过程中 MaxYSlopeError 始终在增加; 而当长度从 180 mm 增加到 250 mm 的过程中最大面形误差存在一个最小值。

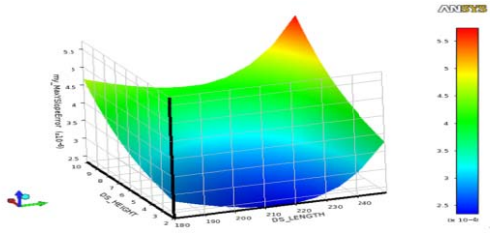

图 2　响应表面图

为了分析接触区域对反射镜面形的影响，选择了 4 种冷却方案进行分析，如表 1 所示。其中方案 A 是一种传统方案—接触区域长度和反射镜相等。而方案 B、C、D 都是接触区域的长度小于光斑的长度。

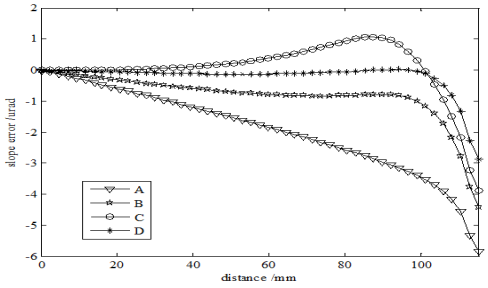

图 3　4 种方案的面形误差曲线

当接触区域的长度大于光斑的长度时，最大的温度位于模型的中心。如果接触区域的长度小于光斑的长度，如 B、C、D，最大的温度向光斑两侧移动，所以这种边冷方案可以从根本上改变反射镜上的温度分布。

4 种方案的面形误差，如图 3 所示。方案 D 是最好的。而且，在光斑 90%的区域面形误差都小于 0.3 μrad，光斑区域的 RMS 值为 0.569 μrad。很明显，由于方案 D 的面形更加均匀，这对于准直是非常有利的。

表 1　4 种方案

方案	高度 /mm	长度 /mm
A	10	250
B	10	205.56
C	9	187.2
D	6	215

参考文献

1. Xu Zhongmin, Wang Naxiu. An optimized side-cooling scheme for a collimationmirror at the SSRF
2. ANSYS Inc. Release 10.0 Documentation for ANSYS Workbench, 2005
3. Khounsary A, Yun W, McNulty I, Cai Z, Lai B. SPIE, 1998, **3447**: 81-91
4. YifeiJaski, MatiMeron, P. James Viccaro. SPIE, 1998, **3447**: 62-71
5. Wah-Keat Lee, Patricia Fernandez, Dennis M. Mills. J Synchrotron Rad, 2000, 7: 12–17
6. Yaming Li, Ali Khounsary, Jorg Maser, Sudhakar Nair. SPIE, 2004, **5193**: 204-210
7. Zhang Lin, Wah-Keat Lee, Michael Wulff, Laurent Eybert. J Synchrotron Rad, 2003 ,**10**: 313–319
8. Artemev A, Artemiev N, Busetto E, Hrdý J, Mrazek D, Plešek I, Savoia A. Nuclear Instrument and Methods in Physics Research A, 2001, 467-468, 380-383

An Optimized Side Cooling Scheme for a Collimation Mirror at the SSRF

XU Zhongmin WANG Naxiu Optical Group Department of Beamline Engineering

Usually, the first collimation mirror in SR beamline will be subjected to high heat load from X-ray source. The mirror surface deformation induced by heat load has bad effect on mirror performance. The criterion employed is the tangential slope error along the centreline of the mirror. Generally, the value is expected to be as small as possible. For side cooling, the length of the contact area between the mirror and cooling blocks should be smaller than the footprint length along the mirror. Then minimum value of slope error can be obtained by optimizing the length and the height of the contact area.

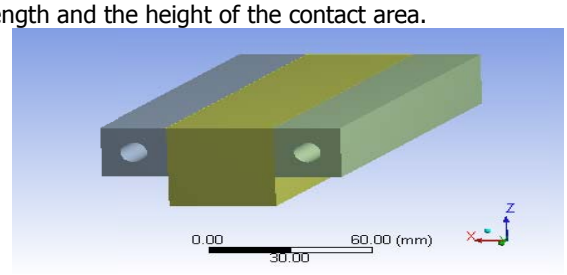

Fig.1 3D illustration of the mirror and copper.

Fig.1 shows the 3D model of collimation mirror made of single crystal silicon and cooling blocks made of OFHC copper. Three dimensions of the mirror are 3 0 mm(X) ×250 mm(Y)×25 mm(Z). The maximum power and power density absorbed by the mirror are 85.7 W and 0.13 W• mm^{-2}, respectively. The centre of the footprint (3 mm(X) ×230 mm(Y)) is coincident with that of reflecting surface on the mirror; The equivalent film coefficient between mirror and cooling block is 3.0×10^{-3} W/ (mm^{2}·°C) and reference temperature is 30 °C.

For optimization design, the length and width of contact area are parameterized and designated as design variables, DS_LENGTH and DS_HEIGHT, respectively. The maximum tangential slope error along the mirror centerline acts as objective function, my_MaxYSlopeError. Then optimization design is performed by AnsysDesignXplorer. After optimization, response surface plot (shown in Fig.2) is obtained. It is helpful to rate how sensitive objective function is based on changes in the design variables. From these plots, it can be seen that MaxYSlopeError is always increasing, when HEIGHT varies from 2 mm to 10 mm; there is a minimum for MaxYSlopeError when LENGTH varies from 180–250 mm.

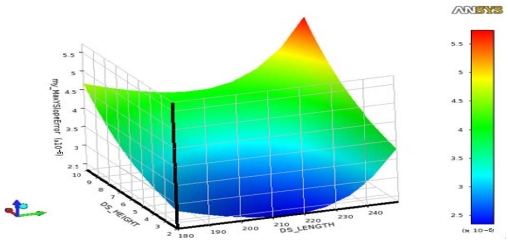

Fig.2 Response surface plot for design variables vs.maximum tangential slope error.

In order to analyze how the size of the contact area affects on slope error of mirror, four kinds of schemes A, B, C and D shown in Table 3 have been chosen, in which scheme A is the traditional scheme, the length of contact area and mirror is equal, while in scheme B, C, D the length of contact area is smaller than that of the footprint.

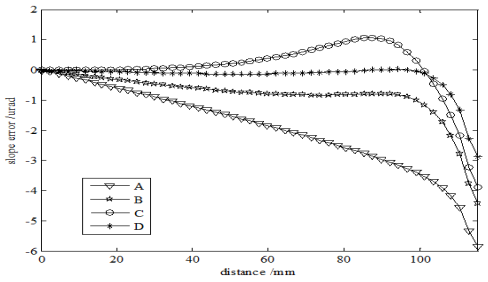

Fig.3 Slope error curves for four Schemes.

When the length of contact area is bigger than that of footprint, maximum temperature is located on the 1/4 model's corner, which is approximately the centre of footprint on full mirror model; if the length of contact area is smaller than that of footprint for scheme B, C and D, maximum temperature points all moved away from the centre of footprint along Y direction similarly. So the sidecooling method can change the temperature distribution on the mirror fundamentally.

Table 1 Four kinds of different cooling schemes

Sheme	Height /mm	Length /mm
A	10	250
B	10	205.56
C	9	187.2
D	6	215

Four slope error curves are plotted in Fig.3. Among the above four schemes, the scheme D is the best one at present. Moreover, slope error value in 90 percent of footprint is smaller than 0.3 μrad and the RMS value for the whole footprint is only 0.569 μrad. It is clearly seen that the slope error is more uniform in the scheme D, which is advantageous for collimation mirror.

Reference

1. Xu Zhongmin, Wang Naxiu. An optimized side-cooling scheme for a collimationmirror at the SSRF
2. ANSYS Inc. Release 10.0 Documentation for ANSYS Workbench, 2005
3. Khounsary A, Yun W, McNulty I Z, Cai Z, Lai B. SPIE, 1998, **3447**: 81-91
4. YifeiJaski, MatiMeron P, James Viccaro. SPIE, 1998, **3447**: 62-71
5. Wah-Keat Lee, Patricia Fernandez, Dennis M. Mills. J Synchrotron Rad, 2000, **7**: 12–17
6. Li Yaming, Ali Khounsary, Jorg Maser, Sudhakar Nair. SPIE 2004, **5193**: 204-210
7. Zhang Lin, Wah-Keat Lee, Michael Wulff, Laurent Eybert . J Synchrotron Rad, 2003, **10**: 313–319
8. Artemev A, Artemiev N, Busetto E, Hrdý J, Mrazek D, Plešek I, Savoia A. Nuclear Instrument and Methods in Physics Research A, 2001, 467-468, 380-383

X 光学测试线

束线工程技术部　光学组　李中亮

X 光学测试线

为解决上海光源二期工程关键设备预研的在线检测，须设计专用于 X 光学检测的光束线。主要研究包括: 光束线设备的检测方法、光学元件的在线检测技术。这些工作为上海光源二期工程中光束线的设备、光学元件的检测提供了技术支持，同时促进同步辐射光束线技术的发展。

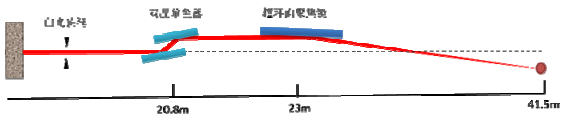

图 1 测试线光路示意图

测试线光路示意图，主要由双晶单色器和超环面镜组成，晶体单色器为 Si(111) 和 Si(311) 2 套切换，满足 4–30 keV 的工作能量范围，超环面镜镀膜为 Pt。

根据光束线建设的科学目标，提供聚焦单色光和直通白光 2 种供光模式(如图 2 所示)，即晶体和超环面镜均可根据实验需求进行调整。

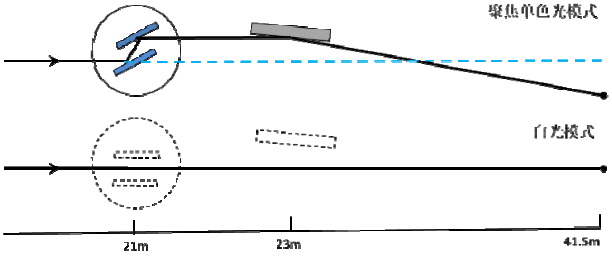

图 2　测试线供光模式

2013 上半年，对需在线检测的光束线设备、光学元件的性能进行了细化，并选择了合理的实验方法及仪器，如表 1 为光束线设备的检测方法及仪器。

表 1 光束线设备检测方法及仪器

设备	检测内容	方法	仪器	光源
晶体单色器	Bragg轴重复性精度 Bragg轴转动精度 出射光束位置稳定性 出射光束指向稳定性 转动时双晶平行度	X射线成像 X射线吸收谱学 XRD	CCD 电离室 五圆衍射仪 分光晶体	白光
	能量分辨率	XRD X射线吸收谱学	五圆衍射仪 硼化镧（Nist标定）	白光
压弯机构	光束位置稳定性 光束指向稳定性	X射线成像	CCD	单色光
白光狭缝	运动重复精度， 运动精度 运动分辨率	X射线成像	CCD 高精度六维样品台	白光 单色光
单色光狭缝	刀口形状，平行度， 单向运动重复精度、 运动分辨率 单向运动定位精度	X射线成像	高精度狭缝 CCD 高精度六维样品台	单色光

2013 年下半年，对光束线的设备的空间位置进行了优化，并进行了直通白光下的辐射防护计算，前端已经进入了工程设计阶段，工程图如图 3 所示：

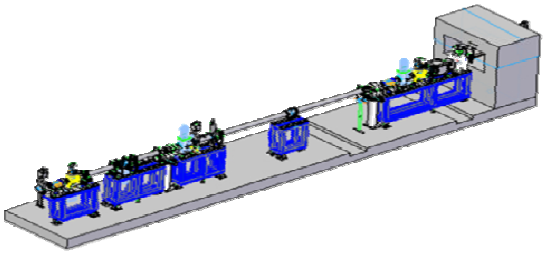

图 3　测试线前端工程图

对测试线的实验方法及检测进行了深入研究，对光束线各设备的性能指标提出具体要求，对特殊要求的部分，如单色器前后的差分系统，进行了计算，并设计出满足 2 种供光模式下的结构。

X-ray Test Beamline

LI Zhongliang Optical Group Department of Beamline Engineering

X-ray test beamline

16 beamlines will be built in the Phase II, most advanced technology will be applied to the beamline equipment. To ensure rapid and successful operation of complex instruments, test facilities to ensure conformance of optics and performance of detector system are essential. To meet the goals, Test beamline is panned.

Test beamline is a flexible and versatile beamline for testing beamline instuments, optical element and detector technology. The beamline provides both white and monochromatic X-rays in two operational modes. The Test beamline works closely with the Optics, Mechanical and Control Group at SSRF, in order to promote the development of beamline technology.

Outline specifications

Photon energy range: 4 keV to30 keV monochromatic focused

White beam: Monochromatic, white beam modes; Beamline acceptance: 2 mrad (h) x0.1 mrad (v); Energy resolution (ΔE/E): 5 x10^{-4}; Monochromator: Water-cooled Si(111) and Si(311)double crystal monochromator; Focusing by a toroidal mirror

A fixed exit double crystal monochromator will be used. The main crystal set will be Si(111) and Si(311) that will cover the 4 keV to 30 keV photon energy range. A toroidal mirror after the DCM will provide focusing in both directions. The mirror substrate would be Si while Pt would be the coating of choice as it does not have any discontinuity in the reflectivity in the 4 keV to30 keV range. The beamline schematic is shown in Fig.1.

The beamline will be operatable in two modes by removing the mirror and crystals. The beamline schematic of the modes is given in Fig.2

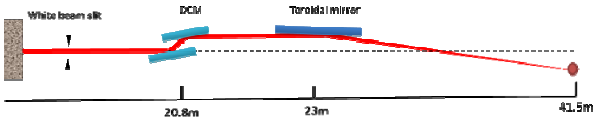

Fig.1 Schematic of the optical layout of the beamline.

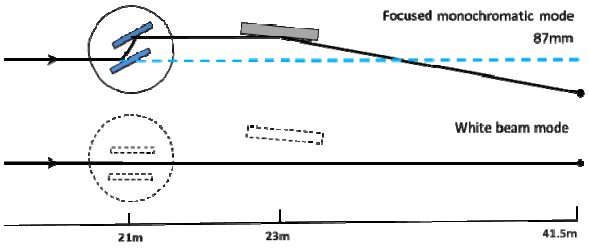

Fig.2 Test beamline schematic of the operational modes.

Diffraction, Imaging, Reflectometry techniques wil be used for the characterization of optics, instrumentation, and development of novel techniques and technologies.
Diffractometer

CCD and Ionization chamber were used for the test experiments. Mechanical design of the beamline front end has been finished, and the drawings is shown in Fig.3.

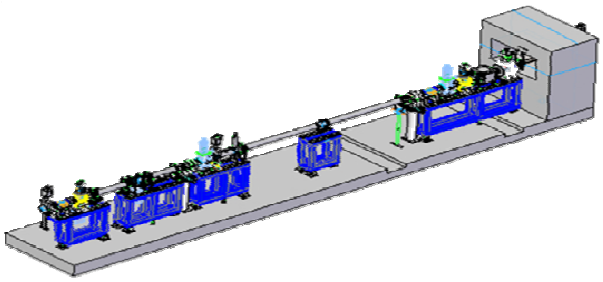

Fig.3 X-ray test beamline Front end.

上海光源的纳弧度精度测量技术研究

束线工程技术部 光学组　何玉梅

为满足第三代同步辐射以及上海光源二期建设中对高质量光学元件纳弧度精度检测的需求，本组研究的纳弧度精度测量技术，通过有效的组合自准直法测量纳弧度角度技术、纳米运动精度的反射镜组合模拟五棱镜技术、纳米级振动控制技术等，实现大尺寸反射镜的纳弧度精度的检测，并研制 1 台实用化的纳弧度检测设备(LTP),实现在 400 mm 范围内，达到 900 nrad 的测量精度目标。研究内容主要包括：高精度角度测量的光学技术的研究；热稳定性对测量精度的影响；机械结构对设备测量精度的影响；相对振动对测量精度的影响；系统集成中各环境因素相互耦合对测量精度的影响。设备的各项功能包括：一维扫描检测，扫描速度、步长可调，一次扫描后得到待测样品的斜率分布与矢高分布。

纳弧度长程面形仪项目由中国科学院重大科研装备研制项目支持，正在按任务计划进行，目前完成系统安装，已进入最后的系统调试及研究测试阶段。

纳弧度长程面形仪

根据纳弧度高精度检测要求，设计方案中考虑采用自准直仪作为高精度测角工具，并使用双反射镜代替传统 LTP 中五角棱镜的扫描光束转折作用，结合高精度气浮导轨、恒温绝热实验环境和高性能隔振系统，通过对各部分的有机耦合，最大限度减小环境因素引起的测量误差，实现对同步辐射用大尺寸光学元件的纳弧度高精度检测。

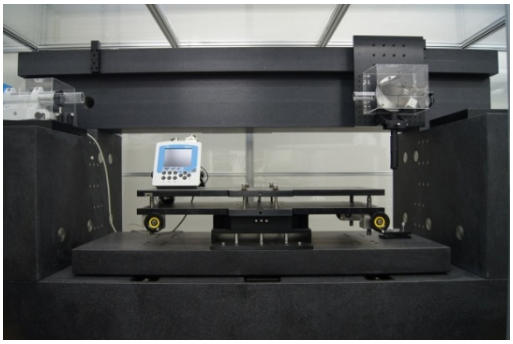

纳弧度长程面形仪

本项目于 2012 年 1 月正式启动，正在按照任务书的计划实施。在完成物理方案设计和系统误差分析的基础上，完成了纳弧度角度检测测试方案的初步设计，全面深入地研究了纳弧度检测中的关键技术、关键问题及相关解决方案；完成主要设备的安装和调试；初步开展了高精度温度控制、空气湍流防护、环境与设备运行导致的振动等因素对纳弧度测量的影响的研究；并与国外的专家就该方面的研究进展进行了深入的技术讨论。

系统结构模态分析

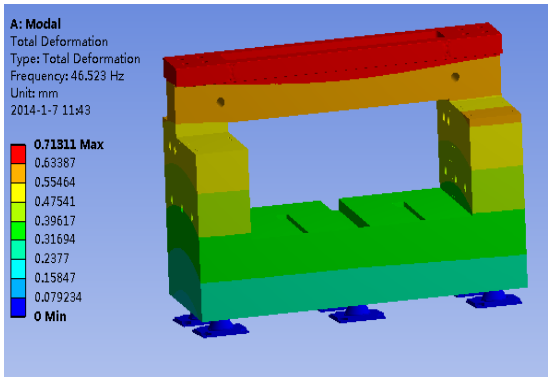

系统结构模态分析

温度稳定性对测量精度稳定性的影响研究

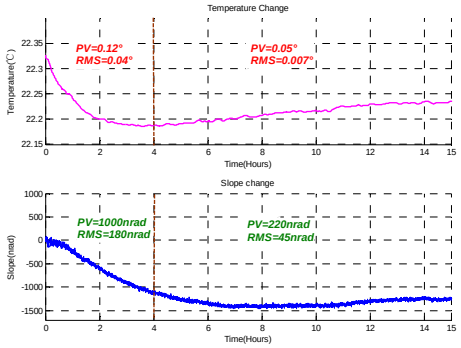

温度稳定性对测量精度稳定性的影响研究

参考文献

1. Assoufid L, Hignette O, Howells M, Irick S, Lammert H, Takacs P. Nucl Instr Meth Phys Res A, 2001, **267**: 467–468
2. Takacs P Z. X-ray optics metrology, in: M. Bass (Ed.), Handbook of Optics, third ed, vol.V, chapter 46, McGraw-Hill, New York, 2009
3. Frank Siewert, Tino Noll, Thomas Schlegel, Thomas Zeschke, HeinerLammert, in: AIP Conference Proceedings 705, American Institute of Physics, Mellville, NY, 2004, 847–850

Development of Nano-LTP Measurement at SSRF

HE Yumei Optical Group Department of Beamline Engineering

Introduction

A high accuracy slope profile measuring instrument, the nano-radian Long trace profiler (Nano-LTP) was recently development at SSRF for the large mirror surface shape testing of grazing incidence optical components in synchrotron radiation. As promotion of the previous LTP, the accuracy of new instrument are possible improved to 100 nrad (rms) in one dimensional surface slope measuring for plane mirrors lengths up to 1 m. We present the feature analyzes of different sources of errors which provide the important reference to the physics and engineering design of the instrument. Appropriate solutions have been investigated to reduce the effect of errors due to optical scanning system, environmental temperature changes, and vibration. System theory, physical analysis and engineering structure design of the Nano-LTP are presented in this paper, experiments are also researched and the results analyzed.

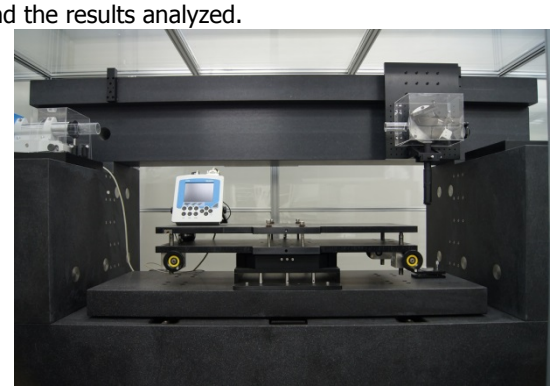

The nano-radian Long trace profiler system.

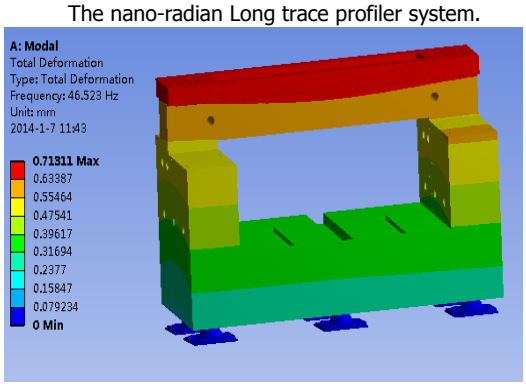

System mode analysis.

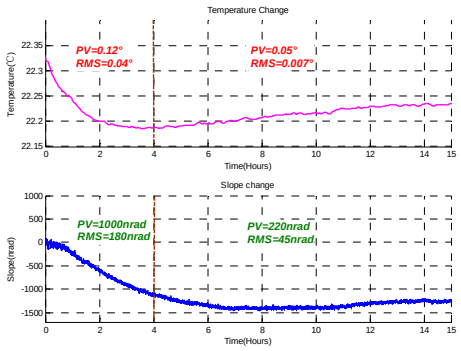

Temperature influence on measurement stability.

In the design, autocollimator is used to instead the light source and detector, which can predigest the light path structure of the measurment system. And dual-reflectors instead traditional scanning pentaprism to avoid the refractive index in homogeneity influence of optical component on Nano-radian measurement. Control the environmental impact from the entire process of measuring, what focuses on the ambient temperature and vibration.

This project is one of the NNSF of China which started in 2012, and everything is going according to plan. Presently, system assembly finished based onthe completion of physical design, engineering design and in key technologies including optical system, scanning system and precise temperature control system. In the next step of the project, by debugging and running working installation, every system can run according to the designing requirement.

References

1. Assoufid L, Hignette O, Howells M, Irick S, Lammert H, Takacs P. Nucl Instr Meth Phys Res A, 2001, **267**: 467–468
2. Takacs P Z. X-ray optics metrology, in: M. Bass (Ed), Handbook of Optics, third ed, vol. V, chapter 46, McGraw-Hill, New York, 2009
3. Frank Siewert, Tino Noll, Thomas Schlegel, Thomas Zeschke, HeinerLammert, in: AIP Conference Proceedings 705, American Institute of Physics, Mellville, NY, 2004, 847–850

利用绝对检测方法检测同步辐射用平面反射镜

束线工程技术部　光学组　宋 丽

同步辐射用光学元件的表面质量和形貌参数将直接影响聚焦或准直后的光束质量及光束线的传输性能。因此，精确测量反射镜的表面轮廓对于同步辐射光束线的整体质量非常重要。在同步辐射光束线上的光学元件通常采用掠入射反射，故镜子的长度达 1 m 多。传统的绝对面形检测方法无法对其进行测量。为解决这一问题，发展了绝对检测方法检测同步辐射用大口径平面反射镜。利用斜入射和 N 次旋转的方法，从而解决小口径面形干涉仪完成大口径同步辐射用平面反射镜的测量。为在 ZYGO 干涉仪上获得干涉图样，引入新的传输镜，测试方法见图 1 所示。

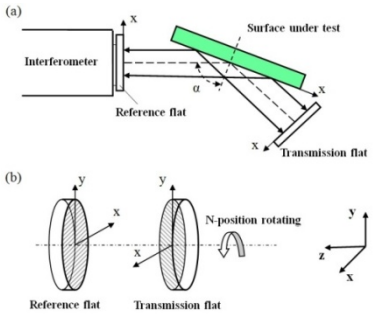

图1　对于大口径反射镜绝对检测示意图: (a)斜入射检测示意图 (b)参考镜与传输镜N次旋转测试

斜入射多次旋转平均测试绝对面形的检测方法的发展，在实验设计上包含 2 步：第 1 步是斜入射检测，从而实现利用小口径干涉面形仪来完成对大口径光学镜面形的检测；第 2 步是多次旋转测量，通过 N 次的旋转平均计算出大尺寸平面光学镜的绝对偏差。干涉仪的上测量的实验数据，经过算法处理，得到了实验数据。测试范围选择为 120 mm×30 mm 的矩形，在 4 个不同的掠入射角的情况下进行多次旋转测试。测试的掠入

射角分别是 38.9º, 61.0º, 72.8º, 81.7º。其测试结果如图 2 所示。

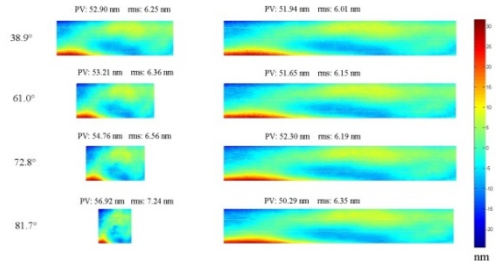

图 2　在斜入射角为 38.9º, 61.0°, 72.8°, 81.7°矩形面的平面度测试结果

为比较斜入射绝对检测的测试结果，利用修正的三平板绝对检测方法[2]对在所选的矩阵范围内进行测试。与修正的三平板测试方法相比较，2 种测试方法的差别小于 0.7 nm RMS。系统不确定度为 0.036 nm RMS，随机不确定度为 2.6 nm RMS。与其它测试大口径平面反射镜方法相比，斜入射绝对检测方的测试方法简单易操作，利用这种方法可以实现对大口径同步加速器光束线光学平面面形绝对测量任务。

参考文献

1. 林维豪, 罗红心, 宋丽等. 同步辐射用光学元件面形绝对检测方法的研究，光学学报 2012, **32**(9):137-143
2. Griesmann U. Three-flat test solutions based on simple mirror symmetry, Appl Optics, 2006, **45**: 5856-5865

Absolute Surface Metrology by Rotational Averaging in Oblique Incidence Interferometry

SONG Li Optical Group Department of Beamline Engineering

Surface figure deviation has been a major consideration in the use of grazing incidence optics in synchrotron beam line instrumentation[1]. Generally, optical surfaces used to reflect x rays at extreme grazing incidence angles have a long tangential dimension with up to 1 meter or more. Owing to the nature of grazing incidence x-ray optics, conventional interferometric techniques for surface figure measurement are not easily employed in the absolute testing. Proposed as an alternative to overcome the aperture limitation, the oblique incidence interferometry combined with multiple rotating measurements at N equally spaced positions is performed to determine absolute flatness of the overall 2D large surface. To obtain the interferometry from the oblique incidence configuration with a Fizeau interferometer, one more transmission flat is required to return back the beam reflected by the long test surface. The method can be illustrated in Fig.1

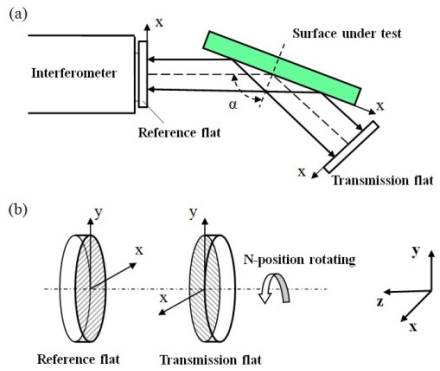

Fig.1 Schematic representation of the absolute flatness testing for long optics. (a) Configuration of oblique incidence measurement in top view. (b) N-position rotating measurements between reference flat and transmission flat in side view.

The method consists of two procedures: The first step was oblique incidence measurement, and the second was multiple rotating measurements. All the experiment data were exported from the Zygo interferometer and processed by our algorithm procedure. we selected 120×30 mm active area of the rectangular plane and carried out the measurements at four different oblique incidence angles with varied rotating numbers. Measurement results of the flatness of the rectangular plane at oblique incidence angle of 38.9°, 61.0°, 72.8°, 81.7° were shown in Fig.2

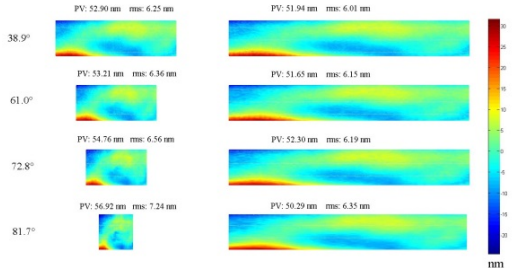

Fig.2 Measurement results of the flatness of the rectangular plane at oblique incidence angle of 38.9°, 61.0°, 72.8°, 81.7°.

To compare the oblique incidence test results, we calibrated the absolute figure of the rectangular plane in active area within the aperture of interferometer, using modified three-flat test approach based on simple mirror symmetry described by Griesmann[2].

From comparison with modified three-flat test results, the difference between two methods is estimated to be better than 0.7 nm rms. The systematic uncertainty is calculated to be 0.036 nm rms while the random uncertainty based on reproducibility is 2.6 nm rms. As compared to other methods of the large surface figure measurement the absolute oblique incidence test is particular simple. This approach could be implemented to facilitate the task of absolute flatness measurement of large synchrotron beam line optics.

References

1. Lin Weihao, Luo Hongxin, Li Song. Absolution Flatness measurement of optical Elements in Synchrotron Radiation, Optical letters, 2012, **32**(9): 137-143
2. Griesmann U. Three-flat test solutions based on simple mirror symmetry, Appl Optics, 2006, **45**: 5856-5865

光束线控制系统

束线工程技术部　郑丽芳

上海光源光束线控制组主要负责控制和监测光束线各光学设备的运行状态，记录和分析各种信息，为实验站用户提供需要的同步光。2011–2012年度，本组完成了光刻分支线等工程建设任务，驱动器国产化研制和其它相关研究工作。

1　束线工程建设

从2011年1月份起，XIL光刻分支线的各个设备陆续到货，工程建设进入设备调试安装阶段。在8月31日前，完成了狭缝、丝扫描、镜箱、快门、金靶、掩膜台等全部设备的在线调试工作。整个分支线于9月17–19日展开第一轮调光就初战告捷，顺利在实验站末端获得单色光。

2011年梦之线和蛋白设施线站工程建设启动，随后进入系统设计、评审及采购工作。2012年8–9月，顺利完成2个项目前端区的控制调试与验收。

在工程实施中，首次使用二相驱动器的ServiceBus功能，配置128细分，驱动狭缝的PI 235.22S滑台，以满足0.1 μm的分辨率。也首次驱动PicoMotor这种类型的电机，为今后的建设工作摸索些经验。

在上海光源一期以及后续光束线站的建设中，控制系统采用EPICS[1](Experimental Physics and Industrial Control System)软件，EPICS是由美国APS光源发展起来的，目前用于全世界多个光源的加速器和光束线控制系统中。

光束线控制系统采用分布式硬件结构，如图1所示。IOC (Input Output Controller)主要有2种：一种是运行在VME系统上的IOC，CPU板采用MVME5500，操作系统采用实时操作系统vxWorks，并采用MAXv8000作为运动控制器，通过SLS驱动器控制电机运动；还有一种是运行在PC主机上的Soft IOC，采用Linux作为操作系统，可以通过串口服务器访问C863运动控制器。

IOC软件采用了EPICS专为光束线开发的synApps[2]软件包中的的motor模块[3]，这是专门用于控制电机的软件模块，包含了motor记录、相应的支持程序以及多种运动控制器驱动程序。同时还采用了calc模块[4]中的transform记录来将多个电机运动转换为设备运动或者将电机运动对应为能量变化。

OPI (Operation Interface)采用了运行Linux的PC主机，主要运行edm显示界面，可以显示电机状态、位置信息等，并且还运行python脚本，执行电机扫描等动作。OPI同时还实时存储电机位置，当IOC重启后可以恢复电机位置。

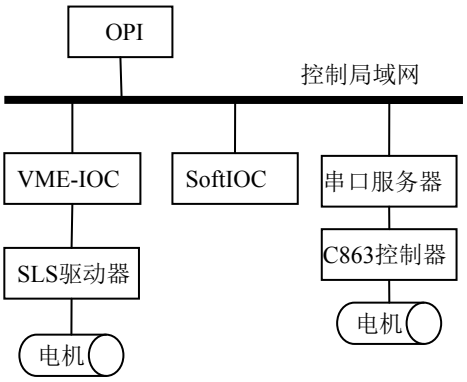

图1　EPICS分布式结构

2　驱动器国产化研究

步进电机驱动器在同步辐射光束线站的控制系统中占有很大数量，针对目前应用的步进电机驱动器存在的不足以及SSRF光束线站的要求，进行了全面的技术改进及整合，最终研制、测试并完成高性能标准化的步进电机驱动器集成系统。在通过完整的性能测试及长时间可靠性评测后，于2011年12月30日通过专家评审，目前自主研制驱动系统已应用在光源线站中。通过驱动器系统的研发，对系统底层硬件技术有了更深的了解，提高了故障的诊断率，并增强了研发能力；能够对市场上快速发展的控制器作出快速反应，进行更优选择，提高工程效率。图2为驱动器及机箱。

图2　驱动器及机箱

3 其它研究

上海光源首期线站的BL14B1和BL16B1的水冷单色器使用的是 Labview 控制软件和厂家配套的驱动控制器，和上海光源统一的 EPICS 运动驱动平台不一致。因此，在2011年4、5月份，在实验室展开技术研究，模拟水冷单色器在 EPICS 平台下的电机控制、温度监测、联动控制等。最后的技术总结，计划用于蛋白设施线站的BL17B1单色器，及改造现有的2台水冷单色器。

虽然目前没有涉及数据采集及探测器控制，但为线站二期着想，也在实验室研究了 SIS 3820 计数器、Hytec 8401/8402 ADC/DAC 变换器、CCD 面探测器等等设备在 EPICS 平台的使用。

时间分辨 X 射线激发发光谱实验(TR-XEOL)，是973计划项目《纳米结构的新型同步辐射表征技术及若干关键科学问题的研究》的子课题之一。同步辐射光源是脉冲光源，脉冲宽度在几十到一百皮秒，相邻脉冲之间的时间间隙为2 ns到1.44 μs可调，再加上其波长是连续可调的，所以同步辐射光源是理想的 TR-XEOL 激发光源。在 SSRF，我们已经完成了 TR-XEOL 相关硬件的设计、选型、采购、光纤布线和测试，包括一套光谱仪系统、一套定时系统和一套 NIM 电子学系统。定时系统利用上海光源加速器主定时系统，在 beamline 大厅，在主定时系统多级结构的基础上，扩展新的一级，作为 beamline 专用，可以为任意一条光束线站提供定时信号。各个子系统的测试已经基本完成，下一步计划在实验室利用激光光源，对整个系统进行集成调试，然后再申请储存环单数团运行模式，在BL08U1实验站实现 TR-XEOL 实验。

参考文献

1. EPICS 官方网站，http://www.aps.anl.gov/epics/
2. synApps 官方网站，http://www.aps.anl.gov/bcda/
3. Tim Mooney, Joe Sullivan, Ron Sluiter, Motor Record and related software, http://www.aps.anl.gov/bcda/
4. Tim Mooney, Transform Record and related software, http://www.aps.anl.gov/bcda/

Beamline Control System

ZHENG Lifang Department of Beamline Engineering

The primarily responsibilities of the Beamline Control Group of SSRF are controling and monitoring the operational status of each beamline's optical equipments, recording and analyzing of every information, providing the proper synchrotron radiation lights which are required by experiment station users. In 2011 and 2012, we have completed the engineering construction of X-Ray Interference Lithography(XIL) branch beamline, the domestic manufactured step motor driver and related research works.

1 Beamline Engineering Construction

From January 2011, the ordered equippments of XIL branch beamline are transferred to the site of SSRF. All the work changed to the equipment debugging and installation. We completed the on-line debugging works of slits, BPMs, mirror chambers, shutters, masks and other devices before August 31.We began the first round commissioning from September 17 to 19. The work was so succeed that we obtained the required monochromatic light form the end of experiment station at that time.

The engineering construction of the Dreamline and the Protein Science Research (Shanghai) Facilities started at 2011.We undertook the work of system design, expert review, manufacture and purchase. We completed the debugging and acceptance of their frontend control systems successfully at August and September 2011.

During the construction, the ServiceBus function of the two-phase step motor driver was adopted first time. In order to satisfy 0.1um resolution of slit, we configured 1/128 step resolution of the driver and applied it to PI 235.22S stage successfully. Also it was the first time to drive the PicoMotor that is a good experience for future construction.

The control system of the beamlines which were set up in SSRF applied EPICS(Experimental Physics and Industrial Control System) [1]. EPICS was created by APS(Advanced Photon Source) in USA, and used in many Synchrontron Radiation Photon Source of the world.

The control system of the beamlines has a distributed structure, as shown in Fig.1:

IOCs (Input Output Controller) have two kinds. Some IOCs run on VME system which use MVME5500 as CPU board and vxWorks as operation system. Vx Works is a realtime operation system. Two or three MAXv8000s slotted into the VME crate are Motion Controllers, and comtrol the motors with SLS motor drivers. The other IOCs named SoftIOC run on the industrial computers, which use Linux as operation system. SoftIOC access the C863 motion controller by serial port server.

Motion control system use motor module in sysApps software package of EPICS which is particularly developed for beamlines. Motor module includes motor record type, support routines and the drivers for many sorts of motion controller. The transform record type in the calc module is also used in the motion control system to change the motor motions to the device motions or to energy plots.

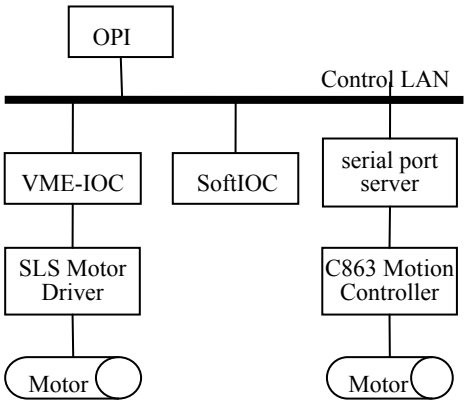

Fig.1 EPICS Structure.

OPIs(Operation Interface) run on the computers using Linux as operation system. EDM displaying interfaces and python scripts both are running on OPI. EDM interfaces display the motor status and positions and support the text input for user. Python scripts carry out some automated controlling tasks. The real time motor positions also are saved on OPI, which will be restored after IOC rebooting.

2 Homemade Motor Driver

A great amount of step motor driver units are used in the beamline control system. The units used in the Phase-Ⅰ project of SSRF don't meet the new needs arose along with the operation of SSRF. Therefore, it is necessary and urgent to improve and integrate the stepper driver techniques so as to develop one high performance and standardized step motor driver integration system. On December 30, 2011, experts are invited to review this integration system after the scheme design, technical and reliability test, and great comments are given on this system. As shown in Fig.2, the homemade motor driver and power rack have been deployed on beamlines at SSRF.

Fig.2 Motor driver and power rack.

Some of the beamline control engineers have learned more deeply about the low level hardware techniques through R&D of the step motor driver system. The ability of R&D as well as handling the motion faults has therefore greatly improved. As a result, control engineers can most efficiatly design and develop the more optimum stepper motion solutions when a new motion controller comes with instrument in our beamline project.

3 Other Research Works

There are two water-cooled monochromators at the BL14B1 and BL16B1 beamline at SSRF. The software of the control system is developed by LabVIEW and the hardware is provided by the manufacturer. It is inconsistent with the EPICS motion control platform which is unified applied at SSRF. We started technical studies at our control lab from April 2011. We simulated the functions of the water-cooled monochromator, including motor control, temperature monitoring, coordinated control, etc. At last, we gave a comprehensive and systematical technique summary which will apply to the monochramator of new beamlineand the two existing monochramators in future.

Although the functions of data acquisition and detector controlling are not referred now, we still set about studying it at our control lab for the further Phase II construction. We studied the application of EPICS platform of SIS 3820 counter, Hytec 8401/8402 ADC/DAC convertor, CCD detector and so on.

TR-XEOL(Time-resolved X-ray excited optical luminescence) is one of the subtasks of the 973 program named 《characterization techniques of nanostructures based on synchrotron and studies on some key scientific problems》. Synchrotron light source produces pulsed X-rays with pulse width of about 100ps and dark time gap of 2 ns to some ms between consecutive pulses. Otherwise, the wavelength of the synchrotron X-ray can be tuned continuously which makes it the most suitable light source to excite the optical samples. We have accomplished designing、model selecting 、purchasing and testing of the hardware including a spectrometer with PMT 、a timing system and a set of NIM-based electronics. We have extended the multi-level SSRF main timing system by adding a new level at the experiment hall which has the capacity to provide timing signals to each beamline. We schedule to integrate and debug all the subsystems in laboratory before the mid of 2014 and to implement the TR-XEOL experiment on beamline BL08U1 at SSRF.

References

1. EPICS 官方网站，http://www.aps.anl.gov/epics/
2. synApps 官方网站，http://www.aps.anl.gov/bcda/
3. Tim Mooney, Joe Sullivan, Ron Sluiter, Motor Record and related software, http://www.aps.anl.gov/bcda/
4. Tim Mooney, Transform Record and related software, http://www.aps.anl.gov/bcda/

蛋白质项目的安全联锁和 XBPM 探测器的工程设计

束线工程技术部　电子学与探测器组

蛋白质项目光束线站的工程设计是这 2 年的主要任务之一，我们课题组承担的任务是安全联锁系统和各种 XBPM 探测器的设计、加工和装调。这是继上海光源一期工程之后，又一次大规模的系统设计和设备安装调试任务。

安全联锁系统的工程设计

蛋白质项目的安全联锁系统包括前端区联锁控制系统、人身安全联锁保护系统、光束线设备保护系统和真空快保护系统。蛋白质项目共有 5 条光束线和 6 个实验站（简称五线六站），1 条弯铁光束线和插入件光束线有和以前同样的设备布局，红外光束线有 2 个实验站，另外 2 条光束线是 Canted 结构；其安全联锁系统的目的是保障光束线站实验运行人员的人身安全和设备安全，在出现紧急情况时，及时关闭光闸或踢除储存环中的束流。

五线六站的 Canted 前端，是 2 个 U20 插入件安装在同一直线节上为 2 条不同的光束线站供光的束线结构，不同于其他 2 条前端（同以前的前端布局，其设计同前），相当于 2 条前端合并在一起，是全新的设计，各个方面都没有经验可借鉴，唯有精心设计、多加讨论交流和听取专家的咨询、集思广益才可设计出满足线站要求的联锁保护控制系统。在 Canted 前端有多个光学设备共用，既要满足各条光束线站的联锁控制逻辑，又要保证 2 条光束线站的实验互不影响、和谐共处，同时，还都要使用操作简便。

Canted 的 2 条光束线共用 1 个光学棚屋，当某条束线需要进入光学棚屋进行设备检修时，必须要考虑到对方的运行情况，不能随意关闭光闸或打开棚屋门。为此，安全联锁系统设置了束线仲裁信号，以实现其联锁要求，当仲裁信号无效时对方可做操作，否则，禁止操作；2 条束线都有自己的束线仲裁信号，束线仲裁信号可以用专门设置的开关按钮来实现，也可以取自各条束线的光闸信号之组合（这是我们根据多方讨论和调研后的选择），即当各自的 PS2 和 SS2 都打开时，则视为束线仲裁信号有效，不管该束线是“用户实验”还是“束线研究”时间，都不能随便开关光闸或棚屋门；PS2 打开且 SS2 关闭时，大多数为用户换样品时间，也应该视为束线仲裁信号有效；PS2 和 SS2 都关闭时，束线不用光，肯定视为束线仲裁信号无效；而 PS2 关闭、SS2 打开时，该束线也没有用光，可视为束线仲裁信号无效。当然，束线仲裁信号还可以将这 2 种信号融合，利用光闸状态的组合和开关按钮来相互弥补对方的不足，进一步保障 2 条束线的和谐共处，但这样会增加操作的复杂性和系统的故障率等。仲裁信号的使用，简化了安全联锁系统的设计，较以前的系统设计，其编程的复杂性增加得不多，又很方便地实现了逻辑功能，在其后的验收测试中，Canted 光束线和其他 2 条光束线的安全联锁功能都达到了物理设计要求。

XBPM 探测器的工程设计

五线六站的 XBPM 探测器包括前端区刀片探测器、荧光靶探测器、丝扫描探测器。前端区刀片探测器是目前各条光束线站输出光斑位置指示的关键设备，自 7 条光束线站建成后，其光斑位置指示的准确性和精度一致备受质疑，究其原因，主要是没有给出有力的测量数据予以证明。为此，先是对各条光束线站前端区刀片探测器的测量数据与其高压电压的关系进行了实验，以求证明高压电压的作用，和其他光源所做的实验结果一致，可以忽略此高压电压的作用；因此，在今后的刀片式探测器设计中，将不再考虑之，以简化其设计。

光束线站输出光斑的位置稳定性问题在于以前记录数据的分析整理不够充分，没有给出各个刀片探测器的位置测量精度范围等参数。因此，在完成 BL17U 前端区刀片探测器的历史记录数据的全面分析和整理，包括对其读出电子学设备的测试后，我们发现其结果比最初的估算要好些，其位置测量精度可以到 5 μm 左右，位置稳定情况一般为 5–10 μm；经过进一步的分析和估算，认为若将其电子学设备加以改进，有望实现 2 μm 的测量精度，若再进一步提高其数据采样率和存储速率，可以消除各线站对其测量结果不真实可信的质疑，同时，还能提供用于光斑稳定反馈控制的输出数据。

在此基础上，设计了能满足五线六站前端光斑测试性能要求的刀片式探测器，改进了刀片探测器的支架热稳定性，选购了国外一家公司专为同步辐

射装置 XBPM 探测器使用的高性能的电子学设备 Libera Photon 仪器，来配套相应的刀片式探测器的读出系统。在最后的束线性能测试中，其光斑位置的读出精度达到了水平方向 2 μm，垂直方向 1 μm，满足其设计要求。

同样地，丝扫描探测器在采用了新研制的 I/V 转换器，加上其结构设计的改进，其测量精度也有了明显的改善，由原来的读数不能准确指示其测量位置，到现在可以将其光斑的中心位置测量精度保证在 100 μm 以内，是一个较大的跨越。这其中的主要改变是丝扫描探测器增加了光栅尺、新型 I/V 转换器具有了自动量程功能和较快的响应时间。所有这些改进都在五线六站的丝扫描探测器的设计中得到应用，在最后的测试中达到了设计要求。

在荧光靶探测器方面，完成了紧凑型单色光荧光靶探测器的升级改造，新研制成功的荧光靶探测器的体积从原来的 300 mm×500 mm×780 mm(长×宽×高)减小到 87 mm×238 mm×383 mm，沿束线方向其长度减少了近 4 倍，且不再需要独立支架，大大缩小了其安放空间；并采用了新型的探测材料 YAG 晶体，其探测灵敏度更高，安装调试更加方便快捷，成功地应用在了五线六站的荧光靶探测器的设计制造中。

参考文献

1. 雷震甲主编. 计算机网络管理，西安交通大学出版社
2. 马明建. 数据采集与处理技术，第 3 版 (下册) 西安交通大学出版社
3. 安毓英，刘继芳，李庆辉. 光电子技术，第 3 版 电子工业出版社

The Design of Safety Interlock System and XBPM for NFPS Engineering

Department of Beamline Engineering Electronics and Detector group

The NFPS (National Facility of Protein Southern project) beamline engineering design is one of the main tasks in two years (from 2011 to 2012), the duty of our research group is to design safety interlock system and various XBPM detectors, include fabrication and assembly. This is, afterwards SSRF phase_I, another large-scale system design and equipment installation tasks.

Safety interlock system brief

Safety interlock system of the protein project includes front end interlocking control system, personal safety interlock protection system, beamline equipment protection system and vacuum fast protection system. There are total five beam lines and six experimental station, one is a bending magnet beamline and is a ID (Insert Device) beamline, which have the same equipment layout with before, the other two is Canted beamline, the fifth is a infrared beamline which there are two end_stations. The Canted and infrared beamline are first design in SSRF. The purpose of safety interlock system is to protect experimental operator and equipment safety, in the event of an emergency, to close the photon shutter or to kick off the electronic beam of the storage ring.

The front end of the Canted beamline is the two U20 ID located in a straight section to feed two different beam lines indevidually. There are some optical equipments to share, not only to meet the interlocking control logic each beamline, but also to ensure the two beamline experiment do not influence each other, live in harmony, however, also must use a simple operation.

The Canted beamline shares one FOE (First Of Enclosure), when a beamline need to enter the FOE for maintenance, they must take into account the operation each other, can not close photon shutter or open the hut door as one pleases. Therefore, safety interlock system set up a beamline arbitration signal, to realize the interlock requirement, when one's arbitration signal is invalid the other can do the operation, otherwise, no operation. There is oneself arbitration signal for each beamline, the arbitration signal can come from a switch button set, can also be taken from each beamline shutter signal combination (this is our selection after more discussion and investigation). When the respective PS2 and SS2 are opened, as the beamline arbitration signal effectively, another beamline can not switch shutter or hut door. If the PS2 is opened and the SS2 is closed, it usually means users is going to change the sample, also the arbitration signal effectively. When the PS2 and SS2 are both closed, no light on the beamline, the arbitration signal of the beamline must be regarded as invalid. While the PS2 closed, the SS2 is opened, nor the beamline with light, the arbitration signal can be regarded as invalid for the beamline. Of course, the beamline arbitration signal can also be the fusion of the combined shutter and button set. It's to make up for each other's deficiencies, to further guarantee the harmonious coexistence of the two beam lines. But it will increase the complexity of the system design and the operation failure rate etc. The use of the arbitration signal, simplifying the design of safety interlock system, and their programming complexity increases not much, in the acceptance test, safety interlock of the Canted beamline and the other 3 beamlines all have been achieving physical design requirements.

Engineering design of XBPM detector

The XBPM detector of the NFPS is the sum of a blade detector, fluorescence screen detector, wire scanning detector. The blade detector located in front end of the beamline is currently one of the key equipment which monitor X-ray beam position, since the 7 beamlines is completed, the accuracy and precision of the light spot position indicating agreement has been questioned, to investigate its reason, mainly is no measurement data are given to prove the strong. To the end, we did some test and data analysis, to reduce the problem. First,we measured the blade detector high voltage which experiments were carried out to prove how its use is, the results is consistent as other sources experimental, can ignore this high voltage; therefore, we will no longer consider high voltage of the blade detector in the future, can be to simplify the design.

In the X-ray beam position stability problem, each beam line previously recorded data analysis is not sufficient, can not give each blade detector position measuring accuracy. Therefore, after a comprehensive analysis of historical data of the BL17U front end blade detector, we found that the results are better than the original estimate, and the position measuring accuracy can be up to 5 microns, position stability is generally 5 to 10 microns. We further think: if the electronics equipment can be improved, it is expected to achieve the measurement accuracy of 2 microns; if the data sampling rate and storage rate can further be improved, the measuring results will not be questioned by anyone, at the same time, can also provide a signal to feedback control in order to insure stability of output of X-ray beam position.

On this basis, we designed a new type blade dector to meet the performance requirements of the x-ray position monitor for each beamline of the NFPS project, and improved the thermal stability of the blade detector bracket, and purchased new readout equipment Libera Photon which is a professional instrument designed for the XBPM detector readout system. In the final test of the beamline performance, measuring accuracy of the X-ray beam position is 2 microns in the horizontal and is 1 micron in vertical.

Similarly, the wire scanning detector adopt a new I/V converter which has the function of automatic range and has faster response time, to improve its structure design, its measurement precision is improved up to 100 microns, it is a larger span. The main change is the wire scanning detector adds the scale ruler and uses new model I/V converter. All of these improvements have been applied in the design of wire scanning detector of the NFPS project.

The fluorescence screen detector, upgrading the compact single color fluorescent detector, the original size 300 mm×500 mm×780 mm (length×width× height) is reduced to 87 mm×238 mm×383 mm, along the beam direction, its length was reduced by almost 4 times, and no longer requires independent bracket, greatly reduced the placing space. YAG crystal is adopt as a new detective material, its sensitivity is higher. The installation and debugging is more convenient; and successfully applied in the design and manufacture of the NFPS project.

References

1. Lei Zhenjia. Computer network management. Xi'an Jiao Tong University Press

红外光束线主动反馈控制系统的设计

束线工程技术部　张永立　蒋建国　龚培荣

2011 年电子学与探测器组承担了红外光束线站主动反馈控制器系统的设计和装调任务。主动反馈控制器是红外光束线站上的关键设备之一。

蛋白质科学设施中的红外光束线是上海光源第一条红外线站。红外光束线的光斑位置稳定直接影响整个光束线的最终性能，光束线从储存环中的发光点到实验站样品台，其振动干扰多而复杂，为了抑制干扰对光斑位置的影响，特在实验站之前的光路中增加主动反馈控制系统，以便尽可能地稳定实验站入射光束，改善其供光品质。该控制系统的核心是主动反馈控制器。

(1) 光路布局　如图 1 所示[1,2]，来自存储环的红外光束，经反射镜 M3、M4（均可通过 PIEZO 的驱动实现其位置的微调）改变光束方向；BS 用来反射红外光束，透射可见光光束，可见光光束用作探测光斑位置，稳定可见光就能稳定红外光，PSD 用作探测光束的光斑位置。M3-PSD1 反馈控制的目的是无论输入光束在反射镜 M3 上的位置如何变化，使得 PSD1 和 M4 上的光斑位置不变；光路设计必须保证 M4、PSD1 到 BS1 的距离相等，以满足 PSD1 上的光斑位置稳定情况和 M4 的完全相同。M4-PSD2 反馈控制的目的是在反射镜 M4 上的入射光斑位置不变的情况下，无论入射光束方向如何变化，PSD2 上的光斑位置不变，以确保经过 BS2 或 BS3 反射到实验站样品点上的光斑位置不变。

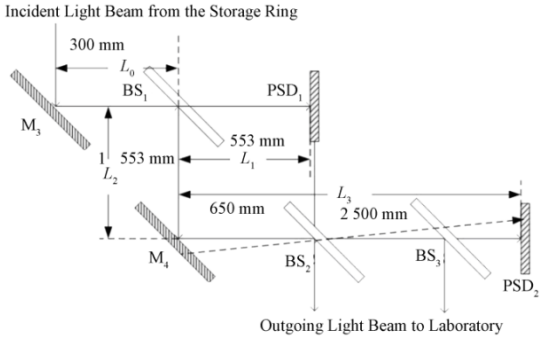

图 1　主动反馈控制器的光路布局图

(2) 实施方案　如图 2 所示，主动反馈控制器由光斑位置探测器(PSD)、执行器(PIEZO)、功率放大器、滤波器、校正补偿器等电路组成；PSD 及其匹配电路板测量、计算 PSD 上的光斑位置，与期望的光斑位置比较后，两者的差值经过滤波器、校正补偿器，再通过功率放大器驱动 PIEZO 执行器，以微调粘贴在其上的平面反射镜(M$_3$ 或 M$_4$)，用于改变入射光束的出射方向，实现其光斑的位置稳定。PSD 的位置及光强测量结果由 5 位 LCD 显示，精确到小数点后三位(可对应 1 μm 的光斑位置变化)，该数据同时可用作功率谱分析。

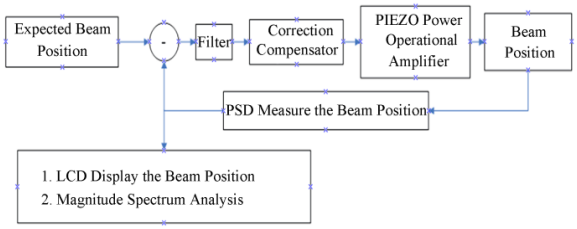

图 2　主动反馈控制器的原理框图

(3) 测试结果　主动反馈控制器在设计完成后先是在实验室进行模拟测试，以寻求不同条件下反馈控制参数的变化情况，并测量其对外加振动干扰的抑制能力，希望在满足幅度裕度 10 dB、相位裕度 45 度的前提下，其控制稳态误差<5 μm，抑制带宽>250 Hz。实验室的测试可概述为，将信号发生器、测量用 PIEZO 及其负载镜片和激光器一起生成特定功率谱的干扰，用来模拟光斑位置抖动，然后通过关闭、开放主动反馈控制器系统定量测量主动反馈对光斑位置抖动的抑制效果。实验室的测量结果显示在满足稳定裕度的前提下，其控制稳态误差<5 μm，抑制带宽>300 Hz，但是在 10 KHz 附近会引入额外的干扰，可能会影响现场光谱仪的测量结果，所以需要根据现场测量情况，进一步优化反馈系统的参数，以降低主动反馈系统本身对光谱仪的测量影响。

参考文献

1. 4-axis implementation of the active feedback mirror system for the IR Beamline 1.4.3.pdf[EB/OL].2000-03. http:// infrared.als.lbl.gov/pubs/Feeback2000 Compendium.PDF
2. Active Feedback Mirror System for the IR Beamline. Pdf [EB/OL]. 1999-09. http://infrared.als.lbl. gov/pubs/ ActiveFeedbackCompendium99.PDF
3. 梅晓榕, 庄显义. 自动控制原理. 北京: 科学出版社, 2007, 139−176

Design of an Active Feedback Controller Used in the Infrared Beam Line of SSRF

ZHANG Yongli JIANG Jianguo GONG Peirong Department of Beamline Engineering

The active feedback controller is one of the key instruments used in the infrared beamline. It is applied in front of the end station to stabilize the incident infrared beam position which mainly disturbed by the external environment due to long optical path from storing ring to end station and all kinds of complicate optical components. The task has been beginning to design by electronics and detector group from 2011, the infrared beamline of National Facility of Protein Southern project (NFPS) is the first infrared beamline of SSRF.

1 Optical path diagram

Fig.1[1,2] shows that the light direction can be altered by the active mirror M3 and M4 driven by PIEZO and the firmed mirror BS1 and BS2 or BS3. The PSD (photo sensitive detector) can receive transmitted part visible light to calculate the beam position. The beam position can be locked on PSD1 by the M3-PSD1 close loop feedback regardless of the incident light position on M3, similarly the beam position can be locked on PSD2 by the M4-PSD2 close loop feedback regardless of the incident light direction on M4. And the special optical design is that the distance from M4 to BS1 must be equal to the distance from PSD1 to BS1, as in order to guarantee the beam position steadiness on the M4 as the PSD1. So regardless of the incident light position and direction how can do, the beam position stability outgoing from the active feedback controller can be guaranteed, unless the beam vibration exceeds the controller system regulated range.

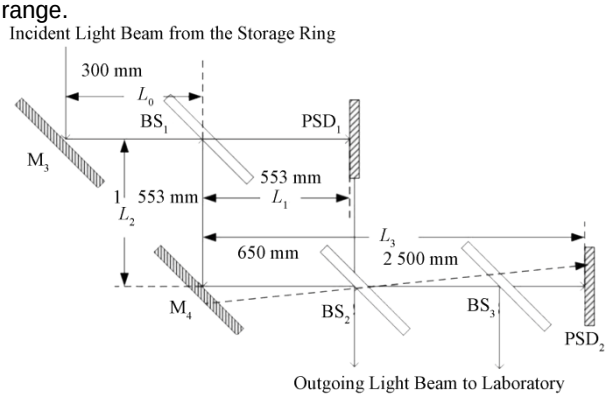

Fig.1 Light-path layout diagram of active feedback controller system.

2 Scheme implemented

Fig.2 shows that the controller system consists of PSD, PIEZO actuator, power amplifier, filter, compensator and other circuit blocks. The PSD and its additional circuit calculate the beam position, the power amplifier drives the PIEZO and its load mirror to change the output light direction, so the close loop feedback can be formed due to controller. The beam position measured by PSD display in LCD, and can be used to indicate the steady error with the maxim 5um position resolution for the controller, and can be used to analyze its power spectrum.

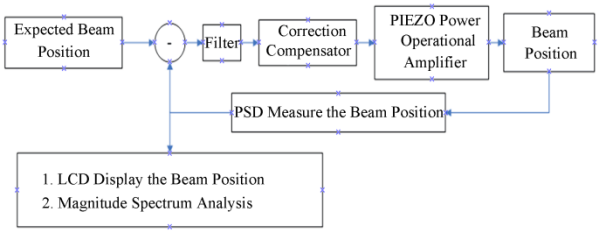

Fig.2 schematic diagram of active feedback controller.

3 Test result

The completed active feedback controller firstly executes the simulation test in electronics laboratory, in order to adjust the controller characteristics parameter under the different operating environment and to test the controller performance with guaranteeing that the controller's minimum effective band is 250 Hz and the maximum steady state error is 5 um within the precondition of 10dB amplitude margin and 45 degrees phase margin. The simulation test was as below. The tested PIEZO and its load mirror is together driven by the power spectrum signal source which is inserted into the light path of the active feedback controller system. Using He-Ne laser as test light source, so the light position signal power spectrum can be given by PSD1 or PSD2. And result of the signal power spectrum will be not difference as the PIEZO driver signal source, when the controller is in open-loop state, if the light position signal power spectrum given by PSD1 or PSD2 is significantly reduced amplitude when the controller is in close-loop state, the controller performance will be verified is good. As expected, the controller performs that the minimum effective band is 300 Hz and the maximum steady state error is 5 um within the precondition of 10 dB amplitude margin and 45 degrees phase margin. But the test result also shows the controller in close loop state will lead to some additional small spectrum peaks in 10 kHz, it's possible to due to PIEZO's resonant frequency affects measurement result of the FTIR spectrometer of the end station. It is necessary to optimize the controller characteristics parameter pass through the ample field test in the future.

References

1. Active Feedback Mirror System for the IR Beamline.pdf [EB/OL]. 1999-09. http://infrared.als.lbl. gov/pubs/ ActiveFeedbackCompendium99.PDF

上海光源实验大厅液氮循环系统线站末端预冷装置

束线工程技术部 工艺组　朱卫华　苏 东　杨建萍　杨 东　黄振国　乌振亮

上海光源实验大厅液氮输送系统的研制水平已接近于国外同类光源液氮输送系统的技术水平，在国内光源装置中还没有先例。实验大厅液氮输送系统在线站液氮支线施工设计时，考虑到插入件线站液氮支线要与进口的液氮循环机组相连，并且，传输管路较长。为液氮循环机组随时补充液氮，但补液时间较长、且时间长短具有不确定性。因此，为解决这些问题，在插入件线站液氮支线的末端分别增加了预冷装置，预冷装置是一种能缩短低温液氮传输时间的技术和设备。通过该预冷装置能做到缩短低温液氮传输时间。这样满足了液氮循环机组及时补液的时间和稳定性的要求。预冷装置由温度控制箱、温度传感器、低温电磁阀、蒸发器、真空液氮传输管道和不锈钢回气管道组成。该装置建成以后，经过一段时间的试运行，2011 年通过验收。由于末端预冷装置是上海光源的首创，我们申请了专利，并取得成功。

上海光源实验大厅液氮输送系统在插入件线站液氮支线的末端增加的预冷装置，充分满足了液氮循环机组及时补液的时间要求。实践证明这一方案效果很好，具有先进性。

线站末端控制预冷装置

The Pre-Cooling Device of the End of the Beamline in the Experimental Hall at the SSRF

ZHU Weihua SU Dong YANG Jianpin YANG Dong HUANG Zhenguo WU Zhengliang
Process Group Department of Beamline Engineering

The development level of the liquid nitrogen source delivery system in the hall at SSRF is close to the level of similar sources of liquid nitrogen technology delivery system in the foreign country, which has no precedent in the light source device in our country. The branch line of the liquid nitrogen of the insert line station should be connected to liquid nitrogen cycle unit, what's more, the transmission lines are lone. It can supply liquid nitrogen for the liquid nitrogen cycle unit anytime, but the time is too long and uncertainly. Therefore, to solve these problems, the pre-cooling device is added to the end of the bench of insert line station, which is a kind of device to shorten the time of transmission of the liquid nitrogen. The pre-cooling device can be done by shortening transmission time of the low temperature liquid nitrogen, which meet the requirements of time and stability for the liquid nitrogen cycle units. The pre-cooling device consists of a temperature control box, temperature sensors, low temperature solenoid valves, evaporators, vacuum liquid nitrogen transfer pipelines and stainless steel gas pipelines。After the device is complished, it has passed the acceptance since a period of trial operation。Since the pre-cooling device of the end of the beamline is our first, we have applied for a patent, and success. The pre-cooling device of the end of the insert beamline is added to the holl of SSRF, which meet the requirements of time and stability for the liquid nitrogen cycle units, which has been proved well and advanced.

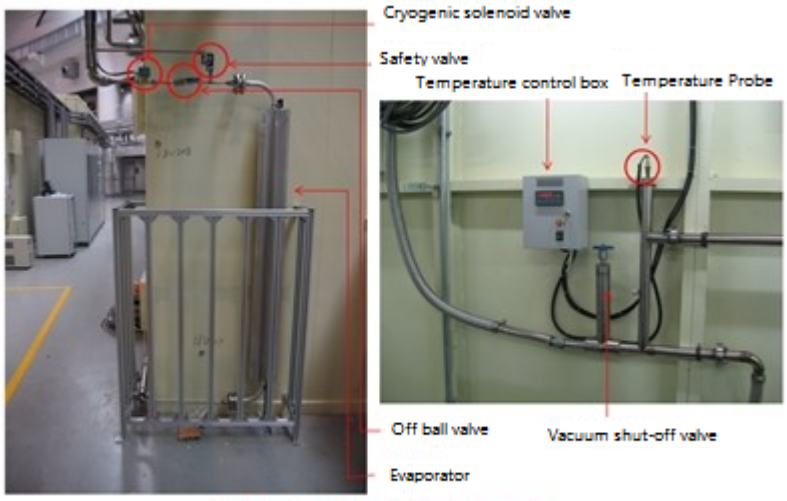

The pre-cooling device controler of the end of beamline

5.0 MeV/120 kW 高频高压型电子加速器研制

应用加速器研究室　李德明　张宇田

中国科学院上海应用物理研究所应用加速器研究室科研人员在长期探索和技术积累的基础上，于 2011 年 9 月研制成功我国首台 5.0 MeV/120 kW 电子辐照加速器，并在珠海瑞欧科技有限公司投入生产试运行。

5.0 MeV/120 kW 工业电子辐照加速器经现场测试，其性能指标达到：空载能量 5.5 MeV，最大束流 24 mA，能量和束流不稳定度小于±3%，扫描不均匀度小于±10%，运行真空度好于 5×10^{-5} Pa。各项技术指标均达到或超过设计指标，符合国家标准“辐射加工用电子加速器工程通用规范”(GB/T25306-2010)规定。该加速器在 5.0 MeV/24 mA 和 5.0 MeV/20 mA 两个束流工况下均按照国标规定通过了连续运行检验。

5 MeV 高频高压电子加速器

5.0 MeV/120 kW 工业电子辐照加速器的研制是产学研结合的成功典范。充分发挥我所在应用加速器研究方面的优势和企业的资金优势，经过科研技术人员充分评估并做了大量研究预案的情况下，于 2009 年同珠海锐欧科技有限公司签署合作研制协议并付诸实施。

5.0 MeV/120 kW 电子辐照加速器的研制成功是我所应用研究的又一项重大科技进展，为此中国同位素与辐射行业协会辐射加工专业委员会发来贺信表示热烈祝贺，这台我国自主研发的首台交付用户生产运行的高能大功率辐照装置，标志着我国工业辐照电子加速器技术又向前迈进了一大步。

该 5.0 MeV/120 kW 电子辐照加速器的研制成功并投入生产应用，对于提高我所工业应用电子加速器的制造水平，扩大社会影响，提高市场竞争力，培养专业人才等都具有重要的意义。对于我国开发高端热缩材料和功能高分子材料制品，实现食品及农副产品的保鲜，医疗卫生用品的消毒等应用打下了坚实的基础，必将为我国辐射加工产业的迅速发展起到积极的推动作用。

5 MeV 电子加速器加工产品

Development of 5.0 MeV/120 kW High-voltage and High-frequency Electron Accelerator

ZHNAG Yutian　Department of Applied Accelerator

The China's first 5.0 MeV/120 kW electron accelerator has been developed successfully in September 2011, and put into production in Zhuhai Ruiou Science & Technology Co. Ltd. The development is base on the massive researches and abundant experience accumulating by the researchers belong to the department of applied accelerator in Shanghai Institute of Applied Physics, Chinese Academy of Sciences.

The 5.0 MeV/120 kW electron accelerator has reached performances that the noload-energy is 5.5 MeV, the maximum beam current is 24 mA, the instability values of energy and beam current are better than ±3%, the nonuniformity value of scan is better than ±10%, the vacuum while accelerator working is better than 5×10^{-5} Pa. All technical specifications meet or even exceed the design requirements, and conform the national standard named "Standard of electron accelerator facility engineering for radiation processing" (GB/T25306-2010). The accelerator has passed the continuous running test of national quality evaluation under the working conditions of 5.0 MeV/24 mA and 5.0 MeV/20 mA.

The 5 MeV high-voltageand high-frequencyelectron accelerator.

It is a successful university-industry cooperation to develop this accelerator. It has taken full advantage of the scientific research of applied accelerator from the research institute and the abundant capital from the enterprise. The cooperative development agreement is signed with Zhuhai Ruiou Scie. & tech. Co. Ltd. in 2009 after fully evaluate and finished abundant of research plan, and then put into action.

The processed product of 5 MeV electron accelerator.

It is also a great progress in the field of applied accelerator research that the 5 MeV/120 kW electron accelerator is successfully developed. Hence, Radiation Processing Professional Committee of China Isotope & Radiation Association sent a letter for congratulations. This one ,which is high-energy accelerator for irradiation processing, is the first self-developed equipment delivered to users for production in China. It marks a big step forward in the technology of industrial electron accelerator for our country.

The successful development and application in production of the accelerator have the important significance to strengthen the level of applied accelerator manufacturing, to expand the social influence, to improve the market competitiveness and to cultivate professional talents. It also lays solid foundation for the development of high-end product of heat shrinkable materials and functional polymer materials, for the preservation of food and agricultural and sideline products and for the sterilization of medical and health products. It will certainly play a positive role to the rapid development of radiation processing industry in the nation.

钍基熔盐堆
核能系统
Thorium Molten Salt Reactor System (TMSR)

钍基熔盐堆核能系统物理设计和分析

反应堆物理部　邹 杨　王纳秀　陈金根　郭 威　王建强　严 睿　傅 瑶
陈玉爽　张金红　胡继峰　王小鹤　沈佳杰　关成志　余笑寒　蔡翔舟

熔盐堆包括固态熔盐堆和液态熔盐堆两类，是国际代堆论坛建议的 6 个候选堆型之一，适合于钍资源利用和高温制氢应用，发展钍基熔盐堆核能系统是解决我国能源和环境问题的一个可能途径。

我们围绕钍基熔盐实验堆的建设，发展相关的研究方法，开展了固态燃料熔盐堆的物理热工设计、钍铀循环物理分析、复合能源系统设计和核能高温制氢等研究。

1　堆芯物理设计分析

本组完成了 2 种不同球床排布的 2 MW 固态燃料熔盐堆堆芯物理设计，其中流动球床堆型在 2012 年 7 月进行了国际评审，规则球床堆型在美国麻省理工大学召开的 IPR 第 4 次研讨会上获得了国际同行的一致认可。2 MW 固态燃料熔盐堆的堆芯物理概念设计工作主要包括，堆芯设计前期方案总体考虑与选型、初步定型后堆芯功能布局设计、静态设计与分析、燃耗分析、衰变热分析、瞬态分析、调试运行实验方案等内容。通过设计分析工作的深入开展，已在上述领域形成了整套计算分析设计的能力，并在相关关键科学问题上进行了较为深入和广泛的研究。

1.1　MW 固态燃料熔盐堆(流动球床)堆芯物理设计

2 MW 流动球床堆的堆芯布局如图 1 所示[1]，整个堆芯(石墨反射层外围) 直径为 330 cm，高为 470 cm。堆芯活性区是由一个直径为 130 cm，高度为 280 cm 和一个锥角为 90° 的圆锥构成，圆锥的上部连接着一个直径为 50 cm，高度为 100 cm 的圆柱形卸料管，活性区内采用燃料球环绕石墨球的燃料排布方式。紧靠堆芯的石墨侧反射层中均匀分布 10 个控制棒和 3 个样品孔道以及 7 个硼球孔道，孔道中心的径向距离为 81.5 cm。其总体物理参数设计为：热功率为 2 MW，堆芯出入口温度为 620 ℃ 和 600 ℃，堆芯平均功率密度为 1.13 $MW\cdot m^{-3}$，冷却剂质量流速为 41.3 $kg\cdot s^{-1}$，堆芯平均冷却剂流速为 0.043 $m\cdot s^{-1}$(球与熔盐混合区，熔盐占空比为 40%)。堆芯中总的 U 燃料球为 10600 个，石墨球为 600 个，堆芯中 ^{235}U 总装量为 10.9 kg。堆中子物理主要参数为：反应堆基准设计情况下(热态，冷却剂平均温度 610 ℃)，堆芯剩余反应性为 0.050，堆芯温度反应性系数为−9.08 $pcm\cdot K^{-1}$。堆芯包含一套反应性控制系统(10 个控制棒)，两套独立的停堆系统(10 根控制棒和 7 个硼球系统)。

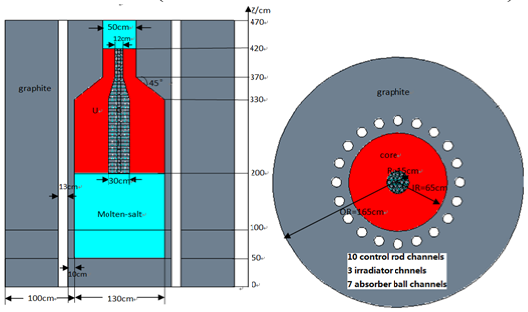

图 1　2 MW 球床钍基熔盐实验堆 PB-FHR 轴向与径向剖面图

1.2　2 MW 固态燃料熔盐堆(规则球床)堆芯物理设计

在 2 MW 固态燃料熔盐堆(规则球床)的堆芯物理设计中，核设计部分做出较大改动[2]。针对中子有效增殖因子、临界质量、堆芯内中子分布、功率分布等物理性能开展堆芯物理设计优化，形成堆芯初步方案。在此设计基础上，开展了运行瞬态分析与事故瞬态分析，给出在反应性引入、失流情况等各种条件下随时间变化的反应性分析、功率分析、温度分析等参数并反馈给堆中子物理静态设计和安全设计。为反应堆安全分析提供堆中子物理事故瞬态分析的依据与各种参数，为反应堆运行、调试与控制提供稳定性分析结果。

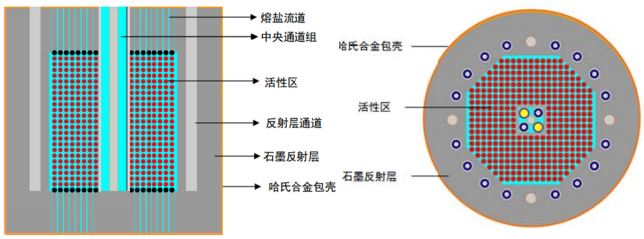

图 2　2 MW 球床钍基熔盐实验堆 TMSR(SF)轴向与径向剖面图

2 MW 规则球床堆的堆芯布局如图 2 所示，堆芯活性区由石墨构件围成，采用八棱柱形规则排列 16924 个直径为 6.0 cm 的燃料球。^{235}U 总装量为

20.2 kg。活性区高度为 168.8 cm，八边形的对边距离分别为 153.0 cm 和 154.5 cm，活性区体积为 3.1 m^3。堆芯活性区中央设石墨柱，其内包含供辐照实验、控制棒、硼吸收球使用的 5 个通道。总体物理参数为：热功率为 2 MW，堆芯出入口温度分别为 620 ℃和 600 ℃，堆芯功率密度为 0.65 MW·m^{-3}，冷却剂质量流速为 41.3 kg·s^{-1}，旁路的冷却剂比例为 0.2，堆芯平均冷却剂流速为 0.031 m·s^{-1}。主要堆中子物理参数为：反应堆基准设计情况下堆芯冷态剩余反应性为 9479 pcm，温度反应性系数为 -7.02 pcm·K^{-1}，最大中子通量密度为 2.31×10^{13} n/cm^2/s。堆芯包含一套反应性控制系统(外圈 12 根控制棒)，两套独立的停堆系统(内圈 2 根控制棒和内圈 2 套硼球系统)。

2 堆热工水力设计分析

本组主要开展钍基熔盐实验堆热工水力概念设计和热安全相关实验及其台架研制两方面的工作。

实验堆热工水力概念设计方面分别完成了液态堆和固态堆 2 种堆型的第一版设计报告[2,3]，其中 2 MW 固态燃料熔盐堆(规则球床)的设计在 2012 年 7 月经过了国际专家评审。

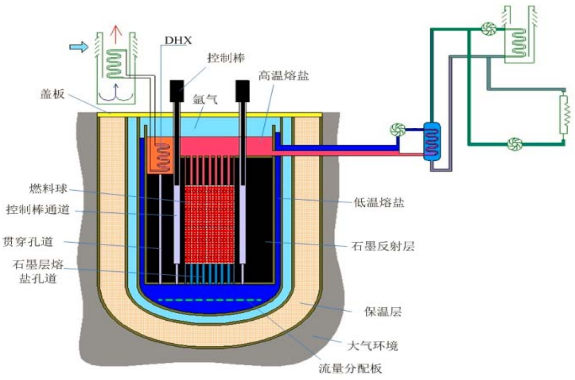

图 3 固态堆堆本体方案

热工水力实验方面完成了堆芯水力实验台架[4]和管内换热系数测量实验方案[5]评审，开展研制并获得硝酸盐圆管内对流换热系数初步测量结果。

堆芯水力实验台架主要配备先进的粒子图像速度场仪(PIV)和超声多普勒流速仪(UDV)、流量计和压力计等仪表，采用模化分析方法设计实验方案，具有开展堆芯水力特性实验研究的能力，包括堆芯入口流量分配、堆芯活性区和上下腔室流场、堆芯旁流或漏流等局部流场分布、堆芯压力损失和整体水力模拟实验。测量参数流量：0–270 m^3·h^{-1}(水)；速度测量维数：一维到三维。

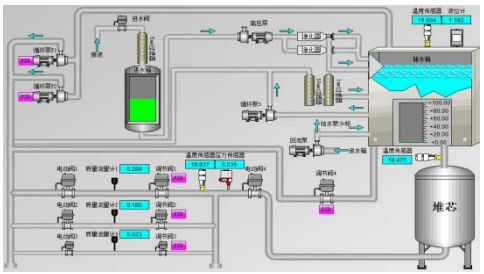

图 4 堆芯实验台架

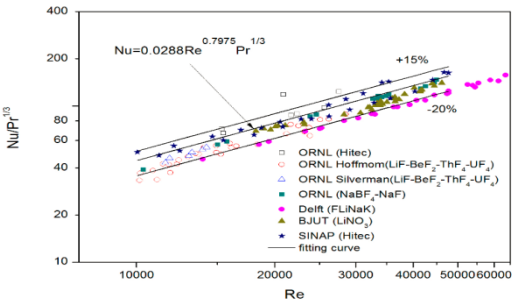

图 5 硝酸盐单根圆管的对流换热关系式

3 钍基核数据和钍铀循环物理分析

本组主要围绕钍铀核数据测量、评价和加工以及钍铀循环物理分析展开研究。钍铀核数据是钍基熔盐堆物理设计的数据基础，主要包括钍铀核数据的测量、评价和截面加工；钍铀循环物理分析是针对钍基熔盐堆(TMSR)的主要堆型开展，包括固态熔盐球床堆(TMSR-SF)、液态熔盐热堆(TMSR-LF)和液态熔盐快堆(TMSFR-LF)。

3.1 钍铀核数据评价

钍铀核数据评价涵盖了全套中子核数据评价、宏观检验、裂变模型研究和钍铀工作数据库研制，为钍基熔盐堆物理设计提供所需核数据库及其评价和检验。完成了钍铀核数据需求分析、钍铀核数据评价框架分析、全套中子核数据评价流程建设，搭建了核数据评价平台。利用该平台，完成了 ^{232}Th、^{233}U 和 ^{155}Gd(包含协方差数据)的全套中子核数据评价。宏观检验的结果显示(见图 6)，重新评价后的 ^{232}Th 数据在快谱区域要好于美国的 ENDF/B-7.0 数据[6]。

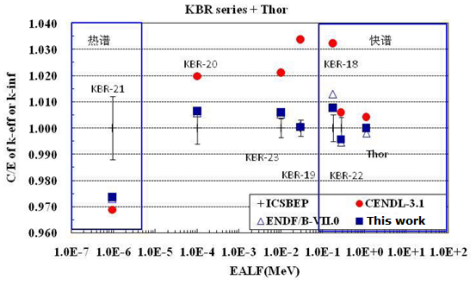

图 6 KBR 系列和 Thor 的宏观检验

3.2 钍铀核数据截面加工

钍铀核数据截面加工以新评价数据和其他现有评价数据为基础，发展处理截面共振问题的方法，进行截面加工，为专门的钍基熔盐堆设计分析程序提供截面库，同时开展关键核素的宏观检验研究。2012 年，利用初步搭建的截面加工平台，完成了 TMSR 混合数据库的 400 个关键核全套中子核数据的初步推荐；针对 TMSR 混合数据库，完成了 24 个温度的连续点截面加工。同时为了检验核数据的可靠性，初步开展了 ^{233}U 连续点截面和 69 群截面的快谱基准题检验。

3.3 钍铀微观核数据测量

钍铀核数据测量的工作主要是建立钍铀循环中子核数据测量平台，补充和完善钍铀循环相关核素反应数据。已经完成了中子物理实验装置(15 MeV 直线电子加速器驱动的白光中子源)物理设计，包括高平均功率电子直线加速器的概念设计、中子源产生靶室系统的模拟和总体设计。中子产生靶和屏蔽体物理及工程设计、实验区终端及探测器设计以及中子物理实验厅改造工程设计等。同时完成了 Th-U 燃料循环主要中子反应截面测量方案设计。

4.3 钍铀循环物理分析

钍铀循环物理分析针对 TMSR 专项基本堆型，进行不同堆型的优化组合，给出未来自持钍铀核能公园的物理设计。主要工作围绕着 TMSR 3 种主要堆型(TMSR-SF、TMSR-LF 和 TMSFR-LF)及 3 种循环模式(一次通过、改进的开环和闭环)的优化分析开展。提出了基于熔盐堆的钍铀循环模式和未来核能公园的雏形，初步开展了 3 种堆型的钍利用设计，给出了利用率比较(见图 7)。结果显示：液态熔盐堆的在线后处理技术可以显著提高燃料利用率，相比熔盐固态堆性能提高约 1 个数量级；同时也表明液态熔盐堆可以实现自持增殖；为了实现核能公园的整体自持，熔盐增殖堆(液态堆)的增殖性能需进一步优化。

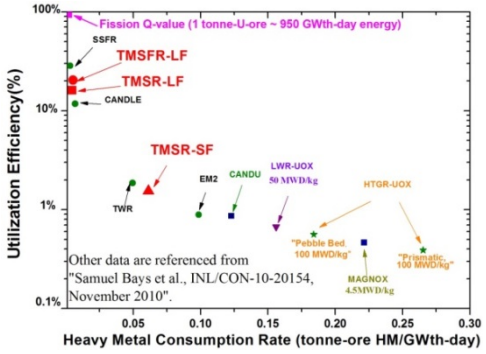

图 7 不同堆型的利用率随燃耗的变化，各类熔盐堆钍利用的结果由红色符号表示，其他数据取自文献[7]

4 钍基熔盐堆设计平台

平台建设总体工作目标是建成国内一流的熔盐堆设计及优化专用计算平台；通过不断的验证、算法的完善，提高软件的计算精度和计算效率，成为国际认可的熔盐堆设计和分析软件，具备各种规模熔盐堆和小型模块堆的设计能力；建立数字化熔盐堆模拟系统，实现漫游仿真、路径优化、动态可视化、在线监测等功能以及反应堆终端控制平台一体化、核数据库等功能。

钍基熔盐堆设计平台硬件系统已经完成阶段性建设任务并开始试运行以支持钍基熔盐堆设计分析的相关计算任务、钍基熔盐堆核数据评价与加工系统已具备并可靠应用到重要核素数据评价及加工工作中、首批液态燃料熔盐堆分析程序模块已经完成开发。

4.1 钍基熔盐堆设计平台硬件系统建设及应用

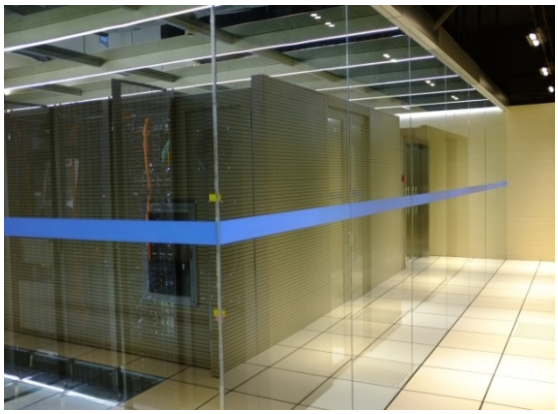

图 8 钍基熔盐堆设计平台

钍基熔盐堆设计平台(见图 8)硬件系统由存储网格、计算网格、互联平台和配套设施构成。到 2012 年末，存储网格调试上线的裸容量为 0.8 PB，采用统一目录的并行文件系统；计算网格共完成 61 个计算节点的调试上线工作，单精度浮点运算峰值计算能力为 118 T·s^{-1}；互联平台采用光纤路径，经调优后最高聚合带宽达 18 GB·s^{-1}，实测不同大小文件块的平均读写速度达 16 GB·s^{-1}。

钍基熔盐堆设计平台采用 64 位 CentOS 6.2 Linux 作为操作系统，并配置了 C/C++/Fortran 等软件开发环境、Intel MPI 并行开发环境、Intel MKL 数学库等。截至 2012 年末，已经为参与钍基核能系统先导专项的 7 个技术部开设账户 100 余个，从 2012 年 11 月底开放运行以来已执行了用户作业 1.4 万余个，累计使用 5.5 万处理器小时，其中 12 月中旬后 CPU 运算资源使用率达 95%[8]。

4.2 钍基熔盐堆核数据评价与加工系统

针对钍基核能系统物理设计对核数据的需求和钍铀循环核数据评价和加工的要求，初步建立了核数据评价和加工系统。该系统包括全套中子核数据评价系统、协方差核数据评价系统、裂变产额核数据评价系统和连续点截面和多群截面加工系统。

目前已经借助该系统完成 ^{232}Th 和 ^{155}Gd 全套核数据评价评价，初步得到了 ^{155}Gd 实验数据协方差矩阵和参数灵敏度矩阵，并完成了 ^{233}U 连续点截面和 69 群截面的快谱基准检验[9]。

4.3 液态燃料熔盐堆分析程序模块

完成了一系列用于执行液态燃料熔盐堆稳态和瞬态分析的程序模块，包括：液态燃料熔盐堆温度反应性计算模块、液态燃料熔盐堆中子输运与单群燃耗耦合计算模块、液态燃料熔盐堆零维点堆和一维少群扩散瞬态分析模块。

液态燃料熔盐堆温度反应性计算模块基于成熟的两步法计算流程，采用超精细群(16500 群)处理共振截面，采用碰撞概率法求解中子输运方程获得组件均匀化截面，采用三角形网格的细网格差分方法求解中子扩散方程[10]。

液态燃料熔盐堆中子输运与单群燃耗耦合计算模块将基于蒙特卡洛方法的中子输运程序与单群点燃耗计算程序耦合起来，以实现中子通量分布与燃耗的耦合计算[11]。

液态燃料熔盐堆零维点堆瞬态分析模块以衰变方程描述多组缓发中子先驱核浓度在一回路中的变化，可以有效描述液态燃料熔盐堆一回路燃料盐流动带来的缓发中子先驱核迁移效应[12]。

液态燃料熔盐堆一维少群扩散瞬态分析模块采用一维二群含时扩散方程描述堆的中子动力学行为，采用一维集总参数法描述堆系统一回路的传热过程，可以用于功率、流量、温度分布等计算[13]。

5 核能综合利用

钍基熔盐堆可以输出 600℃以上的高温热，实现包括核能制氢、工艺热利用、海水淡化在内的核能的综合性利用，提供包括电能、热能、化学能等多种形式的能源产品，大幅度提高核能系统的能效和化石能源系统的碳效。

目前已经开展工作主要包括：核基复合能源系统设计、集成、模拟计算和经济性分析；基于固体氧化物电解池技术的核基高温制氢系统集成研究；高效 CO_2 加氢制甲醇催化剂制备及工业示范。

5.1 核基复合能源系统设计

对于第四代核能系统，如何实现其高温热利用，与现有化石能源系统如何有机结合，如何构建低碳高效的综合性能源体系是一个前沿性课题，这也是推动四代堆研发的重要因素之一。我们与美国爱达荷国家实验室合作开展工作，完成了低碳核基复合能源系统方案设计(见图 9)，对比研究了 TMSR 和 HTGR 构建的复合能源系统特点和差异性。

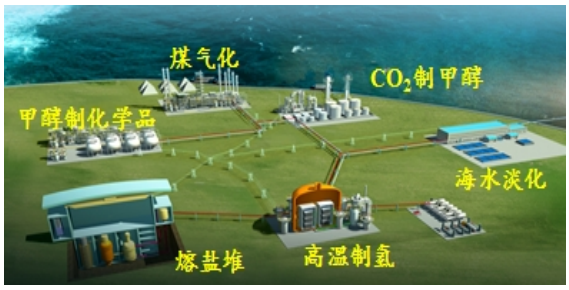

图 9 未来低碳核能综合利用研究示范平台

5.2 高温电解制氢研究

高温电解制氢是核能综合利用研究中的重要方向，已经被 IAES 列为核能非电应用的关键性技术之一。本组在国内率先建设了 kW 级高温电解制氢平台，研究了反应温度、水蒸气含量、电流密度等工作参数对 SOEC 电堆制氢效率、稳定性和电化学性能的影响。图 10 为 1 kW 级高温电解制氢平台，该制氢系统已实现了千小时稳定运行，制氢速率超过百升/小时。

图 10 1 kW 级高温电解制氢平台

为了提高高温固体氧化物电解池系统的稳定性，系统地开展了高温固体氧化物电解池氧电极材料实验，在国际上率先采用同步辐射三维成像技术(TXM)研究了氧电极材料的铬中毒机制。图 11 为 LSCF 电极 Cr 中毒前后的 TXM 表征结果，形象地揭示了 Cr 只在电极表面沉积的反应机制。

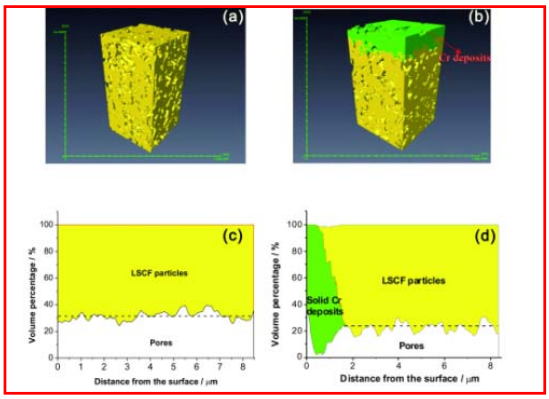

图 11 LSCF 电极上 Cr 沉积的 TXM 表征

参考文献

1. 《2MW 固态钍基熔盐实验堆的物理设计报告》—随机球床堆，2012 年
2. 《2MW 固态钍基熔盐实验堆的概念设计报告》—规则球床堆，2012 年
3. 《2MW 液态钍基熔盐实验堆的概念设计报告》，2012 年
4. 《HTS 回路光管内对流换热系数测量报告》
5. 《堆芯水力实验台架研制报告》
6. 《Th-232 全套中子数据更新评价与基准检验》2012 年
7. Samuel E. Bays, Steven J. Piet, Nick R. Soelberg, Michael J. Lineberry, Brent W. Dixon, Technology Insights and Perspectives for Nuclear Fuel Cycle Concepts, INL/EXT-10-19977, September 30, 2010
8. 王海玲,等. 2013,《TMSR 设计平台基础硬件架构》, XDA02010400.2012.TR11；《2012 年度 TMSR 设计平台运行报告》, XDA02010400.2012.TR12
9. 胡继峰,等. 2013，《整套钍基熔盐堆核数据评价系统报告》，XDA02010400.2012.TR02
10. 张地大，等. 2013，《熔盐堆温度反应性计算模块开发报告》，XDA02010400.2012.TR03
11. 郭威，等. 2013，《熔盐堆中子输运与单群燃耗耦合程序开发报告》，XDA02010400.2012.TR07
12. 何龙，等. 2013，《适用于液体燃料的熔盐堆点堆动力学模块开发报告》，XDA02010400.2012.TR04
13. 战志超，等. 2013，《熔盐堆一维中子扩散及初步瞬态分析耦合程序开发报告》，XDA02010400.2012.TR06
14. Xing L. Yan, Ryutaro Hino. Nuclear Hydrogen Production Handbook. 2011, 47-52
15. O'Brien J E, Stoots C M, Herring J S, *et al*. High Temperature Electrolysis for Hydrogen Production from Nuclear Energy-Technology Summary. INL/EXT-09-16140

Physical Design and Analysis of TMSR Nuclear Energy System

ZOU Yang WANG Naxiu CHEN Jingen GUO Wei WANG Jianqiang YANG Rui
FU Yao CHEN Yushuang ZHANG Jinhong HU Jifeng WANG Xiaohe SHEN Jiajie
GUAN Chengzhi YU Xiaohan CAI Xiangzhou Department of Reactor Physics

Being one of the six Gen-IV reactor candidates, Molten Salt Reactors (MSRs) have two main subclasses. The first subclass is also known as Liquid-fueled MSR(MSR-LF), where fissile material is dissolved in the molten fluoride salt and it serves both as fuel and coolant in the primary circuit. Dry reprocessing can be applied in MSR-LF system, so that fuel breeding can be achieved. Such a scenario is particularly suitable for the use of Thorium fuel. The second subclass is also known as Solid-fueled MSR(MSR-SF),where the molten fluoride salt serves at the coolant to a coated particle fuelled core similar to that employed in Very High-Temperature Reactors. This concept is an integration of proven technologies from other reactor types. It can achieve excellent performance on safety and economy with a high temperature output. It has outstanding suitability for the Nuclear Hydrogen and small modular reactor application.

MSRs operate at high temperature and at near atmospheric pressure. MSRs are very suitable for Thorium energy utilization and hydrogen production at high temperature. These properties made MSR one of the best approaches to solve energy and environment issues of China.

Around the constructions of both a MSR-SF and an MSR-LF in principle-test scales for experimental investigations, our research covers neutronicsand thermal-Hydraulics design and analysis, nuclear data and physical analysis for Th-U fuel cycle, integration of Hybrid Energy System and its economy analysis, nuclear hydrogen production via high-temperature steam electrolysis etc.

Neutrionics design of 2 MW TMSR-SF1

Two design schemes of 2 MW TMSR-SF1 (Thorium Molten Salt Reactor - Solid fuel 1) were accomplished by the Core Physics Design Group. The random pebble bed TMSR-SF (Scheme was reviewed by international specialists group in July, 2012. The ordered pebble bed TMSR-SF scheme gained recognition at the IPR fourth meeting in USA MIT University. Design covers lectotype, core layout, neutronics design and analysis, transient analysis, debugging and running scheme and so on. TMSR developed the ability to complete the whole set of core design and analysis and an in-depth research would be performed in the key science and technologies of TMSR-SF1.

1.1 Neutroncis design of 2 MW random pebble bed TMSR-SF

Fig.1 shows the core layout of 2 MW random pebble bed TMSR-SF with diameter 330 cm, height 470 cm[1]. The core active region is comprised of two parts: a cylinder with diameter 130 cm and height 280 cm, and a circular truncated cone with coning angle 90°. Above the circular truncated cone, attached a cylindrical discharge tube with diameter 50 cm and height 100cm.The fuel spheres circle the centered graphite spheres in the active region and there are 10 control rod channels, 3sample channels and 7 boron ball channlesdistributed homogeneously around the active region in the radial reflector, with all centre distance from the active region is 81.5cm. The overall physical parameters describe that the thermal power is 2MW,the core inlet and outlet temperature is 620 ºC and 600 ºC, average core power density is 1.13 $MW\cdot m^{-3}$, the coolant mass flow rate is 41.3 $kg\cdot s^{-1}$ and the average core coolant flow rate is 0.043 $m\cdot s^{-1}$ (molten salt fraction 40%). 10600 fuel spheres and 600 graphite spheres locate in the core, and the total ^{235}U inventory is 10.9 kg. The general neutron physics parameters show thatfollowing the reactor benchmark design cases (hot state, coolant average temperature 610 ºC), the core excess reactivity is 0.050 and the core temperature reactivity coefficient is $-9.08\ pcm\cdot K^{-1}$. One set of reactivity control system (10 control rods) and two sets of independent shutdown system (10 control rods and 7 boron ball system)are included in the core scheme.

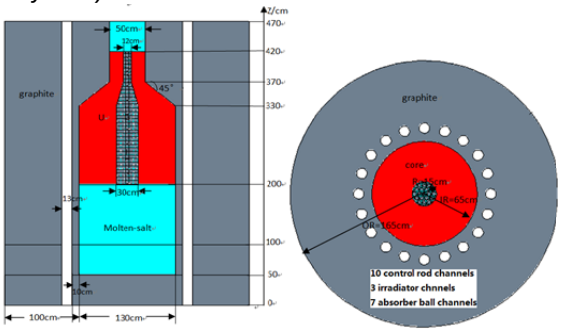

Fig.1 Axial and radial profiles of 2 MW random pebble bed TMSR-SF.

1.2 Neutroncis design of 2 MW ordered pebble bed TMSR-SF

Neutronics design improves a lot in the physical design and analysis of the core in 2 MW ordered pebble bed TMSR-SF. Taking into account of the characters of K-eff、critical mass、neutron distribution、power distributiong, ect., a serious of work been done, achieved a preliminary scheme. Then running sate transient analysis and accident state analysis was performed, gave the parameters of reactivity、power and temperature, which are also treated as the feedback of the statics design and safety design in neutron physics analysis. This provides a basis for transient analysis and various parameters for the

safety analysis in accident state, and supplies stability analysis results for reactor running、debugging and controlling.

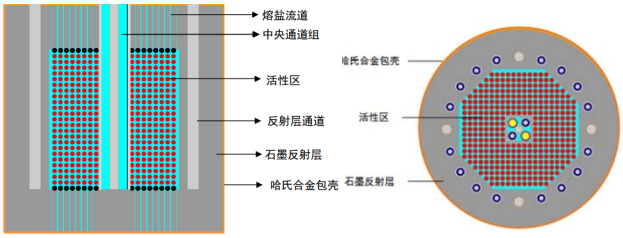

Fig.2 Axial and radial profiles of 2 MW ordered pebble bed TMSR-SF.

Fig.2 shows the core structure of 2 MW ordered pebble bed TMSR-SF[2]. The reactivity area be piled up by the graphite assemblies, appears octagonal shape and contains 16924 fuel spheres with diameter 6.0 cm and ^{235}U inventory 20.2 kg for initiate. The height of reactivity area is 168.8 cm, and the opposite side distance of the octagon is 153.0 cm and 154.0 cm respectively. The volume of reactivity area is 3.1 m^3, whose centre be arranged 5 channels for irradiation experiment、control rods or Boron absorption ball. The overall physical parameters show that the thermal power is 2MWth, Inlet/outlet operating temperature (°C) is 600 and 620 respectively, the mass velocity of coolant is 41.3 $kg \cdot s^{-1}$, the average mass velocity in the core is 0.031 $m \cdot s^{-1}$ and coolant in the side-tube occupies 0.2 of the total coolant volume. The neutron physical parameters illustrate that, in the reference design case, the cold state core excess reactivity is 9479 pcm, the temperature coefficient of reactivity is -7.02 pcm$\cdot K^{-1}$, and the maximum neutron flux density is 2.31×10^{13} n/cm^2/s. One set of controlling system (12 control rods) and two sets of shut-down systems (2 control rods and 2 sets of Boron systems) are also desigened in this design scheme.

2 Thermal-Hydraulics Design and Analysis of Molten Salt-cooled Reactor

The tasks of thermal hydraulics group are conceptual design and V&V experiment on thermal safety of molten salt-cooled reactor.

A preliminary conceptual design of liquid fuel-salt reactor and molten salt-cooled pebble bed reactor has been developed and reviewed respectively[3]. Especially the first edition of 2 MW orderly packed pebble bed reactor design had been evaluated by the international experts. The layout of 2 MW TMSR-SF1 is in Fig.3.

The experimental scheme of reactor core hydraulic test bench[4] and heat transfer coefficient measurements in tube[5] has been evaluated. The preliminary result of convective coefficient of nitrate in circle tube is obtained in Fig.4.

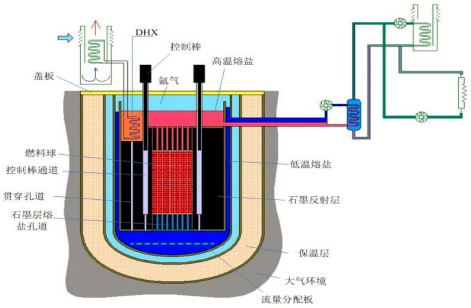

Fig.3 Layout of TMSR-SF1.

The reactor core hydraulic test bench in Fig.5 is equipped with advanced instruments such as particle image velocimetry (PIV) and ultrasonic Doppler velocimetry (UDV), flow meter and differential pressure transducer etc. Scaling analyses have been performed on the integral reactor vessel test facility, which simulates flow distribution in reactor core, upper and lower plenum, core bypass flow or leakage flow, core pressure loss and the integral hydraulic simulation experiments. The flow measurement parameters: 0 to 270 $m^3 \cdot h^{-1}$ (water); velocity measurement dimension: one-dimensional to three-dimensional.

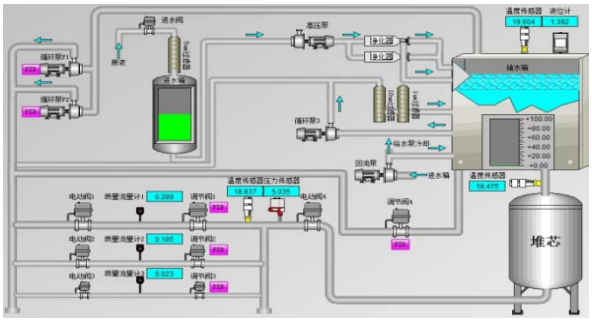

Fig.4 Convective heat transfer coefficient of nitrate in circle tube.

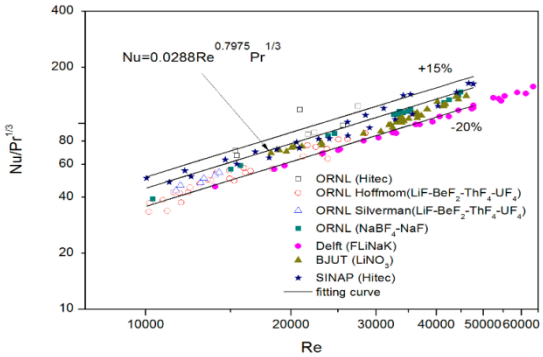

Fig.5 The reactor core test bench.

3 Nuclear data and physical analysis for Th-U fuel cycle

Th-U fuel cycle physics group focuses on the nu-clear data measurement, evaluation and processing for Th-U fuel cycle, which is the foundation of TMSR physical design. It is also concentrated on the physical analysis of Th-U fuel cycle which aims at three types of reactors including TMSR-SF, TMSR-LF and TMSFR-LF.

3.1 Evaluation of nuclear data for Th-U fuel cycle

Evaluation of the Th-U nuclear data contains the development of the fission model, evaluation of the complete neutron reaction data, producing of the Th/U cycle special nuclear data library and the benchmark testing to supply nuclear data for physical design of TMSR. The requirement for Th-U nuclear data has been firstly performed. Then the building of the software and hardware platform for researching the Th-U nuclear data was completed. With the platform, the complete C.S of ^{232}Th, ^{233}U and ^{155}Gd (including the co-variance data) were evaluated. The comparison C/E of Keff between KBR and Thor (Fig.6) shows that the complete C.S of ^{232}Th is better than ENDF/B-VII.0 in fast spectrum[3].

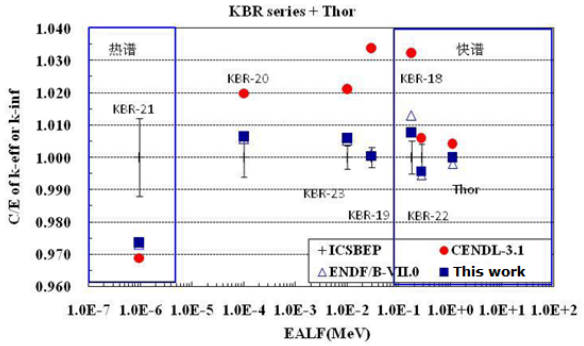

Fig. 6 C/E comparison of Keff between KBR and Thor.

3.2 Processing of nuclear data for Th-U fuel cycle

Based on the evaluated nuclear data, the processing of nuclear data for Th-U fuel cycle is concentrated on developing the method to deal with cross-section re-so-nance, supplying nuclaer data Lib. for analysis software of the physical design in TMSR and benchmark testing of key nuclei. The complete neutron nuclear data of 400 key nuclides were recommended and cross section files with continuous energy at 24 temperature points were processed in 2012. The benchmark testing of consecu-tive energy c.s and 69 groups for ^{233}U in fast spectrum has been carried out to verify the reliability of nuclear data.

3.3 Measurement of nuclear data for Th-U fuel cycle

This subject is engaged in building a platform for measurement of nuclear data of key nuclei in Th-U fuel cycle. The conceptual design of neutron physical ex-perimental device (i.e. whitle neutron source driven by a 15 MeV electron linear accelerator) has been finished, including the physical design of high average power electron linear accelerator, integrated design of neutron source generated target chamber system. The en-gi-neering design of neutron generated target, shield, terminal detector design and renewal of neutron phys-ical experimental hall have been crried out. In the meanwhile, the measurement project design of neutron reaction cross section for Th-U fuel cycle has been proposed.

3.4 Physical analysis for Th-U fuel cycle

Based on TMSR, physical analysis for Th-U fuel cycle is implementing with future vision of nuclear park. Optimization and physical analysis for Th-U fuel cycle pay attention on three kinds of reactors (TMSR-SF, TMSR-LF and TMSFR-LF) and three types of fuel cycle modes (once-through fuel cycle, modified open fuel cycle and closed fuel cycle). The fuel cycle based on TMSR is proposed to compose the future nuclear energy park. The fuel utilization compared between three kinds of Th-based reactor designs is given in Fig.7. The re-sults show that TMSR-LF with online processing can significantly improve the fuel utilization for about one magnitude compared with TMSR-SF and realize self-sustain breeding. However, the breeding perfor-mance of TMSR-LF should be optimized in order to maintain the self-sustain utilization of Th-fuel in the future nuclear energy park.

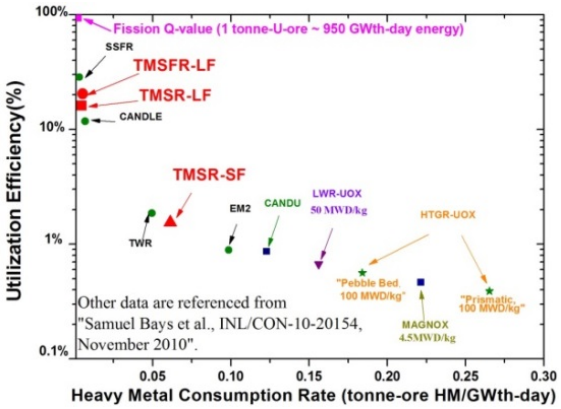

Fig.7 Resource utilization efficiency as a function of consumed mass-in heavy metal [4].

4 The TMSR designing platform

The overall goal of TMSR platform is to build a first-class computing platform system in China for dedicated to the designing and opti-mization of the molten salt reactors in China; to estabilish an internaltional recognized software system for MSR design and analysis by exalta-tion of accuracy and efficiency through contin-uous verification and improvement of the algo-rithm qualified for designing variety molten salt reactors and small modular reactor, and interna-tionally recognized MSR designing and analysis software through improving the accuracy and efficiency by continuous verification and im-provement of the algorithm, ; tobuilt realize a digital MSR simulation system for including roaming simulation, Roaming Simulation , path optimization, dynamic visualization, on-line monitoring, integrative terminal control platform of reactors and nuclear databases.

The hardware system of TMSR designing platform has already finished staged construc-tion task and begin running in support of the related calculation jobs to support the designing and analysis of TSMR TMSR. The evaluation and processing system of nuclear data in TMSR has already be qualified and applied on evalua-tion and processing of the important nuclear da-ta. The first group batch of analysis program modules of for Liquid Fueled MSR-LF have already been completed.

4.1 Hardware system construction and application

The hardware system of TMSR designing platform is composed with storage grid, grid computing, Internet platforms and ancillary fa-cilities. By the end of 2012, the bare capacity of on-line debugging storage grid is 0.8 PB, with unified directory of parallel file system. The computing grid has completed the on-line opera-tion of 61 compute nodes. The compution peak of the single-precision floating is 118 T per sec-onds; The internet platform use optical fiber path. The highest aggregate bandwidth after optimi-zation is 18 GB per second, the average meas-ured speed of reading and writing with different size files is 16GB per second.

Fig. 8 TMSR designing platform.

The TMSR designing platform use linux operating system of CentOS 6.2 with 64-bit, and configure with the C/C++/FORTRAN software development environments, Intel MPI parallel development environments, Intel MKL math libraries. Until the end of 2012, more than 100 accounts have been opened for seven technical department which participating the TMSR spe-cial project. Since the open running of platform in end of November 2012, more than 14,000 us-ers' jobs have been performed by using 55,000 processor hours, in which usage rate of the computing resource is up to 95% after middle of December[8].

4.2 The evaluation and processing system of nuclear data in TMSR

Based on the nuclear data requirement of physical design of TMSR, preliminarily builted the evaluation and processing system of nuclear data which incude the evaluation of the com-plete C.S、the covariance data and the fission yield production and the processing of the con-tinuous energy C.S and the multi-groups.

With the system, evaluated the complete C.S of ^{232}Th and Gd-155(include covariance of experimental data and sensitivity parameters), and completed the benchmark testing of ^{233}U[9].

4.3 The Analysis program modules of LF-MSR

A series program modules of steady state and transient analysis for LF-MSR have been completed in 2011 to 2012, including: temperature reactivity calculation module for LF-MSR, cou-pled module with neutron transport and single group burnup calculation for LF-MSR, ze-ro-dimensional point group and one-dimensional few-group diffusion transient analysis module for LF-MSR.

The temperature reactivity module of LF-MSR is based on the proven two-step calcu-lation process, using ultra-fine group (16,500) on the treatment of resonance cross section, us-ing the collision probability method for solving the neutron transport equation to obtain uniform cross section of components, using fine mesh grid finite difference method with triangular mesh for solving the neutron diffusion equation[10].

The coupled module with neutron transport and single group burnup calculation for LF-MSR is based on the coupling of neutron transport program by Monte Carlo method and the single group burnup program, in order to achieve the coupling calculation with neutron flux distribu-tion and burnup[11].

The zero-dimensional point reactor analysis module of LF-MSR describe the concentration of several delayed neutron precursors by the decay equations in first loop, which can effec-tively describe the migration effect of delayed neutron precursors by flow of fuel salt in the first loop of LF-MSR[12].

The one-dimensional few-group diffusion transient analysis module of LF-MSR describe the dynamic behavior of neutrons in reactor by using the one-dimensional and time-dependent diffusion with two groups, us-ing the one-dimensional The lumped parameter method to describe the heat-transfer process in first loop of reactor system, which can be used to calculate power, flow, temperature distribu-tion and so on[13].

5 Nuclear Hybrid Energy Research in TMSR

Nuclear heat from thorium molten salt reactor (TMSR) can be used not only for electricity generation, but also for hydrogen production, industrial process, and seawater desalination. A hybrid energy system (HES) based on TMSR will improve the energy utilization efficiency, meet the clean energy demand, diminish the use of coal and oil, and diminish the emission of pollutants.

Our current research covers three issues: integration of TMSR Hybrid Energy System and its calculation and economy analysis; nuclear hydrogen production via high-temperature steam electrolysis (HTSE); synthesis of catalysts for CO2 hydrogenation and large-scale methanol production.

5.1 Integration of TMSR Hybrid Energy System

For the Gen-IV nuclear energy system, the utilization of the nuclear heat, combination with fossil-fuel based energy systems, and establishment of effective carbon-friendly hybrid energy system, are pioneering work, which in turn will promote the development of Gen-IV nuclear energy system. We have been cooperating with the Idaho National Laboratory (INL) in developing HES based on advanced nuclear system. Fig.9 demonstrates a sketch map for effective and carbon-friendly nuclear hybrid energy system based on TMSR. And a comparative evaluation of HES based on TMSR and high temperature gas-cooled reactor (HTGR) has been finished.

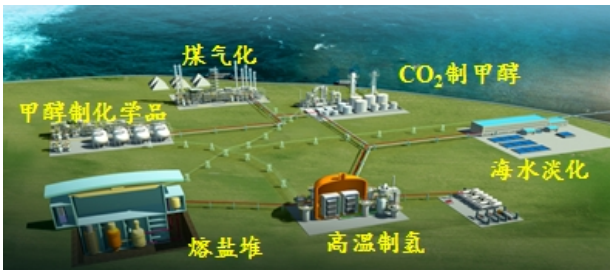

Fig.9 A sketch for effective and carbon-friendly nuclear hybrid energy system based on TMSR.

5.2 Hydrogen production via HTSE

Hydrogen production is an attractive option to import nuclear energy to traditional energy utilization. And HTSE has been recognized as one of the key technologies in non-electric applications for nuclear energy by IEAS. We have integrated the first 1 kW-SOEC hydrogen production system of China and reveal the influence of different parameters, such as current density, temperature and steam concentration on the stack performance. The facility shown in Fig.10 has run stably for more than 1000 hours and the hydrogen production rate reaches more than 100 L/min.

Fig.10 1 kW integrated SOEC evaluation platform.

One of the crucial issues relevant to the durability of HTSE system is the degradation of solid oxide cell (SOC) materials, such as Cr-contamination at the O_2-electrode side. Performance of the electrodes will decrease due to the formation of Cr depositions on the electrode surface, increasing the gas diffusion resistance. Therefore, we have investigated several perovskite-structure O_2- electrodes, and choose the transmission X-ray microscope (TXM) technique to clarify the 3D distribution of Cr deposits and the porosity change as a function of the distance from the electrode surface. Fig.11 shows the morphology of Cr-deposition on porous LSCF electrode, indicating that Cr species occupy the holes in the surface layer.

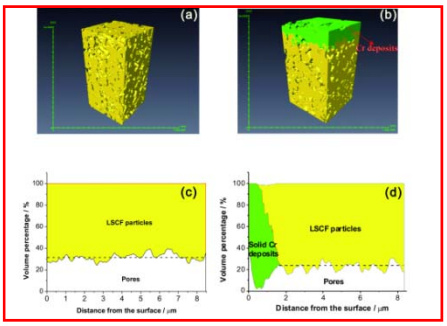

Fig.11 3D distribution of Cr deposition at LSCF electrode via TXM technique.

参考文献

1. Conceptual design of 2 MW pebble bed TMSR-SF, Year 2012
2. Physical design of 2 MW pebble bed TMSR-SF, Year 2012
3. Conceptual design of 2MW Liquid-fueledthorium-based molten salt reactor experimental facility. 2012
4. Test report of convective heat transfer coefficient of nitrate in circle pipe
5. Development report about hydraulic test bench
6. Reevaluation of the complete neutron cross sections of ^{232}Th and its benchmark testing. Year 2012
7. Samuel E. Bays, Steven J. Piet, Nick R. Soelberg, Michael J. Lineberry, Brent W. Dixon, Technology Insights and Perspectives for Nuclear Fuel Cycle Concepts, INL/EXT-10-19977, September 30, 2010
8. Wang H L. The designing platform of hardware architecture for TMSR, XDA02010400. 2012.TR11；The operational report of the designing platform of TMSR in 2012, XDA02010400. 2012.TR12
9. Hu J F. The report on evaluation system of nuclear data inTMSR. XDA02010400.2012.TR02
10. Zhang D D. The development report of temperaturereactivity calculation modulefor MSR, XDA02010400. 2012. TR03
11. Guo W. The development report of coupled programwith neutron transport andsingle group burnup calculationfor MSR, XDA02010400.2012.TR07
12. He L, The development report of point reactor kinetics module for LF-MSR, XDA02010400.2012.TR04
13. Zhan Z C. The development report of coupled program of one-dimensionalneutron diffusion analysis and Preliminary transient analysis for MSR, XDA02010400.2012.TR06
14. Xing L. Yan, Ryutaro Hino. Nuclear Hydrogen Production Handbook. 2011, 47-52
15. O'Brien J E, Stoots C M, Herring J S, *et al.* High Temperature Electrolysis for Hydrogen Production from Nuclear Energy-Technology Summary. INL/EXT-09-16140

反应堆工程技术部

反应堆工程部负责 TMSR 堆工程的设计及研制任务，具体包括堆结构及结构力学，仪控和厂房工艺。目前完成了 TMSR-SF1 概念设计和部分关键系统的样机研制，如控制棒驱动机构原理样机、保护系统原理样机、燃料球装卸机构原理样机等。

控制棒驱动机构原理样机的研制

控制棒是熔盐堆的关键部件之一，主要由(1)中子吸收毒物炭化硼的棒芯体，和(2)驱动步进电机与行星齿轮驱动链轮链条组成的控制棒驱动机构等组成。控制棒的棒位置测量是由旋转变压器和拉伸磁尺共同承担，二者互补。控制棒研制于 2012 年年初开始，2012 年 7 月底正式确定方案与加工厂商，经历整 1 年时间，于 2012 年 12 月底研制成功(见图 1)。初步的运行试验和落棒试验结果表明：(1) 控制棒运行良好无异响，棒位置显示精度好于 0.2 mm；(2) 落棒时间为 4.6 s，详细落棒如图 2 所示，这个落棒时间水平跟清华大学高温气冷堆研制的控制棒落棒时间为 4–8 s 相当。在此平台上开展了控制棒运动实验、落棒实验等验证。

图 1 控制棒驱动机构原理样机装置

熔盐反应堆的控制棒控制与位置监测系统是反应堆功率控制系统的重要组成部分。基于熔盐堆控制棒驱动机构样机的棒控棒位系统的研制为熔盐堆功率控制系统设计和设备选型积累了宝贵经验。

熔盐堆控制棒驱动机构的棒控/棒位系统采用数字化设计，通过采用数字化控制器、网络技术、热备冗余技术等设计，来提高系统可靠性和安全性，实现控制棒逻辑控制、故障报警和棒位历史数据记录、在线监控、落棒参数测量、棒动作波形记录以及在授予高级权限下关键参数的修改等系统功能。

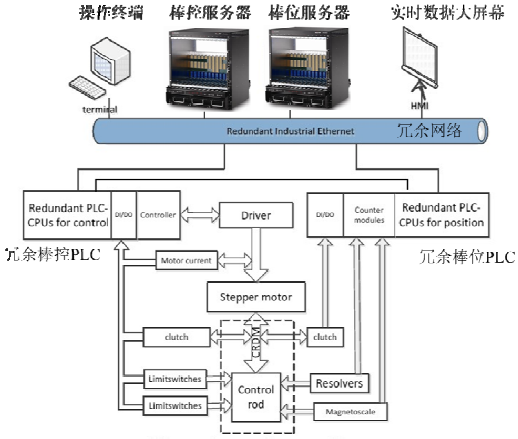

图 2 棒控棒位系统架构

熔盐堆控制棒驱动机构样机由步进电机作为驱动源，结合磁滞伸缩传感器和旋转变压器作为位置测量机构[1]。控制棒控制和位置检测硬件配置完全独立，采用冗余的西门子 S7-400 PLC。冗余 CPU 之间的无扰动切换能力，大大提高了系统的可靠性。

系统的服务器采用高可靠性的 ATCA 架构的服务器如图 2 所示。其标准平台支持灵活开发和配置的重复使用，它的系统设计可以达到最小 99.99%的可用性。ATCA 拥有先进完善的系统管理功能，开发工程师可以非常方便地对每一张板卡以及机箱内部环境进行监控，可以实时监测每个板卡的电压、温度、控制器 CPU 的状况以及机箱风扇的参数。另外，该硬件平台支持板卡的热插拔功能以及支持多个系统控制器以冗余方式工作，极大地保证了系统管理的安全可靠性。

系统的监控层的软件采用基于 EPICS 即实验物理与工业控制系统软件开发平台。结合系统硬件特点，设计了冗余的 EPICS IOC(输入输出控制器)软件结构。软件的设计的目标是为实现比单一 IOC 运用更高的可靠性。冗余系统所具有对系统错误的“预见性”，可驱动冗余设备进行切换。冗余的软件结构主要包括 2 部分如图 3 所示。

RMT 是整个 IOC 冗余控制软件的核心，其主要任务有建立 2 条以太网通信线路进行状态监测和与 IOC driver 进行通信，根据状态信息 RMT 决

定哪个 IOC 承担控制任务，哪个 IOC 处于备用状态。CCE 功能为维持主备 IOC 数据库同步。经优化，系统 IOC 冗余切换时间为 1–2 s.

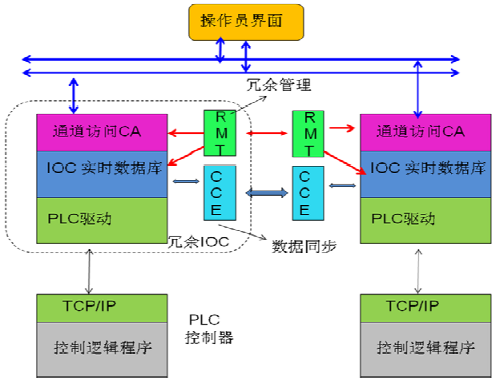

图 3　冗余 EPICS IOC 软件结构示意图

在系统测试中，棒控棒位系统达到了如表 1 所示的设计指标。棒控棒位系统的 3 个月测试(累计行程 153096.4 m，模拟落棒次数 50 次)，系统连续运行无故障。

表 1　控制棒控制系统运动参数

运行参数	指标
控制棒正常运行速度	10 mm• s^{-1}
控制棒运动方向反转时间	< 0.5 s
控制棒运动停止时间	< 0.25 s
控制棒运动行程	>1600 mm
位置控制精度	< ±2 mm

燃料球装卸机构原理样机

燃料球装卸装置是 TMSR 固态堆熔盐堆的重要组成部分，主要功能是实现燃料球的循环管理。该装置有自动进球、出球、分球等复杂机构组成。由于熔盐环境下的在线燃料球装卸装置在国际上尚无研制先例，因此，需要从模拟装置开始对整个系统进行研究。

燃料球提升机构　　模拟堆芯

图 4　燃料球装卸机构原理样机

本模拟装置于 2012 年 7 月开始设计，11 月下厂加工，2013 年 1 月 26 日开始现场安装，2 月 4 日安装结束，初步调试成功(见图 3)。即将开展(1)模拟燃料球自动注入模拟堆芯的实验；(2)模拟燃料球在堆芯顶部自动卸料的实验；(3)模拟燃料球自动提升、分球的实验；(4)球在堆芯中的流动和排布规律研究及部分水力实验研究等。

堆结构力学分析

(A) 完成了 FLiNaK 高温熔盐回路管道、熔盐泵、加热器、换热器、储罐、冷冻阀、冷冻法兰和溢流罐等的热力学分析和优化设计；(B)参照 MSRE 的经验，提出采用柔性支撑方式解决热应力过大的方案，大大减小了整个系统的热应力；(C)参照 ASME NH 规范对核级工程样泵进行了高温力学评定工作，掌握了高温应力评定、变形评定和蠕变-疲劳评定的方法，该方法可推广使用到整个 TMSR 的安全级设备力学评定中；(D)对冷冻阀和熔盐泵的高温应变进行了测试，并和力学分析结果进行了对比验证，掌握了高温结构力学测试的关键方法。

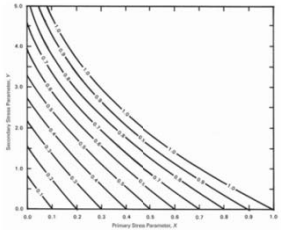

图 5　ASME NH B-1 和 B-3 试验中参数 Z 的取值

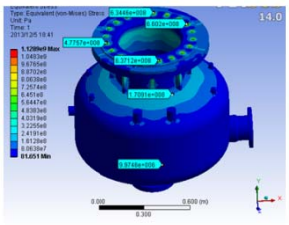

图 6　熔盐泵等效应力云图

建立了石墨砖辐照力学计算的方法: (a) 编写了热分析子程序，并对不同间隙、不同温度和不同辐照剂量下的石墨辐照应力进行了分析，在此基础上，初步运用 ASME 第三卷 HHA 对石墨进行了应力评定，掌握了辐照石墨应力评定的方法；(b) 对压力容器进行了较为全面的力学分析和优化，主要包括热应力分析、屈曲分析、抗震分析和蠕变分析，并按照 ASME NH 卷，首次运用非弹性计算方法，对容器进行了变形评定；(c) 对控制棒在熔盐中的落棒特性和流体阻力进行了研究，并对控制棒在地震工况下与石墨砖碰撞的可能性以及棒体的柔性设计进行了初步的分析，在理论分析钢珠缓冲器缓冲性能基础上，设计了基于正交优化的试验方案，并完成了相应的落棒缓冲试验。

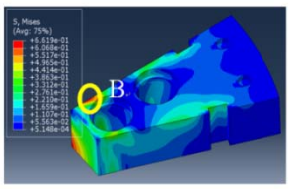

图 7 石墨砖辐照下的应力分布

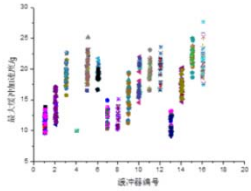

图 8 16 组缓冲器最大缓冲加速度

基于 FPGA 的反应堆保护系统原理样机

结合 TMSR 项目的长期规划与现代核电仪控发展的趋势，考虑到纯硬件系统的高可靠性及先进性，TMSR 拟采用基于 FPGA 的数字化系统作为安全级系统平台，开展基于 FPGA 技术数字化保护系统平台的自主研制作为长线技术储备和人才培养及训练的平台。

保护系统原理样机着重于保护系统主要功能的实现，通过硬件设计加工测试来验证方案可行性及合理性，积累相关技术经验。样机总体设计采用四重冗余、四选二符合逻辑的结构如图 9 所示，每个保护序列均由信号调理单元、定值比较单元、逻辑符合单元和触发执行单元组成。参加保护的信号通过信号隔离单元后经过定值比较产生该序列的保护逻辑信号，各序列逻辑信号在逻辑符合部分完成局部 2/4 符合逻辑之后产生相应的保护动作信号。原理样机采用主处理板卡、后走线板、背板、机箱的组成结构。主处理板卡通过 FPGA 芯片和模块化的 I/O 子卡完成样机的主要信号和逻辑处理功能，每块主处理板卡包含 2 片 FPGA 处理芯片，1 片主要完成逻辑处理功能，1 片负责完成通讯相关功能。针对保护功能对象的特点，样机设计考虑了 3 种不同的停堆逻辑。样机还研制了测试和显示子系统以方便对系统进行测试。

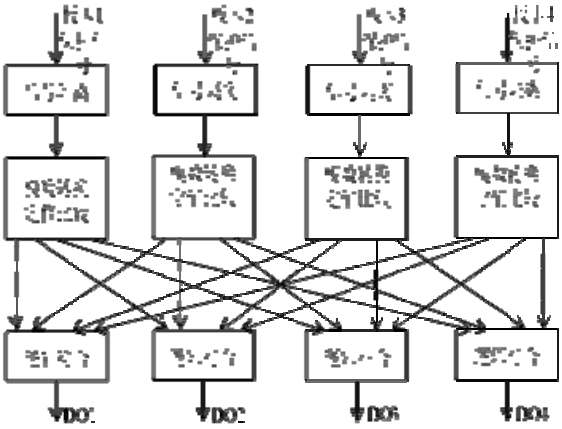

图 9 保护系统结构图

原理样机实物如图 10 所示，其逻辑功能测试、响应时间测试及与 CRDM 样机的联合调试结果表明样机研制完成了系统的设计功能要求，样机系统对数字信号变量的停堆响应时间为 30 μs，对模拟信号变量的停堆响应时间为 3.2 ms，响应时间符合要求，能够正确输出停堆信号，实现了原理样机的目标，掌握了基于 FPGA 保护系统的关键技术。

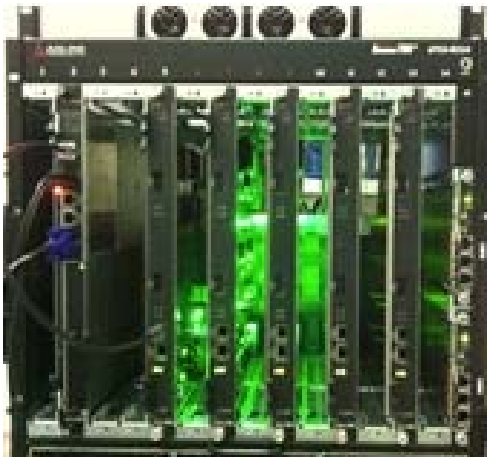

图 10 保护系统原理样机

超声波流量计在 HTS 和 FLiNaK 回路上的应用

堆测量组针对超声波流量计开展了一系列的应用研究工作：

(1) 在常温状态下，完成了实验室水流量标定平台上的仪表标定工作，掌握了超声波流量计的安装和调试方法，标定精度小于 1%，标定结果获得了上海计量院的确认。

(2) 在专项的 HTS 回路(200 ℃–400 ℃)和 FLiNaK 回路(550 ℃)上进行了高温熔盐的流量测量应用研究。根据 HTS 与 FLiNaK 回路的管径(DN32、DN50)，选择了 4 MHz 的高频探头，以保证能够正常测量。由于熔盐的熔点较高，熔盐管路需要保温以保证其内部熔盐的正常流动，虽然 FLEXIM 超声波流量计采用了波导板的方式能够提高耐受管路壁温，但针对 400 ℃ 以上高温仍然需要对波导板局部降温，使换能器能安全稳定的工作。因此，工程上需要权衡保温与冷却方案以同时满足熔盐和流量计的需求。

由于 FLiNaK 回路运行温度为 550 ℃，且熔盐的熔点约为 450 ℃，因此，对该回路的流量计进行了风冷的改造，实物图如图 11-b 所示。实验结果表明，当泵频率增加，流量增加，最小为 17.7 $m^3 \cdot h^{-1}$，最大约为 24.8 $m^3 \cdot h^{-1}$，拟合曲线如图 11-c 所示。

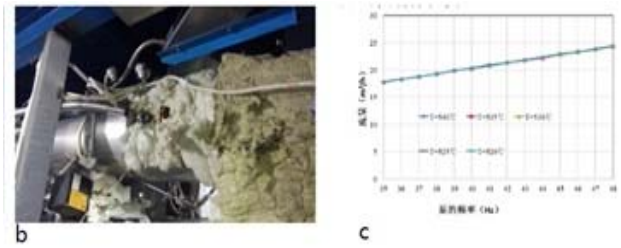

图 11 (b) 超声波流量计在 FLiNaK 回路上的实物图; (c)流量与泵的转速关系图

通过实验室标定及 HTS 和 FLiNaK 回路上的工作，积累了超声波流量计在不同工况下的安装调试经验，获得了超声波在 HTS 和 FLiNaK 熔盐中大致的传播速度。

反应堆工程技术部 2011–2012 年主要完成了控制棒驱动机构原理样机的研制、燃料球装卸机构原理样机的研制、堆结构力学分析、基于 FPGA 的反应堆保护系统原理样机的研制、超声波流量计在 HTS 和 FLiNaK 回路上的应用研究。这些工作的顺利圆满完成，为熔盐反应堆项目的进一步展开提供了有利保障，为反应堆工程部下一阶段的工作打下了坚实基础。

参考文献

1. 刘斌,刁兴中,周惠忠,黄志勇. HTR-10 控制棒驱动机构的设计经验,全国新堆与研究堆学术会议,新疆伊犁
2. 袁润, 刘延山. 高温气冷堆用控制棒位置指示器的可靠性设计 江苏理工大学学报 1997, 1
3. 张冰蔚, 刘延山. 10 MW 高温气冷试验堆控制棒驱动系统结构设计, 江苏工学院学报, 1994 年 01 期
4. 魏利强,马涛, 陈晓明,等. HTR-10 数字化运行仪表与控制系统更新设计, 原子能科学技术, 2011, **45**(9)
5. HOU Xuemei, LIU Guimin. Study of Control rod worth in the TMSR. Nuclear Science and Techniques, 2013, **24**: 010601
6. E Zio. Reliability engineering: Old problems and new challenges. Reliability Engineering and System Safety, 2009, **94**: 125-141
7. Wang Quanquan, Li Yongping, Lifeng Han,*et al*. TMSR Single Control Rod Drive Mechanism Control System and its Reliablity Analysis. 2nd International Conference on Measurement, Information and Control, Harbin, CHINA,Volume 1:737-741
8. 刘冲. 核电站反应堆棒控棒位控制系统数字化软硬件设计及其可靠性研究, 南华大学, 2010
9. 谭平, 周剑良, 姚秋果, 等. 基于 PLC 的秦山一期棒控棒位系统的数字化, 核电子学与探测技术, **27**(6)
10. 左文, 阎玉辉. 秦山核电二期工程棒控棒位系统设计, 核动力工程, 2003, z1
11. 彭小强, 郑养波. AP1000 控制棒棒位的数字化测量技术分析,核电子学与探测技术, 2012, 5

Department of Reactor-Engineering

Department of Reactor Engineering, is responsible for the design and development of TMSR, including reactor structural and structural mechanical, instrumentation and control (I&C), and plant layout. The concept design of TMSR-SF1 has been finished, and some critical devices, such as prototype for the control rod drive mechanism, protect-system prototype, prototype for spherical fuel handling system, *et al*.

Development of control rod drive mechanism prototype

Control rod, one of the key parts in TMSR-SF1, consists of the core-rod made of boron carbide, and the control rod drive mechanism included stepper motor and planetary gear chain. The position of the control rod is measured by a rotary transformer and a magnetic scale. The rod (Fig.1), after one year hard work, has proved that (i) the position resolution is less than 0.2 mm and no accident happened, (ii) the drop time is less than 4.6s (Fig. 2), compared to that in HTR-10. Using this experiment platform, lots of verifying tests, such as rod movement, rod drop, and et.al have been done.

Fig.1 Control rod drive mechanism prototype.

As the sub-system of the power control system，the development of the rod control and position measurement system is the basic design of the power control system. Considering the systems reliability and security, digital has been used for the rod control and position measurement system, including digital controllers, network technology, and hot-redundancy technology. And then the rod control measurement system has such functions, the rod logical-control and dropping parameters measurement, alarming and online monitor, the records of the rod position historical data and the rod movement waveform, and the modification of the key parameters with the advanced permissions.

The control rod drive mechanism consists of a stepper as the driving source, a rotary transformer and a magnetic scale as the position measurement mechanism. The detection hardware of the rod control and position measurement system is independent, and the redundant s7-400 PLCs are used, which greatly improve the system security by their bumpless transfer.

The system servers, as shown in Fig.2, are based on the ATCA architecture, more than 99.99% can used and agile development and reuse of the configure supported. By its excellent management function, any boards and the inter-environment in the platform can be easily monitored, including boards' voltage and temperature, controller's CPU status, and the parameters of the chassis fan. The security and reliability of the management system is supported by the platform hot-plug function and controllers working in the redundant way.

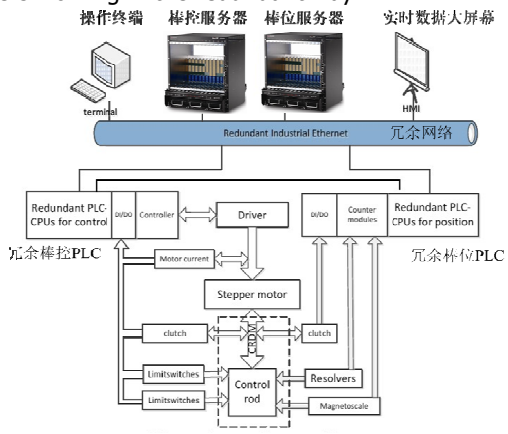

Fig.2 Architecture of the rod control and position measurement system.

The software of the system monitor layer is based on the EPICS, and used the redundant EPICS-IOC for the reliability request since its predictability for the system errs and ability of redundancy switch, as shown in Fig.3.

At the heart of the redundant IOC is RMT, responsible for choosing the IOC to take the control task according to the status- information-RMT by the two Ethernet lines, one for the status monitor, the other IOC driver communication. The two databases of the redundant IOCs are synchronized by CCE. The redundant switch time of the system IOCs is about 1–2 seconds.

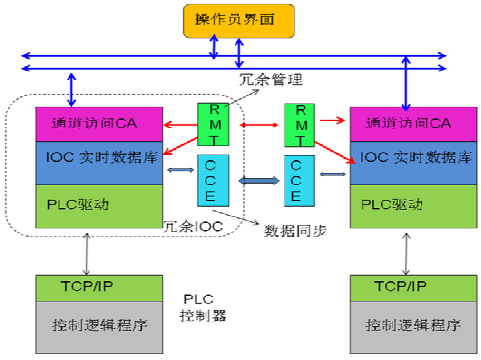

Fig.3 The structure of the redundant EPICS-IOC.

After 3 months tests, the rod control and position measurement system was safe without fault during total 153096.4m, and total 50 rod-drop times running. The system has reached the design standard requirements listed in Table 1.

Table 1 Parameters of the rod control and position measurement system

Parameters	Standard
Speed	10 mm• s^{-1}
Switch time of the motion direction	< 0.5 s
Stop time	< 0.25 s
Travel	>1600 mm
Resolution of the position control	< ±2 mm

Prototype for spherical fuel handling system

The spherical fuel handling system, one important sub-system of the TMSR-SF1, consists of auto-ball-in, auto-ball-out, auto-ball-separated parts, responsible for the spherical ball management. The system was needed to be designed completely from the simulator since no similar system had been designed or used under the molten salt environment.

After half of a year, the spherical fuel handling system was designed successfully, as shown in Fig. 4. In the next step, experiments as follows will be done, (i) simulator spherical fuel auto-injected to the simulator reactor core, (ii) simulator spherical fuel auto-removed from the top of the simulator reactor core, (iii) simulator spherical fuel auto-lifted and auto-separated, (iv) the flow and distribution of the simulator spherical fuel in the simulator reactor core and some waterpower researches.

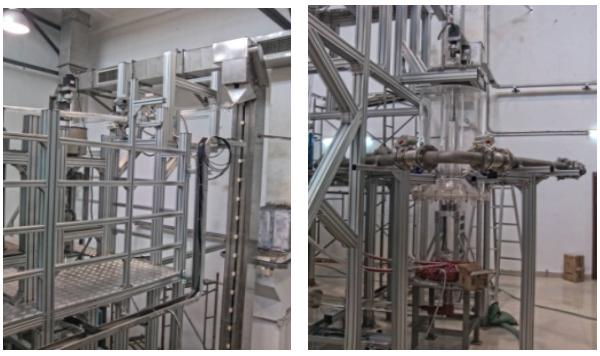

Spherical fuel handling system Simulator reactor core

Fig.4 Prototype for spherical fuel handling system.

Mechanical analysis

(a) Thermal analysis and structural optimization of loop system and equipment at Elevated Temperature in FLiNaK have been finished. The analysis objects include pipe, molten salt pump, heater, heat exchanger, storage tank, Freeze-Valve, Freeze-Flange and weir tank, and so on. (b) Flexibility support has been adopted to solve the problem of high thermal stress according to the experience of MSRE, which can greatly reduce the thermal stress of entire system. (c) The structural evaluation of engineering pump at elevated temperature has been conducted based on the ASME NH code. The methods of stress, deformation and creep-fatigue evaluation progress had been studied. These methods can be further applied to the safety mechanics evaluation of all equipment in TMSR. (d) The strain tests of Freeze-Valve and molten salt pump has been compared with the thermal analysis results. The key method of high temperature structural mechanics test was mastered.

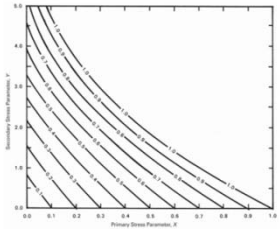

Fig.5 Parameter Z of test B-2 In ASME.

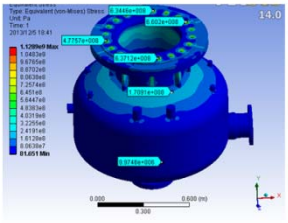

Fig.6 Equivalent stress of molten salt pump.

(a) For the graphite safety analysis, we have developed a methodology for stress analysis of irradiated graphite and written a user subroutine for graphite thermal analysis after irradiation. Furthermore we have analyzed irradiated graphite brick under different brick clearances, temperature profiles and fluence profiles. All the stress analyses have been assessed according to ASME HHA standard. (b) The structure of pressure vessel has been assessed according to ASME NH standard. Several analyses have been performed to optimize the design of the pressure vessel including thermal stress analysis, seismic analysis, buckling analysis and creep analysis. Furthermore the pressure vessel subjected to elevated temperature working condition has analyzed by inelastic analysis. (c) For the mechanical analysis of the control rod: fluid resistance calculation and rod drop analysis, impact possibility of the control rod and the graphite channel, preliminary analysis on the flexibility design of control rod, theoretical analysis of the shock absorber, orthogonal experiment design of the shock absorber and absorbing test.

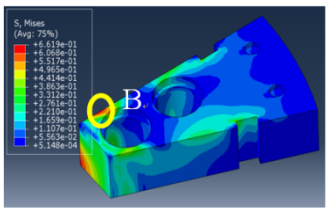

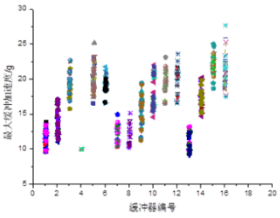

Fig.7 Stress distribution of the graphite brick (left).
Fig.8 Maximum acceleration of the shock absorbers (right).

FPGA-based Prototype Reactor Protection System

TMSR intends to use FPGA-based digital system as the safety system platform and use the independent development of the FPGA-based digital reactor protection system as the long-term technical reserves and training platform, after combining the trend of modern nuclear instrument & control system development with long term

planning of TMSR project and taking into account the reliability and advanced pure hardware system.

The Prototype Reactor Protection System (PRPS) focus on the realization of main function of the Reactor Protection System (RPS). And it is used to verify the feasibility and reasonableness of the solution of FPGA-base system and get the relative technical experience, during the hardware design, producing and tests. The PRPS have four redundant protection parts using 2 out of 4 logic with each part make up by signal conditioning unit, comparator unit, 2oo4 logic unit and trigger to execute unit showing as Fig.9. The protection related signal inputs into the system after isolation compared with the setting value of the comparator unit to generate a protection logical signal of one part. This logical signal with three other the same signal from other parts get into the 2oo4 logic unit to generate the final shut down or not signal of this part. The PRPS is made up with processing motherboard, back line board, back board and ATCA chassis. The processing motherboard within two FPGA chips one of which does logical functions and another one does communication function, work with modular I/O child board to process the main signals and logical works of the protection system. Due to the characteristics of the protected objects, three different shut down logics are designed. Meanwhile there are testing and display mini system designed to make the PRPS tests easier.

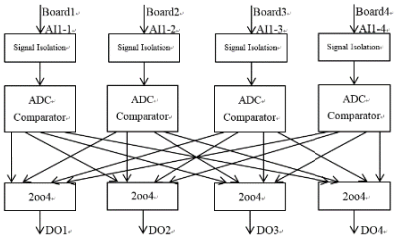

Fig.9 The Structure of PRPS.

Fig.10 shows the picture of the PRPS. The result of logical function test shows the prototype's functions reach the design goals and in response time test the prototype gets 30μs with digital signal and 3.2 ms with analog signal both of which achieve the design goal. Further, the PRPS do send the right shutdown signal into the CRDM system to cut the power of the driver motor of the control rods during the combining test of the PRPS and the CRDM system. Above all, the PRPS design is success and the key technology of FPGA-based Reactor Protection System is mastered.

Fig.10 Prototype Reactor Protection System.

The applied research work about ultrasonic flow meter at HTS loop and FLiNaK loop

A series of applied research work about ultrasonic flow meter is carried out by measured group.

1. In normal condition, calibration was done on the water calibration platform, and installation and commissioning skills was mastered in this process. Calibration measurement result was confirmed by Shanghai Measurement and Testing Institute.

2. Applied research for high temperature molten salts is carried out at HTS loop and FLiNaK loop. Transducers of 4MHz frequency were selected according to pipe diameter. Due to high melting point of molten salt, heat insulation is needed to ensure melting molten salt flow. Although FLEXIM ultrasonic flow meter uses a waveguide plate, it is still needed to cool down the transducer when the temperature is above 400 ℃. Therefore in engineering process, it is necessary to keep balance of insulation and cooling solutions.

Since FLiNaK loop operating temperature is 550 degrees, and molten salt melting point is about 450 degrees, so air-cooled modification is applied on ultrasonic flow meter on FLiNaK loop, as shown in Fig. 11-b. Experimental results show that when the pump frequency is increased, the flow rate also increases, the fitting curve is shown in Figure 11-c. The minimum flow is 17.7 $m^3 \cdot h^{-1}$; a maximum flow is 24.8 $m^3 \cdot h^{-1}$.

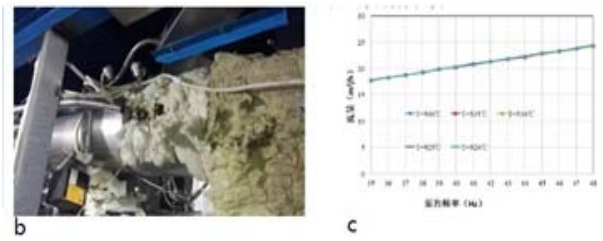

Fig.11 The ultrasonic flow meter at FLiNaK loop (left); The relation of the pump frequency and flow rate (right).

In calibration and loop application process, installation and commissioning experience is accumulated and ultrasonic velocity of HTS and FLiNaK molten salt is also obtained.

During 2011-2012, Reactor-Engineering Department finished the developments of the prototype for the control rod drive mechanism, the prototype for spherical fuel handling system, protect-system prototype, as well as the Mechanical analysis and the applied research work about ultrasonic flow meter at HTS loop and FLiNaK loop. All of these have supplied a strong guarantee for the TMSR future work and laid a solid foundation for the next stage of work of the Reactor-Engineering Department.

Reference

1. 刘斌,刁兴中,周惠忠,黄志勇. HTR-10 控制棒驱动机构的设计经验,全国新堆与研究堆学术会议, 新疆伊犁
2. 袁润, 刘延山. 高温气冷堆用控制棒位置指示器的可靠性设计 江苏理工大学学报, 1997, 1
3. 张冰蔚, 刘延山. 10 MW 高温气冷试验堆控制棒驱动系统结

构设计, 江苏工学院学报, 1994, 01
4. 魏利强,马涛, 陈晓明,等. HTR-10 数字化运行仪表与控制系统更新设计, 原子能科学技术, 2011, 45(9)
5. HOU Xuemei, LIU Guimin. Study of Control rod worth in the TMSR, Nuclear Science and Techniques, 2013, **24**: 010601
6. E Zio. Reliability engineering: Old problems and new challenges. Reliability Engineering and System Safety, 2009, **94**: 125-141
7. Wang Quanquan, Li Yongping, Lifeng Han,*et al*. TMSR Single Control Rod Drive Mechanism Control System and its Reliablity Analysis. 2nd International Conference on Measurement, Information and Control, Harbin, CHINA,Volume 1:737-741
8. 刘冲. 核电站反应堆棒控棒位控制系统数字化软硬件设计及其可靠性研究，南华大学, 2010
9. 谭平, 周剑良, 姚秋果, 等.基于 PLC 的秦山一期棒控棒位系统的数字化, 核电子学与探测技术, **27**(6)
10. 左文,阎玉辉. 秦山核电二期工程棒控棒位系统设计,核动力工程, 2003, z1
11. 彭小强, 郑养波. AP1000 控制棒棒位的数字化测量技术分析, 核电子学与探测技术, 2012, 5

熔盐化学与工程年报

熔盐化学与工程技术部　左 勇　俞国军　傅 远　唐忠锋　李玉兰　谢雷东

1　熔盐化学研究进展

熔盐化学课题组的主要任务是解决熔盐制备、纯化及分析检测中的技术难题，为获取合格的反应堆氟盐冷却剂扫清技术障碍。2011–2012 年度主要完成熔盐化学各类研究平台的建立，具体进展如下。

1.1　熔盐物性测试与相图研究平台

熔盐物性测试研究平台

建立熔盐物性与相图研究平台，包括密度仪、高温 DSC、表面张力仪、熔盐粘度仪、激光导热仪、熔盐物性综合测定仪等设备，购置了热力学计算软件，具备开展氟化物熔盐相关物性测试研究的能力。

1.2　熔盐分析化学实验室

熔盐分析化学实验室

建立熔盐分析化学实验室，包括 ICP 光谱、离子色谱、电位滴定等仪器分析技术和重量法、容量法等常规化学分析技术，具备开展 FLiNaK 熔盐主要组分及常规杂质的分析检测能力。

1.3　熔盐氧化物净化研究平台

建立熔盐氧化物净化研究平台，包括 HF-H2 脱氧净化实验装置、熔盐电化学净化研究装置、熔盐水分分析装置、熔盐总氧含量分析仪器等设备，具备开展化学和电化学脱氧净化熔盐的能力。其中，熔盐氧化物净化水平达 100 ppm，所研制的熔盐参比电极寿命达 200 h。

熔盐氧化物净化研究平台

2　熔盐回路研究进展

本组主要任务是熔盐回路及其关键设备的研制工作。在 2011–2012 年开展了 HTS 热工试验回路和 FLiNaK 熔盐高温试验回路的设计建设及调试运行工作；开展了熔盐泵、冷冻阀等关键设备的研制工作。开展熔盐回路技术研究主要是获得熔盐回路系统设计和建造技术，开展熔盐回路热工和力学特性研究，为 TMSR 回路设计、建造和运行提供依据。关键设备是回路成功运行的保障。

HTS 热工试验回路已在规定的时间和经费下，成功完成调试测试，达到设计指标，并开展了热工水力性能测试和长期运行考验。FLiNaK 熔盐高温试验回路已经在规定时间内完成了物理设计和工程设计，主要设备已经完成加工。关键设备及其原型设备，也已在规定的时间和经费下，成功完成系统参数的测试验证，达到设计指标。

2.1　HTS 熔盐热工试验回路

HTS 熔盐热工试验回路系统主要由循环泵，加热器，空气散热器，管路和阀门，实验段、保温和预热(伴热)设备，温度、流量、液位测量仪表等组成。熔盐由循环泵驱动进入加热器，经加热升温达到出口温度(类似熔盐堆堆芯)，然后进入换热器，经冷负荷降温释放热能(类似熔盐堆发电设备负荷)，冷却后的熔盐再进入加热器升温，从而实现熔盐回路的循环和热工水力实验参数的测试。

HTS 熔盐热工试验回路 2011 年初完成方案设计，2011 年 10 月开始设备安装，2012 年 1 月完成安装工作。2012 年 2 月完成系统的调试运行，后期主要开展 HTS 回路系统的运行技术研究及热工水力特性测试。全年总计运行超过 1600 h，获得了回路运行技术经验，完成了 HTS 熔盐的热工实验

数据测试，为 FLiNaK 熔盐高温试验回路的设计提供了重要的技术参考。

HTS 熔盐热工试验回路

表 1　HTS 熔盐热工试验回路系统参数

类别	系统参数
熔盐介质	KNO_3-$NaNO_2$-$NaNO_3$ (53-40-7 mol%)
结构材料	Incolnel 600
运行温度/℃	250–450
系统压力/MPa	＜0.5
熔盐流量/$m^3 \cdot h^{-1}$	＜2

2.2　FLiNaK 熔盐高温试验回路

FliNaK 盐（LiF-NaF-KF/46.5-11.5-42 mol%）是 FliBe 熔盐的模拟体系，其熔点、密度、热容、热导和腐蚀性等与熔盐堆使用的 FliBe 熔盐体系十分接近，由于不含铍，毒性相对较低。建造 FliNaK 熔盐高温试验回路，目的在于研究和解决熔盐回路及其相关设备的耐高温和耐氟盐性能，开展高温氟盐流动特性(流速、压力损失)和传热特性(换热系数、换热面积、换热损失) 研究，为关键设备性能试验、氟盐除氧净化试验以及控制、安全联锁、安全防护改进等提供研究平台。

本组承担完成 FLiNaK 熔盐高温试验回路机械系统工程设计及设备跟加工。该机械系统包括熔盐循环系统、存储系统和钢平台。熔盐循环系统由循环泵，加热器，空气散热器，管道，保温和预热(伴热)设备、支承件等组成。熔盐由循环泵驱动进入加热器，经加热升温达到出口温度，然后进入换热器，经冷负荷降温释放热能，冷却后的熔盐再进入加热器升温，实现熔盐回路的循环。熔盐存储系统由储罐、冷冻阀(兼安全阀)、液位计、压力计、气压计、加热和保温等设备组成，其主要作用是：a)系统运行前，将固态盐加热熔融为液态熔盐，经气压输送至熔盐循环系统；b)系统停机后，全部熔盐流回储罐，防止熔盐在回路中凝固；c)在紧急情况下，如发生运行故障、系统过热、断电等情况，要求冷冻阀自动打开，熔盐可以在重力下自动流回储罐中。

表 2　FLiNaK 熔盐高温试验回路系统参数

类别	系统参数
熔盐介质	LiF-NaF-KF(46.5-11.5-42 mol%)
结构材料	哈氏 C276
运行温度/℃	500~650
系统压/MPa	＜0.5
熔盐流量 $m^3 \cdot h^{-1}$	＞5

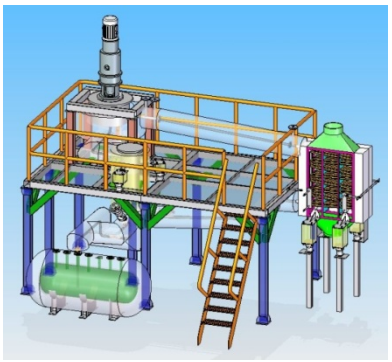

FLiNaK 熔盐高温试验回路三维设计图

至 2012 年底，FLiNaK 熔盐高温试验回路机械系统已完成加工，回路钢平台已完成安装。

2.3　熔盐泵

回路组与桂林市广汇泵业有限责任公司联合研制了高温熔盐泵。该熔盐泵应于于 FLiNaK 熔盐高温试验回路。设计最高使用温度 650℃，流量>5 $m^3 \cdot h^{-1}$，过流部件材料采用哈氏 C276 合金，设计额定转速为 1180 rpm，扬程 20 m。该泵为立式悬臂离心泵，轴承采用自润滑形式，轴封采用干气密封形式。该泵为国内首台高温密封氟盐泵。于 2012 年 12 月完成加工制造、装配及水力测试。

冷冻阀利用“非能动”设计理念通过熔盐的“冷却-凝固/加热-熔融”原理实现阀的开启与关闭。采用硝酸盐作为媒介，通过多个循环及改变加热速率和冷冻速率等措施，至 2012 年底完成冷冻阀关闭时间、开启时间、温度分布等实验规律测试。

FLiNaK 熔盐高温试验回路熔盐泵三维效果图冷冻阀

冷冻阀三维设计及加工实物图

本组还完成了机械阀、冷冻法兰等回路设备的研制；协同设计院完成了回路熔盐存储设备的工程设计；完成了熔盐泵水力试验台架设计。

3 高温合金熔盐腐蚀研究进展

高温腐蚀是 TMSR 结构合金面临的重大问题之一。本组承担对包括 Hastelloy N 合金在内的多种候选合金的高温熔盐腐蚀性能的评估与腐蚀行为的研究。2011–2012 年度的工作任务是筛选商用合金，并对国产 Hastelloy N 合金进行熔炼工艺的腐蚀评定。

3.1 静态腐蚀测试平台的建立

静态浸泡是腐蚀测试的常用手段。高温熔盐浸泡实验对设备、耗材、环境的要求极为苛刻。我们立足自身，借鉴国际先进经验，建立了完善的静态腐蚀测试平台，并形成了极为严格的测试作业流程，确保数据的可靠性与重复性。

静态腐蚀测试平台与测试流程(排 1 左：盐锭&盐块&石墨容器；排 1 右：用于熔盐破碎、烘烤、封装的手套箱；排 2 左：装好盐块和样品的 Capsule；排 2 右：手套箱内 Capsule 焊接；排 3 左：准备加热腐蚀的 Capsules；排 3 右：高温取出 Capsule；排 4 左：高温 Capsule 倒置，样品脱盐；排 4 右：Capsule 切割)

3.2 合金腐蚀性能排序与筛选

对进口 Hastelloy N、Hastelloy C276、Haynes 242、Inconel 600、316 SS 等商业合金进行腐蚀性能排序，发现合金的腐蚀性能与铬(以及铁)含量密切相关，含量越高，腐蚀性能越差。综合考虑后，选定 Hastelloy C276 作为 FLiNaK 热工回路的结构合金。

另外，对 5 种工艺的国产 Hastelloy N 合金进行腐蚀性能评定，发现影响合金腐蚀性能的最关键因素为合金组分。

3.3 镍基合金的腐蚀机理的研究

迄今为止，国际上对于镍基合金在燃料盐中的腐蚀机理的认识，已达成共识。不过，对于在冷却剂盐中的腐蚀机理的认识尚不深入。我们通过对腐蚀产物的显微表征，发现镍基合金在 FLiNaK 熔盐中的腐蚀产物为复杂的复合离子化合物 K_3MF_6、K_2NaMF_6 和 KMF_3。合金基体内部析出 M_6C 碳化物，以及少量的 $Cr_{23}C_6$ 化合物。这有利于从热力学角度，推导出腐蚀机理以及腐蚀反应的平衡浓度，为 Hastelloy N 在熔盐的腐蚀总量估算提供依据。

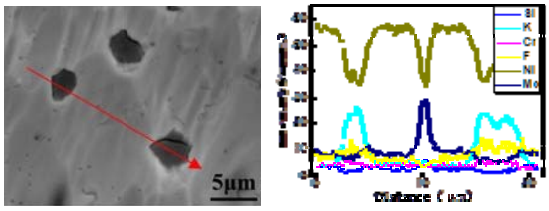

(a) (b)

700 ℃、 400 h N 合金在 FLiNaK 熔盐中腐蚀后 SEM 观察 (a)腐蚀形貌；(b) 元素分布

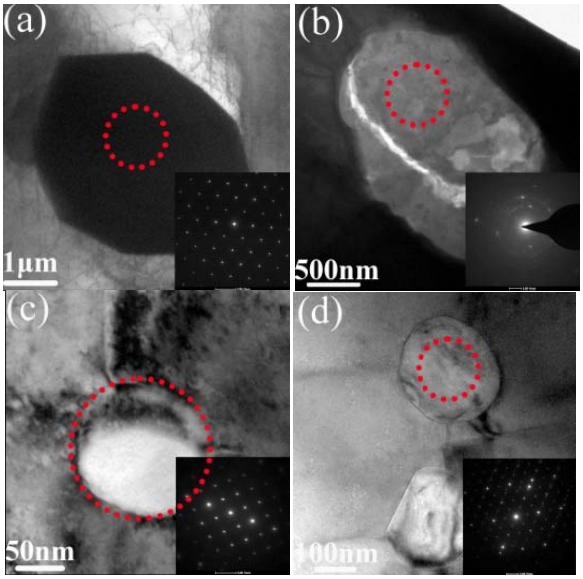

图 1 N 合金在 FLiNaK 熔盐中腐蚀后 TEM 观察(a)富 Mo 析出相；(b)腐蚀产物；(c)腐蚀产物；(d) 富 Cr 析出物

图 1 中对 Hastelloy N 腐蚀后的表面形貌及成分分布进行了 SEM 观察和表征。从图中可以看出，腐蚀后表面产生了腐蚀坑，元素分布表明，腐蚀坑内富集 K 和 F。在腐蚀坑周围，存在富 Mo 的析出相。对腐蚀产物的 TEM 观察结果如图 1 所示。图 1(a)中给出了富 Mo 析出相的形貌和衍射图，结合成分和衍射结构的分析，富 Mo 相主要为 M6C。图 1(b)中给出了腐蚀产物的形貌和衍射结构，对多晶衍射环进行分析，结合面间距计算和能谱的成分分析，腐蚀产物的结构与 K_3MoF_6、K_3FeF_6、K_3CrF_6、K_2NaCrF_6、K_2NaNiF_6 和 K_2NaMoF_6 等相符。因此，腐蚀产物主要为复杂的 K_3MF_6 和 K_2NaMF_6 复合化合物。图 1(c)和图 1(d)所示的近似球形的析出相，经分析主要为为 KMF_3 腐蚀产物(图 1c)和 $Cr_{23}C_6$ 析出碳化物(图 1d)。

参考文献

1. 于平安, 朱瑞安, 等. 核反应堆热工分析. 北京: 原子能出版社, 1986
2. 朱聘冠. 换热器原理及计算. 北京: 清华大学出版社,1987
3. 史美中, 王中铮. 热交换器原理与设计, 南京:东南大学出版社, 2009
4. 钱颂. 换热器设计手册; 北京: 化学工业出版社, 2002
5. 姚玉英. 化工原理(上册). 天津: 天津大学出版社, 2003
6. Robert W. Bradshaw and Nathan P. Siegel. Molten nitrate salt development for thermal energy storage in parabolic trough solar power systems. Energy Sustainability, 2008, **8(**10): 1-7
7. Janz G J, Truong G N. Melting and premelting preoperties of the KNO_3-$NaNO_2$-$NaNO_3$ eutectic system, Journal of chemical and engineering Data, 1983, **28**: 201-202
8. 陶文铨, 传热学. 西安: 西北工业大学出版社, 2006

Annual report of Molten Salt Chemistry and Engineering

ZUO Yong YU Guojun FU Yuan TANG Zhongfeng LI Yulan XIE Leidong

Department of Molten Salt Chemistry and Engineering

1 Molten Salt Chemistry

To obtain qualified fluoride salt reactor coolant, our molten salt chemistry research group should master the skill of the preparation, purification, analysis and detection of the fluoride salts. In the year of 2011 to 2012, we have established research platform for molten salt chemistry as follows.

1.1 Physical Properties and Phase Diagram Lab

Physical properties and phase diagram research platform

Establish the physical properties and phase diagram research platform, including density meter, hightemperature DSC, surface tension meter, molten salt viscometer, laser thermal conductivity meter, molten salt physical properties comprehensive measurement instrument etc., possessing ability to study and measure fluoride molten salts relative physical properties.

1.2 Analytical Chemistry Lab for Molten Satls

Molten Salts Analytical Chemistry Lab.

Establish the molten salts analytical technologies such as ICP-OES, ion chromatography, potentiometric titratoretc, and some conventional chemical analysis technologies including weight method, volumetric method etc.Possess the ability to analyze and measure components and impurities in FLiNaK molten salt.

1.3 Molten Salts Purification Lab

Establish the molten salt purification research instruments including HF-H2 purification system, electrochemical purification devices, molten salt water analyzer, and molten saltoxygen analyzer. Possess the ability to purify the fluoride molten salts by chemical and electrochemical methods. For the electrochemical purification process, a FLiNaK product with oxygen content of 100 ppmwas achieved. And the life of molten salt reference electrode developed by us was over 200 h.

Molten Salt Purification Lab

2.2 Molten Salt Loop

This team devotes to the research& development of molten salt loops and their key equipments. Technological experience is obtained through the design, construction and commissioning of the HTS thermal test loop and FLiNaK high temperature test loop. Key equipments, such as molten-salt pump, freeze valve were designed for the loop's functional operation. A series of thermal and mechanical research were conducted to provide the basis for TMSR loop design, construction and operation.

So far, the HTS thermal test loop has successfully fulfilled the design objects and conducted long-term operation for thermo-hydraulics tests within stipulated time and funds.As for FLiNaK high temperature test loop, physical and engineering design was completed on schedule, and the fabrications of major equipments were finished as well. Tests and verifications of system parameters for key equipments and prototype instruments were completed on schedule and on budget. Design objectives were achieved.

2.1 HTS thermal test loop

The HTS thermal test loop consists of circulating pump, main heater, radiator, interconnecting piping, valves, test section, thermal insulation and heaters, and measuring instruments, etc.

The centrifugal pump transfers molten salts to main heater (simulating reactor) where they are further heated and then flow directly to the circulating pump. Salts discharged by the pump flow through the radiator where they are cooled down (simulating conventional island), and then flow back to the main heater to complete a circulation. The thermohydraulic test is conducted on this

loop.

HTS thermal test loop.

The design of HTS thermal test loop was completed in early 2011, fabrication started in October 2011 and completed in January 2012. The HTS loop commissioning was completed in February 2012. Later, researchemphasis was mainly focused on operation and thermohydraulic test. Experience was obtained as HTSloop yearly operated for more than 1600 hours. Thermohydraulic test was completed, which provided technical reference for the design of FLiNaK high temperature test loop.

Table 1 System parameters of HTSthermal test loop

Category	System parameters
Salts composition	KNO_3-$NaNO_2$-$NaNO_3$ (53-40-7 mol%)
Structure material	Incolnel 600
Operation temperature	250–450℃
System pressure/MPa	＜0.5
Flow /m^3• h^{-1}	＜2

2.2 FLiNaKmolten salt high temperature loop

FLiNaK(LiF-NaF-KF/46.5-11.5-42 mol%) salt has thermophysical properties very similar to those of FLiBe and is therefore an excellent simulant salt system for FLiBe salt. However, it eliminates the safety issues associated with berylliumcontaining materials, making testing much less restrictive. Construction of FLiNaK high temperature test loop aims to examine high temperature resistance and corrosion resistance of loop and major equipments, and to study flowing properties and heat transfer charactors of fluoride salt, providing research platform for key equipments, fluoride salts purification, and for the system improvement of control, interlocking and safty protection.

This team is responsible for the design of the system and supervision of key equipmentsfabrication. FLiNaK test loop consists of molten salts circulating system, storage system, gas circuit system and steel platform. Molten salts circulating system consists of circulating pump, main heater, air radiator, interconnecting piping, thermal insulation and heaters, and supports, etc.The centrifugal pump transfersmolten salts to main heater (simulating reactor) in which they are further heated, and then flow directly to the circulating pump. Salts discharged by the pump flow through the radiator where they are cooled down (simulating conventional island), and then flow back to the main heater to complete a circulation. Molten salts storage system consists of storage tank, freeze valve (safety valve), level indicators, pressure-gages, heating and insulating devices. The functions of the salts storage system are as follows:

Before operation, FLiNaK salts are pre-heated and moved to circulating system by pressurized argon.

After system shutdown, all the molten salts flow back to storage tank in order to avoid salts solidfication.

In an emergency, for instance, operation faults, system over-heating and power off, freeze valve will be automaticly thawed to make sure the salts flow back to tank by gravity.

Table 2 FLiNaKmolten salt high temperature test loop system parameters

Category	System parameters
Salts composition	LiF-NaF-KF (46.5-11.5-42 mol%)
Structure material	HASTOLLEY C276
Operation temperature	500–650℃
System pressure/MPa	＜0.5
Flow /m^3• h^{-1}	＞5

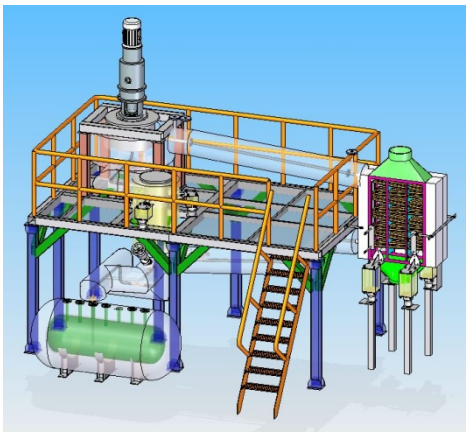

The 3D model for FLiNaK molten salt high temperature test loop.

By the end of 2012, the fabrication of FLiNaK high temperature test loop and the construction of the steel platform had been completed.

2.3 Molten salt pump

As the first high temperature sealed fluoride molten salts pump in china, this pump is jointly developed by this team and GUILIN GUANGHUI PUMP CO., LTD. This pump was applied in FLiNaK loop. In the design, the highest operation temperature was 650℃, the flow was >5m3/h, the head was 20m, the rated speed was 1180rpm. The

flow passage componentswere made up of HASTELLOY C276. The pump has a vertical shaft and an overhung impeller which are equipped with self-lubricated ball bearings and dry-gas shaft seal. Fabrication, assembling and hydraulic tests of the pump were completed in December 2012.

The 3D model for FLiNaK loop molten salt pump.

2.4 Freeze Valve

Freeze valve, which has no moving parts, is controled by freezing and thawing the salts plug in a specially fabricated pipe. Nitrite salts are used as medium in the valve. By the end of 2012, tests of valve open, close, and temperature distribution had been completed through multiple cycles and various heating-cooling rates tests.

The 3D model and pictures of freeze valve.

In addition, this team also developed equipments such as mechanical valve and freeze-flange and designed the molten salts hydraulic test bench. It also co-designed the molten salt storage equipments with the design institute.

3 Molten Salt Corrosion in Superalloy

High temperature corrosion is the most challenge for structural materials and components in TMSR. The corrosion group was committed to the assesement and investigation of high temperature molten salt corrosion behavior for several candidate materials, especially Hastelloy N alloy. In the stage from 2011 to 2012, the major task was to screen the commercial candidates, and to evaluate the manufacture process of domestic Hastelloy N alloy by corrosion testing.

3.1 Construction of test platform for static corrosion

Static immersion was the most common method for corrosion test in molten salt. The high temperature molten salt corrosion test was demanding for test apparatus, supplies and the operating environment. We take advantage of the international working experience and improve our ability on molten salt corrosion testing. The test platform for static corrosion was completely constructed. Moreover, the rigorous conducting process for corrosion test was formed to make sure the reliability and repeatability of experimental results.

The test platform and operating process for static molten salt corrosion.From left to right and from top to bottom: molten salt ingot and graphite crucible; glove box for test preparation; graphite bearing small salt block; stainless steel capsule welding shut; the welded capsule preparing for testing; taking out capsule from high temperature furnace after exposure; inverting the capsule to drain out the molten salt from test coupons; cutting open the capsule after test.

3.2 Corrosion properties sorting and screening of candidate alloys

It was confirmed that the corrosion property was closely related to Cr (and Fe) content by sorting the corrosion resistance to molten salt of Hastelloy N, Hastelloy C276, Haynes 242, Inconel 600 and 316SS. The resistance to corrosion decreased with increasing Cr content. Considering the combination of such factors as cost, high-temperature strength and corrosion resistance, Hastelloy C276 was finally chosen as the structural material for thermal loop.

Corrosion tests were performed on five types of domestic Hastelloy N alloy. From these results, it was

concluded that the chemical component and microstructure were the most significant factors dominating the corrosion behavior.

3.3 Study of corrosion mechanism inNi-base alloy

Up to now,concensus oncorrosion mechanism of Ni-base alloy in fuel salt had been formed. While the fundamental understanding corrosion mechanism in coolant salt was not yet clarified. We focused on the corrosion products characterization of Hastelloy N, aiming to comprehensive understanding of corrosion process and mechanism. The corrosion products of Ni-base alloy in FLiNaK molten salt were mainly such complex compounds as K_3MF_6, K_2NaMF_6 and KMF_3 fluoride. The main M6C type and dispersed $Cr_{23}C_6$carbides were observed in the matrix after corrosion exposure. The equilibrium concentration could be derived by thermaldynamic calculation due to the comfirmation of corrosion products. The total corrosion amount of Hastelloy N in the molten salt reactor could be derived based on the equilibrium concentration.

As shown in Fig.1, EDS line scanning of the pits revealed the enrichement of F and K, and the depletion of Ni. The enrichement of Mo in the line scanning was corresponding to the precipitates in the matrix.

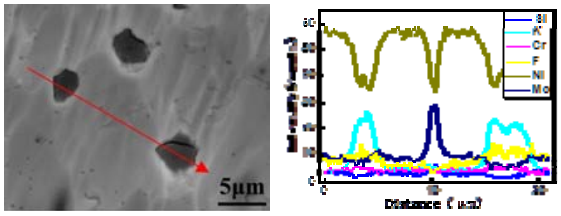

(a) (b)

Fig.1 SEM observation of Hastelloy N after corrosion tests in FLiNaK at 700℃,(a) surface plan view and (b) EDS line scanning.

The Mo enriched precipitates were observed by TEM, as shown in Fig.2a. The crystal structure and its lattice parameter of the Mo enriched precipitate was identified as M6C type carbides. In Fig.2b, the corrosion products were observed as the bright area.The corrosion product was comfirmed to be such complex as K_3MF_6 and K2NaMF6fluoride. In addition, some dispersed KMF_3 type fluoride and $Cr_{23}C_6$ carbide precipitates were observed, as shown in Fig.2c and Fig.2d.

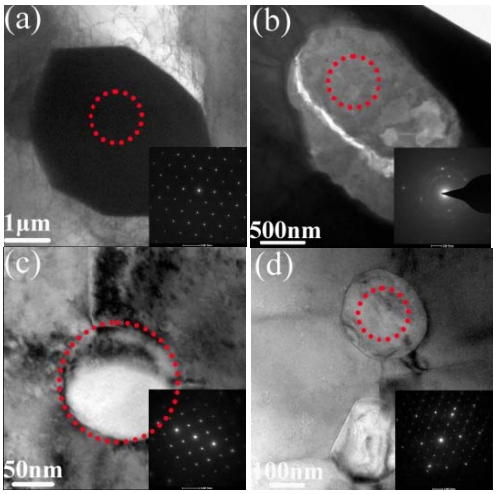

Fig.2 TEM images of Hastelloy N after corrosion tests.

References

1. YU P A, ZHURA. nuclear reactor thermal analysis. Beijing: Publishing House of atomic energy, 1986
2. ZHU P G. the principle and calculation of heater exchanger. Beijing: Publishing House of Qinghua University, 1987
3. DU M Z, WANG Z Z. the principle and design of heater exchange. NANJING: Publishing House of Dongnan University, 2009
4. QIAN S. heater exchanger design book, BEIJING: chemical industrial press, 2002
5. YAO Y Y. principles of chemical engineering, tianjin: Publishing House of Tianjing University, 2003
6. Robert W. Bradshaw and Nathan P. Siegel. Molten nitrate salt development for thermal energy storage in parabolic trough solar power systems, Energy Sustainability, 2008, **8**(10): 1-7
7. Janz G J, Truong G N. Melting and premeltingpreoperties of the KNO_3-$NaNO_2$-$NaNO_3$ eutectic system. Journal of chemical and engineering Data, 1983, 28: 201-202
8. TAO W Q, Heat transfer theory. Xian: Publishing House of Xibei industrial University, 2006

熔盐堆材料

堆材料与工程技术部　周兴泰

本部门自 2011 年成立以来，着重研发熔盐堆用结构材料。TMSR 中心钍基熔盐堆的建设需各种合格的结构材料，即制备熔盐堆构件所用的各自材料，如制备堆芯容器、回路管道所用的特种合金，制备慢化体所用的核石墨等。目前，国内尚没有能满足熔盐堆建设所用的特种合金和核石墨，需自行研制或从国外进口。同时，现阶段即便从国外进口的专用材料也需另外积累足够的数据，建立各种材料的数据库方能得到这些材料的进堆使用许可。我们的研究内容一方面为材料获取、材料加工、材料数据库的建立，另一方面为材料研发能力的建设。

合金结构材料

合金结构材料的 5 年总目标：为 2 MW 固态熔盐堆提供反应堆所用的合格的合金结构材料和部件。总技术路线为进口和自行研制两条路线并行推进，并探索合金的各种加工工艺。2011–2012 年，我们推进了 Hastelloy N 合金的进口；放大了自主研制的 GH3535 合金的冶炼规模，探索了研制合金的制备、加工工艺，进行了合金的高温热力学性能测试等。我们和金属所相关研究组合作，经过小试，中试，现采用双联工艺制备了重量达 1 t 的 GH3535 合金料，图 1 为本次合金锭的自耗锭。

图 1　直径 360 mm 合金 GH3535 自耗锭

实验室进行了 GH3535 合金热轧板、冷轧板(见图 2)、棒材和丝材加工工艺探索和优化，在实验室制备出合金无缝管材(见图 3)、焊丝和棒材，这些材料达到了美国汉斯公司材料指标。进行了合金板焊接试验，包括对接焊缝、板材角焊缝、管材角焊缝等。

图 2　合金 GH3535 冷轧板(4 mm×950 mm×2000 mm)

图 3　合金 GH3535 无缝管成品

核石墨

核石墨的 5 年总目标：为 2 MW 固态熔盐堆提供合格的反应堆中子慢化体材料和构件。总技术路线也是进口和自行研制两条路线并行推进。2011–2012 年，我们推进了首选核石墨材料-IG110 的进口；确定了备选核石墨材料-国产方大石墨(NG-CT-10)。对 IG110 进行了系统的评估并进行了表面涂层的研究工作，完成了 2012 年高温回路所用的加热石墨球的筛选和加工，进行了燃料球石墨的评估。

我们在 10 atm 的压强下对不同的牌号及尺寸的石墨进行 FLiNaK 盐的浸泡。在此条件下 FLiNaK 盐在 IG-110 中的最大浸渗量约为 15 wt%，在国产的 NG-CT 石墨中的最大浸渗量为 10.2 wt%，在石墨球基体石墨中的最大浸渗量为 13 wt%。由于 FLiNaK 盐与石墨的接触角约为 90°，而 FLiBe 盐与石墨的接触角约为 147°，因此 FLiNaK 盐对石墨的浸渗实验可用于评估 FLiBe 盐在石墨中的最大浸渗量，FLiBe 盐在各种石墨中的浸渗量将远小于这个值。根据回路加热要求，选取了适当的商用石墨并探索出回路感应加热用石墨球(见图 4)的加工工艺，并对其相关性能进行了检测，各项指标均达到要求。

图 4　高温回路所需的石墨球

碳基材料

碳基材料包括碳基复合材料(C/C、SiC/SiC)和

烧结 SiC 陶瓷材料。尽管碳基材料不是熔盐堆建设的主体材料，但它们作为潜在的高温反应堆材料受到极大的重视。碳基材料 5 年总目标为探索它们在 2 MW 固态熔盐堆中应用的可能性，并制备部分小型、简单的回路部件。2011–2012 年，我们对复合材料的特性进行了系统的研究，制备出 Φ38×440 mm C/C-SiC 熔盐管道器件(见图 5)，完成了 2012 高温回路中 SiC 烧结陶瓷加热罐构件的制备和加工(见图 6)。

图 5 C/C-SiC 熔盐管道

图 6 高温回路 SiC 加热罐

材料进堆服役性能评估

在调研的基础上确定主要堆用材料现有的数据以及按 ASME 标准材料进堆仍需通过测试获取的数据。在现有条件下对材料进行了部分性能测试，制定了材料进堆辐照计划，开展了材料在服役环境中结构/性能演化的理论模拟。根据 2 MW 固态熔盐堆的设计方案，分析了熔盐堆内各构件所用材料服役的高温、强腐蚀以及强辐照环境，在此基础上，对冷却剂氟化盐、合金结构材料以及核石墨 3 大类材料在堆内的服役行为进行全面的分析(见图 7)。对堆用主要材料的熔盐腐蚀行为进行评估，并制定了它们的进堆辐照计划及辐照后各种材料样品的测试项目。

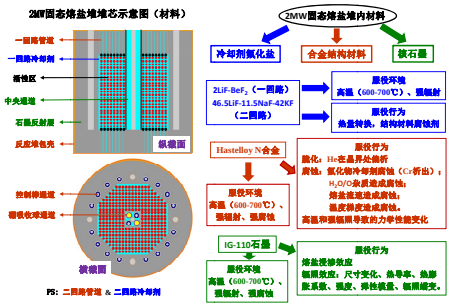

图 7 2 MW 固态熔盐堆服役环境与服役行为分析示意图

实验室建设

2011–2012 年，已完成多台设备的购置或研制，如完成了拉伸试验机、疲劳试验机、蠕变试验机、冲击试验机等设备的购置、安装、调试和验收，组建了材料力学性能测试平台；完成了 XRD、直读光谱仪、质谱分析仪、金相显微镜等设备的购置；专门设计了适用于高温熔盐静态腐蚀测试的反应釜。初步形成了堆材料评估和测试能力(见图 8–10)。

图 8 蠕变实验室

图 9 热分析实验室

图 10 熔盐腐蚀实验室

Materials for Molten Salt Reactor

ZHOU Xingtai　Department of Nuclear Materials Science and Engineering

The department of nuclear materials science and engineering was founded in 2011. Since that time, the staffs in our division have been developing the materials for Th- based molten salt reactor (TMSR). TMSR components are made of materials, for instance, the reactor container and tubes are made of a special Ni-based alloy (Hastelloy N alloy), and the reactor reflector of nuclear graphite. Currently, there are commercially available Hastelloy N alloy but not nuclear graphite for the construction of TMSR. In addition, either Hastelloy N alloy or nuclear graphite　has not been allowed to be exported to China due to the sensitivity of the nuclear materials. Now, we are trying to get the above materials in two ways for the fabrication of the TMSR components. One is to apply for the export and import permit so that we can order the materials in the international market; the other is to develop home-made materials for the TMSR. So, the duties of our division are: a) the acquisition of the materials and the fabrication of the components, b) the collection of the data for the licensing of the materials, and c) the establishment of the platform for the nuclear materials analysis.

Alloy

The 5 years' target about the alloy is to provide the alloy products with various sizes and the components made of the alloy for the construction of TMSR. We have been trying to get the alloy products in two ways (to order the commercially available alloy-Hastelloy N products from US and to develop home-made alloy-GH3535) and to develop the fabrication techniques for these alloys. In 2011 and 2012，we are still applying for the export and import permits from US and Chinese governments, respectively. The home-made alloy GH3535 was developed successfully in Institute of Metal Research (IMR), and now the alloy ingot (Fig.1) with weight of more than 1000kg can be prepared.

Fig.1　An alloy GH3535 ingot with diameter of 360 mm.

Fig.2　A rolled alloy GH3535 plat with size of 4 mm×950 mm×2000 mm.

We also developed the rolling and welding techniques for the alloy GH3535 and prepared the rolled alloy plats (Fig.2), rods, wires and tubes. The quality of all these alloy products is pretty good and their properties are comparable to those of the commercial Hastelloy N alloy.

Fig.3　Alloy GH3535 tubes prepared.

Nuclear graphite

The 5 years' target about the nuclear graphite is to provide the nuclear graphite products with various sizes and the components made of nuclear graphite for the construction of TMSR. Similarly to the alloy, we have been trying to get the nuclear graphite products in two ways (to order the commercially available nuclear graphite products from other countries or to develop home-made nuclear graphite) and to develop the fabrication techniques for the nuclear graphite. In 2011–2012, based on the evaluation of various commercial nuclear materials, we chose IG110, a commercial nuclear graphite made in Japan, as the preferred TMSR reflector candidate material, while a home-made graphite, NG-CT-10, as the alternate reflector candidate material. We also finished the selection of the graphite used as the heating component of a FLiNaK loop and the fabrication of the graphite balls (Fig.4).

We focused on the compatibility between the nuclear graphite we selected and fluoride salts. As FLiBe has not been available in our lab so far, FLiNaK was used as molten salt currently. The penetration of FLiNaK (pressure: 1MPa, temperature: 700℃) into graphite products was analyzed. The quantities of FliNaK into IG110, NG-CT-10, and heating ball graphite are 15 wt%, 10.2 wt% and 13 wt%, respectively.

Fig.4　Graphite heating balls prepared.

Cabon-based materials

Carbon-based materials on which we are focusing include composites (C/C、SiC/SiC) and sintered ceramic (SiC). They can be used as TMSR components because of their excellent properties at high temperature. Actually, Carbon-based materials are looked as next generation materials of TMSR, especially when the working temperature of reactor becomes higher. The 5 years' target about the carbon-based materials is to make sure that they can be used in TMSR and further to provide some simple components with smaller size made of composites for the construction of TMSR. In 2011 to 2012, we have been trying to prepare a few small components made of the above carbon-based materials, for example, a molten salt tube made of C/C composite (Fig.5) and a heating pot of sintered SiC (Fig.6).

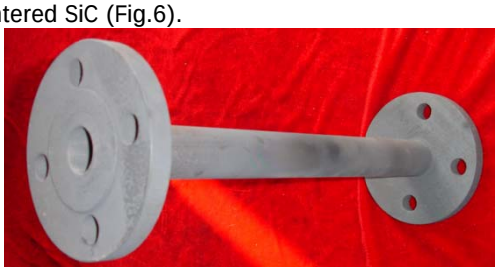

Fig.5 A C/C composite tube prepared (38 mm×440 mm).

Fig.6 A pot made of sintered SiC.

Evaluation of the TMSR materials

We have collected all the data in literature and further figured out the data we should get by ourselves by conducting experiments based on the ASME standards for all TMSR materials. Actually, we did the measurements of some properties of the materials (The anti-corrosion behavior of the alloy, for example) and scheduled the neutron irradiation experiments for the alloy and nuclear graphite. The TMSR environments (High temperature, strong corrosion and radiation) for all materials and components are analyzed closely (Fig.7) and the simulation about the evolvement of some materials in the TMSR environments is also did.

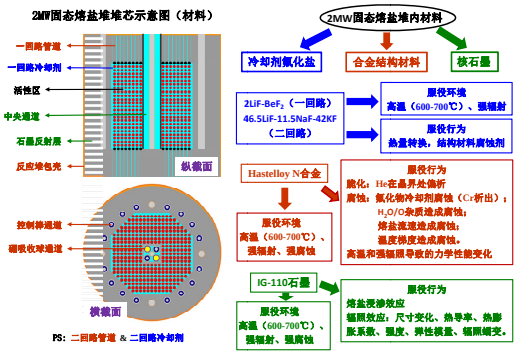

Fig.7 Environments for materials in the 2 MW TMSR.

Establishment of the labs for materials analysis

In 2011–2012, we bought or developed some facilities employed to do the evaluation of the TMSR materials, for example, tensile testers, fatigue testers, creep testers and impact testers for the measurement of the mechanical properties of materials, a thermal expansion tester and a thermal conductivity tester for the measurement of the thermal properties of materials, optical microscopies, mass spectrographs and a x-ray diffraction system for the structural analysis of materials. A special system used to do the analysis of the static corrosion behavior of materials in molten salts was also developed. Some labs for the TMSR materials analysis are established (Fig. 8 to 10).

Fig.8 Lab for creep test.

Fig.9 Lab for thermal properties analysis.

Fig.10 Lab for molten salt corrosion evaluations.

先进反应堆材料的开发和性能测试

堆材料与工程技术部　怀 平

反应堆材料在核能的发展中处于关键地位，由于裂变核反应堆运行于极端苛刻的服役环境，要求选取的材料不仅需要优异的高温强度与可加工性，更重要的是具备优良的耐中子辐照和耐腐蚀性能。熔盐堆是第四代反应堆中唯一采用液体燃料的堆型，堆材料长期工作于高温、中子辐照、熔盐腐蚀多重极端环境中，对材料性能提出了极高的要求。

TMSR 中心建设了综合性的材料制备/加工平台、评估/测试平台，现已具备了国内领先的镍基合金实验室、核石墨实验室等一系列堆材料研发平台(见图 1)，形成了高温镍基合金、高致密核石墨的研发、测试、生产能力。

图 1　熔盐堆材料平台各实验室

TMSR 中心建立完备的熔盐堆材料辐照研究平台。基于 4 MV 加速器新建了 1 台专用辐照装置，以研究 TMSR 堆材料的辐照效应。该装置可用于多种核材料，如合金、核石墨、SiC 等。辐照损伤速率 10^{-8}–10^{-3} dpa·s^{-1}，辐照温度从液氮温度到 950ºC。整个装置的辐照剂量、辐照均匀性、辐照温度都可控，为堆材料辐照测试提供支持。

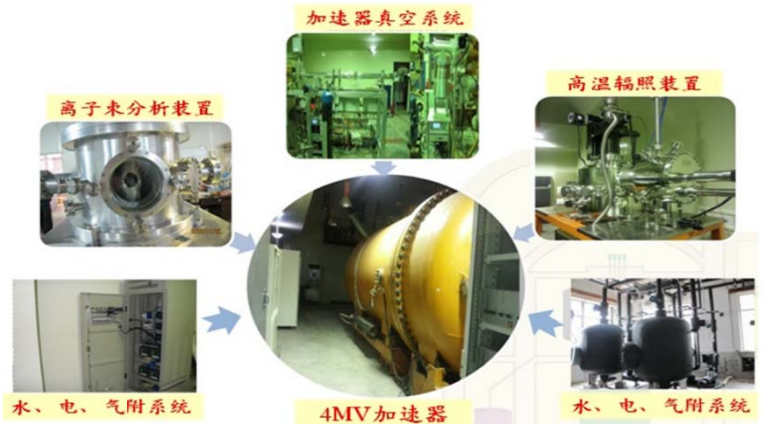

图 2　4 MV 加速器及离子束辐照平台

TMSR 中心运用先进的材料研究手段制备适合熔盐堆的成熟工程材料，探索改进或提升现有的熔盐堆材料的可行途径。已自主研发出了用于熔盐堆的国产 GH3535 合金材料、用于液态燃料熔盐堆的高致密核石墨，并在基础研究中也获得了材料微观结构、辐照损伤机理等成果。

合金材料

现有熔盐堆采用的成熟结构材料仍是上世纪 60 年代美国橡树岭国家实验室研发的 Hastelloy N 高镍合金，使用温度上限为 700℃。TMSR 中心自

主研发了用于熔盐堆的国产高温镍基合金-GH3535 合金材料(见图 3)，其性能达到和进口 Hastelloy N 合金相当的水平，目前已完成小试、中试(吨级)，已具备大规模生产的条件。

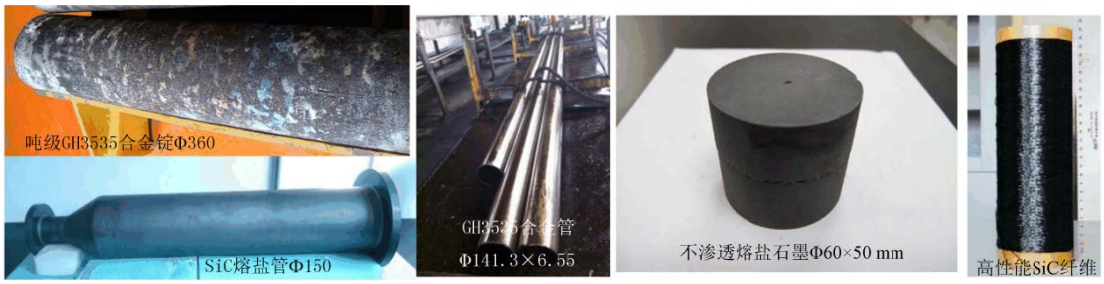

图 3　TMSR 中心研发的熔盐堆材料

TMSR 中心针对 GH3535、Hastelloy N 合金的腐蚀、辐照性能展开了研究。研究母材、不同焊后热处理、塑性变形、焊丝、单双面焊接等工艺对腐蚀行为的影响，获取焊接接头不同区域的腐蚀形式，并且发现对于氩弧焊和激光焊，材料表现出完全不同的区域腐蚀程度排序。对于合金的耐辐照性，首先在室温下对钍基熔盐堆中候选合金结构材料 Ni-Mo-Cr 合金进行了能量为 132 MeV 的 $Ni10^{+}$离子辐照研究。结果表明: 离子辐照损伤的峰值出现的深度介于 8.1–12.3 μm 之间，也发现了辐照产物 Te 对纯镍的表面形貌及内部晶界的影响。此研究填补了目前关于高温镍基合金的辐照、腐蚀性能研究的空白。

核石墨

TMSR 中心自主研发了用于液态燃料熔盐堆的高致密核石墨，具备防止熔盐渗透能力(见图 3)。采用 X 射线衍射及拉曼的方法研究熔盐对石墨的浸渗问题，发现熔盐浸渗对石墨的堆叠有序度的增强作用，这是由于熔盐与石墨膨胀率的差别而产生的压应力所导致，此压应力减小了石墨层间距的波动以及消除了石墨中部分的微裂纹，从而增加了石墨的堆叠有序度。探索和改进现有核石墨的研究中，成功制备了石墨烯掺杂的核石墨并进行测试[1]，结果表明掺加石墨烯起到润滑作用，提高原料混合均匀性、生坯热导率、成品率和成品热导率。发现当石墨烯掺入量 0.8 wt.%时，成品热导率可以达到 120.4 W/m·K，从而较好的调制材料的导热性能。

复合材料

TMSR 中心立足于成熟的熔盐堆材料,同时探索研发具备更高工作温度及耐辐照、腐蚀能力的新型结构材料，系统化地开展纤维增强陶瓷基复合材料的研究。在目前国际核能材料界备受关注的 SiC/SiC 复合材料的熔盐堆应用中，中心自主研发了高质量的 SiC 纤维(见图 4)，其力学性能等各项指标到了美、日等国商用的水平，为 SiC 复合材料的研制奠定了基础。针对复合材料在熔盐堆中的应用，与上海硅酸盐研究所合作成功研制出 SiC/SiC 复合材料热交换器板和 SiC 陶瓷热交换器板。由国防科大第一代纤维编织成的 SiC/SiC 复合材料在熔盐中出现腐蚀，熔盐中的 Si 元素含量明显增加，且复合材料中的 SiC 纤维被熔盐明显腐蚀。国防科大、厦门大学、SINAP 的 SiC 纤维进行的静态熔盐实验显示，厦门大学和 SINAP 的 SiC 纤维未被熔盐明显腐蚀，优于国防科大第一代 SiC 纤维。

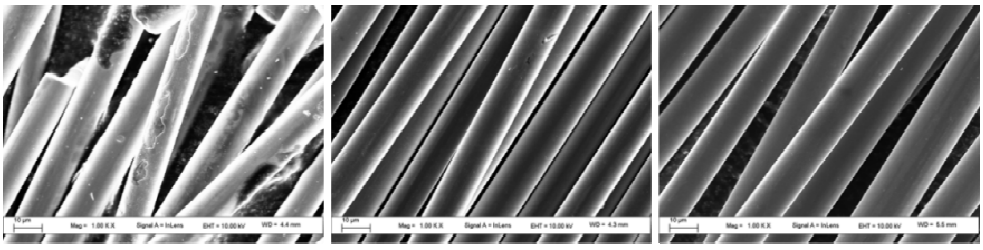

图 4　SiC 纤维的 FLiNaK 熔盐腐蚀(700ºC)结果

材料理论研究

材料理论研究的对象是 TMSR 系统工程与核心技术研发中提炼出的关键科学问题，重点是新型核燃料、干法化学分离，新型熔盐与结构材料，以及材料与熔盐的相互作用等。材料物理组建立了熔盐堆材料的多尺度模拟计算方法，实现了基于超级计算平台计算的堆材料性能的初步预测。

采用 DFT 理论对包含铀的富勒烯材料 U2@C61 系统进行了结构特性研究，发现其成键特性来自于 U 原子与存在于富勒烯表面的缺陷 C 原子共同自旋极化的贡献，U 原子上的单占据电子与 C61 富勒烯上缺陷附近的单占据电子发生铁磁耦合作用[2]。在此基础上研究了 UC2 与石墨之间作用的化学吸附特征[3]。

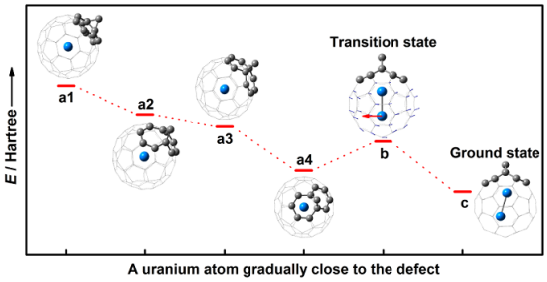

图 5 内含式铀富勒烯缺陷结构 $U_2@C_{61}$

采用分子动力学的方法模拟不同组分的 Ni-Fe 合金中 PKA 能量为 10 keV 的辐照级联过程，揭示缺陷演化过程是原子离位能和缺陷形成能共同作用的结果[4]。并将此研究拓展到 Ni、Mo 金属以及 Ni-Mo 二元合金，分析辐照温度以及 PKA 能量对级联结果的影响。

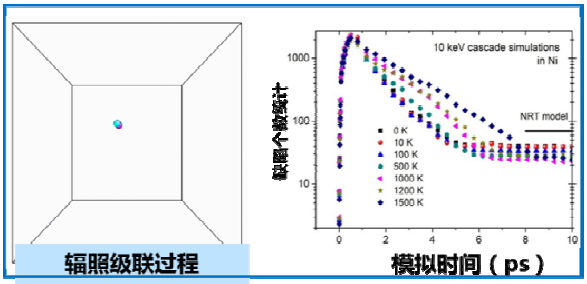

图 6 镍基合金辐照缺陷演化规律

考虑合金与辐照产物的作用，系统研究了氦泡在近镍表面的释放机制，获得了氦泡释放与温度/浓度的关系。为了初步考察合金与氟盐的作用，研究氟原子在金属镍表面及铬掺杂镍表面的行为，结果表明，氟与铬原子的结合可使其更易从镍的表面析出[5]。

参考文献

1. Ding G. Q, *et al.* Carbon, 2013, **53**: 321
2. Dai X, *et al.* Scientific reports, 2013, **3**: 1341
3. Han J, *et al.* J Phys Chem C, 2013, **117**: 26849
4. Wang C B, *et al.* Nucl Inst Meth B, 2014, **321**: 49
5. Wang S, *et al.* Applied Surface Science, 2014 **292**: 488

The Development and Performance Testing of Advanced Nuclear Reactor Materials

HUAI Ping　Department of Reactor Materials and Engineering

Reactor materials play a key role in the development of nuclear energy. Since nuclear fission reactors operate in extremely harsh environment, nuclear materialsare required to have enough strength and workability under high temperature. More importantly, they should have-superior resistance to neutron irradiation and corrosion. In generation-IV reactors, Molten Salt Reactor is aunique one thatis based on liquid fuel. Therefore, the nuclear materials in TMSR have to work in extreme environment with high-temperature, high neutron irradiation and high molten salt corrosion, which rises a challenge for the material research.

TMSR center has established comprehensive material research platform for material preparing, machining, analyzing and testing. Up to now, a series of laboratories have been established, including nickel-based alloys and nuclear graphite research laboratories (as shown in Fig.1). We also own the capability to develop, test and product high-temperature nickel-based alloys and high-density nuclear graphite.

Fig.1　Labs of Molten salt reactor material research platform.

TMSR center has also established a comprehensive materials irradiation platform for molten salt reactor(as shown in Fig.2). Based on a 4MV accelerator, a new radiation chamber has been built for the radiation effects of TMSR material. The device can be used to test a variety of nuclear materials, such as alloys, nuclear graphite, SiC, etc. The irradiation damage rate is 10^{-8} to 10^{-3} dpa$\cdot s^{-1}$, and the irradiation temperature ranges from liquid nitrogen temperature to 950 ℃. The irradiation dose, uniformity and temperature are all controllable, so as to provide support for material irradiation testing.

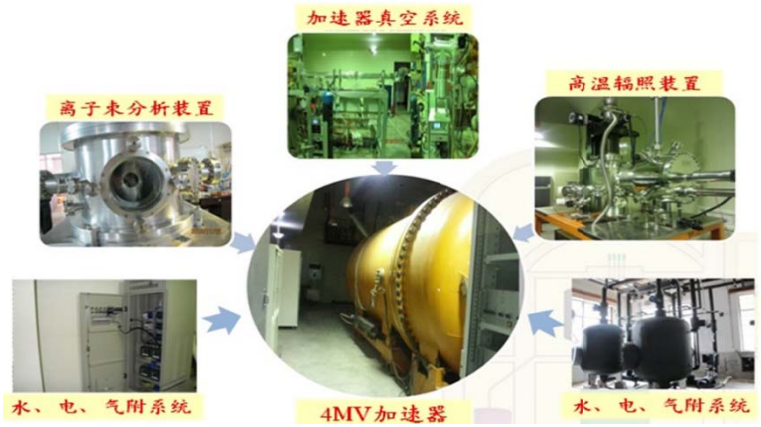

Fig.2　The 4 MV accelerator and ion beam irradiation chamber.

Using advanced materials research method, TMSR center has developed mature engineering materials for molten salt reactor, and dedicated to improve MSR materials. We have developed a domestic GH3535 alloy material for molten salt reactors and high-density nuclear graphite for Liquid Fueled Molten Salt Reactor. Furthermore, we also obtained some achievements in fund amentalresearch, such as the microstructure of material and mechanism of irradiation damage.

Alloy

The nickel-based Hastelloy N alloy developed by Oak Ridge National Laboratory (ORNL) in the 1960s, is mature structural material for molten salt reactor up to 700℃. The TMSR research center independently develops the domestic high-temperature nickel-based alloys - GH3535 alloy for MSR (as shown in Fig.3), which has equivalent performances as Hastelloy N alloy. Up to now, TMSR has completed the preparation of small & medium batch (tonnage) GH3535 alloy, and are ready for large-scale production. The TMSR research center has been investigated the corrosion & radiation resistances of GH3535 and Hastelloy N alloys. TMSR center has studied the effects of welding process, such as heat treatment, plastic deformation, welding wire, single/double-side welding etc, and the corrosion behavior of the weld. The results revealed that Argon arc welding exhibit a completely different way of corrosion compared to laser welding. As for the radiation effects of alloys, the Ni-17Mo-7Cr alloy, as a candidate structural material for Thorium-based Molten Salt Reactor(TMSR), was irradiated by 132 MeV Ni10+ ions. The micro-indentation results revealed that the peak of ion irradiation damage occur at a depth ranging from 8.1 to 12.3 μm, which is consistent with the theoretical results calculated with TRIM. Meanwhile, the research also shows corrosion by fission product Te on surface morphology and internal grain boundaries of pure nickel. The research aforementioned fills the gap in corrosion & irradiation properties of high-temperature nickel-based alloys.

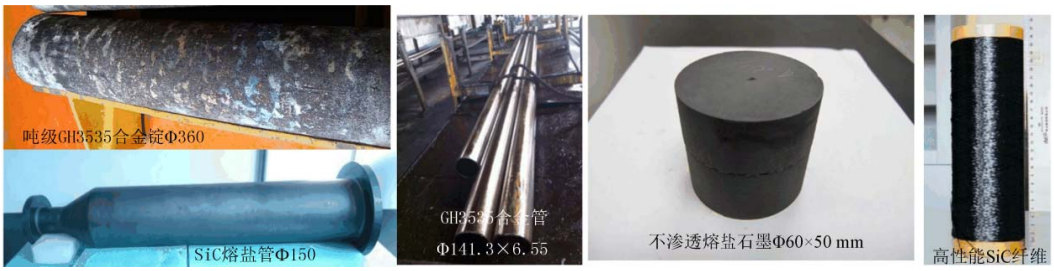

Fig.3 Molten salt reactor materials developed by TMSR center.

Nuclear Graphite

TMSR center have developeda kind of high-density nuclear graphite used in Liquid Fueled Molten Salt Reactor, which significantly reduces molten salt permeation (as shown in Fig.3). The molten salt impregnation in graphite was investigatedby using X-ray diffraction and Raman. Molten salt impregnation is induced bycompressive stress due to difference between the expansion of the molten salt and the graphite. Compressive stress reduces variation of inter-layer space and eliminates part of the micro cracks in graphite, thereby increases the degree of graphitization. In the study of novel nuclear graphite, the nuclear graphite doped graphene was developed successfully[1]. It is proved that doped graphene improves the mixing uniformity, the thermal conductivity and the yielddue to lubrication action. The graphene has elevated performance in material's thermal conductivity of 120.4 W/m.K, if graphene is dope by 0.8wt.% graphene.

Composites

We are developing Ceramic matrix composites with high temperature resistance, radiation resistance and corrosion resistance. Recently, we have fabricated SiC fiber and fiber reinforced ceramic matrix composites for molten salt reactor (SiC/SiC) (as shown in Fig.4). Our studies reveal that the SiC/SiC composite weaved with the first generation SiC fiber made by NUDT is corroded by FLiNaK salt. Further studies reveal that there is no obvious corrosion in SiC fibers made by SINAP and Xiamen University. The SiC fiber made by SINAP has similar properties as commercial SiC fibers made in US and Japan. Systematic studies on SiC fiber pave the way for the development of high quality SiC/SiC composite used in molten salt reactor. Recently, we developed SiC/SiC composite plates and SiC ceramic plates for heat exchanger applied in molten salt system.

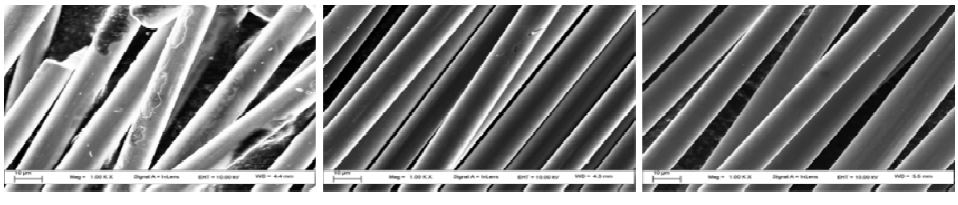

Fig.4 The corrosion testing results of the SiC fiber under FLiNaK molten salt (700 ℃).

Modelling and Simulation

Theoretical studies of nuclear material focuses on the key scientific problems in TMSR material, e.g. new advanced nuclear fuel, dry chemical separation of spent fuel, new structural materials, new molten salt, and the interactions between structural materials and salts. TMSR materials physics group has developed multi-scale simulation methods to study MSR material. Some preliminary results about nuclear material properties has been obtained base on supercomputing.

The structural properties of U2@C61 were studied by using DFT theory.U2@C61 is a fullerene system containing two uranium atoms(as shown in Fig.5). It was found the interesting properties of bonding come from the co-contribution of U atoms and spin-polarized C of the surface defects in the fullerene. Electronic structure analysis shows that the inner U atoms and the C ad-atom on the surface of the cage contribute together to this spin state. The high spin is induced by a ferromagnetic coupling between the spin of the unpaired electrons of the Uatoms and the C ad-atom[2]. Based on this study, chemical adsorption properties of the interaction between UC_2 and graphite were also investigated[3].

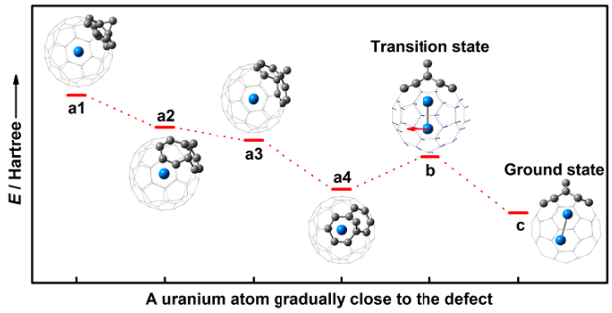

Fig.5 The structures of defective U2@C61.

The radiation cascade process of Ni-Fe alloytriggered by a 10 keV PKA was simulated by molecular dynamics simulation[4] (as shown in Fig.6).. The results revealed the evolution of defects are determined by both the defect formation energy and atomic-displacement energy. We further studied the properties of Ni, Mo and Ni-Mo binary alloys toanalyze the effect of irradiation temperature and PKA energy.

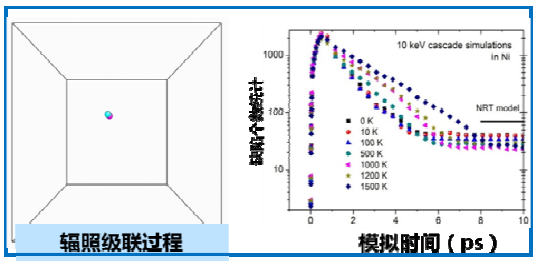

Fig.6 The evolution of radiation defects in nickel based alloy.

To understand the interaction between alloy and fission products, we systematically studied the behavior of helium bubbles near the nickel surface. In order to investigate the interaction between the alloy and fluoride salts, we studies fluorine atoms near the surface of metallic nickel/nickel-chromium-doped. The results show that the bonding of fluorine and chromium atoms may make it easier for chromium to segregation from the nickel surface [5].

Reference

1. Ding G. Q, et al. Carbon, 2013, **53**: 321
2. Dai X, *et al.* Scientific reports, 2013, **3**: 1341
3. Han J, *et al.* J Phys Chem C, 2013, **117**: 26849
4. Wang C B, *et al.* Inst Meth B, 2014, **321:** 9
5. Wang S, *et al.* Applied Surface Science, 2014, **292**: 488

钍铀放射化学研究进展

放射化学与工程技术部

放射化学与工程技术部设有钍铀燃料技术、干法后处理、水法后处理和放化设施等 4 个专业组，承担 TMSR 专项中燃料供应和研发、钍基熔盐堆辐照后燃料的化学分离与重构及放化设施的建设。2011–2012 年重点开展了 TMSR 实验堆燃料获取与可行性分析、钍基熔盐燃料干法处理技术、钍铀燃料水法后处理技术等研究，取得实质性进展。

TMSR 实验堆燃料的获取与可行性分析

TMSR 实验堆确定采用现高温气冷堆使用的球形包覆颗粒燃料元件。我们根据国家的相关法规(HAF501、HAF501-01 等)确定了核材料许可证申请、核专料采购和燃料元件生产的流程。

在 2 MW 固态钍基熔盐实验堆中，球形包覆颗粒燃料元件工作于 2LiF-BeF_2 熔盐环境。为了评估燃料元件在 TMSR 实验堆中的性能，根据 2 MW-TMSR 预概念设计(2012 年 6 月的版本)提供的燃料元件服役环境(卸料燃耗 11%FIMA，单球功率 189 W/FE，冷却剂出/入口温度 620/600℃)，对球形燃料元件的温度分布和包覆颗粒 SiC 层的应力进行了计算分析。

图 1 显示了单球功率分别为 0.19 kW、1.89 kW 时燃料元件内的温度分布。即使工作在高的功率密度条件下，燃料球内 TRISO 颗粒的最高温度也不会超过包覆颗粒燃料正常工况下的限值温度(1250℃)。根据压力壳模型计算了在不同燃耗和温度时包覆颗粒 SiC 层受到的应力(见图 2)。由图可见，在实验堆燃料的寿期内，SiC 层受到的应力远低于 SiC 未辐照和快中子注量为 1.8×10^{21} n•cm^{-2} (EDN) 时的极限拉伸强度(分别为 834 MPa 和 687 MPa)。

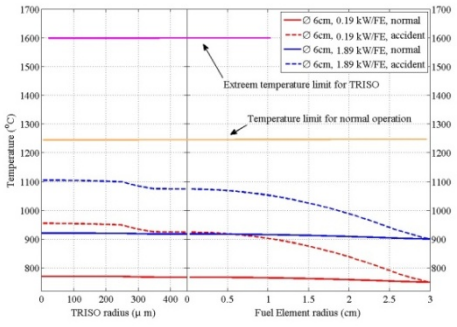

图 1 在不同功率密度和表面温度下元件和 TRISO 颗粒内的温度分布

计算结果表明，在实验堆预概念设计的运行环境下，球形燃料元件及其中的包覆颗粒处于安全的工作范围以内。

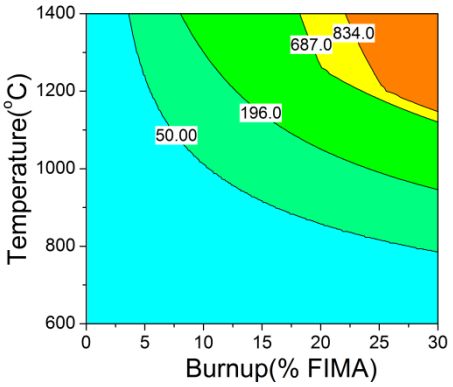

图 2 包覆颗粒 SiC 层的应力与燃耗和辐照温度的关系

钍基熔盐燃料干法处理技术研发

基本确定了以氟化挥发技术、减压蒸馏技术和熔盐电化学技术为主的钍基熔盐燃料干法处理流程。

完成了首套小型非放射性高温氟化实验装置的安装、调试和验收。小型非放射性高温氟化反应系统由供气、氟化反应、产物净化(1 级 NaF 阱)、UF6 吸附(2 级 NaF 阱)和尾气处理等 5 个子系统组成(见图 3)。该系统作为开展铀氟化实验研究的基础设施，主要承担常温和高温气体实验、熔盐实验、NaF 吸附研究、反应进程研究和材质腐蚀性研究。在尚不能进行真正铀氟化实验的条件下，开展了基于第一套实验装置的 FLiNaK 熔盐体系 MoF_6(模拟 UF_6)挥发及反应过程在线红外分析研究，为后续的 FLiNaK 熔盐体系开展 UF4 氟化挥发研究优化工艺及积累经验。

图 3 高温氟化挥发实验装置

针对干法后处理所面临的挑战和困难，特别是氟化挥发工艺(环境最苛刻，腐蚀最严重)的困难，

拟在后处理过程中引入“冷冻壁”技术。我们设计的冷冻壁是指通过调节容器壁外部和内部的温差，在容器壁上形成一层与熔盐堆载体盐同一组分的固态氟盐，这层冷冻壁成为天然的保护“内衬”，达到防止液态熔盐、氟气与器壁的直接接触、同时又不影响熔盐的组成的目的。

计划从硝酸盐入手，先研制一套硝酸盐冷冻壁技术研究实验装置(见图 4)，通过硝酸盐体系下冷冻壁的形成和维持的研究，掌握冷冻壁厚度检测和控制技术，在此基础上，对该装置进行能力提升，使其适合于氟盐体系的研究。目前研制的由“一罐一泵一试验段”组成的硝酸盐冷冻壁技术研究实验装置由熔盐加热系统、熔盐输送系统、气体预热及流量控制系统、管路加热及保温、冷冻壁试验罐、冷冻壁试验罐外壁循环导热油系统、尾气处理系统、运行参数监测系统等 8 个子系统组成。硝酸盐冷冻壁技术研究实验装置的运行，综合了流体流动、器壁换热等技术，需要解决的关键技术有：熔盐泵的顺利运转及熔盐流量控制、冷冻壁试验罐夹套换热控制、冷冻壁厚度的准确检测等。

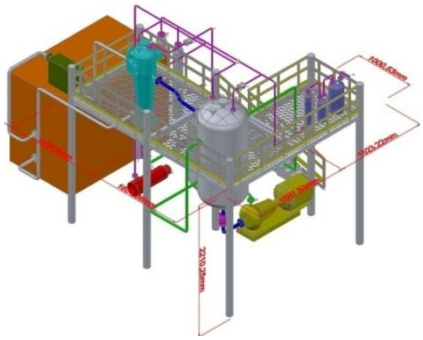

图 4　硝酸盐冷冻壁技术研究实验装置

自行研制了立式分段式减压蒸馏装置(见图 5)，用于减压蒸馏分离熔盐载体与稀土氟化物的可行性研究，测得 NdF_3、SmF_3 相对于 LiF 的相对挥发度分别为 2.0×10^{-2} 和 2.2×10^{-4}，并实现了 95%以上载体盐的冷凝收集。建立了熔盐电化学实验室，确定了氟盐电解用的标准参比电极和固定面积工作电极的设计方案，研制了一套能进行公斤级熔盐电化学实验的手套箱-电解槽一体式熔盐电解装置；开展了 FLiNaK 熔盐中目标元素电化学参数的测量，并获得 Nd、Y、Gd、Eu、Sm 在 FLiNaK 中的氧化还原电位、扩散系数、电极反应电子转移数等关键参数(见表 1)；并开展了 FLiNaK 中 Nd 的电解分离初步实验，在现有条件下稀土元素的去除率达到 86 %以上。

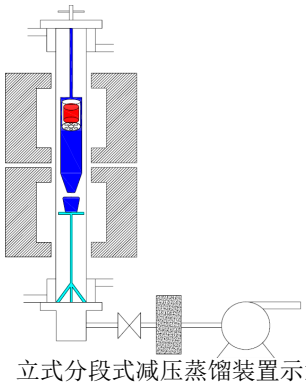

图 5　立式分段式减压蒸馏装置示意图

表 1　目标元素在 FLiNaK 中的电化学参数(723K)

电极反应	平衡电势电位 E(V. vs. Ni/NiF_2)	扩散系数
$Gd^{3+}+3e^- \rightarrow Gd^0$	-2.02	3.2×10^{-4}
$Y^{3+}+3e^- \rightarrow Y^0$	-1.96	5.4×10^{-6}
$Nd^{3+}+3e^- \rightarrow Nd^0$	-1.95	1.1×10^{-5}
$Sm^{3+}+e^- \rightarrow Sm^{2+}$	-1.65	7.4×10^{-6}
$Eu^{3+}+e^- \rightarrow Eu^{2+}$	-1.03	9.6×10^{-6}

钍铀燃料水法后处理技术研发

重点发展基于萃取技术的 ^{233}U 提取工艺和 Thorex 流程，开展了工艺段中氧化钍溶解、调料等水法后处理头端工艺以及铀产品离子交换纯化工艺等研究工作，初步确定了上述工艺段的工艺条件并研制了溶解装置、调料装置、混合澄清槽(见图 6)、离子交换装置等试验设备。

通过系统的 ^{233}U 单级萃取实验考察不同条件下钍、铀分配比的影响因素，初步确定了萃取剂浓度、料液、洗涤液及反萃液酸度等主要工艺参数，然后利用多级逆流串级萃取实验确定了萃取、洗涤及反萃级数，并对主要工艺参数进行了进一步优化。在此基础上，完成了混合澄清槽台架冷试验，对上述 ^{233}U 提取工艺进行了验证，台架冷试验运行时间 60 h，结果表明，在我们提出的 ^{233}U 提取工艺中，钍铀分离系数可达到 2.5×10^5 以上(铀产品中钍含量＜0.04%)，铀回收率可达到 99.6%以上。通过上述工作为建立完整的钍基核燃料水法后处理流程提供了初步的技术基础。

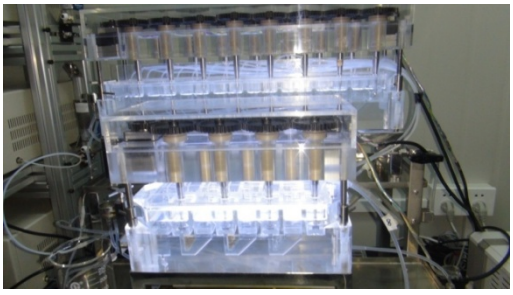

图 6　混合澄清槽实物图

Research Progress of Th-U Radiochemistry

Department of Radiochemistry-Engineering

Radiochemistry engineering and technology department undertakes the task of supply and development of fuel for TMSR, chemical separation and reconstituent of irradiated fuel from TMSRs, and construction of radiochemical facilities. In the past two years, our work focused on feasibility study of TMSR-SF1 fuel, development of pyroprocess and aqueous reprocess technologies planed to process irradiated Th-U fuel.

Performance of Spherical fuel element in TMSR-SF1

Spherical fuel element (TRISO element), which has been widely adopted in HTGR (such as HTR-10 of INET, China) is a reliable selection for molten salt cooled reactor.

In TMSR, TRISO element will be immersed in molten salt consisting of LiF and BeF_2. In order to evaluate the performance of fuel in service within the TMSR, both the temperature distribution of the fuel elements and the stress in SiC layer of coated particles are calculated and analyzed according to the environments of fuel elements in service (End of life burnup: 11%FIMA, power density: 189 W per element, average coolant inlet/outlet temperature: 600℃/620℃), which are provided by pre- conceptual design for 2 MW-TMSR (2012.6 version).

Fig.1 illustrates the temperature distribution of fuel elements with the power densities of 0.19 kW/FE and 1.89 kW/FE, respectively. As we can see, even if the fuel elements work on the high power density condition, the maximum temperature of TRISO coated particles in the fuel elements will not exceed its limitation under normal operation, 1250 ℃. In addition, according to pressure shell model, the stress in SiC layer of TRISO coated particles with various Burnups and temperatures are calculated, the result is shown in Fig.2. As we can see, stress in SiC layer is far below the ultimate tensile strength of 834 MPa or 687 MPa, each for un-irradiated SiC and fast neutron fluence 1.8×10^{21} n• cm^{-2} (EDN).

Based on above results, both the spherical fuel elements and coated particles are working within safe scope according to both the normal operation and accident conditions provided by TMSR's pre-conceptual design.

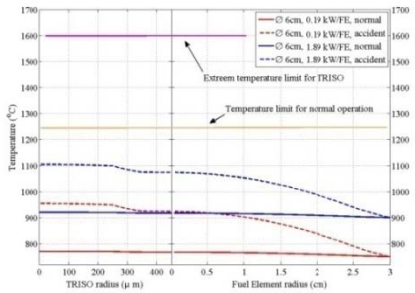

Fig.1 Temperature distribution for fuel elements and TRISO particles with various power density and surface temperature.

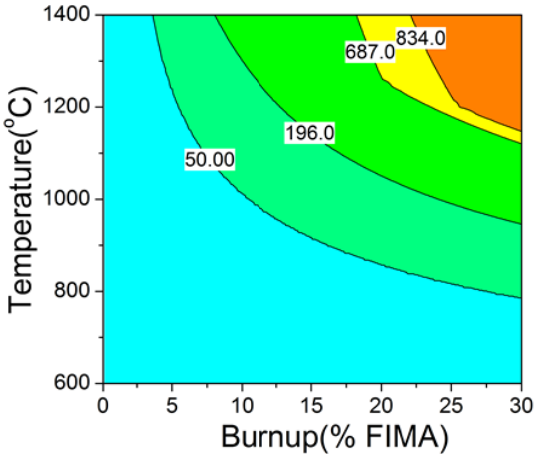

Fig.2 The relationship between stress in SiC layer and Burnup or irradiated temperature.

Development of pyroprocess technologies

We have developed a pyroprocessing flowsheet for TMSR fuel cycle on the basis of three technologies, namely, fluoride volatility, low pressure distillation and electrochemical separation techniques.

We have completed the construction of a set of non-active fluoride volatility experimental equipment, which constitutes of gas supply system, reaction tank, volatile products purification (primary NaF tank), UF6 absorption tank (secondary NaF tank) and off-gas treatment (Fig.3). Working on this setup, we have carried out gas flow experiments at ambient and high temperature, the salt melting experiments, absorption experiment of NaF, reaction process monitoring. we have operated volatile experiments, using MoF6 as surrogate and also monitoring the reaction process by FT-IR spectrometer.

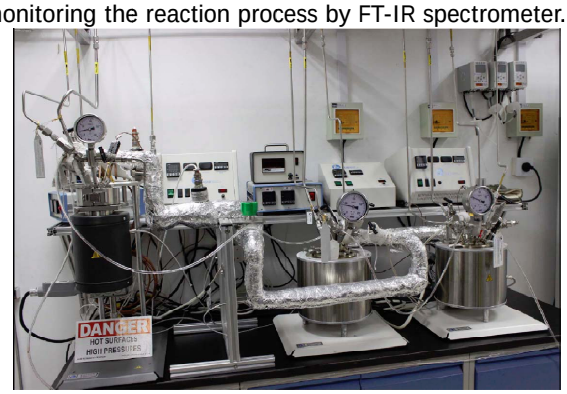

Fig.3 Fluoride volatility experimental setup.

In order to solve the corrosion challenge, especially in fluoride volatility method, we planed to adopt a frozen wall protection technique. The mechanism of frozen wall protection technique is based on the temperature intergradient of the inner and outer side of the reaction tank, and then formation of a layer of solid salt, which have the

same constitution of the liquidus salt, at the surface of reaction tank. The formation of frozen layer would protect the attack to construct material from molten salt, fluorine gas and could not affect the chemical constitution of the molten salt.

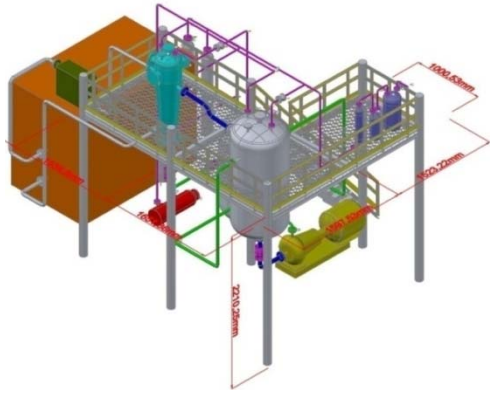

Fig.4 Nitride molten salt frozen wall experimental equipment.

Initially, we have built up a molten salt equipment operating with nitride salts. We have been developing the formation and maintain techniques of a given thick frozen wall. In the future, a equipment suitable for fluoride molten salt will be designed. Now, the equipment is composed of “tank-pump-experimental section” including heating system, transport system, gas heating system and flow controlling system, heating system for pipes, experimental tank, oil cooling system for experimental tank, off-gas treatment, and control panel. The developing of frozen wall technique has close relation to hydraulic theory and heat exchange theory, and the key points including the operation of molten salt pump and flow rate control, the heat exchange technique for experimental tank, precisely measurement of frozen wall etc.

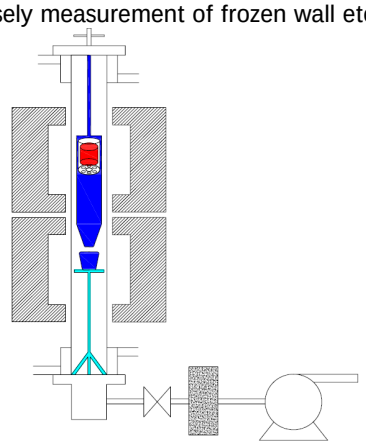

Fig. 5 Vertical low pressure distillation experimental device.

To evaluate the feasibility of low pressure distillation, we have designed a vertical three-gradient-temperature device for measuring the relative volatility of rare earth fluorides to LiF. The obtained results are 2.0×10^{-2} and 2.2×10^{-4} for NdF_3 and SmF_3, respectively, and the recovery of carrier salt is over than 95%.

A full function electrochemistry laboratory has been built up. The fabrication of molten salt reference electrode and the production of fixed area working electrode have been developed. A kilo-scale molten salt electrochemical setup has been installed. Systematic investigation of electrochemical behavior of Nd, Y, Gd, Eu and Sm in the FLiNaK eutectic, such as the reduction potentials, diffusion coefficients, and the exchange electron numbers of the electrode reactions, have been performed. Preliminary electrodeposition experiments of Nd in FLiNaK was carried out and the extraction of Nd from FLiNaK is over than 86%.

Table 1 Key parameters of target elements in the FLiNaK molten salt

Electrode reaction	Reduction potential E(V. *vs* Ni/NiF_2)	Diffusion coefficient
$Gd^{3+}+3e^- \rightarrow Gd^0$	-2.02	3.2×10^{-4}
$Y^{3+}+3e^- \rightarrow Y^0$	-1.96	5.4×10^{-6}
$Nd^{3+}+3e^- \rightarrow Nd^0$	-1.95	1.1×10^{-5}
$Sm^{3+}+e^- \rightarrow Sm^{2+}$	-1.65	7.4×10^{-6}
$Eu^{3+}+e^- \rightarrow Eu^{2+}$	-1.03	9.6×10^{-6}

Development of aqueous thorium-uranium fuel reprocessing process

Focus on developing the ^{233}U extraction and THOREX flowsheet based on liquid-liquid extraction technique, including ThO_2 dissolution and feed solution adjustment of the head-end process, the extraction separation of thorium, uranium and fission products, and an ion-exchange process for further purification of uranium. The operating parameters and experimental equipments of above processes were preliminarily determinated and developed.

In the research of ^{233}U extraction process, the primary processing parameters, including extractant concentration, acidity of feed, scrubbing and stripping solution, were firstly determinated by investigating the distribution coefficient of thorium and uranium under different conditions using single stage extraction. Then, the number of stages of extraction, scrub and strip were determinated, and the primary processing parameters were further optimized by using multistage countercurrent extraction. On the basis of above experiment, the 233U extraction process was tested by using “cold” bench experiment in the mixersettler. The total run time was 60h and the results showed that the separation factor of Th/U and recovery of U was above 2.5×10^5 and 99.6%, respectively. The above work could provide preliminary technical support for building a complete thorium-fuel aqueous reprocessing process.

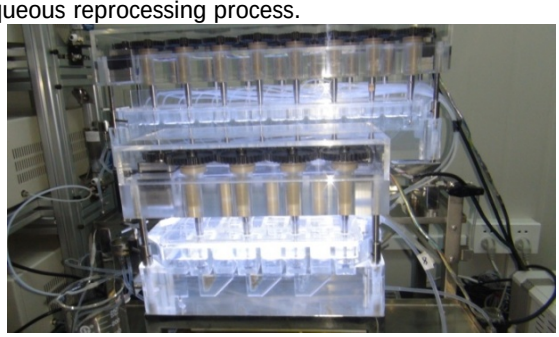

Fig.6 Mixer-settler.

海水提铀吸附材料的制备研究

辐射化学与辐照技术部　吴国忠　李景烨　胡江涛　马红娟　虞 鸣　邢 哲

为确保核燃料稳定供应、实现核能可持续发展，海水提铀技术近年重新受到国际关注。海洋中铀的储量约45亿吨，但铀的浓度仅为3.3 ppb，从海水中富集铀的技术难度远高于铀矿开采，因此，开发高性能、低成本的吸附材料是实现规模化海水提铀的关键。课题组以超高分子量聚乙烯(UHMWPE)纤维为基材，通过辐照接枝丙烯酸和丙烯腈共聚物，然后使用盐酸羟胺肟化将腈基转变为能与铀酰离子配位的偕胺肟基团，获得海水提铀吸附材料。

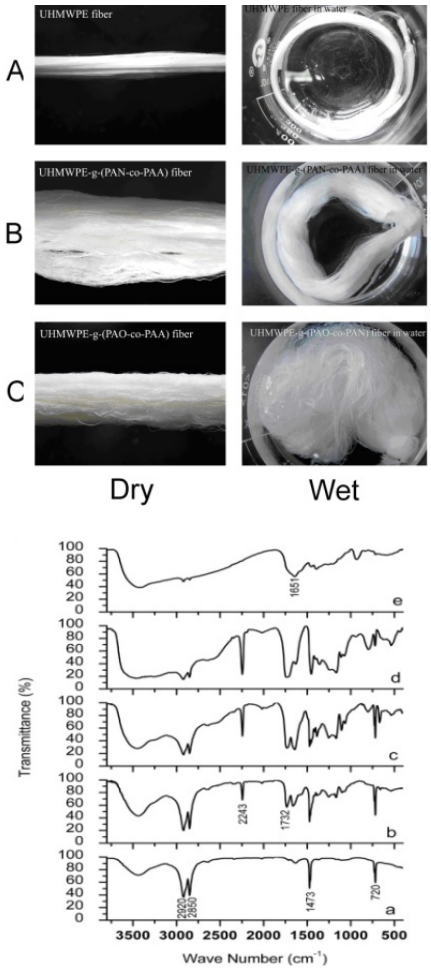

图 1　UHMWPE 纤维(A,a)进行接枝(B,b-d)和胺肟化(C,e)反应前后在水中的外观变化及其红外吸收光谱

结果表明，UHMWPE 纤维基吸附材料的接枝率达 300%以上，在接枝聚合过程中丙烯腈和丙烯酸共聚接枝在纤维基材上。辐照剂量和盐酸洗提对纤维吸附材料的拉伸强度影响较大，而接枝聚合及胺肟化反应对纤维力学性能的影响较小。吸附材料对铀和钒的选择性主要受胺肟化反应液 pH 值影响，当在 pH 值较高时制备吸附材料的吸附容量为铀大于钒；在 pH 较低的条件下制备的吸附材料的吸附容量铀小于钒。在美国能源部实验室帮助进行的 42 d 真实海水吸附试验中吸附材料的铀酰吸附能力为 2.3 $mg \cdot g^{-1}$。

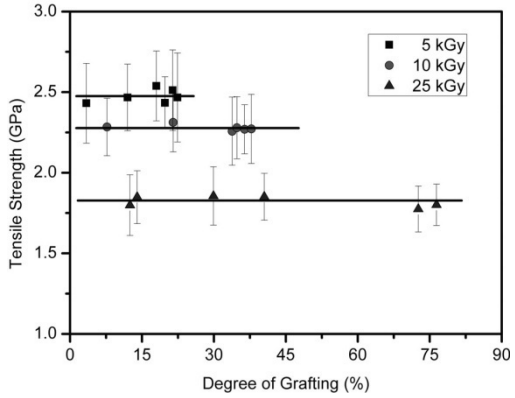

图 2　吸收剂量、接枝率对 UHMWPE 纤维拉伸强度的影响

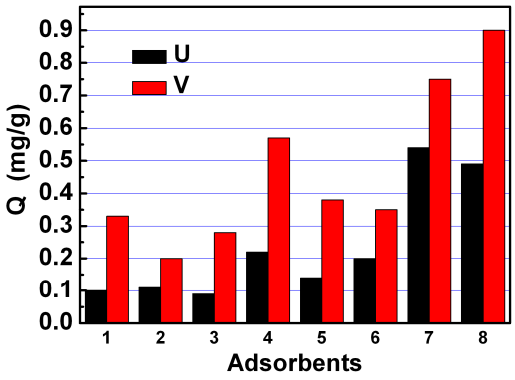

图 3　不同条件下制备的吸附材料对铀和钒的选择性分析 (24 h 吸附, 100 倍海水浓度)

参考文献

1. Kim J, Tsouris C, Mayes RT, Oyola Y, Saito T, Janke CJ, Dai S, Schneider E, Sachde D. Separ Sci Technol, 2012, **48**: 367–387
2. Takahashi A, Igarashi S. Solvent Extr Res Dev-Jpn, 1999, **6**: 61–71
3. Liu H Z, Yu M, Deng B, Li L F, Jiang HQ, Li J Y. Rad Phys Chem, 2012, **81**: 93–96
4. Liu X Y, Liu H Z, Ma H J, Cao C Q, Yu M, Wang Z Q, Deng B, Wang M, Li J Y. Ind Eng Chem Res, 2012, **51**: 15089−15095

Study on the preparation of adsorbent materials for extraction of uranium from seawater

WU Guozhong LI Jingye HU Jiangtao MA Hongjuan YU Ming XING Zhe

Department of Radiation Chemistry and Technology

Uranium is an important resource for sustainable development of nuclear energy. The total amount of uranium in ocean is 4.5 billion tons, which is equivalent to 1000 times of that in terrestrial reserve. However, since the uranium concentration is only 3.3 ppb in seawater, the collection of uranium is more difficult from seawater than from uranium mining. To realize the uranium collection from seawater in large scale advanced adsorbent with good performance and low cost has to be developed. In this study, amidoxime-based fibrous adsorbent was prepared by radiation-inducedgrafting of acrylonitrile and acrylic acid ontoultra-high molecular weight polyethylene (UHMWPE) fiberand subsequent amidoximation of the grafted fiber.

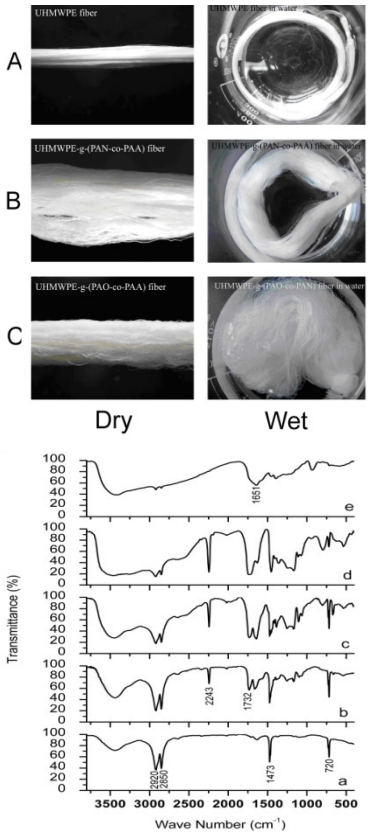

Fig.1 Photographs and FT-IR spectra of the UHMWPE (A, a), UHMWPE-g-(PAN-co-PAA) (B, b-d) and UHMWPE-g-(PAO-co-PAA) (C, e) fiber.

The results show that the degree of grafting can be higher than 300%. The acrylonitrile molecule chain segments comprise of a majority of the copolymer graft chains. The tensile strength of the fibrous adsorbents was primarily influenced by the absorbed dose and elution with HCl solution, but independent of graft polymerization and amidoximation. The selectivity between U and V might be dependent on the pH value of the amidoximation solution. In detail, adsorbents prepared at pH=8 exhibit higher sorption capacity of U than V, while adsorbents prepared at pH=6.7 and 7 exhibit lower capacity of U than V. The adsorption of uranium of the amidoxime-based fibrous adsorbent reached 2.3 mg $\cdot g^{-1}$ in the adsorption test in seawater for 42 days, conducted in PNNL of DOE, USA.

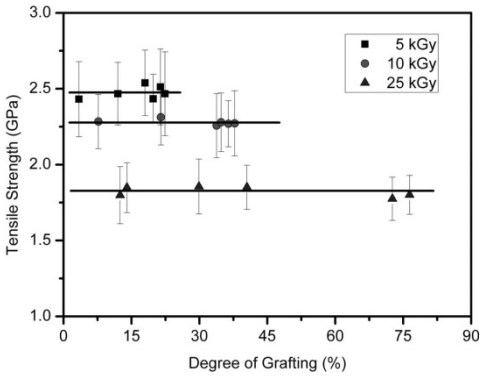

Fig.2 Effect of dose, degree of grafting on the tensile strength of the UHMWPEfibersamples.

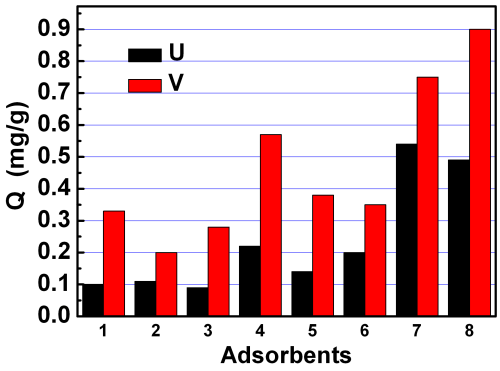

Fig.3 Adsorption capacity of U and selectivity between U and V(24 h adsorption, 100 times C_0 as in seawater).

References

1. Kim J, Tsouris C, Mayes R T, Oyola Y, Saito T, Janke C J, Dai S, Schneider E, Sachde D. Separ Sci Technol, 2012, **48**: 367–387
2. Takahashi A, Igarashi S. Solvent Extr Res Dev-Jpn, 1999, **6**: 61–71
3. Liu H Z, Yu M, Deng B, Li LF, Jiang HQ, Li J Y. Rad Phys Chem, 2012, **81**: 93–96
4. Liu X Y, Liu H Z, Ma H J, Cao C Q, Yu M, Wang Z Q, Deng B, Wang M, Li J Y. Ind Eng Chem Res, 2012, **51**: 15089−15095

堆用高分子材料及其耐辐照寿命考验

辐射化学与辐照技术部　李景烨　张 聪　李林繁

TMSR中使用聚合物材料主要用于电缆的绝缘层和护套，通常核电站用电缆根据安装区域不同可分为安全壳外和安全壳内两类，根据功能不同可以分为电力电缆、控制电缆、仪表电缆及补偿导线。

核用电缆分布在核电站不同区域内，对应不同的工况条件。目前，第二代、第三代反应堆已经对核电站用电缆以建立了相关标准，对核电站不同区域使用的电缆提出了详细的技术指标。

与第二代、第三代反应堆相比，TMSR在核岛中心区域的工作温度更高、辐射剂量更大，而外围区域工作环境与第二、三代反应堆相似。因此，TMSR堆用电缆可分为两类：一、在非中心区域使用的电缆，可以使用符合第二代、第三代核电站(如AP1000)相关指标的电缆；二、中心区域使用的电缆，这部分电缆需符合TMSR运行的特定要求，在较高温度和较高辐射剂量的环境中长期使用并在事故状态下能维持正常运行。

根据相关标准和要求，研制了核电K1内绝缘料、外绝缘料及护套料3种材料，采用此3种材料制备了1根核电K1电力电缆和1根核电K1控制电缆。并委托上海电缆研究所开展性能鉴定。


检 验 报 告
Test Report
样品名称 Name of sample　核电站用1E级K1类电缆料
样品型号 Type of sample　/
委托方 Consigner　中国科学院上海应用物理研究所
试验类型 Kind of test　委托检验
国家电线电缆质量监督检验中心
CHINA NATIONAL CENTRE FOR QUALITY SUPERVISION AND TEST OF ELECTRIC WIRE AND CABLE

所研制核电站用 1E 级 K1 类电缆料检验报告

三代核电如AP1000核电站，在安全性能方面比二代要求更高，因此，在二代核电的基础上，其对核电设备辐照老化和事故辐照考验提出了更加苛刻的要求，在γ射线辐照考验的基础上，增加β射线辐照考验，按照AP1000要求，β辐射的能量为1.2 MeV，其事故条件下辐照剂量率为20 kGy·h^{-1}，总剂量率为3000 kGy以验证材料辐照老化性能。

在现有工业用地纳米电子加速器下，通过遮蔽材料遮蔽部分剂量计，然后同时进行辐照。经过多次实验，证明经遮蔽材料遮蔽后在能量为1.2 MeV稳定电子束下方1.5 m处可以得到1 h连续静态辐照剂量为20 kGy (误差为±15%)的区域用以进行满足AP1000要求的β射线辐照实验。同等条件下的重复实验证明，电子束辐照区域剂量重现性良好，数据误差均小于10%。同样利用二次扫描法可以获得每小时15 kGy±15%的剂量率区域。实现了满足AP1000要求的β射线辐照考验条件的研究目标。

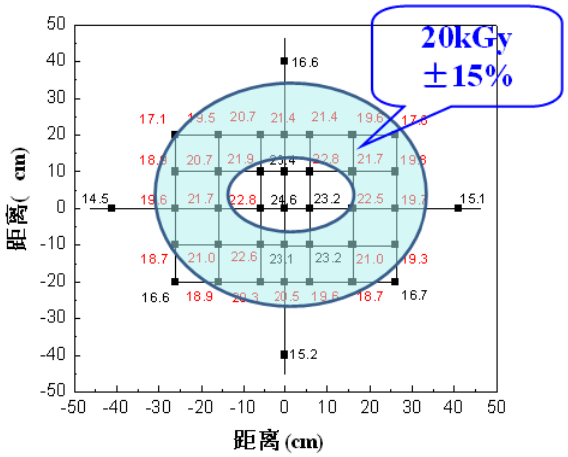

遮蔽法实验结果

参考文献

1. 核用电缆无卤阻燃绝缘料、电缆绝缘层、制备方法和应用,申请号: 201210356203.5
2. 核用电缆无卤阻燃护套料、电缆护套、制备方法和应用,申请号: 201210352803.4
3. 无卤无红磷阻燃热收缩材料、热收缩管、制备方法和应用，申请号: 201210356195.4
4. 电子射线源产生装置及产生低剂量率电子射线的方法,申请号: 201210425491.5
5. 电子射线源产生装置及产生低剂量率电子射线的方法,申请号: 201210348278.9
6. 电子射线源产生装置及产生低剂量率电子射线的方法,申请号: 201210556558.9

Nuclear Polymer Materials and Its Resistance to Radiation Test

LI Jingye ZHANG Cong LI Linfan

Department of Radiation Chemistry and Technology

TMSR polymeric materials are used principally for cable insulation and sheath. The nuclear cable, according to the different service regions, usually can be divided into two categories, inside and outside the containment. However, according to the different functions, the nuclear cable can be divided into power cables, control cables, instrument cables and compensation wire.

Corresponding to different service conditions, nuclear cables distribute in various regions of the nuclear power plant. By now, the relevant standard shave been established for nuclear cables in the second or third generation reactors. The detailed technical specifications have been proposed for different areas' cables of nuclear power plants.

Compared with the second and third generation reactors, TMSR central region of the nuclear island has higher operating temperatures, greater radiation doses. But the work environments of peripheral areas in TMSR are similar with the second and third generation reactors. Therefore, TMSR nuclear cable can be divided into two categories. The first, the relevant specifications cable in accordance with the second and third generation reactors (such as AP1000) can be used in the TMSR non-central region. The second, for the TMSR central area, the cables must meet the specific requirements including the normal using in the accident state and sustaining long-term high temperature and high radiation doses in the normal operation state.


检 验 报 告
Test Report

The test report of developed class 1E K1 nuclear cable materials.

According with the relevant standards and requirements, the three materials, inner insulation materials, outer insulation materials and sheath material of K1nuclear cable have been developed. Moreover, a K1 power cable and a K1 control cable are achieved by using of three materials mentioned above. The performance appraisals of these cables have been carried out by Shanghai Electric Cable Research Institute.

The third generation nuclear power plants, such as AP1000, the safety requirements are higher than the second generation reactor. Therefore, based on γ ray radiation test of the second generation reactor, more stringent requirements in its equipment radiation aging and accident radiation tests have been discussed. Thus, the β ray radiation test has been proposed. In according with the AP1000 β ray radiation test requirements, the β ray energy is 1.2 MeV, the radiation dose rate of the accident conditions is 20 kGy $\cdot h^{-1}$, the radiation total dose is 3000 kGy, which were used to verify material aging properties.

Under industrial dynamitron accelerator, by using partial shielding method, a dose rate area 20 kGy$\cdot h^{-1}$ (±15% error) to be required to meet the AP1000 β-ray radiation test experiments has been achieved successfully after 1.2 MeV electron beam continuous irradiation. The experiment was repeated under the same conditions and the data errors were less than 10%.Using the same technology, the 15±15% kGy$\cdot h^{-1}$ dose rate area can be obtained by secondary scanning method. The research objective to meet the requirements of the AP1000 β ray radiation test has been achieved.

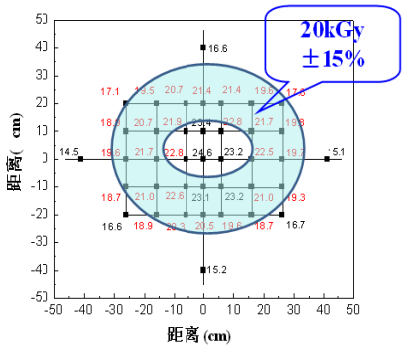

The experimental result to meet the AP1000 β-ray radiation test using partial shielding technology.

Reference

1. The preparation and application of flame retardant nuclear cable material and insulation. Application No.201210356203.5
2. The preparation and application of flame retardant nuclear cable material and insulation. Application No.201210352803.4
3. The preparation and application of flame retardant nuclear cable material and insulation. Application No. 201210356195.4
4. Electron beam generation instrument and the method to acquire low dose rate β ray. Application No. 201210425491.5
5. Electron beam generation instrument and the method to acquire low dose rate β ray. Application No. 201210348278.9
6. Electron beam generation instrument and the method to acquire low dose rate β ray. Application No. 201210556558.9

核科技与前沿交叉研究

Nuclear Science and Frontier Interdiscipline Research (NSFI)

相对论重离子对撞物理研究

核物理研究室

位于美国布鲁克海汶国家实验室的相对论重离子对撞机上(RHIC)产生了类似于宇宙大爆炸早期的物质形态，是研究宇宙早期新物质形态包括反物质的理想实验场所。2011–2012 年我们在 RHIC-STAR 上主要开展了关注反物质和超氚核的实验研究，并在理论上利用唯象输运模型对相对论重离子对撞动力学进行研究。

1 RHIC-STAR 实验研究

利用 RHIC-STAR 实验探测器开展了多方面的实验研究。我们和 STAR 实验组其它单位合作，首次观测到迄今为止最重的反物质原子核，反氦 4 核[1]。该工作是继 2010 年我们发现反物质超核之后的又一个重要成果，是反物质研究领域的另一个力作。同时也提出了在 STAR 能量扫描实验中开展超核研究的新观点，并且在实验上开展了相应的研究，取得了初步的成果。分析了 $\sqrt{S_{\rm NN}}$=500 GeV 质子碰撞中非光电子与带电强子的方位角关联函数，以此来研究重味夸克的产生及其能量损失机制。

2 RHIC 物理唯象动力学研究

用多相粒子输运模型对相对论重离子碰撞实验中的两粒子关联中双峰和山脊结构的物理机制进行了深入研究，通过使用不同的初态涨落条件来区分三角流、热斑和喷注-介质相互作用对双强子关联的贡献[2]，通过比较光子喷注和双强子喷注的不同结构揭示更多的有关新部分子介质的信息[3–5]。开展了 RHIC 和 LHC 能量下，初态涨落对于末态各向异性流的影响的系统研究[6]。开展 RHIC 能量下椭圆流关联函数的研究，发现椭圆流涨落之间的关联对于关联函数起着很重要的作用[7]。系统的研究了相对论重离子碰撞中双强子方位角关联的对碰撞系统尺寸的依赖性，提出了利用系统尺寸扫描来寻找核物质的 QGP 相变和 QCD 临界点[8]。尝试从实验数据中抽取了强子化时刻部分子的横向动量分布，结果与夸克组合模型的思想保持一致[9]。使用一个简单的组合模型研究了在金核+金核中心碰撞中的轻核、超核、双 Λ 的产额，相关结果很好的解释了实验数据，并和热力学统计模型的预言保持一致[10]。使用强子输运模型和组合强子化的方法研究了在略低于 Λ 产生阈值能量下轻核的产额情况，发现在 CSR 能区得重离子碰撞中有可观的超氚核产额[11]。将初态电荷分离机制引入到多相粒子输运模型中，发现末态相互作用对手征磁效应产生的初态电荷分离是不容忽略的[12]。使用夸克质量密度依赖的模型描述了无限核物质和有限尺寸原子核的性质，并推广至有限温度和密度的情况下，较好的解释了核物质的饱和性质和退禁闭相变[13]。使用夸克－介子耦合模型研究了夸克的能谱，发现在低于 50 MeV 的温度下激发态的夸克被压抑，为有关热力学势的计算提供了理论简化[14]。

参考文献

1. Abelev B I, *et al*. (the STAR Collaboration), Nature, 2011, **473**: 353
2. Ma G L,Wang X N. Phys Rev Lett, 2011, **106**: 162301
3. Li H L, *et al*. Phys Rev Lett, 2011, **106**: 012301
4. Ma G L, Wang X N. J Phys G: Nucl Part Phys, 2011, **38**: 124156
5. Ma G L, Wang X N. Acta Phys Pol B, 2012, **43**: 697
6. Han L X, *et al*. Phys Rev C, 2011, **84**: 064907
7. Han L X, *et al*. Phys Rev C, 2011, **83**: 047901
8. Zhang S, *et al*. Nucl. Phys. A, 2011, **860**: 76
9. Jin F, *et al*. Indian J Phys, 2011, **85**: 161
10. L Xue, *et al*. Phys Rev C, 2012, **85**: 064912
11. Zhang S, *et al*. Chin Phys C, 2011, **35**: 741
12. Ma G L, Zhang B. Phys Lett B, 2011, **700**: 39
13. Wu C, *et al*. Eur Phys Lett, 2012, **98**: 21005
14. Wu C, *et al*. Phys Rev C, 2012, **86**: 068201

The Researches on Relativistic heavy-ion collisions

Department of Nuclear Physics

The Relativistic Heavy-Ion Collider at BNL created a condition similar to the earlier universe at a few microseconds just after the Big Bang, thus it is the ideal lab to understand the early state of the universe including the antimatter. During 2011 and 2012, our research focus are observations of antimatter helium4 and (anti) hypernuclei in Au+Au collisions at RHIC-STAR. Meanwhile, we use phenomenological models to study the partonic dynamics in relativistic heavy-ion collisions.

1 Experimental researches at RHIC-STAR

We have observed the first antimatter helium-4 in Au+Au collision with a combined of the available data accumulated by the STAR detector until 2010[1]. This is the continual project after the observation of antimatter hypernuclei[2], which was also lead by our group. We also proposed to carry out hypernuclei study in STAR Beam Energy Scan program. The data analysis is on progress. We studied the charm quark production mechanism by non-photonic electron azimuthal correlation in proton-proton collisions at $\sqrt{S_{\rm NN}}$ =500 GeV.

2 Phenomenological study on partonic dynamics in relativistic heavy-ion collisions

The mechanism of double peak and ridge structure in dihadron correlation in the relativistic heavy-ion collision experiment is intensively studied by using a multiphase transport (AMPT) model. To distinguish the contributions of triangular flow, hot spots and jet-medium interaction on dihadron correlation, we use different fluctuations in initial parton density[3]. By comparing the different structure between photon jet and dihadron jet, which reveal more information about the new partonic medium[4–6]. We have a systematic study on the influence of initial fluctuation on final-state anisotropic flow at the RHIC and the LHC energies[7]. A study of elliptic anisotropy correlation at the RHIC energy shows the correlation of elliptic fluctuation plays an important role on the correlation function[8]. Considering system-size dependence of dihadron azimuthal correlations, we propose to use system-size scan to look for the QGP phase transition and QCD critical point[9]. Our attempt of the parton transverse momentum distribution from the experimental data at hadronization indicates a good agreement with the idea of quark coalescence model[10]. A simple coalescence model is employed to investigate the production of light nuclei, hypertriton and di-Λ, the results agree with experimental data as well as thermal model predictions[11]. Utilizing a dynamical coalescence model coupled with the ART model to study the production of light nuclei at sub-threshold energy of Λ production, we find a considerable yield of hypertriton at the CSR energy[12]. Within the framework of AMPT model, we introduce the initial charge separation mechanism, our results show the effects of final state interactions on initial charge separation cannot be negligible[13]. We use quark mass density-dependent (IQMDD) model to describe the properties of both infinite nuclear matter and finite nuclei. Furthermore, we extend the IQMDD model to finite temperature and finite nuclear matter density, which can describe the saturation properties of nuclear matter, and explain the quark deconfinement phase transition successfully[14]. To study the quark energy spectrum, a quark-meson coupling model is adopted. It is found that when the temperature is less than 50 MeV, the excited quark is suppressed, therefore the corresponding thermodynamic potential can be theoretically simplified[15].

References

1. Abelev B I, *et al.* (the STAR Collaboration), Nature, 2011, **473**: 353
2. Alelev BI, *et al.* (the STAR Collaboration), Science, 2010, **328**:58
3. Ma G L, Wang X N. Phys Rev Lett, 2011, **106**: 162301
4. Li H L, *et al.* Phys Rev Lett, 2011, **106**: 012301
5. Ma G L, Wang X N, J Phys G, 2011, **38**: 124156
6. Ma G L, Wang X N. Acta Phys Pol B, 2012, **43**: 697
7. Han L X, *et al.* Phys Rev C, 2011, **84:** 064907
8. Han L X, *et al.* Phys Rev C, 2011, **83**: 047901
9. Zhang S, *et al.* Nucl Phys A, 2011, **860**: 76
10. Jin F, *et al.* Indian J Phys, 2011, **85**:161
11. Xue L, *et al.* Phys Rev C, 2012, **85**: 064912
12. Zhang S, *et al.* Chin Phys C, 2011, **35**: 741
13. Ma G L, Zhang B. Phys Lett B, 2011, **700**: 39
14. Wu C, *et al.* Eur Phys Lett, 2012, **98**: 21005
15. Wu C, *et al.* Phys Rev C, 2012, **86**: 068201

低中能重离子碰撞物理

核物理研究室

本研究方向主要在丰质子核结构、核物质状态方程与对称能密度依赖、重离子碰撞中产生的核物质的约化粘滞系数及液气相变现象等方面开展了系列实验或理论研究。

1 丰质子核 ^{31}Cl 的外层质子动量分布实验研究

在兰州重离子加速器装置的 RIBLL 束流线上开展了 ^{31}Cl 的碎片动量分布测量实验。^{31}Cl 用 82A MeV 的 ^{36}Ar 主束轰击 Be 产生靶(0.5 mm)得到。产生的次级束从 T0 起通过二级铁的磁刚度及 Al 降能片进行分离和选择并传输到 T1 靶室的次级靶上(1 mm 的 C)。靶前粒子通过 Bρ-ΔE-TOF 的方法进行鉴别。从 T1 到 T2 靶室 RIBLL 可看成一个磁谱仪，通过该磁谱仪可以鉴别 ^{31}Cl 擦去一个质子后的碎片 ^{30}S 并测量其从 T1 到 T2 的飞行时间，从而确定碎片的动量。假设 ^{31}Cl 为核芯 ^{30}S +价质子结构，我们用少体 Glauber 模型对其碎片动量分布进行了计算。^{30}S 动量分布宽度的实验数据与价质子处于 d 态的计算结果一致，而与 s 态的结果相差很大。这说明 ^{31}Cl 的价质子主要处于 d 态[1]，结果表明 ^{31}Cl 虽然单质子分离能较小，但价质子的轨道与壳模型预言符合。

2 核物质态方程及对称能密度依赖研究

核物质的状态方程是目前核物理领域的最重要的研究课题之一，因为它与尚待解决的核力性质问题息息相关。尤其是其同位旋矢量依赖部分(对称能)，尚未有确切的描述，即使是其唯象的密度依赖行为，也只是在饱和密度附近才有明确的数值形式描述。我们用同位旋依赖的量子分子动力学模型在这方面做了一序列的研究。主要有：首次完整给出，费米能量附近到 1A GeV 能量范围内，核阻止本领的激发函数，并限定了较软的核物质状态方程[2]。在饱和密度以下，利用多重碎裂反应中的自由核子和中等质量碎片中的中质比来限定对称能的密度依赖行为[3]。在饱和密度以上，利用自由中质子的产额比，给出了对称能的高密依赖行为的理论计算结果[4]，在不同密度依赖对称能下，计算了自由中子多重数(Mn)和束缚质子多重数(Zbound)的相关性，并给出了 ALADIN-2000 合作组的实验数据的理论解释，给出了较软的对称能密度依赖性[5]。在半周边反应下，给出了不同弹靶同位旋不对称性，以及类弹类靶与参与区域源的同位旋组成的对称能依赖性，并提出使用这样的依赖性，作为同位旋漂移理论所预言的实验测量的有效探针[6]。

3 核物质的约化粘滞系数与液气相变现象研究

约化粘滞系数定义为剪切粘滞系数对熵密度的比值，最近发现在物质发生相变时总是会取得局部的极小值，因而它是物质相变时一个灵敏的探针。我们利用 BUU 和 IQMD 模型来模拟中能区对心 Au+Au 碰撞，提取碰撞中心区域核物质的约化粘滞系数来研究核物质的液气相变问题。

在 BUU 模型的框架下，我们用 Green-Kubo 公式来提取粘滞系数、用 Gibbs 公式来提取熵密度。研究发现提取的约化粘滞系数会随着碰撞能量有一个下降过程，然后会逐渐达到饱和[7]。在 IQMD 框架中，我们发现存在一个极小值[8]。

其次我们还尝试了另外一种提取粘滞系数的方法- Danielewicz 参数化公式。计算结果表明在 IQMD 框架下还是有极小值出现，尽管我们选择不同的体积大小对约化粘滞系数的数值有一定的影响[9]。

总的来说，我们使用了不同的方法来提取核的约化粘滞系数，并且计算结果支持核物质在中能重离子碰撞中能发生液气相变的结论。其次，提取的约化粘滞系数的极小值大概是预言的 KSS 下限的 10 倍。

参考文献

1. Fu Y, Fang D Q, Ma Y G, *et al*. Phys Rev C, 2011, **84**: 037603
2. Zhang G Q, Ma Y G, Cao X G, *et al*. Phys Rev C,2011 **84**: 034612
3. Kumar S, Ma Y G, Zhang G Q, *et al*. Phys Rev C, 2011, **84**: 044620
4. Kumar S, Ma Y G, Zhang G Q, *et al*. Phys Rev C, 2012: **85**: 024620
5. Kumar S, Ma Y G. Phys Rev C, 2012, **86**: 051601(R)
6. Kumar S, Ma Y G, Zhang G Q. Phys Rev C, 2012, **86**: 044616
7. Li S X, Fang D Q, Ma Y G, *et al*. Phys Rev C, 2011, **84**: 024607
8. Zhou C L, Ma Y G, Fang D Q, *et al*. Phys Rev C, 2013, **88**: 024604
9. Zhou C L, Ma Y G, Fang D Q, *et al*. Plasma Scince and Technology, 2012,16

Low and Intermediate Energy Heavy Ion Collision Physics

Department of Nuclear physics

This research field focuses on experimental and theoretical studies of the following subjects: structure of proton-rich nuclei, nuclear equation of state (EOS) and density dependence of symmetry energy, the shear viscosity and its relation with the liquid-gas phase transition of nuclear matter formed during heavy ion collisions.

1 Experimental study on the momentum distribution of the valence nucleon in ^{31}Cl

The experiment was performed at the RIBLL beamline in the Heavy Ion Research Facility in Lanzhou. Secondary beams were produced through the projectile fragmentation of an 82A MeV ^{36}Ar primary beam bombing on a Be target (0.5 mm) at the target chamber (T0). The produced exotic nuclei, such as ^{31}Cl, were separated and selected by means of magnetic rigidity ($B\rho$) and an Al degrader and transported to T1 where the carbon reaction target (1 mm) was placed. The particle identification for the incident ^{31}Cl before the reaction target was made by the $B\rho$-ΔE-TOF method. From T1 to T2, RIBLL can be used as a spectrometer to measure the momentum distribution ($P_{//}$) of the ^{30}S fragment after one proton removal from ^{31}Cl. We performed a few-body Glauber model analysis for $P_{//}$ of the $^{31}\mathrm{Cl} \rightarrow {}^{30}\mathrm{S}$ process to interpret the experimental momentum distributions. In this model, a core plus valence proton structure is assumed for the projectile. The calculation shows that the width of the momentum distribution for a proton in an l = 2 orbit is consistent with the measured $P_{//}$ data[1], which suggests a dominant *d* wave for the valence proton in ^{31}Cl as predicted by the shell model.

2 Nuclear Equation of State and density dependent Symmetry energy

Nuclear Equation of State (EoS) is one of the most important topics in nuclear study, due to its tight connection with the unknown properties of nuclear force. Especially, its isospin dependent part which is called symmetry energy needs further study to uncover its density dependent behavior. Using the isospin quantum molecular dynamical (IQMD) model, we have done serious of works on this topic.

A detailed analysis of the wide excitation function of nuclear stopping has been conducted and a softer EoS is proposed based on the quantitatively comparison between experimental results and our calculation ones[2]. At subsaturation densities, it is suggested to probe the density dependence of the symmetry energy via multifragmentation[3]. While the sensitivity of neutron to proton ratio toward the high density is also discussion for behavior of symmetry energy in heavy-ion collisions[4]. The dependence of the sum of the charge number for fragments with Z≥2 (Zbound) on the multiplicity of neutrons (Mn) from the projectile spectator fragmentation is compared with the experimental results of the ALADIN-2000 Collaboration, which also suggests a soft symmetry energy[5]. The sensitivities of isospin asymmetry and collision geometry dependencies of participant -spectator matter towards the symmetry energy are explored. The difference of the number of nucleons in the overlapping zone to the quasi-projectile-target matter is found to be quite sensitive to the symmetry energy at semiperipheral geometries compared to the individual yield. It gives us a clue that this quantity can be used as a measure of isospin migration [6].

3 Number-of-nucleon scaling of elliptic flow for light particles and photo production

The specific viscosity, defined as the ratio of shear viscosity to entropy density， has been studied in the intermediate energy heavy ion collisions both in the Boltzmann-Uehling-Uhlenbeck model (BUU) and isospin dependent quantum molecular model (IQMD). The specific viscosity is found to be a new probe of phase transition for the minimum is exhibited at the critical temperature. The Au+Au head-on collisions are simulated, and the nuclear matter in the central region of center of mass frame is selected.

The Green-Kubo formula is employed to calculate the shear viscosity and the Gibbs formula is used to calculate the shear viscosity and in the BUU and IQMD. The calculated results show that the specific viscosity decreases as the increasing energy and shows a saturated value in BUU[7] or reaches a minimum in IQMD[8].
On the other hand, the Danielewicz's parameter formula is also employed to calculate the shear viscosity, a minimum is also found in IQMD model[9].

In a word, different methods are used to study the specific viscosity of nuclear matter created in the intermediate energy heavy ion collisions. And our results support the conclusion that the liquid gas phase transition could occur in this energy region. Besides, the minimum value of specific viscosity is about 10 times of the predicted KSS bound.

References

1. Fu Y, Fang D Q, Ma Y G, *et al*. Phys Rev C, 2011, **84**: 037603
2. Zhang G Q, Ma Y G, Cao X G, *et al*. Phys Rev C,2011 **84**: 034612
3. Kumar S, Ma Y G, Zhang G Q, *et al*. Phys Rev C, 2011, **84**: 044620
4. Kumar S, Ma Y G, Zhang G Q, *et al*. Phys Rev C, 2012: **85**: 024620
5. Kumar S, Ma Y G. Phys Rev C, 2012, 86: 051601(R)
6. Kumar S, Ma Y G, Zhang G Q. Phys Rev C, 2012, **86**: 044616
7. Li S X, Fang D Q, Ma Y G, *et al*. Phys Rev C, 2011, **84**: 024607
8. Zhou C L, Ma Y G, Fang D Q, *et al*. Phys Rev C, 2013, **88**: 024604
9. Zhou C L, Ma Y G, Fang D Q, *et al*. Plasma Scince and Technology, 2012,16

上海激光电子伽玛源（SLEGS）

核物理研究室

上海激光电子伽玛源(SLEGS)是基于激光康普顿原理建设的高质量 γ 光装置，γ 光的低能区为 0.4–20 MeV，高能区为 330–550 MeV。其科学目标如下：通过光核反应开展核天体物理、核结构、极化物理、介子物理等领域中的基础物理研究，特别是解决核天体物理中具有重大科学价值的问题；此外，还开展与航天、国防、核能等战略需求相关的应用基础研究，如利用 γ 射线开展航天电子元器件空间辐射效应中的总剂量效应和抗辐射加固评估的研究，以及航天用 γ 探测器的精确定标。SLEGS 的低能区覆盖了光核反应热点能区(几百 keV 到十几 MeV)的绝大部分，并且其能量也可连续或多个离散点调节，高能区能量范围也能兼顾部分介子物理(K 介子和 π 介子)的研究。建成的 SLEGS 有望成为一个以低能为主兼顾高能、开展基础物理和应用研究相结合的多功能实验平台。

目前，SLEGS 已经被正式纳入上海光源二期工程。2011–2012 年度主要进行 SLEGS 的初步设计(SLEGS 整体设计示意图如图 1 所示)。具体开展的设计工作如下：

3 完成光束线设计

(1) 设计指标

能量范围：低能区：0.4–20 MeV；高能区：330–550 MeV；单色性：5%（加准直器）；γ光通量：低能区：10^5–10^7 phs/s；高能区：10^5–10^6 phs/s；发散度：0.5 mrad。

(2) 光源和前端区设计。光源和前端区的功能是产生γ光并将产生的γ光引出。光源系统主要包括：1)碰撞点靶室，用于激光和储存环电子发生康普顿散射；2)激光系统，用于激光的引入和检测；3)测量系统，用于激光和电子的检测。前端区主要包括真空管道、真空泵、真空阀、光阑、γ 光准直器和位置监测器等。

(3) 束线主要光学元件设计。光束线的功能是将前端区引出的γ光引到实验站，并对γ光的性质进行检测。光束线系统主要包括：1) 相干公司高功率连续激光器(型号：Diamond GEM-100L，Paladin 355)，用于背散射情况下的激光产生；高功率连续激光器(型号：Diamond GEM-100L)，用于斜入射情况下的激光产生；2) 光子流强测量仪：用于测量伽玛光流强。3) 伽玛光准直器：用于准直伽玛光，为铅制空心圆柱体，长度 20 cm，外径 10 cm，内径小于 40 mm，具体可根据需要选取。4) 标记计数器：用于测量高能伽玛光能量，能量分辨率约为 5–10 MeV，覆盖的能量范围为 330–550 MeV。

4 完成实验站设计

(1)实验方法。SLEGS 实验站采用的实验方法主要包括：散射法测量光致裂变截面、核共振荧光方法以及伽玛光成像法。

(2)主要配置设计及功能。实验站将建设低能散射实验平台，高能散射实验平台和核共振荧光实验平台。主要配置包括：1) 靶室，用于为反应提供真空环境；2) 多组探测器系统，用于对反应后产生的多种粒子进行测量；3) 电子学和数据获取系统，用于数据的采集。

SLEGS 初步设计的顺利完成为即将开展的 SLEGS 工程建设打下了坚实的基础。

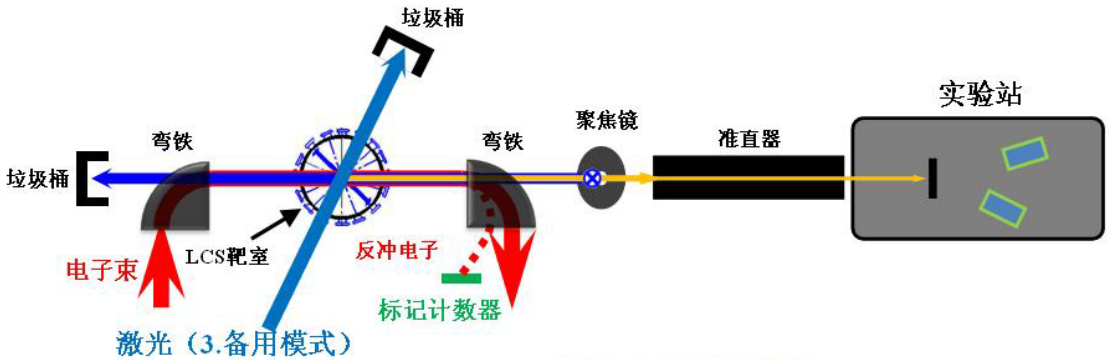

图 1 SLEGS 整体设计示意图

Shanghai Laser Electron Gamma Source (SLEGS)

Department of Nuclear Physics

Shanghai Laser Electron Gamma Source (SLEGS) is the designed one of the high quality gamma sources based on Laser Compton Scattering (LCS). The low and high energy regions of SLEGS are 0.4 MeV to20 MeV and 330 MeV to 550 MeV, respectively. Based on the method of photon nuclear reaction, SLEGS aims at basic physics researches, such as nuclear astrophysics, nuclear physics, polarization physics, and meson physics. In addition, SLEGS also tends to carry out applied research relating to aerospace, national defense, nuclear energy and other strategic demand of our country, such as space radiation effect research of the aerospace electronic components, and accurate calibration of the gamma detector for aerospace. The low energy region of SLEGS covers the hot zone of photon nuclear reaction (hundreds of keV to several MeV). More importantly, the energy of the gamma ray in low energy region is continuously adjustable. The high energy region of SLEGS covers part of meson physics (such as Kaon and Pion). SLEGS is expected to become a multi-function experimental platform for basic physics and applied physics researches at low energy and high energy in the future.

At present, SLEGS has been formally incorporated into the second phase of the project of Shanghai Synchrotron Radiation Facility (SSRF). Preliminary design of SLEGS has been carried out from 2011 to 2012 (The overall layout of SLEGS is shown in Fig.1). Details are listed below:

1 Beam line

(1) Design index

Photon energy range: 0.4 MeV to 20 MeV in low energy region: 330 Mev to 550 MeV in high energy region: Energy resolution: 5 % (using collimator); Flux: 10^5–10^7 phs/s at low energy; 10^5–10^6 phs/s at high energy; Emittance: 0.5 mrad.

(2) Light source system and front end system. The light source system includes LCS chamber, multi-way component, laser system and measurement system. The front end system includes vacuum tubes, vacuum pumps, vacuum valves, shutters, collimators, and position monitor etc.

(3) Major components of the beam line. 1) Laser: (a) High power CW laser for Slanting Scattering mode (type: Diamond GEM-100L, Coherent); (b) High power quasi-CW laser for Backward Scattering mode (type: AVIA 355 series, Coherent); (c) collimators for the installation and commissioning of laser. 2) Photon-flux instrument: for measurement of the flux of gamma ray. 3) Gamma calorimeter: for measurement of the gamma ray energy with resolution of 5–10 %, and with range from several keV to tens of MeV. 4) Gamma collimators: for narrowing the low energy gamma ray. The collimators will be made of plumbum and shaped into 200 mm long hollow cylinders with external radius of 100 mm and inner radius of less than 40 mm. 5) tagging counter: for tagging the high energy gamma ray with resolution of 5 MeV to10 MeV, and with range from 250 MeV to 550 MeV.

2 Experimental station

(1) Experimental methods. The methods employed by SLEGS's experimental station are photon nucleus scattering for measurement of photo fission cross section, nucleus resonance fluorescence and gamma-ray imaging.

(2) The main configuration of experimental station includes target chamber, experimental platform, detector system, electronics and DAQ system.

The preliminary design of SLEGS lays a soiled foundation for building SLEGS in the nearly future.

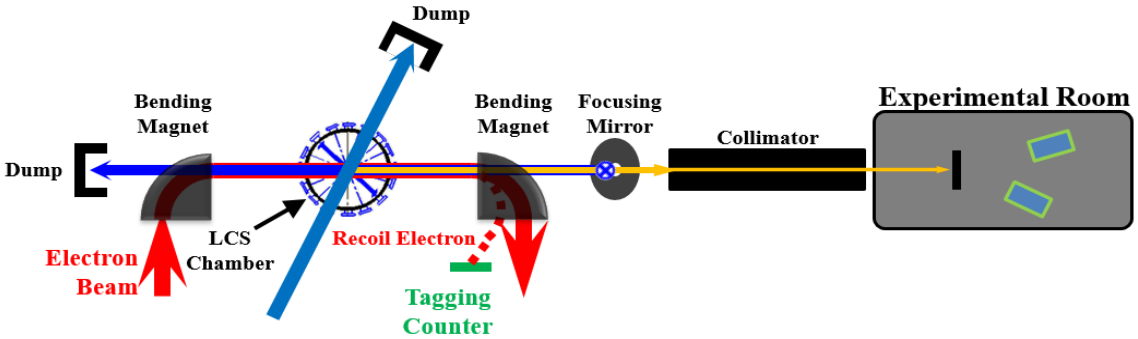

Fig.1 The overall layout of SLEGS.

CUORE 及 PandaX 合作组

核物理研究室

本研究方向主要在丰质子核结构、核物质状态方程与对称能密度依赖、重离子碰撞中产生的核物质的约化粘滞系数及液气相变现象等方面开展了系列实验或理论研究。

1 中微子国际合作(CUORE)

CUORE(Cryogenic Underground Observatory for Rare Events) 目前研究目标是测量 ^{130}Te 的无中微子双贝塔衰变事件，通过无中微子双贝塔衰变的半衰期测量，进而得到中微子的质量谱。探测器材料采用 TeO_2 晶体，在 CUORE 合作中我们负责该探测器单元晶体粉末的本底辐射、原材料纯度和宇宙射线本底测量。主要通过等离子体质谱仪(ICP-MS)测量 Te 金属，TeO_2 等原材料中的微量元素如 Ag，Au，Pt，Pb，Bi，Th 和 U 的含量，保证这些微量元素的杂质含量在实验允许值之下；研制了进行低本底γ测量的探测器和宇宙射线探测器。2011–2012 年继续为 CUORE 项目测试样品纯度(45 个样品，第 8–12 批次)，至 2012 年 10 月圆满完成了近 5 年(2008–2012)的所有晶体材料的纯度检测任务，完成了全部的 12 个批次，总计 91 个样品的等离子体质谱仪 ICPMS 检测分析工作，为 CUORE 的 TeO_2 晶体探测器按期在地下实验室陆续的组装、测试提供了强有力的支持。2011 年 12 月参加 CUORE 合作组会议，2012 年 1–4 月参加意大利 Gran Sasso 地下实验室 CUORE-0 准备实验的值班，并学习、参与 CUORE 的数据获取工作[1-7]。

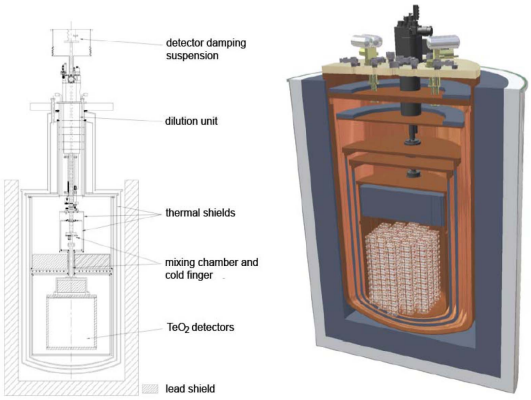

CUORE 探测器示意图

2 暗物质测量液氙探测器研究(PandaX)

PandaX (Particle and Astrophysical Xeon TPC, 粒子和天体物理液氙探测项目，又称为“熊猫 X 计划”)，利用液氙组建大型时间投影室探测器 Xe-TPC(吨级)研究暗物质以及中微子的基本性质，目前主要的研究目标是液氙探测器屏蔽材料以及探测器的放射性检测，低本底伽马监测站设计和加工，^{3}He 中子正比计数器的模拟分析、测试等[4]。

低本底伽马测量：HpGe 伽马检测站在上海实验室初步组建后，2012 年主要完成 PandaX 部分重要样品的测试；2012 年 7 月转移到锦屏山地下实验室重新组装，经测试宇宙射线本底降低一个量级以上，开始低本底的伽马测量；低本底中子测量：2011 年在实验室利用天然环境中子本底测试，刻度 ^{3}He 正比计数器，2012 年4 月和7 月分别进行了 2 次调试[8]。

锦屏山地下实验室 PandaX 伽马监测站

参考文献

1. The CUORE Collaboration, arXiv:1109.0494v3
2. The CUORE Collaboration, arXiv:1210.1107, Astropart. Phys. 45, 13 (2013)
3. The CUORE Collaboration, arXiv:1108.4757, Astropart. Phys. 35, 839 (2012)
4. The CUORE Collaboration, arXiv:1209.2800, J COSMOL ASTROPART P 05, 007 (2013)
5. doi:10.1088/1475-7516/2013/05/007The CUORE Collaboration, arXiv:1209.2519, J COSMOL ASTROPART P 01, 038 (2013)doi:10.1088/1475-7516/2013/01/038
6. The CUORE Collaboration, 2011 LNGS Report
7. The CUORE Collaboration, 2012 LNGS Report
8. 刘应都, 张国强, 王宏伟, 田文栋. 核技术, 2012, 35(3): 175

CUORE and PandaX Collaborations

Department of Nuclear Physics

The topic mainly focus on neutrinoless double beta decay (0**ν**DBD) and experimental study related with dark matter and dark energy under conditions of underground laboratory and non-accelerator. The later one was partially supported by a sub-project named "Developing liquid xeon detector for dark matter measurement" in a 973 project. We have carried out a series of experimental and detector investigations in nuclear physics and particle physics frontier, such as ultralow background detector development. Some interesting results have been obtained.

1 0vDBD international collaboration

The aim of CUORE (Cryogenic Underground Observatory for Rare Events) is to obtain mass spectrum of neutrino by measuring half-life of the neutrinoless double beta decay of ^{130}Te. The detector is made of TeO_2 crystals. We are responsible for measuring background radioactivity of crystal power, purity of raw materials and background of comic ray. The contents of trace elements of such as Ag, Au, Pt，Pb，Bi，Th and U in TeO_2 power, which is measured by ICP-MS, must be guaranteed below the allowed value. We developed detectors to measure low background Gamma and cosmic rays. During 2011–2012, we continued to measure the purity of samples for CUORE (45 samples, 8th-12th batch). Till Sept. 2012, we finished measurements of total 12 batches, 91 crystal materials samples in almost last 5 years (2008–2012). Our work provides strong support for testing and assembling of crystals underground on time.

We participated in CUORE collaboration meeting in Dec. 2011. In addition, we took part in the shift for the CUORE-0 experimental preparation, also learn and involved DAQ work at Gran Sasso from Jan. to Apr. in 2012 [1-7].

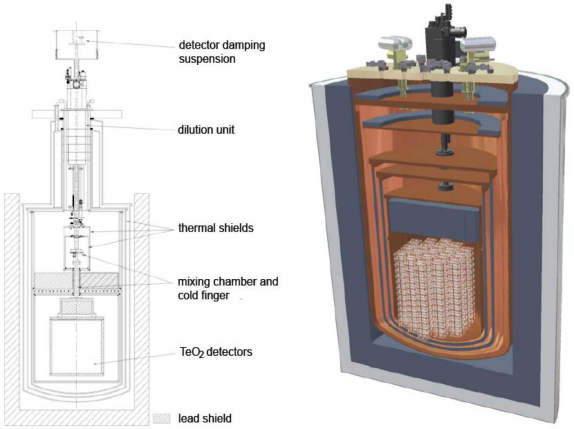

The schematic diagram of CUORE detector

2 The study of liquid xeon detector for dark matter (PandaX)

The aim of PandaX (Particle and Astrophysical Xeon TPC) is to build large scale time projection chamber: Xe-TPC which is used to search for dark matter and investigate properties of neutrino. The main task now is to measure background radioactivity of shielding materials and detectors, design and machine of Gamma counting station，simulate and test ^{3}He neutron proportional counter.

HpGe Gamma counting station has been assembled in Shanghai firstly. The measurements of part of important samples have been carried out in 2011–2012. The station was transported to Jinping underground lab and reassembled in July 2012. The measurement results show that the background of cosmic ray is one order magnitude lower. The ^{3}He neutron proportional counter was tested using natural neutron aboveground in 2011. The debug was carried in Apr. and Jul. of 2012, respectively[8].

γ ıd
laboratory

References

1. The CUORE Collaboration, arXiv: 1109.0494v3
2. The CUORE Collaboration, arXiv: 1210.1107, Astropart. Phys. 45, 13 (2013)
3. The CUORE Collaboration, arXiv: 1108.4757, Astropart. Phys. 35, 839 (2012)
4. The CUORE Collaboration, arXiv: 1209.2800, J COSMOL ASTROPART P 05, 007 (2013)
5. doi: 10.1088/1475-7516/2013/05/007The CUORE Collaboration, arXiv: 1209.2519,J COSMOL ASTROPART P 01, 038 (2013)doi:10.1088/1475-7516/2013/01/038
6. The CUORE Collaboration, 2011 LNGS Report
7. The CUORE Collaboration, 2012 LNGS Report
8. Liu Y D, Zhang D G, Wang H W, *et al*. Nucl Tech, 2012: **35**: 175

中子物理实验装置（白光中子源）

核物理研究室

本研究方向是 TMSR 关键核数据测量系统研制及测量，TMSR 专项中“反应堆物理与工程”项目的课题之一，为反应堆设计所需的评价核数据提供最基础的，精确全面的实验数据。主要为钍基熔盐堆(TMSR)相关的中子截面核数据测量，研制一台 15 MeV 电子直线加速器驱动的白光中子源，即中子物理实验装置，在中子产生靶，中子物理实验终端，中子探测器的研制等方面开展了一系列研制与模拟研究，设计了中子物理实验装置等。

该装置的主要目的在于：(1) 产生白光中子谱，进行钍基熔盐堆相关的 Th-U 反应链核数据的初步测量。(2) 为更高能量(约 100 MeV)电子加速器驱动的白光中子源做技术性尝试。(3) 利用中子源，检验，刻度中子探测器，设计、研发新型的中子探测器装置。(4) 中子， γ 与熔盐及燃料、包壳材料中轻元素的相互作用研究。(5) γ 活化、材料和生物辐照效应、屏蔽研究，探测器的 γ 辐照效应研究。

整个中子物理实验装置可以分为电子加速器、中子产生靶、中子实验终端，数据获取与控制系统等 4 个主要部分

1 中子产生靶

钨具有较高的熔点温度，杨氏模量和较高的热导能力，为首选的固体靶材料，与钽元素相比，钨元素在光核反应后生成的放射性同位素半衰期更短，产额更低；钨的热导率是钽的 3 倍左右，钨具有比钽更好的散热效果，模拟计算给出钨的光子溢出产额要低于钽，钨靶光子本底要稍微低于钽。另外，强辐射条件下，高压冷却水会严重腐蚀靶材料，须采用适当的措施避免直接接触。钨靶设计为圆柱形，直径 60 mm，厚度 48 mm，纯度为 98 %，为了降低温度和保持真空，设计了铜座冷却以及不锈钢真空壳[1-3]。

2 中子能谱 TOF 测量

在中子能谱测量中，飞行时间法是一种最直接、最精确的测量方法。随着快闪烁计数器的出现和纳秒脉冲技术的发展，飞行时间法也用到了快中子的测量中，飞行时间法的精确性和分辨率都远高于其它方法。要测量中子的飞行时间，必须记录中子从起点出发的时刻和到达飞行距离终点的时刻。后者由路程终点处的中子探测器中出现的脉冲时间来给出，路径的长度决定了测量的精度，在我们的设计中由于空间的限制，采用约 5 m 的飞行路径。

3 中子实验终端

中子束引出以后，还要经过滤波，准直，吸收、屏蔽以后才能到达中子实验终端，目前我们正在设计不锈钢中子准直管道，在 15 MeV 装置上将直接使用其中的一段(约 5 m 长度)。实验装置主要集中在总截面和俘获截面的实验测量上，设计制作了 ^{6}LiI[4]，^{6}Li-ZnS，^{6}Li-Glass 等中子探测器用于总截面 TOF 测量，设计了 C_6D_6，CsI(Tl)阵列用于俘获截面测量。

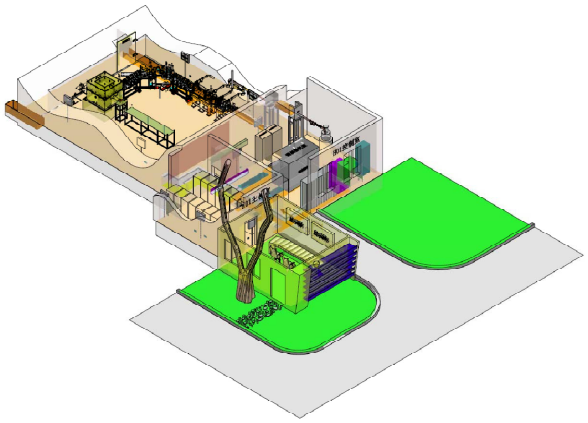

图1 15 MeV 电子直线加速器驱动的中子物理实验装置示意图(白光中子源)

参考文献

1. 王宏伟,李琛,张松, 等. 15 MeV 直线电子加速器驱动的白光中子源物理设计，设计报告，2012.
2. LIN Zuokang, SUN Guomin, CHEN jingen, *et al*. Nuclear Science and Techniques, 2012, **23**: 272
3. LIN Zuokang, ZOU Xin, CAO Yun, *et al.* Atomic Energy Science and Technology, Suppl Sep, 2012, **46**: 26
4. 杜龙，常乐，王玉廷等，核技术，2014, **37**: 040201

Neutron Physics Experimental Facility（White Light Neutron Source）

Department of Nuclear Physics

This topic is to develop measurement system and method for TMSR key nuclear data, which is a sub –project of reactor physics and project. The aim of this project is to provide the basic, complete and accurate neutron nuclear data for reactor engineering design. Our task is to develop a white light neutron source driven by 15MeV electron LINAC accelerator. The work is related with simulation and development of neutron production target, neutron experimental terminal, neutron detector etc.

The specific aim of the project is shown as following. (1) Producing white light neutron spectrum used for preliminary measurements of nuclear data related with Th-U reaction chains. (2) Accumulating technical experiences for higher energy (~ 100 MeV) white light neutron source driven by electron LINAC accelerator. (3) Test and calibration of neutron detectors using the white light neutron source. Furthermore, to develop new type neutron detectors. (4) Study the interactions among neutron, Gamma, molten salts, fuels and light elements in canning materials. (5) Study Gamma activation, irradiation effects of materials and biology, shielding and Gamma irradiation effects.

The whole facility consists of four main parts: electron LINAC accelerator, neutron production target, neutron experimental terminal and DAQ & Control system.

1 Neutron production target

Tungsten (W) has high melting point, Young's modulus and heat conductivity. Therefore, W is the preferred solid target material. Compared with Titanium (Ta), the radioactive isotopes produced by photonuclear reactions have lower yields and shorter half-life. The heat conductivity of W is three times higher than Ta. Therefore, W has more better heat dissipation effect. Our simulation shows that yield of light overflow is lower than Ta. So the light background is also lower than Ta. In addition, in order to avoid the severe erosion of target from high temperature cooling water under strong irradiation surrounding, proper measures must be adopted. The W target has the cylindrical shape with diameter 60 mm, length 48 mm and purity 98%. In order to keep low temperature and vacuum, cooling pedestal is made of Cu and a stainless vacuum shell is adopted[1-3].

2 TOF measurement of neutron energy spectrum

Time of flight (TOF) is the most direct and accurate method to measure neutron energy spectrum. Later, with the emergence of fast scintillation counter and the development of nanosecond pulse technology, TOF is also used for fast neutron, which has more high accurate and resolution compared with other methods.

In order to measure the time of flight of neutron, the starting time and stop time must be recorded. The later is recorded by pulse time in neutron detector. The accuracy depends on the path length of flight. In our scheme, 5 m flight length is adopted due to limit space.

3 Neutron experimental terminal

The neutron beam needs to be filtered, collimated, absorbed and shielded to reach neutron experimental terminal after extraction. We designed stainless collimation pipe. A 5 m long pipe will be used for 15 MeV facility. Due to the main aim of our facility is focus on total and capture cross section, we have developed ^{6}LiI[4], ^{6}Li-ZnS, ^{6}Li-Glass detectors to measure total cross section by TOF method. C_6D_6, CsI(Tl) array detectors are designed to measure capture cross section.

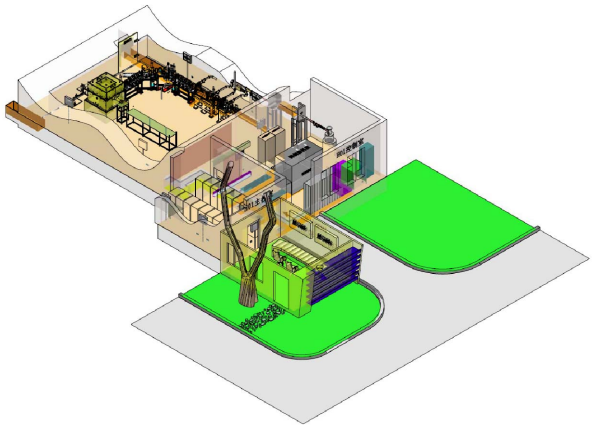

Fig.1 Schematic diagram of neutron physics experimental facility driven by 15MeV electron accelerator.

References

1. Wang H W, Li C, Zhang S, *et al*. The design report of neutron physics experimental facility driven by 15 MeV electron accelerator, 2012
2. LIN Zuokang, SUN Guomin, CHEN jingen, *et al*. Nuclear Science and Techniques, 2012, **23**: 272
3. LIN Zuokang, ZOU Xin, CAO Yun, *et al*. Atomic Energy Science and Technology, Suppl Sep, 2012, **46**:26
4. Du L，Chang L, Wang Y T Y, *et al*. Nuclear Technique, 2012, **37**: 040201

生物传感器研究

物理生物学研究室　樊春海

课题组依托上海光源和物理生物学实验室，与相关课题组紧密合作，主要从事纳米生物传感器、微流控生物芯片、生物光子学与生物电化学、分子机器、DNA 纳米技术与 DNA 计算机等方面的研究，旨在发展可用于分子诊断、环境检测、生物安全性防御的新一代高灵敏、高特异性、廉价、快速、便捷的集成化生物传感器与生物芯片。

DNA 纳米技术

DNA 纳米技术近年来成为一个研究热点。发展了一种固定在金电极表面的三维 DNA 纳米结构框架，为 DNA 双螺旋结构介导的界面电荷耦合传递提供了新的证据[1]，并将这种 DNA 纳米结构修饰金电极界面的传感器用于食管鳞状细胞癌病人 microRNA 靶标的超灵敏检测，检测限可达 aM(10^{-18} mol·L^{-1})水平(<1000 个分子)[2]。

创新性地将 DNA 纳米技术与 DNA 计算相结合，设计了一系列基于三维 DNA 纳米结构的新型“DNA 逻辑门”，实现了复杂的分子运算和活细胞内的分子成像，为实现智能载药系统提供新可能[3]。

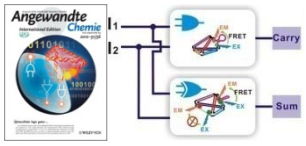

DNA 逻辑门

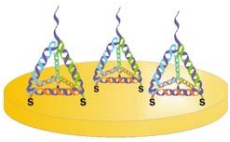

DNA 纳米结构修饰金电极

新型检测平台

我们发展了一种基于金纳米粒子的高通量长片段单倍型分型技术，至少可以在长达 34 kb 人类基因组片断中实现高特异性扩增，并获得清晰的测序图谱，从而实现单倍型的规模化检测[4]。

基于氧化石墨烯与 DNA 分子相互作用研究，我们提出了“集合适配体”新概念，构建了一种新的检测平台，实现了多种生物靶标的特异性识别与检测，并成功应用于不同肿瘤细胞和细菌的识别[5]。

纳米复合探针

发展了一种制备高性能DNA-金纳米粒子复合探针的新方法[6]。采用天然 DNA 序列设计成双嵌段寡核苷酸，即探针部分用于 DNA 识别，连续的腺嘌呤碱基(polyA) 用于 DNA 固定在金纳米粒子上。这种探针避免了使用修饰 DNA 分子，而且可通过改变 A 碱基的长度精确调控纳米金表面上 DNA 密度，从而避免了 DNA 分子间的相互作用，实现了探针的高识别活性。

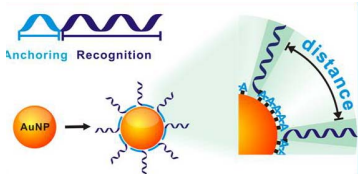

DNA-AuNPs 复合探针

金纳米粒子的催化特性

将金纳米粒子类似天然葡萄糖氧化酶的催化活性与金纳米粒子催化生长耦合，我们提出了一种自限的生长机制[7]。利用暗场光学显微镜技术实时、动态地观测到 DNA 分子可以调控单个金纳米粒子的自限生长[8]。

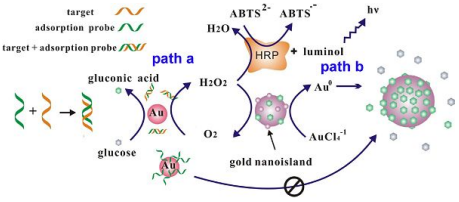

DNA 调控金粒子的自限生长

参考文献

1. Lu N, Pei H, Ge Z, *et al*. J Am Chem Soc, 2012, **134**: 13148-13151
2. Wen Y, Pei H, Shen Y, *et al*. Sci Rep 2012, **2**: 867
3. Pei H, Liang L, Yao G, *et al*. Angew Chem Int Ed, 2012, **51**: 9020-9024. (当期杂志封底)
4. Chen P, Pan D, Fan C, *et al*. Nature Nanotechnol, 2011, **6**: 639-644
5. Pei H, Li J, Lv M, *et al*. J Am Chem Soc, 2012, **134**: 13843-13849
6. Pei H, Li F, Wan Y W, *et al*. J Am Chem Soc, 2012, **134**: 11876-11879
7. Luo W, Zhu C, Su S, *et al*. ACS Nano, 2010, **4**: 7451-7458
8. Zheng X, Liu Q, Jing C, *et al*. Angew Chem Int Ed, 2011, **50**: 11994-11998

Progress in Biosensor Research

FAN Chunhai Department of Physical Biology

Relying on the Shanghai Synchrotron Radiation Facility and Laboratory of Physical Biology, our research group is mainly engaged in the research of nano-biosensors, microfluidic biochip, bio- photonics and bio-electrochemistry, DNA computation and DNA machine. Our research is aimed at developing next generation sensors to meet China's requirement for molecular diagnostics, environmental monitoring and biological safety. The next generation biosensors are meant to have high sensitivity and selectivity, and to be cost-effective with short detection time and capable of further devising into portable chips.

DNA Nanotechnology DNA nanotechnology is a hot research field in the world. We developed 3D DNA nanostructures fixed on gold electrodes, which provided new evidence for the interface charge coupled delivery mediated by double helix DNA[1]. This was also used as the sensor for ultra sensitive detection of microRNA target of esophageal squamous cell carcinoma, with a detection limit up to aM (10^{-18} mol·L^{-1}) (<1000 molecules)[2].

By combing DNA nanotechnology with DNA computation, we designed 3D DNA nanostructure-based logic gates, which could carry out complex molecular computation and cellular molecular imaging. The DNA logic gates may provide new possibilities for intelligent drug delivery systems[3].

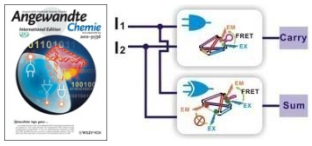

DNA logic gates.

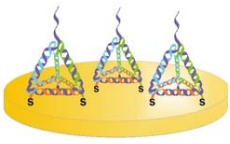

DNA nanostrcure-Au sensor.

New Detection Platform We developed a strategy based on gold nanoparticles (AuNPs) for high-throughput genotyping of long-range haplotype, achieved high specific amplification of 34 kb human genome and obtained clear capillary sequencing. AuNPs-enhaced allele-specific sequencing may provide an in-depth understanding of complex genetic diseases[4].

Based on the interaction between 2D graphene oxide nanosheets and DNA, we reported a new concept of adaptive "ensemble aptamers" and provided a new biological detection platform. We demonstrated that this platform provides a highly discriminative and adaptive tool for high-precision identification of a wide range of targets for diagnostic and proteomic applications[5].

Multicomponent Nanoprobes We reported a novel strategy for spatially controlled functionalization of AuNPs with designed diblock oligonucleotides that are free of modifications[6]. Poly adenine (polyA) can serve as an effective anchoring block for preferential binding with the AuNPs surface, and the appended recognition block adopts an upright conformation that favors DNA hybridization. The lateral spacing and surface density of DNA on AuNPs can also by systematically modulated by adjusting the length of the polyA block. The diblock oligonucleotide strategy results in DNA-AuNPs nanoconjugates with high and tunable hybridization ability, which formed the basis of rapid plasmonic DNA sensors.

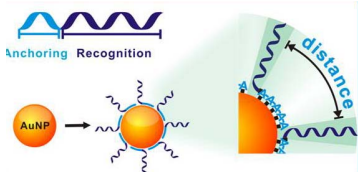

DNA-AuNPs Nanoprobes.

The Catalytic Properties of AuNPs Our research indicated the catalytic activity of AuNPs is similar to natural glucose oxidase. Based on this, we proposed a mechanism of self-limitation growth of AuNPs[7]. Through real-time and dynamic observation using dark-field optical microscopy, we observed that DNA molecules could regulate the self-limitation growth of single gold nanoparticle[8].

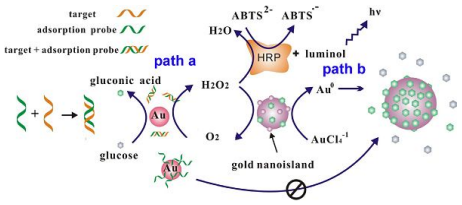

Self-limitation growth of AuNPs regulated DNA.

References

1. Lu N, Pei H, Ge Z, *et al*. J Am Chem Soc, 2012, **134**: 13148-13151
2. Wen Y, Pei H, Shen Y, *et al*. Sci Rep 2012, **2**: 867
3. Pei H, Liang L, Yao G, *et al*. Angew Chem Int Ed, 2012, **51**: 9020-9024. (当期杂志封底)
4. Chen P, Pan D, Fan C, *et al*. Nature Nanotechnol, 2011, **6**: 639-644
5. Pei H, Li J, Lv M, *et al*. J Am Chem Soc, 2012, **134**: 13843-13849
6. Pei H, Li F, Wan Y W, *et al*. J Am Chem Soc, 2012, **134**: 11876-11879
7. Luo W, Zhu C, Su S, *et al*. ACS Nano, 2010, **4**: 7451-7458
8. Zheng X, Liu Q, Jing C, *et al*. Angew Chem Int Ed, 2011, **50**: 11994-11998

纳米材料的生物效应研究

物理生物学研究室　　黄　庆

本课题组依托于上海光源和物理生物学研究室，主要从事纳米科学、化学、物理学和生物科学领域的交叉研究。研究内容包括：纳米材料的制备和表征、纳米材料与生物大分子的相互作用、纳米材料的生物学效应及分子机制以及同步辐射技术和超分辨显微成像技术在纳米生物效应研究中的应用。

纳米材料的细胞生物效应

纳米材料的大比表面积和高吸附活性直接影响其生物学效应。在石墨烯氧化物(Graphen oxide, GO)的细胞毒性研究中，我们发现 GO 在低血清浓度(含 1%血清)的培养基中，表现出浓度依赖的细胞毒性；在正常培养基中(含 10%血清)，细胞毒性显著性减弱[1]。在纳米金刚石的生物效应研究中也发现，在无血清培养时，纳米金刚石可以吸附并携带培养基中的大量钠离子进入细胞，改变细胞内渗透压和 ROS，导致细胞受损；当在正常培养基(含有 10%血清)，纳米金刚石表面被血清包被，几乎没有细胞毒性[2]。

量子点的生物相容性问题一直是其临床应用的瓶颈问题。课题组系统比较了 3 种不同结构的镉系量子点的细胞毒性，发现量子点的细胞毒性与其解离的镉离子相关[3]。同时，基因芯片分析和上海同步辐射光源软 X 射线显微成像技术证明量子点的细胞毒性与纳米材料的尺寸效应和表面效应造成的“纳米毒性”也密切相关[4,5]。这一系列工作为理解量子点的生物安全性问题提供了新角度，对量子点在生物成像、医学诊断和治疗中具有一定指导作用。

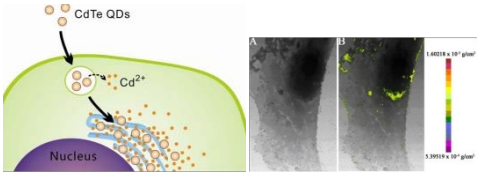

量子点的细胞毒性机制

纳米载药体系

CpG 寡核苷酸可以作为一种良好的免疫佐剂用于抗感染和肿瘤等的辅助。当 CpG 寡核苷酸负载到金纳米粒子表面后，可以很容易地被细胞内吞，并产生显著的免疫刺激作用，刺激产生的 TNF-alpha, IL-6, IL-12 等细胞因子浓度相对于裸寡核苷酸提高了两个数量级。而且,纳米载药体系的核酸运载率也显著高于商品试剂 lipofectamin[6]。另一研究中，我们将刚性的 DNA 四面体结构与 CpG 寡核苷酸结合，发现 DNA 纳米结构可以有效地将 CpG 寡核苷酸载运到细胞内，在胞浆内可以稳定存在 8 h 以上，极大增强了 CpG 寡核苷酸的免疫刺激效果。DNA 纳米结构作为核酸分子，更容易与待载运核酸分子偶联，且在体内可降解、无免疫原性，在疾病诊疗中显示了广阔应用前景[7]。

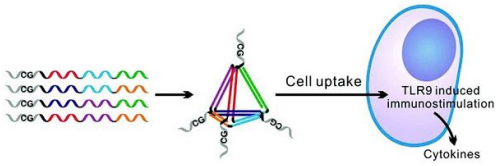

DNA 四面体载药系统

纳米材料的动物毒性

以果蝇为动物模型，我们发现经食物摄取的金纳米粒子能够显著增强果蝇代谢途径中胰岛素和生长因子下游的 PI3K/Akt 信号通路，促进细胞对食物中营养成分的吸收和利用。该研究预示金纳米粒子在糖尿病等代谢紊乱疾病的治疗中具有应用潜力[8]。

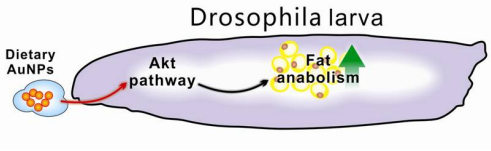

金纳米粒子对果蝇代谢信号通路的调控

参考文献

1. Hu W, Peng C, Lv M, *et al.* ACS Nano, 2011, **5**: 3693-3670
2. Zhu Y, Li W, Zhang Y, *et al*. Small, 2012, **11**: 1771-1779
3. Su Y, He Y, Hao T, *et al*. Biomaterials, 2009, **30**:19–25
4. Su Y, Hu M, Fan C, *et al*, Biomaterials, 2010, **31**: 4829-4834
5. Chen N, He Y, Su Y, *et al*. Biomaterials, 2012, **33**: 1238-1244
6. Wei, M, Chen H, Li J. Angew Chem Int Ed, 2012, **51**: 1202-1206
7. Li J, Pei H, Zhu B, *et al*. ACS Nano, 2011, **5**: 8783-8789
8. Wang B, Chen N, Wei Y, *et al*. Sci Rep, 2012, **2**: 563

Biological Effects of Nanomaterials

HUANG Qing Department of Physical Biology

Relying on the Shanghai Synchrotron Radiation Facility and Laboratory of Physical Biology, our research group mainly focuses on interdisciplinary studies combining nanoscience, chemistry, physics and biology. On-going research programs include preparation and characterization of nanomaterials, investigation on interactions between nanomaterials and biological molecules and studies on biological effects and molecular mechanisms of nanomaterials, in which synchrotron radiation techniques and super-resolution microscopy techniques have served as important tools.

Cellular Bio-effects of Nanomaterials

The bio-effects of nanomaterials are directly affected by their large surface area and extraordinary adsorption properties. Our studies on cytotoxicity of graphene oxide (GO) revealed that human cells were sensitive to the presence of GO, which showed concentration-dependent cytotoxicity at low concentrations of FBS (1%). The cytotoxicity of GO was greatly mitigated at 10% FBS, which is the concentration usually employed in cell medium[1]. For the cytotoxicity of nanodiamonds (NDs), the results showed NDs adsorbed and delivered a large amounts of sodium ions into cells in serum-free medium, which induced the change of osmotic stresses and concentrations of reactive oxygen species (ROS) to cellular damage. In complete culture medium, serum proteins wrapped around the NDs effectively and thus prevented the adsorption of sodium ions onto NDs, therefore, NDs showed no cytotoxicity[2].

The biocompatibility of quantum dots is the bottleneck for their clinical applications. We systematically studied the cytotoxicities of a series of cadmium-based quantum dots. The results showed the cytotoxicity was resulted from cadmium ion dissociated from QDs[3]. Additionally, the cellular toxicity is closely related to "nano-toxicity" caused by nano-size and surface effect of QDs suggested by gene chip analysis and synchrotron radiation X- ray microscopic technique[4,5]. This series of research work provide a new perspective for understanding the biological security of quantum dots, which can guide applications of QDs in biological imaging and medical diagnosis and treatment.

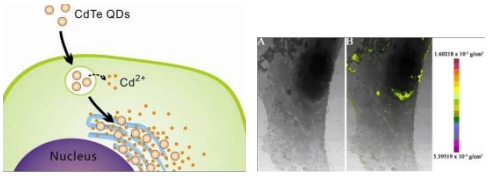

The toxic mechanism of QDs.

The System of Nano-drug Dilvery

CpG oligonucleotides have been used as an adjuvant for assistance in anti-infection and anti-tumor treatment. The study showed CpG loaded on the surface of gold nanoparticles (AuNPs) was easily cellular uptaken, which led to immune stimulation. The concentrations of cytokines, such as TNF-alpha, IL-6 and IL-12, in cells stimulated by AuNPs-CpG are two orders of magnitude higher than those induced by naked oligonucleotides. Moreover, delivery efficiency of nucleic acids by AuNPs is significantly higher than lipofectamin[6]. In the other study, when rigid DNA tetrahedron structures were combined with CpG oligonucleotides, we found DNA nanostructures can effectively carry CpG into cells, which can stably exist for more than 8 h in the cytoplasm, and thus greatly enhances the immune effect induced by CpG. Additionally, as nucleic acids, DNA nanostructures are bio-compatible, easily degradable *in vivo* and exhibit no-immunogenicity, therefore, they can be potentially applied in diagnosis and treatment[7].

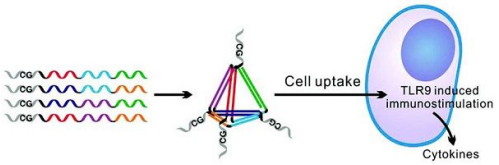

DNA tetrahedron as drug delivery system.

The toxicity of nanomaterials in animals

The study found the food intake of AuNPs by Drosophila could significantly enhance the PI3K/Akt signaling pathways, which are downstream of insulin and growth factor pathways, which consequently improved cellular uptake and use of nutrients in food. The results indicate that the AuNPs have application potential in the treatment of metabolic disorders such as diabetes. [8]

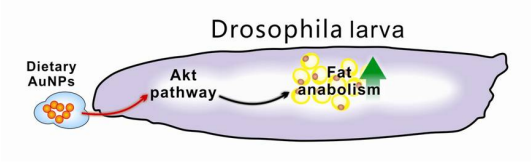

Regulation of AuNPs on metabolic pathway in Drosophila.

References

1. Hu W, Peng C, Lv M, *et al*. ACS Nano, 2011, **5**: 3693-3670
2. Zhu Y, Li W, Zhang Y, *et al*. Small, 2012, **11**: 1771-1779
3. Su Y, He Y, Hao T, *et* al. Biomaterials, 2009, **30**:19–25
4. Su Y, Hu M, Fan C, *et al*, Biomaterials, 2010, **31**: 4829-4834
5. Chen N, He Y, Su Y, *et al*. Biomaterials, 2012, **33**: 1238-1244
6. Wei, M, Chen H, Li J. Angew Chem Int Ed, 2012, **51**: 1202-1206
7. Li J, Pei H, Zhu B, *et al*. ACS Nano, 2011, **5**: 8783-8789
8. Wang B, Chen N, Wei Y, *et al*. Sci Rep, 2012, **2**: 563

应用理论物理研究

水科学研究室　计算物理组　方海平

本组从事理论物理学与生物学的交叉研究，主要是纳米生物学和纳米尺度界面水的特性研究。本组以上海光源和我所重要研究方向为导向，与相关实验组密切结合开展应用基础理论研究，并建设相关的模拟计算平台，为实验提供模拟计算支持。已与所内多个实验组合作，并取得成功；也开展一些建立基本理论的探索性研究。

带有极性基团的表面也有疏水特性

表面的浸润性或者叫表面的亲疏水性，在大量的物理、生物、化学过程中和工程学上起着关键的作用。例如：蛋白质折叠、两亲分子的自组装、微流动技术、分子的识别检测技术和自清洁表面材料的制备等。对表面的亲疏水性质的误判，会导致对表面和表面附近物质的相互作用的错误理解，进而影响对整个系统的物理分析和相应的实验、应用设计。

由于水分子是极性分子，带有极性基团的分子对水有很强的亲和力，可以吸引水分子并且易溶于水。因此，一般认为这类带有极性基团的分子形成的固体材料表面容易被水润湿，是亲水表面。所以目前使表面变亲水的最普遍方法是表面极性基团修饰。

带有极性基团的表面总是亲水的吗？最近，中国科学院上海应用物理研究所水科学和技术研究室的王春雷博士和方海平研究员等通过理论分析发现，固体表面的亲水和疏水特性(浸润性)，还明显依赖于表面上极性分子的偶极长度。通过理论模型和分子动力学模拟证明，偶极长度存在一个临界值，当表面上极性分子的偶极长度小于此临界长度时，无论极性分子的偶极矩有多大，水分子仍无法“感受”到固体表面偶极的存在，从而使带有极性基团的表面也有疏水特性；当偶极长度大于此临界长度时，随着偶极矩和偶极长度增大，固体表面会变得越来越亲水。相关研究结果发表在国际学术期刊 Scientific Reports (Sci. Rep., 2012, 2, 358)上。http://www.nature.com/srep/2012/120411/srep00358/full/srep00358.html。

这种极性表面为什么会疏水呢？水中带有极性基团的分子，其正、负极性基团分别被水中的氧和氢原子所吸引(水中的氧和氢原子分别带有负、正电)，或者形成氢键，会导致这个分子与水分子产生强大的亲和力。当这些分子形成固体材料的表面时，如果分子小，偶极长度短，水分子之间的空间位阻效应(拥挤效应)不能保证水分子中的氢原子被吸引到表面上的负电荷，同时氧原子被吸引到正电荷(如图的下面部分)。这导致整体表面的偶极与水之间的相互作用较弱，表现出“意外的”疏水特性。当偶极长度增大，空间位阻效应减弱，更多的水分子中的氢原子(或氧原子)被吸引到表面上的负(或正)电荷很近的距离，界面变得更亲水。分子动力学模拟还证实该临界偶极长度的存在具有普适性，即很多类型的极性表面上均存在这样的临界偶极长度。2012 年，美国实验组 Wong 等人也发现了类似现象，即电偶极长度较小的表面上会表现出疏水行为(Phys. Rev. E 2012, 85, 031501)。

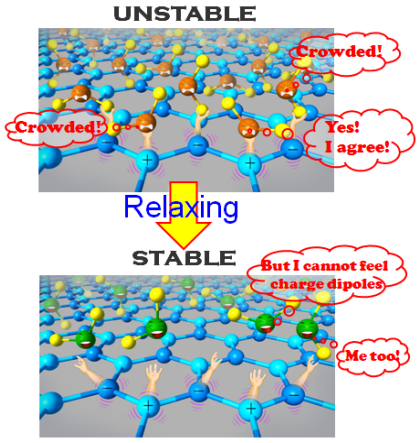

图 1　上图: 水中的氧原子(桔黄色哭脸)和氢原子(黄色小球)分别被表面上正、负极性基团所吸引，空间位置受到约束。当表面上正、负极性基团的距离比较小时，表面附近的水分子会非常拥挤，导致不稳定。下图: 表面附件的水分子间距离增大后，系统达到稳定。但不能保证水分子中的氢原子(黄色小球)被吸引到表面上的负电荷，同时氧原子(绿色笑脸)被吸引到正电荷，使水分子感受不到表面电荷的吸引力，从而使固体表面表现出疏水特性

在此以前，该研究组曾在 2009 年提出，当固体表面的电偶极排布合适，吸附在表面的第一层水表现出有序，可以导致第一层水上面出现(只有不完全亲水表面才有的)水滴，该表面呈现“表观的疏水” (Phys. Rev. Lett., 2009, 103, 137801; J. Phys. Chem. C, 2011, 115, 3018)。2013 年，《自然•材料》(Nat. Mater. 2013, 12, 289)对该发现和物理机制还给予专门评述。这些工作使人们从表面偶极排布的

角度来审视表面的亲疏水的物理机制，引发了包括美国科学院院士 Chandler 在内的许多国际学者在理论及实验上的后续工作，他们分别在滑石、金属铂(100)、羟基化的氧化铝表面、羟基化的二氧化硅表面、红宝石、尾端为羧基(-COOH)的自组装表面以及牛血清蛋白-Na_2CO_3 膜表面上都看到了类似的现象；这些工作说明了有极性基团的表面也可以表现出疏水或者“表观的疏水”性质，并有助于描绘表面的亲疏水性质与极性基团之关联的完整图像。

该项研究工作由中国科学院上海应用物理研究所、上海大学、四川大学和浙江大学的研究人员合作完成，得到了中国科学院、国家自然科学基金委、科技部、中国博士后科学基金会、上海市科学技术委员会和上海市人民政府(通过上海超级计算中心)的共同资助。

通过第一性原理分子动力学研究在碳纳米管束中锂离子的插入与迁移

利用基于密度泛函的第一性原理分子动力学方法对在碳纳米管束中锂离子的插入与迁移进行了研究。我们发现会锂离子很快渗透进碳纳米管中。在锂离子浓度较低的情况下，锂离子倾向于处在纳米管管口。有意思的是，我们发现锂离子能够在碳管中渗透并从碳管一端移动到另一端。我们同时发现锂离子可以处在两个近邻碳管之间，这是一种全新的锂离子插入与储存的机制。重要的是，碳管对处在三个近邻碳管之间的锂离子有非常强的吸附势，是其处在一个单层碳管中心轴线时的四倍。这说明处在三个近邻碳管之间的锂离子非常难以移除，表明这种情况下的锂离子储存是不可逆的。我们的研究有助于对锂离子在碳管中插入以及扩散机制的理解，并且对锂离子电池的实验发展与应有借鉴作用。

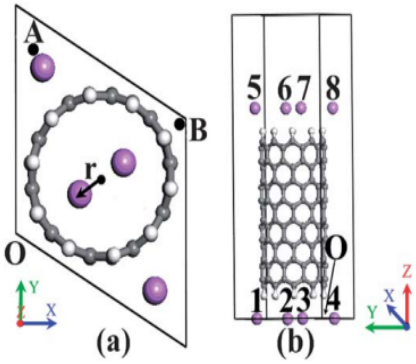

图 2　典型单元电池的初始构象从头开始分子动力学模拟

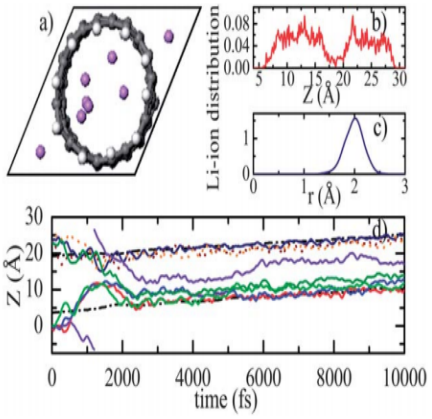

图 3　锂离子嵌入和扩散内或碳纳米管之间的反应。

设计一种分子尺度质子通道开关

我们设计了一种当施加合适电场时可以高效传输质子的纳米通道。通过对其本征传输率的研究，我们发现这种通道是具有开关性质的。通道的打开需要强电场与质子的吸附。当电场较小或者关闭的时候，质子传输会因为乙酸与碳管内壁之间的位阻效应而关闭。由于通道可以根据场强的强弱而在开闭状态之间切换，利用这种特点可以控制传输的方向，从而建立并且维持两侧的化学势。势的强度可以通过控制旋转集团的化学构成以及通道直径来调节。

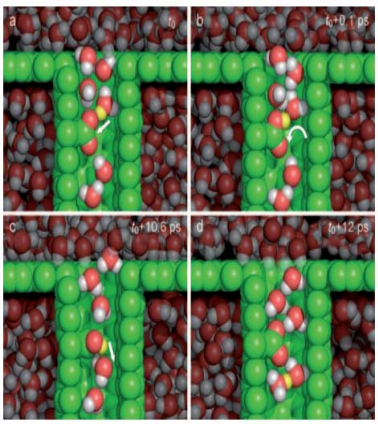

图 4　从一个完整的传导过程所设计的质子通道中封闭的质子传导机制（空间填充模型：氧原子：红色，碳原子：绿色，氢原子：白色）。

Cation⊗3π：阳离子与碳的一种新的作用形式

中国科学院上海应用物理研究所水科学与技术研究室的宋波博士、方海平研究员等科研人员与四川大学合作，提出了阳离子与三个苯环的协同相互作用，发现了反常相互作用行为并阐述了相关物理机理。研究结果发表于《美国化学学会杂志》[J. Am. Chem. Soc. 134, 12104-12109 (2012)]

该项工作提出一个阳离子可以与三个苯环结

构同时相互作用——Cation⊗3π 相互作用（这里 π 代表一个苯环结构内部的电子特性）。正常情况下，阳离子与一个或两个苯环结构的作用，其强度跟阳离子直径相关。阳离子直径越大，阳离子与苯环结构距离越远，相互作用越小。对应三种典型的一价离子，阳离子与一个苯环结构的作用强度的次序是 K+ < Na+ < Li+。但是，对于 Cation⊗3π 相互作用，研究发现，其作用强度随离子直径的增大而增大，即：Li+ < Na+ < K+。这种反常行为背后的物理机制是阳离子与苯环结构、相邻苯环结构间相互作用的协同效应。相邻苯环结构间相互作用导致直径小的阳离子与每个苯环结构的作用发生偏离，减弱的阳离子与每个苯环结构的作用强度。需要说明的是，阳离子与三个苯环结构相互作用强度和阳离子与两个苯环结构相互作用强度相当。

碳是生命的基本元素之一。由六个碳原子构成的苯环状结构广泛存在于 DNA 碱基、氨基酸等生物分子。包含苯环状结构的碳基纳米材料（例如富勒烯、碳纳米管、石墨烯、碳纳米线）被认为在分子器件、生物检测、能源储存等领域有广泛的应用。另一方面，阳离子广泛存在于土壤、大气等自然界，并且是生物体内的必要元素和材料中常用的掺杂元素。阳离子与苯环状结构的相互作用，在生物体系、纳米材料中起着关键的影响，Cation⊗3π 的发现为进一步理解生物分子的结构与功能、新型碳基材料与器件提供了新的视角。

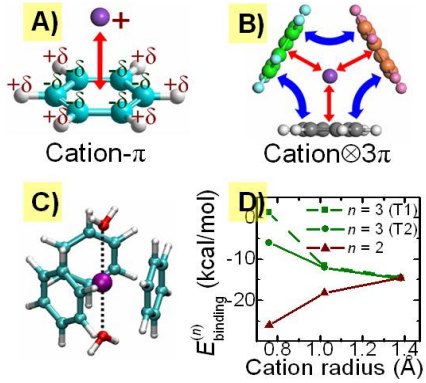

图 5 Cation⊗3π 相互作用与 Cation-π 相互作用的比较。大球、小球和紫色的球分别表示碳原子、氢原子和阳离子(钾离子、纳离子和锂离子)。红色箭头表示 Cation-π 相互作用，蓝色箭头表示 π-π 相互作用。A) Cation-π 相互作用。带正电的阳离子(cation)能够诱发苯环中的 π 电子重新分布，即：靠近阳离子的碳原子带负电荷(-δ)，远离阳离子的氢原子带正电荷(+δ)，从而产生 cation-π 相互作用。B) Cation⊗3π 相互作用。C) Cation⊗3π 相互作用在水中，以水合 Cation⊗3π 形式存在。黑色虚线表示阳离子与水分子之间的电荷相互作用。D) Cation⊗3π 与 Cation⊗2π 相互作用随阳离子大小变化的规律

该项研究工作由中国科学院上海应用物理研究所和四川大学、中国工程物理研究院流体物理研究所的研究人员合作完成，得到了中国科学院、国家自然科学基金委、国家科技部和上海市人民政府的共同资助。

超配位碳的新进展

作为第一作者和通讯联系人，高嶷和国内外 3 个单位合作，理论预测了最大配位数的碳体系。碳作为生物圈最重要的组成元素，其化学键组成一直以来是化学的终极问题之一。自 1857 年凯库勒(苯的发现者)提出四配位碳的概念以来，范托夫(第一届诺贝尔化学奖)、路易士(30 次诺贝尔化学奖提名)、鲍林(诺贝尔化学奖、和平奖)、霍夫曼(诺贝尔化学奖)等都在碳的配位理论方面作出杰出贡献。特别是随着 2000 年前后《科学》杂志连续发表了 5 篇研究工作，通过红外光谱对于五配位碳的理论预言进行了实验证实，又掀起了超配位碳的研究热潮。高嶷等通过最新发展的全局寻优技术结合第一性原理，借助于超级计算机，理论预测了至今具有最高配位数的碳配位体系[CTi_7^{2+}]，并存在室温下形成一维纳米线的可能。这一工作发表在 2012 年的《物理化学快报》(J. Phys. Chem. Lett., 2012, 3, 224-2268)后，迅速被英国皇家化学会旗舰新闻期刊《化学世界》(Chemical World)在网站主页上以封面故事“Carbon Clusters Score Lucky Seven”形式报道。英国伦敦帝国学院的实验化学家 Henry Rzepa 教授评论说：

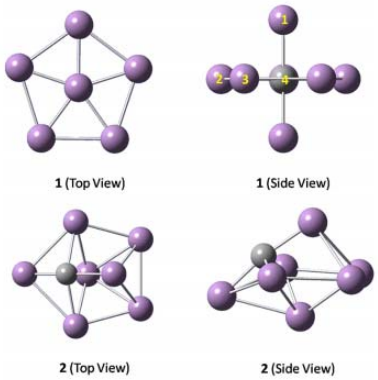

图 6 [CTi_7^{2+}]的超优化结构配位碳的异构体 1 和异构体 2 灰色球体表示的碳原子数,和紫色球体表示钛原子

“新思想可以来自理论计算就像来自实验一样，两者相互作用会更有活力和富有成果，CTi_7^{2+} 体系正是这一绝佳体现。这一思想可以促使并激励实验化学家去合成。”(“New ideas are as likely to come from computation as from experiment, and there is a vibrant, fruitful, interplay between these. The CTi_7^{2+} system here is a wonderful example of

how this process happens. The strength of ideas such is that it inspires experimental chemists to go make it in the lab.")

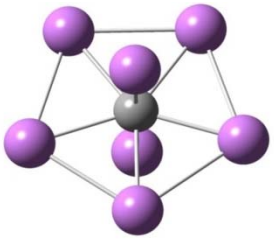

这一研究成果也入选由中国科学院院士和中国工程院院士评选的瀚霖杯“2012 年中国十大科技进展新闻”提名。

参考文献

1. Wang Chunlei, Zhou Bo, Tu Yusongu, Duan Manyi, Xiu Peng, Li Jingyei, Fang Haiping. Critical Dipole Length for the Wetting Transition Due to Collective Water-dipoles Interactions. Scientific Reports, 2012, **2**: 358
2. Wang Shen, Tu Yusong, Wan Rongzheng, Fang Haiping, Evaporation of Tiny Water Aggregation on Solid Surfaces of Different Wetting Properties. J Phys Chem B, 2012, **116**: 13863-13867
3. Duan Manyi, Song Bo, Shi Guosheng, Li Haikuo, Ji Guangfu Hu Jun, Chen Xiangrong, Fang Haiping. Cation⊗3π Cooperative Interaction of a Cation and Three Benzenes with an Anomalous Order in Binding Energy. JACS, 2012, **134**: 12104-12109
4. Song Bo, Yang Junwei, Zhao Jijun, Fang Haiping. Intercalation and diffusion of lithium ions in a carbon nanotube bundle by ab initiomolecular dynamics simulations. Energy & Environmental Science, 2011, **4**: 1379-1384
5. Gu Wei, Bo Zhou, Tihamr Geyer Geyer, Michael Hutter, Fang Haiping, Volkhard Helms. Design of a Gated Molecular Proton Channel. Angew Chem Int Ed, 2011, **50**: 768-771
6. Gao Yi, Shao Nan, Zhou Rulong, Zhang Guiling, Zeng Xiaocheng. [CTi_7^{2+}]:Heptacoordinate Carbon Motif? J Phys Chem Lett, 2012, **3**: 2264-2268
7. Gao Yi, Zeng Xiaocheng. Water-Promoted O2 Dissociation on Small-Sized Anionic Gold Clusters. ACS catalysis, **2**: 2614-2621
8. Zhou Xibin, Liu Guande, Kazuhiro Yamato, Shen Yi, Cheng Ruixian, Wei Xiaoxi, Bai Wanli, Gao Yi, Li Hui, Liu Yi, Liu Futao, Daniel m Czajkowsky, Wnag Jingfang. Michael J. Dabney, Zhonghou Cai, Jun Hu, Frank V Bright, He Lan, Zeng Xiaocheng, Shao Zhifeng, Bing Gong. Self-assembling subnanometer pores with unusual mass-transport properties,nature communications, 2012, **3**:1-8

Theoretical Physics for Nanobiology and Interfacial Water

FANG Haiping Department of Water Science Group of Computational Physics

The group is engaged in interdisciplinary studies on theoretical physics and nanobiology, focusing on molecular dynamics simulation and other computational studies on biomolecules and interfacial water. These provide theoretical assistance to synchrotron radiation studies and other experimental research programs at SINAP. Collaborating well with the experimental groups, the group has made remarkable progresses. It works on other fundamental researches, too, such as nanobubbles, nanochannels, biological channels and the structure of biomolecules.

Is polar surface always hydrophilic?

The wetting properties of surfaces, named hydrophobicity and hydrophilicity, play a critical role in extensive physical, chemical, biological and/or engineering sciences, such as protein folding, self-assemble of amphiphiles, micro-fluids devices design, biosensors and fabricating self-clearing materials. The misleading of the surface hydrophobicity and hydrophilicity would lead to the misunderstanding of the interactions and dynamics property at the interface, thus greatly affect the analysis and the design of the experiments.

As a polar molecule, water molecule has a high affinity with other polar molecules/groups. Namely, the surface with polar molecules or groups are easily hydrated by water. Thus the surfaces with polar molecules or groups are usually regarded hydrophilic. Actually, modifications of polar groups are always chosen by the experimental scientists to create the hydrophilic materials.

However, is the polar surface always hydrophilic? Recently, Dr. Chunlei Wang and Prof. Haiping Fang at Shanghai Institute of Applied Physics, Chinese Academy of Sciences, have shown that the length of the charge dipoles on the solid surface plays a key role on the wetting behavior. Both the theoretical analysis and the molecular dynamics simulations show that there is a critical length of the charge dipoles on the solid surface, below which the charge dipoles on the solid surface plays unexpectedly negligible role in the wetting property. The solid surface still exhibits hydrophobic behavior when the dipole length is less than the critical value, indicating that the water molecules on the solid surface seem not to "feel" attractive interactions from the charge dipoles on the solid surface, no matter how large the moment magnitude of the charge dipoles is. When the charge dipole lengths are greater than this critical length, it is found that the surfaces become more hydrophilic with the dipole lengths increase. Those results have been published on Scientific Reports (Sci. Rep., 2012, 2, 358) http://www.nature.com/srep/2012/120411/srep00358/full/srep00358.html.

Those unexpected observations result from the collective interactions between the water molecules and charge dipoles on the solid surface, where the steric exclusion effect(crowded effect) between water molecules prevents those hydrogen atoms of water molecules from staying very close to the negative charge and those oxygen atoms of water molecules from staying very close to the positive charge, reducing the interactions between the water molecules and the charge dipoles. Interestingly, the steric exclusion effect was also important for surfaces with charge dipole lengths greater than this critical length. When the charge dipole lengths are greater than this critical length, it is found that the surfaces become more hydrophilic with the dipole lengths increase. Further analysis shows that existence of the critical length is universal for various types of surface. Recently, Wong's group researchers have experimentally (Phys. Rev. E 85, 031501 (2012)) shown that the surface with extremely high dipole density displays similar hydrophobic property on the basis of inelastic x ray scattering techniques.

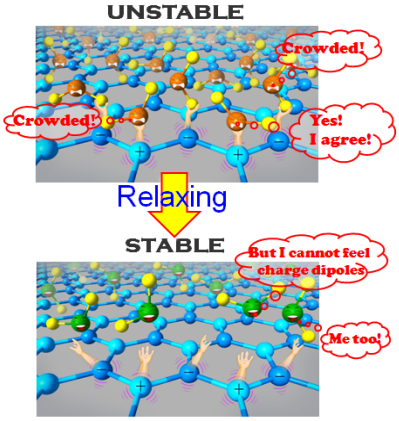

Fig.1 Upper Figure: the oxygen atoms of water (orange crying face) and the hydrogen atoms of water (yellow balls) are bind by the surface positive and negative charges. When the distance between surface charges is small, the water molecules would be very crowded and unstable. Bottom Figure: when the water molecules relax themselves and distance between water molecules is large, the system is stable. However, those hydrogen atoms (yellow balls) of water molecules are prevented from staying very close to the negative charge and those oxygen atoms (green smile faces) of water molecules are prevented from staying very close to the positive charge. This leads that the water molecules cannot feel the interactions between the water molecules and the charge dipoles, making the surface hydrophobic.

At the year 2009, this research group have proposed that a stable liquid water droplet on a monolayer may emerge on a well-defined charged solid surface at room temperature, which is termed of "ordered water monolayer that does not completely wet water" (Phys. Rev. Lett., 2009, 103, 137801; J. Phys. Chem. C, 2011, 115, 3018).In 2013, this phenomenon and the physical me-

chanism were highlighted in Nature Materials (Nat. Mater. 2013, 12, 289).These worksshed a light on the effect of surface polarity on the surface wetting behavior, and evoke several subsequent works in both theoretical and experimental aspects. Scientists have found the similar phenomenon "ordered water monolayer that does not completely wet water" on talc surface, Pt(100) surface, hydroxylated Al_2O_3 surface, hydroxylated SiO_2 surface, sapphire c-plane surface, self-assemble monolayer (SAM) surface with the terminal of -COOHand BSA-Na_2CO_3(BSA, bovine serum albumin) membrane surface. All of these works draw a relatively complete picture on how the surface charges and charge dipoles affect the wetting property and have clearly shown that the polar surfaces may be unexpected hydrophobic, contrary to our common sense.

This work was performed in cooperation by researchers at Shanghai Institute of Applied Physics, Chinese Academy of Sciences, Shanghai University, Sichuan University and Zhejiang University. The funding supports are from the National Science Foundation of China, the National Basic Research Program of China, Shanghai Leading Academic Discipline Project, E-Institutes of Shanghai Municipal Education Commission, the Knowledge Innovation Program of the Chinese Academy of Sciences, Innovation Program of Shanghai Municipal Education Commission, China Postdoctoral Science Foundation, Shanghai Postdoctoral Scientific Program and Shanghai Supercomputer Center of China.

Intercalation and diffusion of lithium ions in a carbon nanotube bundle by ab initiomolecular dynamics simulations

The intercalation and diffusion of lithium ions in a bundle of carbon nanotubes (CNTs) are investigated viaanab initiomolecular dynamics simulation method based on the density functional theory. We found that lithium ions quickly penetrate into the CNTs and the space between neighboring CNTs. With a low Li ion density, the Li ions tend to stay close to the nanotube ends. Interestingly, Li ions are able to penetrate through the carbon nanotube and move from one end to the other. We also discovered that Li ions may remain between two neighboring CNTs, which presents a new approach for Li ion intercalation and storage. Importantly, Li ions located among three neighboring CNTs have very strong adsorption potentials that are a factor of four larger than those of Li ions located along the central axis of a single-walled nanotube (SWNT). This indicates that Li ions located among three neighboring CNTs would be very difficult to remove from a nanotube bundle, which suggests that Li storage capacity in this case is possibly irreversible, and that keeping the nanotubes apart with an appropriate distance would hinder or promote the formation of irreversible intercalation. Our findings contribute to the understanding of lithium intercalation and diffusion in CNTs, which has implications for the experimental development and application of rechargeable Li ion batteries.

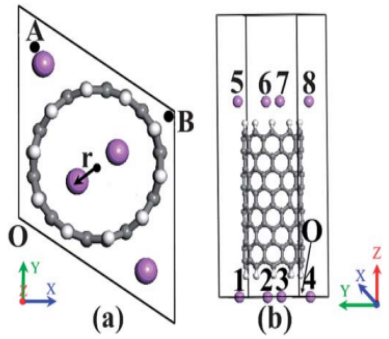

Fig.2 Typical initial conformation of the unit cell for ab initio molecular dynamics simulations.

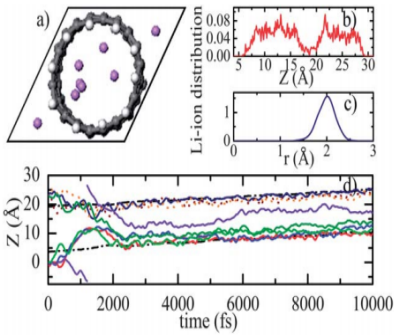

Fig.3 Behavior of the eight Li ions intercalating and diffusing inside or between the carbon nanotubes.

Design of a Gated Molecular Proton Channel

We have shown that the designed nanochannels can conduct protons in a very efficient way when a suitable electric field is applied. Analyzing the intrinsic conducting rate proves that these devices are also switchable.The opening of the gate requires both a strong electric field and the binding of a proton. When the electric field is small or turned off, the conduction of protons is turned off as a result of the steric clash between the acetic acid and the tube inner wall and because of its higher pKa. Since the designed channel is "switched on" under stronger fields and "switched off"under weaker (or no) fields, it is possible to control the direction of the conduction, and therefore establish and kinetically maintain a chemical potential across the two sides of the devices. The magnitude of the potential is controllable by adjusting the chemical properties of the rotating group and the diameter of the channel.

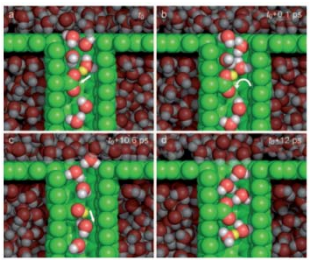

Fig.4 Mechanism of gated proton conduction in the designed proton channels from snapshots of a complete conduction process(space-filling model; oxygen atoms: red, carbon atoms: green, hydrogen atoms: white).

Cation⊗3π：New Interaction Between Cations and Carbon

Cation-π or cation-π-π interaction between one cation and one or two structures bearing rich π-electrons (such as, benzene, aromatic rings, graphene and carbon nanotubes) plays a ubiquitous role in various areas. We analyzed a new type interaction, cation⊗3π, whereby one cation simultaneously binds with three separate π-electron-rich structures. Surprisingly, we found an anomalous increase in the order of the one-benzene binding strength of the cation⊗3π interaction, with K^+> Na^+> Li^+. This was at odds with the conventional ranking of the binding strength which usually increases as the radii of the cations decrease. The key to the present unexpected observations was the cooperative interaction of the cation with the three benzenes and also between the three benzenes, in which a steric-exclusion effect between the three benzenes played an important role. Moreover, the binding energy of cation⊗3π was comparable to cation⊗2π for K^+ and Na^+, showing the particular importance of cation⊗3π interaction in biological systems.

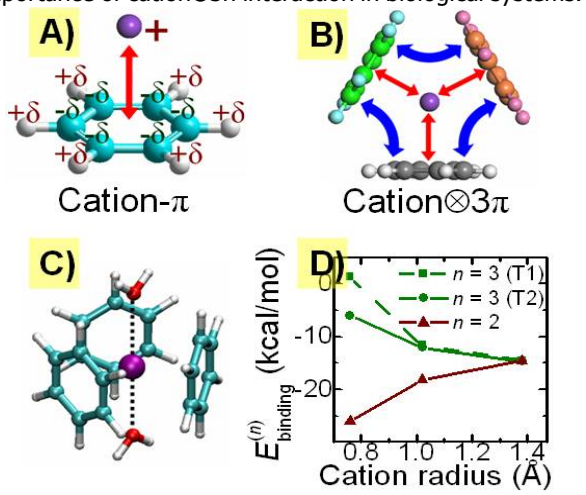

Fig.5 Cation⊗3π interaction compared with Cation-π interaction. The big ball, small ball and the purple ball denote carbon atom, hydrogen atom and cations (K^+, Na^+, Li^+), respectively. The red arrows stand for the interaction of Cation-π, the blue arrows stand for the interaction of π-π. A) Cation-π interaction. B) Cation⊗3π interaction. C) Cation⊗3π in water, hydration of Cation⊗3π. The black dash lines denote interaction between water molecules and cations. D) Cation⊗3π and Cation⊗2π interaction varied with the size of cations.

New Advances in Hyper-coordinated Carbon

As the first and correspondence author, Yi Gao collaborated with the researchers from three institutes to predicted the highest coordinated carbon species [CTi72+] theoretically. As the most important element of the biocycle, the coordination of carbon is always the most fundamental question in chemistry. Since Kekulé proposed the concept of tetracoordinate carbon in 1857, Van't Hoff (First Nobel Laureate in Chemistry), Lewis (30+ Nobel Prize Nominees), Pauling (Nobel Laureate in Chemistry and Peace), Hoffmann (Nobel Laureate in Chemistry)have made the significant contributions in the coordination of carbon.In particular, five experimental

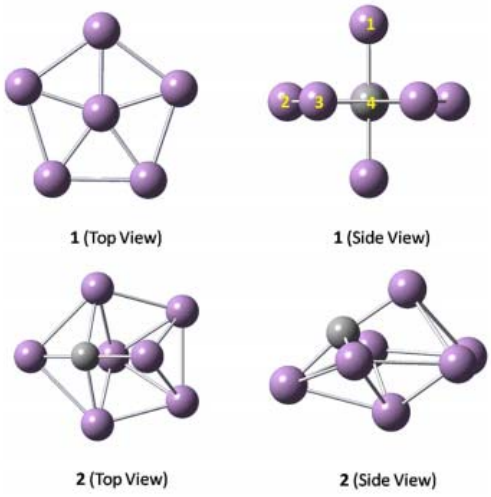

Fig.6 Optimized structures of hypercoordinate carbon isomer1and isomer2 of [CTi72+]. Gray spheres represent carbon atoms, and purple spheres represent titanium atoms.

papers published in Science around 2000 confirm the existence of CH5+, which arouse the enthusiasm to explore the higher coordinated carbon species. Yi Gao and co-workers employed the state-of-the-art techniques to combine the basin-hopping global-minimum optimization method and density functional theory to predict the highest coordinated carbon species [CTi_7^{2+}] theoretically. They also discussed the possibility to form one-dimensional nanowire. Once this work was published in The Journal of Physical Chemistry Letters (J. Phys. Chem. Lett., 2012, 3, 224-2268), it was immediately highlighted by the RSC flagshipjournal "Chemistry World" as the cover story "Carbon Clusters Score Lucky Seven"in the website's homepage. Prof. Henry Rzepa from Imperial College London commented: "New ideas are as likely to come from computation as from experiment, and there is a vibrant, fruitful, interplay between these. The CTi72+ system here is a wonderful example of how this process happens. The strength of ideas such is that it inspires experimental chemists to go make it in the lab."

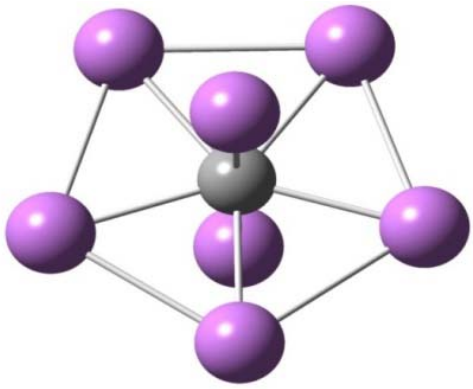

This research output was the nominee of "Top 10 Science News of China in 2012".

References

1. Wang Chunlei, Zhou Bo, Tu Yusongu, Duan Manyi, Xiu Peng, Li Jingyei, Fang Haiping. Critical Dipole Length for the Wetting Transition Due to Collective Water-dipoles Interactions. Scientific Reports, 2012, **2**: 358
2. Wang Shen, Tu Yusong, Wan Rongzheng, Fang Haiping, Evaporation of Tiny Water Aggregation on Solid Surfaces of Different Wetting Properties. J Phys Chem B, 2012, **116**: 13863-13867
3. Duan Manyi, Song Bo, Shi Guosheng, Li Haikuo, Ji Guangfu Hu Jun, Chen Xiangrong, Fang Haiping. Cation⊗3π Cooperative Interaction of a Cation and Three Benzenes with an Anomalous Order in Binding Energy. JACS, 2012, **134**: 12104-12109
4. Song Bo, Yang Junwei, Zhao Jijun, Fang Haiping. Intercalation and diffusion of lithium ions in a carbon nanotube bundle by ab initiomolecular dynamics simulations. Energy & Environmental Science, 2011, **4**: 1379-1384
5. Gu Wei, Bo Zhou, Tihamr Geyer Geyer, Michael Hutter, Fang Haiping, Volkhard Helms. Design of a Gated Molecular Proton Channel. Angew Chem Int Ed, 2011, **50**: 768-771
6. Gao Yi, Shao Nan, Zhou Rulong, Zhang Guiling, Zeng Xiaocheng. [CTi_7^{2+}]:Heptacoordinate Carbon Motif? J Phys Chem Lett, 2012, **3**: 2264-2268
7. Gao Yi, Zeng Xiaocheng. Water-Promoted O2 Dissociation on Small-Sized Anionic Gold Clusters. ACS catalysis, 2: 2614-2621
8. Zhou Xibin, Liu Guande, Kazuhiro Yamato, Shen Yi, Cheng Ruixian, Wei Xiaoxi, Bai Wanli, Gao Yi, Li Hui, Liu Yi, Liu Futao, Daniel m Czajkowsky, Wnag Jingfang. Michael J. Dabney, Zhonghou Cai, Jun Hu, Frank V Bright, He Lan, Zeng Xiaocheng, Shao Zhifeng, Bing Gong. Self-assembling subnanometer pores with unusual mass-transport properties,nature communications, 2012, 3:1-8

太赫兹技术及应用研究

水科学研究室　太赫兹实验组　赵红卫　张建兵　亓文鹏

本组主要从事太赫兹技术及其应用研究工作。主要包括基于飞秒加速器的高功率太赫兹源探测、晶体切伦科夫辐射，以及基于飞秒激光和新型光导天线的太赫兹时域光谱系统研制等。物质在太赫兹波段的光谱吸收包含有丰富的物理化学信息。经机械激活处理的固态反应可以有效避免溶剂参与，并实现对特定分子构型的控制。太赫兹光谱技术在反应的动态过程检测和分子微观机制研究方面发挥重要的作用。

手性酒石酸固态反应

在机械力研磨作用下，酒石酸成盐反应得以高效进行。通过测量不同时刻反应体系的太赫兹吸收信号，清晰地观察到 L-酒石酸与碳酸盐之间的机械力化学反应的动态过程。对反应的定量分析表明，反应为二级反应，遵循球形扩散控制模型机理。研究提示太赫兹光谱技术在生物制药分析和在线检测中具有重要的应用前景。

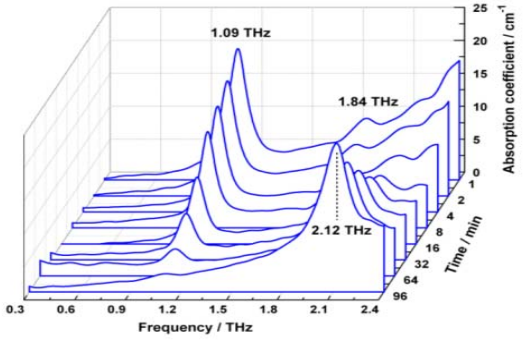

图 1　L-酒石酸和碳酸氢钠固态反应的太赫兹吸收光谱

THz 辐射和飞秒加速器

经过 2 年时间的努力，我们和俄罗斯托木斯克理工大学，设计、加工、搭建了一套基于飞秒加速器电子束团长度测量的综合实验平台。包括真空腔室、相干衍射双靶、CsI 晶体靶、传动机构和迈克尔逊干涉仪等。分别用相干度越辐射(CTR)、相干衍射辐射(CDR)和 CDR

干涉双靶成功地测量了飞秒加速器的电子束团长度(500–600 fs)。此外进行了 CsI 晶体的相干切伦柯夫辐射实验，测得了 CChR 的角分布。通过实验实现了飞秒电子束团长度的无阻拦测量。

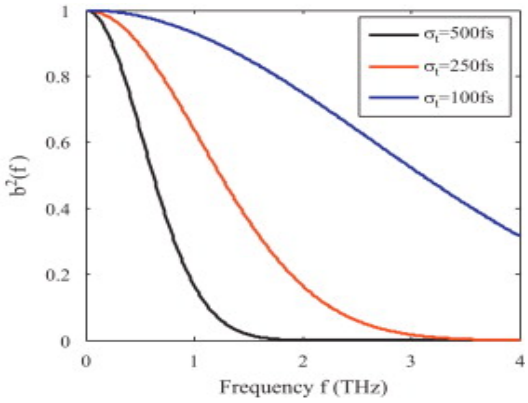

图 2　聚束因子 b 群与一个相同的高斯相关电子,在脉冲持续时间是 σ_t 的半最大值宽度。如果假设标准 b2 > 0.2，相干辐射频率低于 2 可以显著提高太赫兹使用 250 fs 电子群

参考文献

1. Liu Xiaohong, Zhao Hongwei, Wu Yuting, *et al*. Investigation of solid-state reaction by terahertz time-domain spectroscopy. Nuclear Science and Techniques. 2011, **22**: 139-143
2. Liu Xiaohong, Liu Guifeng, Zhao Hongwei, *et al*. The quantitative monitoring of mechanochemical reaction between solid L-tartaric acid and sodium carbonate monohydrate by terahertz spectroscopy. J Phys Chem Solids, 2011, **72**: 1245-1250
3. Zhang Jianbing, Deng Haixiaog, Lin Xulingn, *et al*. Tunable few-cycle coherent terahertz radiation with watt-level power from relativistic femtosecond electron beam. Nucl Instr Meth A, 2012, **693**: 23-25

Terahertz Technique and Applications

ZHAO Hongwei ZHANG jingbing QI Wenpeng
Department of Water Science THz experimental group

The group is engaged in the studies on terahertz (THz) technique and its applications. The research including the detection of high power THz source based on femtosecond accelerator and THz time-domain spectroscopy based on femtosecond laser and THz photoconductive antenna. The THz spectra of materials contain plenty chemical and physical information. Mechanochemical reactions are usually effective and environmentally benign and have the capability to control the molecular configuration. THz spectroscopy and imaging provide effective novel approaches to study the dynamics and mechanism of chemical reactions.

Solid-State Reaction of Chiral Tartaric Acid

Solid sodium L(+)-tartrate was synthesized efficiently by mechanical grinding, which is particularly sustainable and environmentally benign. Distinct Terahertz (THz) absorptions were observed for L(+)-tartaric acid, alkali carbonate and the proposed products. The reaction process could be clearly visualized by THz spectral patterns at different grinding time. The reactions were quantitative analyzed. The reaction kinetics could be expressed by the Second-order equation and the Jander equation which is consistent with a three-dimensional diffusion mechanism. The study demonstrates that THz time-domain spectroscopy is an effective novel tool to monitor solid-state reactions in pharmaceutical industry.

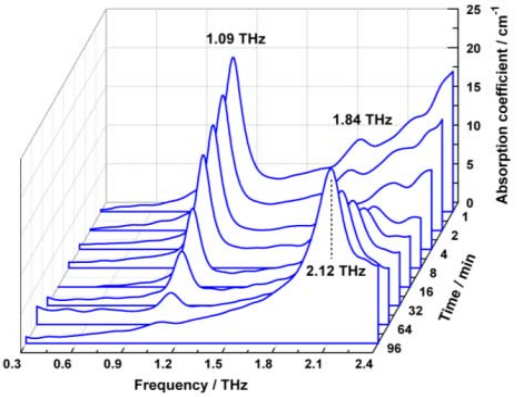

Fig.1 THz spectra of the reaction process of L(+)-Tartaric acid and sodium hydrogen carbonate by grinding.

THz Radiation and Femtosecond Accelerator

After two year's efforts, we had designed, manufactured and established a multi-purpose beam diagnostic test bed for the femtosecond accelerator, including the vacuum chamber, diffraction target, CsI crystal target, transformstage and Michelson interferometer. Successfully, we measured the bunch length about 500-600fs with the coherent transition radiation (CTR), coherent diffraction radiation (CDR) and Double diffraction interferometry (DDI) base method. Moreover, we observed the (1, 2) (CChR) from the CsI crystal and measured the angular distribution of CChR, which can be used to derive the electron bunch length. With these two phase beam experiment, we have successfully measured the bunch length with a non-invasive way.

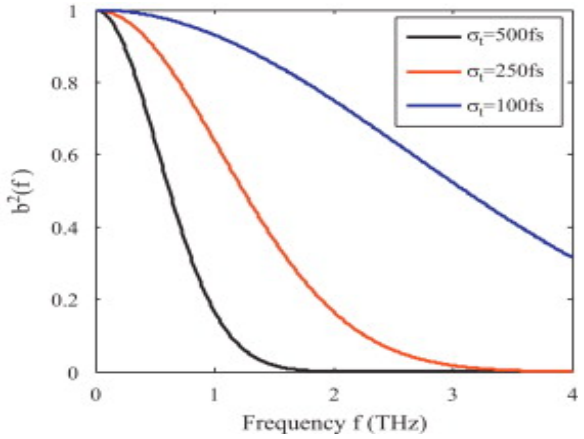

Fig.2 Bunching factor b associated with an identical Gaussian electron bunch, where σ_t is the FWHM pulse duration. If the criterion b2>0.2 is assumed, coherent radiation with frequency below 2 THz could be significantly enhanced by use of a 250 fs electron bunch.

References

1. Liu Xiaohong, Zhao Hongwei, Wu Yuting, *et al*. Investigation of solid-state reaction by terahertz time-domain spectroscopy. Nuclear Science and Techniques. 2011, **22**: 139-143
2. Liu Xiaohong, Liu Guifeng, Zhao Hongwei, *et al*. The quantitative monitoring of mechanochemical reaction between solid L-tartaric acid and sodium carbonate monohydrate by terahertz spectroscopy. J Phys Chem Solids, 2011, **72**: 1245-1250
3. Zhang Jianbing, Deng Haixiaog, Lin Xulingn, *et al*. Tunable few-cycle coherent terahertz radiation with watt-level power from relativistic femtosecond electron beam. Nucl Instr Meth A, 2012, **693**: 23-25

工业应用界面水研究

水科学研究室　纳米材料实验组　候铮迟　杨海军

本组长期从事糖类物质的辐射化学基础应用研究、生物材料及纳米材料的研制、高分子材料的辐射改性研究、过滤膜结构与性质研究等。主要研究：高分子材料改性及其在膜过滤技术及有机无机复合材料制备中的应用、同步辐射技术应用和水科学应用基础。

聚醚砜(PES)是制备超滤膜的典型高分子材料，具有良好的化学、热学稳定性、机械性能、耐酸碱性。大量研究表明，制膜溶液组成(如聚合物浓度、溶剂、添加剂等)、凝胶浴溶液组成以及制膜条件(如温度、湿度等)都会不同程度地影响 PES 超滤膜的结构和性能。在实际应用中，改变添加剂种类和浓度是一种常用的超滤膜性能调控手段。添加剂可以改变铸膜液中各组分间的相互作用，改变聚合物在溶液中的聚集态、热力学动力学行为。我们采用非溶剂致相分离(NIPS)法，以 2 种分子量的 PES 为制膜材料，NMP 为溶剂，改变添加剂的种类(PEG400，PEG6000，PVP K30)及其在铸膜液中的浓度，通过测定热力学相图、铸膜液粘度及膜过滤性能，研究添加剂对不同分子量聚醚砜超滤膜性能的影响。

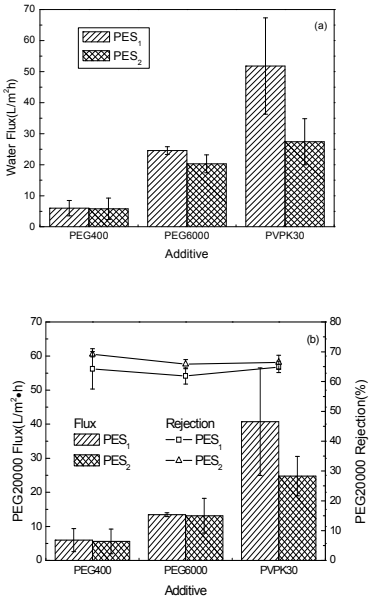

图 1　不同添加剂对膜通量及截留率的影响(a 为膜的纯水通量；b 为膜对 PEG20000 的通量及截留率)

添加剂为 PEG400、PEG6000 时，由图 1(a)可知，与 PES2 超滤膜相比，PES1 超滤膜的纯水通量略有增加；由图 1(b)可知，PES1 超滤膜对 PEG20000 的通量略大，而截留率略低。添加剂为 PVP K30 时，由图 1(a)可知，PES1 超滤膜的纯水通量为 51.8 L/m^2·h，远大于 PES2 超滤膜纯水通量 27.4 L/m^2·h；由图 1(b)可知，与 PES2 超滤膜相比，PES1 超滤膜对 PEG20000 的通量较大，而截留率较低。这说明，使用同种添加剂时，随着 PES 分子量增大，超滤膜通量增大截留率降低。从图 1(b)还可以看到，超滤膜对 PEG20000 通量按添加剂为 PEG400，PEG6000，PVP K30 的顺序依次增大；添加剂为 PEG400 时，PES 超滤膜截留率大于添加剂为 PEG6000 时超滤膜的截留率，这是由于添加剂 PEG400、PEG6000 体系相分离过程中热力学影响大于动力学影响，由于按照 PEG400，PEG6000 的顺序铸膜液体系热力学稳定性变差，加速了相分离使形成的膜孔尺寸变大，导致超滤膜的通量增大截留率下降。添加剂为 PVPK30 时，PES 超滤膜截留率大于添加剂为 PEG6000 时超滤膜的截留率，由于 PVP K30 体系铸膜液粘度较大，动力学上阻碍了相分离，导致膜孔变小，但 PVP K30 是一种强水溶性致孔剂，可增加膜表面孔隙率。因此,与添加剂为 PEG6000 的超滤膜相比，添加剂为 PVP K30 的超滤膜有较大的通量和较高的截留率。

参考文献

1. Rabiller-Baudry M, Bégoin L, Delaunay D, *et al*. Chemical Engineering and Processing: Process Intensification, 2008, **47**(3): 267-275
2. Rahimpour A,Madaeni S S. Journal of Membrane Science, 2007, **305**(1-2): 299-312.
3. Bil'dyukevich A V, Semenkevich N G, Pratsenko S A. Chemical Engineering Science, 2007, **2**:74-79
4. 4.Zhou C, Hou Z C,Lu X F, *et al*. Industrial& Engineering Chemistry Research, 2010, **49**: 9988- 9997
5. 李磊, 孙伟娜, 陈翠仙. 高分子材料科学与工程, 2008, **24**(7): 59-62.
6. Li Liang, Hou Zhengchi, Lu Xiaofeng, *et al*. Membrane Science and Technology, 2011, **31**(6): 6-12

发明专利

1 一种 PVDF 接枝 NVP 的方法及由其制得的接枝共聚物。

2 预辐照 PVDF 接枝 NVP 的制备方法和所制得的共聚物。

Industrial Application of Interfacial Water Research

HOU Zhengchi YANG Haijun
Department of Water Science Group of Nanomaterials experimental

Basic and applied research radiation chemistry of carbohydrates has long been engaged in this group, the development of biological materials and nano-materials, radiation modification of polymer materials, filtration membrane structure and properties research. The main study: modification of polymer materials and its application in the preparation of membrane filtration technology and organic-inorganic composite material, synchrotron radiation applications and scientific applications of water-based technology.

Polyethersulfone(PES) with two kinds of molecular weights were chosen to prepare ultrafiltration membranes by the nonsolvent induced phase separation method using N-methyl-2-pyrrolidone (NMP) as solvent and polyethyleneglycol(PEG400,6000), polyvinylpyrrolidoneK30(PVP K30) as additivesin the study. The effects of additive species and concentrations on performance of ultrafiltration membranes with different PES molecular weights were systematically investigated. Based on the ternary phase diagram and cast solution viscosity data, the experimental phenomena were explained from the perspectives of thermodynamics, dynamics and polymer aggregate dimensions. It was found that increasing PES molecular weight would lead to higher permeability and lower rejection with the same additive. Solute fluxes of membranes increase in the order: PEG400< PEG6000< PVP K30. Solute rejections of membranes with PVP K30 and PEG400 were higher than the membrane with PEG6000.

With the same cast solution composition, increasing additive concentration would increase the thickness of membranes and lead to higher permeability and lower rejection.

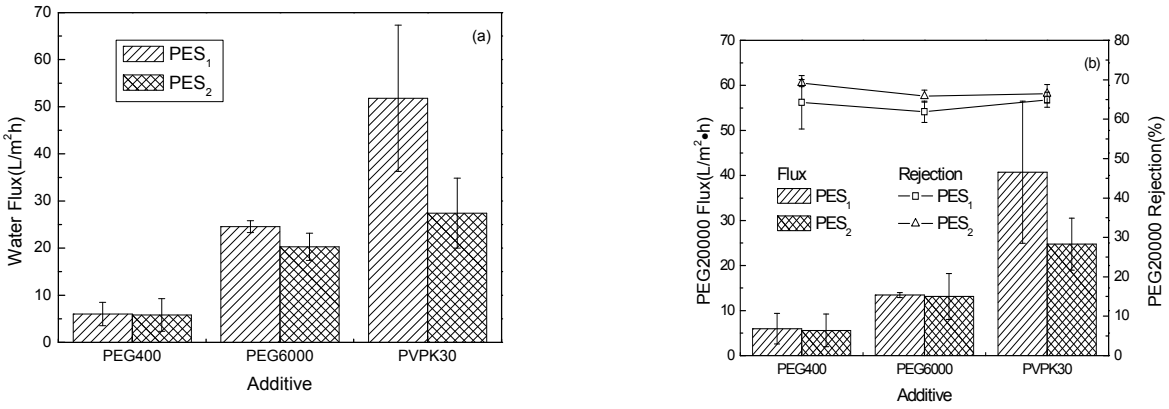

Fig.1 Effect of different additives on membrane permeability(a) water flux of membrane; (b) PEG20000 flux and rejection of membrane

References

1. Rabiller-Baudry M, Bégoin L, Delaunay D, *et al*. Chemical Engineering and Processing: Process Intensification, 2008, **47**(3): 267-275
2. Rahimpour A,Madaeni S S. Journal of Membrane Science, 2007, **305**(1-2):299-312.
3. Bil'dyukevich A V, Semenkevich N G, Pratsenko S A. Chemical Engineering Science, 2007, **2**:74-79
4. 4.Zhou C, Hou Z C,Lu X F, *et al*. Industrial&Engineering Chemistry Research, 2010, **49**: 9988-9997
5. 李磊, 孙伟娜, 陈翠仙. 高分子材料科学与工程, 2008, **24**(7): 59-62.
6. Li Liang, Hou Zhengchi, Lu Xiaofeng, *et al*. Membrane Science and Technology, 2011, **31**(6): 6-12

Patent for invention

1. A method of PVDF grafted NVP and made by the graft copolymer
2. Methods for preparing pre-irradiation and the NVP grafted PVDF copolymers prepared

附录 1

2011–2012 年学术论文统计

Papers Published in 2011–2012

1 Luo W, Xu W, Pan Q Y, *et al*. A 4D monte carlo laser-compton scattering simulation code for the characterization of the future energy-tunable SLEGS, Nuclear Instruments & Methods in Physics Research Section A-Accelerators Apectrometers Detectors and Associated Equipment, 2011, **660(**1): 108

2 Liu Gang, Chen Haode, Peng Hongzhen, *et al*. A carbon nanotube-based high-sensitivity electrochemical immunosensor for rapid and portable detection of clenbuterol, Biosensors & Bioelectronics, 2011, **28**(1): 308

3 Wu Wenhe, Hu Haiyan, Li Fan, *et al*. A graphene oxide-based nano-beacon for DNA phosphorylation analysis, Chemical Communications, 2011, **47**(4): 1201

4 Wang Lihua, Pu Kanyi, Li Jing, *et al*. A graphene-conjugated oligomer hybrid probe for light-up sensing of lectin and escherichia coli, Advanced Materials, 2011, **23**(38): 4386

5 Zhu Changfeng, Wen Yanqin, Peng Hongzhen, *et al*. A methylation-stimulated DNA machine: an autonomous isothermal route to methyltransferase activity and inhibition analysis, Analytical and Bioanalytical Chemistry, 2011, **399**(10): 3459

6 Sun Xiaoyan, Fang Deqing, Ma Yugang, *et al*. A new probe of neutron skin thickness, Chinese Physics C, 2011, **35**(6): 555

7 Cai Jun, Xu Xunjiang, Xia Xiaobin, *et al*. A real-time beam loss monitoring system for storage ring of SSRF, Nuclear Science and Techniques, 2011, **22**(1): 5

8 Zuo Guanghong, Zhou Xin, Huang Qing, *et al*. Adsorption of villin headpiece onto graphene carbon nanotube and c60: effect of contacting surface curvatures on binding affinity, Journal of Physical Chemistry C, 2011, **115**(47): 23323

9 Zhang Xuezhu, Qi Yujin. An analytical simulation technique for cone-beam CT and pinhole SPECT, Nuclear Science and Techniques, 2011, **22**(6): 338

10 Zhang Ning, Wang Baopeng, Leng Yongbin. An on-line data acquisition system of oscilloscope-embedded input/output controller for cavity BPM measurement, Nuclear Science and Techniques, 2011, **22**(6): 321

11 Hou Hongtao, Liu Jianfei, Zhao Yubin, *et al*. Analysis of superconducting cavity quench events at SSRF, Chinese Physics C, 2011, **35**(2): 179

12 Sun Peijian, Huai Ping, Zhang Wei, *et al.* Angle-resolved photoemission spectra in one-dimensional Hubbard- Holstein model, Nuclear Science and Techniques, 2011, **22**(5): 299

13 Wang Jingyan, Li Yongping, Zhang Ying, *et al.* Bag-of-features based medical image retrieval via multiple assignment and visual words weighting, IEEE Transactions ON Medical Imaging, 2011, **30**(11): 1996

14 Chen Zhichu, Leng Yongbin, Zou Yi, *et al.* Baseline recovery method to measure bunch charge under low-current mode of SSRF, Nuclear Science and Techniques, 2011, **22**(5): 261

15 Luo Shihai, Gao Mei, Chen Jun, *et al.* $BiFeO_3$ as Electrode material for lithium batteries, Journal of New Materials for Electrochemical Systems, 2011, **14**(3): 141

16 Zuo Guanghong, Gu Wei, Fang Haiping, *et al.* Carbon nanotube wins the competitive binding over proline-rich motif ligand on SH3 domain, Journal of Physical Chemistry C, 2011, **115**(25): 12322

17 Zheng Xiaoxue, Liu Qing, Jing Chao, *et al.* Catalytic gold nanoparticles for nanoplasmonic detection of DNA hybridization, Angewandte Chemie-international Edition, 2011, **50**:(50): 11994

18 He Zifeng, Zhang Jinling, Liu Yonghao, *et al.* Characteristics of a symmetrical Cockcroft-Walton power supply of 50 Hz 1 2 MV/50 mA, Review of Scientific Instruments, 2011, **82**(5)

19 He Zifeng, Zhang Jinling, Liu Yonghao, *et al.* Characteristics of a symmetrical Cockcroft-Walton power supply of 50 Hz 1 2 MV/50 mA (2011, **82**(5): 055116), Review of Scientific Instruments, 2011, **82**(8)

20 Deng Haixiao, Feng Chao, Liu Bo, *et al.* Characterizing the temporal structure of a relativistic electron bunch, Chinese Physics Letters, 2011, **28**(12)

21 Li Yong, Zheng Liping, Zhang Wei, *et al.* Charge and mass effects on low energy ion channeling in carbon nanotubes, Chinese Physics Letters, 2011, **28**(6)

22 Wang Lihua, Wang Changsui. Co speciation in blue decorations of blue-and-white porcelains from Jingdezhen kiln by using XAFS spectroscopy, Journal of Analytical Atomic Spectrometry, 2011, **26**(9): 1796

23 Ahmad Ishaq, Akram Waheed, Husnain G, *et al.* Coalescence of multi-walled carbon nanotubes and their electronic conduction nano-networks, Current Nanoscience, 2011, **7**(5): 790

24 Ye Ming, Li Bin, Zhang Yi, *et al.* Confined water nanofilm promoting nonenzymatic degradation of DNA molecules, Journal of Physical Chemistry B, 2011, **115**(12): 2754

25 Ma G. Conical emission: p(T) and system dependences and the first result with identified particles from STAR, Indian Journal of Physics, 2011, **85**(6): 797

26 Li Guang, Liu Mingyang, Liu Huajie. Controlled synthesis of porous flowerlike Cu_2S microspheres with nano-sheet-assembly, Crystengcomm, 2011, **13**(17): 5337

27 Zhang Manzhou, Hou Jie, Li Haohu. Coupling measurement and correction at the SSRF storage ring, Science CHINA-Physics Mechanics & Astronomy, 2011, **54**: S201

28 Lai Longwei, Leng Yongbin, Yi Xing, Yan Yingbing, Zhang Ning, Yang Guisen, Wang Baopeng, Xiong Yun, DBPM signal processing with field programmable gate arrays, Nuclear Science and Techniques, 2011, **22**(3): 129

29 Wang L, Wu H, Li S Y, *et al.* Design and Analysis of a self-centered cold mass support for the MICE coupling magnet, IEEE Transactions on Applied Superconductivity, 2011, **21**(3): 2259

30 Fang Wencheng, Tong Dechun, Gu Qiang, *et al.* Design and experimental study of a C-band traveling-wave accelerating structure, Chinese Science Bulletin, 2011, **56**(1): 18

31 Gu Wei, Zhou Bo, eyer Tihamer, *et al.* Design of a gated molecular proton channel, Angewandte Chemie- international Edition, 2011, **50**(3): 768

32 Fang Wencheng, Gu Qiang, Tong Dechun, *et al.* Design optimization of a C-band traveling-wave accelerating structure for a compact X-ray Free Electron Laser facility, Chinese Science Bulletin, 2011, **56**(32): 3420

33 Fan Chunhai. Designing DNA probes, Current Organic Chemistry, 2011, **15**(4)

34 Chien Chiachi, Zhang Guilin, Hwu Y, *et al.* Detecting small lung tumors in mouse models by refractive-index microradiology, Analytical and Bioanalytical Chemistry, 2011, **401**(3): 827

35 Li Haixia, Zhang Peng, Song Xiyu, *et al.* Determination of astaxanthin and canthaxanthin triplet properties in different polarities of the solvent by laser flash photolysis, Chinese Journal of Chemistry, 2011, **29**(7): 1535

36 Zhu Yan, Li Xiaolin, Li Yulan, *et al.* Determination of platinum group elements in fall dust by isotope dilution inductively coupled plasma mass spectrometry, Chinese Journal of Analytical Chemistry, 2011, **39**(5): 695

37 Yu Yang, Zhang Bowu, Yang Xuanxuan, *et al.* Determining the degree of grafting for poly(vinylidene fluoride) graft-copolymers using fluorine elemental analysis, Nuclear Science and Techniques, 2011, **22**(1): 25

38 Zhang XueZhu, Qi Yujin. Development of fully 3D image reconstruction techniques for pinhole SPECT imaging, Chinese Science Bulletin, 2011, **56**(3): 340

39 Zhao Jie. Dielectron continuum production from root $\sqrt{S_{\rm NN}}$ =200 GeV p+p and Au+Au collisions at STAR, Journal of Physics G-nuclear and Particle Physics, 2011, **38**(12)

40 Yuan Renxian, Leng Yongbin, Yu Luyang, *et al.* Digital bunch-by-bunch transverse feedback system at SSRF, Science China-Physics Mechanics & Astronomy, 2011, **54**: S305

41 Gao Anran, Liu Xiang, Li Tie, Zhou Ping, *et al.* Digital microfluidic chip for rapid portable detection of mercury(II), IEEE Sensors Journal, 2011, **11**(11): 2820

42 Zhou Guangzhao, Tong Yajun, Chen Can, *et al.* Digital simulation for coherent X-ray diffractive imaging, Acta Physica Sinica, 2011, **60**: 2

43 Zhang Xiaoyong, Yin Jilei, Peng Cheng, *et al.* Distribution and biocompatibility studies of graphene oxide in mice after intravenous administration, Carbon, 2011, **49**(3): 986

44 Qi Wenpeng, Song Bo, Lei Xiaoling, Carbon DNA base pair hybridization and water-mediated metastable structures studied by molecular dynamics simulations, Biochemistry, 2011, **50**(44): 9628

45 Qi Wenpeng, Lei Xiaoling. DNA conformational variations induced by stretching 3' 5'-termini studied by molecular dynamics simulations, Chinese Physics Letters, 2011, **28**: 4

46 Wen Yanli, Pei Hao, Wan Ying, *et al.* DNA nanostructure-decorated surfaces for enhanced aptamer-target binding and electrochemical cocaine sensors, Analytical Chemistry, 2011, **83**(19): 7418

47 Bian Xiaokai, Sin Liuqing, Yang Xuanxuan, *et al.* Effect of nano-TiO_2 particles on the performance of PVDF PVDF-g-(Maleic anhydride) and PVDF-g-poly (acryl amide) membranes, Industrial & Engineering Chemistry Research, 2011, **50**(21): 12113

48 Wang Chunlei, Zhou Bo, Xiu Peng, *et al.* Effect of surface morphology on the ordered water layer at room temperature, Journal of Physical Chemistry C, 2011, **115**(7): 3018

49 Ma Guoliang, Zhang Bin. Effects of final state interactions on charge separation in relativistic heavy ion collisions, Physics Letters B, 2011, **700**(1): 39

50 Fang Deqing, Ma Yugang, Cai Xiangzhou, *et al.* Effects of neutron skin thickness in peripheral nuclear reactions, Chinese Physics Letters, 2011, **28**(10):

51 Ge Zhilei, Pei Hao, Wang Lihua, *et al.* Electrochemical single nucleotide polymorphisms genotyping on surface immobilized three-dimensional branched DNA nanostructure, Science China-Chemistry, 2011, **54**(8): 1273

52 Peng Mingfa, Li Yang, Gao Jing, *et al.* Electronic structure and photoluminescence origin of single-crystalline germanium oxide nanowires with green light emission, Journal of Physical Chemistry C, 2011, **115**(23): 11420

53 He Zhoutong, Yang Xinmei, Xia Huihao, *et al.* Enhancing the ferromagnetization of graphite by successive C-12(+) ion implantation steps, Carbon, 2011, **49**(6): 1931

54 Ma Yufei, Yu Junfeng, Han Yanjiang, *et al.* Evaluation of a ^{188}Re-radiolabeled Arg-Gly-Asp peptide for tumor overexpressed alpha(v)beta(3) receptors, Journal of Labelled Compounds & Radiopharmaceuticals, 2011, **54**: 602

55 Mao Chengwen, Yu Xiaohan, Xiao Tiqiao, *et al.* Exact revision of the elliptically bent mirror theory, Applied Optics, 2011, **50**(16): 2413

56 Yang Haijun, Wang Huabin, Hou Zhengchi, *et al.* Fabrication and application of high quality poly(dimethylsiloxane) stamps by gamma ray irradiation, Journal of Materials Chemistry, 2011, **21**(12):4279

57 Yan Fen, Zhang Jichao, Li Aiguo, *et al.* Fast scanning X-ray microprobe fluorescence imaging based on synchrotron radiation, Acta Physica Sinica, 2011, **60**(9)

58 Deng Biao, Yang Qun, Xie Honglan, *et al.* First X-ray fluorescence CT experimental results at the SSRF X-ray imaging beamline, Chinese Physics C, 2011, **35**(4): 402

59 Huang Wei, Chen Shimou, Liu Yusheng, *et al.* Fluoride ion yield and absorption spectral analysis of irradiated imidazolium-based room-temperature ionic liquids, Radiation Physics and Chemistry, 2011, 80(4): 573

60 Han L X, Ma G L, Ma Y G, *et al.* Forward-backward elliptic anisotropy correlations in parton cascades, Physical Review C, 2011, **83**(4)

61 Fu Haiying, Lin Mingzhang, Katsumura Yosuke, *et al.* Free-radical scavenging activities of silybin and its analogues: A pulse radiolysis study, International Journal of Chemical Kinetics, 2011, **43**(10): 590

62 Deng Bo, Yu Yang, Zhang Bowu, *et al.* Graft polymerization of acrylic acid and methacrylic acid onto poly(vinylidene fluoride) powder in presence of metallic salt and sulfuric acid, Radiation Physics and Chemistry, 2011, **80**(2): 159

63 Peng Cheng, Jiang Bowei, Liu Qing, *et al.* Graphene-templated formation of two-dimensional lepidocrocite nanostructures for high-efficiency catalytic degradation of phenols, Energy & Environmental Science, 2011, **4**(6): 2035

64 Liu Jianfei, Hou Hongtao, Mao Dongqing, *et al.*Great progress in developing 500 MHz single cell superconducting cavity in China, Science China-Physics Mechanics & Astronomy, 2011, **54**: S169

65 Zhang Yi, Hu Xiaofang, Sun Jielin, *et al.* High-resolution imaging and nano-manipulation of biological structures on surface, Microscopy Research and Technique, 2011, **74**(7): 614

66 Zhang Song, Chen Jinhui, Ma Yugang, *et al.* Hypertriton and light nuclei production at A-production subthreshold energy in heavy-ion collisions, Chinese Physics C, 2011, **35**(8): 741

67 Liu Ping, Wang Yong, Tai Renzhong, *et al.* Implementation of effective control system for variable-included angle plane-grating monochromator, Nuclear Science and Techniques, 2011, **22**(1): 9

68 Yan Long, Zhou Guangying, Ishaq Ahmad, *et al.* Improving the electrical conductivity of multi-walled carbon nanotube networks by H ion beam irradiation, Carbon, 2011, **49**(6): 2141

69 Wu Na, Zhou Xingfei, Czajkowsky Daniel M, *et al.* In situ monitoring of single molecule binding reactions with time-lapse atomic force microscopy on functionalized DNA origami, Nanoscale, 2011, **3**(6): 2481

70 Su Yuanyuan, Peng Fei, Jiang Ziyun, *et al.* In vivo distribution pharmacokinetics and toxicity of aqueous synthesized cadmium-containing quantum dots, Biomaterials, 2011, **32**(25): 5855

71 Zhou P, Tian W D, Ma Y G, *et al.* Influence of statistical sequential decay on isoscaling and symmetry energy coefficient in a GEMINI simulation, Physical Review C, 2011, **84**(3)

72 Wu Zhongliang, Shen Yue, Zhou Xingfei, *et al.* Influencing factors on local reduction of graphene oxide with a heated AFM tip, Nuclear Science and Techniques, 2011, **22**(4): 245

73 Han L X, Ma G L, Ma Y G, *et al.* Initial fluctuation effect on harmonic flows in high-energy heavy-ion collisions, Physical Review C, 2011, **84**(6)

74 Liu Xiaohong, Zhao Hongwei, Wu Yuting, *et al.* Investigation of solid-state reaction by terahertz time-domain spectroscopy, Nuclear Science and Techniques, 2011, **22**(3): 139

75 Zhang Haiou, Dai Dongdong, Tang Ziyi, *et al.* Investigation of vacuum performances of TiZrV coated pipe, Nuclear Science and Techniques, 2011, **22**(6): 326

76 Ye Ming, Zhang Yi. Irreversible transformation of the porphyrin supramolecular structures under a water vapor environment, Nuclear Science and Techniques, 2011, **22**(1): 30

77 Tian Wendong, Ma Yugang, Cai Xiangzhou, *et al.* Isospin and symmetry energy study in nuclear EOS, Science China-Physics Mechanics & Astronomy, 2011, **54**: S141

78 Zheng Liping, Zhu Zhiuyuan, Li Yong, *et al.* Isotopic mass effects for low-energy channeling in a silicon crystal, Rad-

iation Effects and Defects in Solids, 2011, **166**(11): 861

79 Ma Guoliang, Wang Xinnian. Jets mach cones hot spots ridges harmonic flow dihadron and gamma-hadron correlations in high-energy heavy-ion collisions, Physical Review Letters, 2011, **106**(16)

80 Li Dongguo. Laser Compton scattering for a linearly polarized laser, Chinese Physics C, 2011, **35**(4): 405

81 Fu Haiying, Xing Zhaoguo, Wu Guozhong, *et al.* Laser photolysis studies of quaternary ammonium ionic liquids aqueous solution, Research on Chemical Intermediates, 2011, **37**(1): 79

82 Fu Haiying, Xing Zhaoguo, Wu Guozhong. Laser photolysis studies on pyrene in ionic liquids and conventional solvents, Spectroscopy and Spectral Analysis, 2011, **31**(5): 1344

83 Wang Jingyan, Li Yongping, Bai Xiang, *et al.* Learning context-sensitive similarity by shortest path propagation, Pattern Recognition, 2011, **44**: 2367

84 Yang Xinmei, He Zhoutong, Li Weifeng, *et al.* Localized defects closely related with the magnetism of graphite induced by C-12(+) ion implantation, Journal of Applied Physics, 2011, **109**(8):

85 Fan Yingcai, Zhao Mingwen, Zhang Xuejuan, *et al.* Manifold electronic structure transition of BNC biribbons, Journal of Applied Physics, 2011, **110**(3)

86 Feng Chao, Zhang Tong, Chen Jianhui, *et al.* Measurement of the average local energy spread of electron beam via coherent harmonic generation, Physical Review Special Topics-Accelerators and Beams, 2011, **14**(9)

87 Fu Y, Fang D Q, Ma Y G, Cai X Z, *et al.* Measurement of the longitudinal momentum distribution of S-30 after one- proton removal from Cl-31, Physical review C, 2011, **84**(3)

88 Ma Yugang, Fang Deqing, Sun Xiaoyan, *et al.* Measurements on diproton emission from the break-up channels of ^{23}Al and ^{22}Mg, Science China-Physics Mechanics & Astronomy, 2011, **54**: S18

89 Liu Yusheng, Fu Haiying, Tang Zhongfeng, *et al.* Melting point and structure of ionic liquid [EMIM][PF_6] on the surface of nano-SiO_x particles, Acta Physico-Chimica Sinica, 2011, **27**(7): 1725

90 Dou Qiang, Sha Maolin, Fu Haiying, *et al.* Melting Transition of Ionic Liquid [bmim][PF_6] Crystal confined in nanopores: A molecular dynamics simulation, Journal of Physical Chemistry C, 2011, **115**(39): 18946

91 Wen Yanqin, Peng Cheng, Li Di, *et al.* Metal ion-modulated graphene-DNAzyme interactions: design of a nanoprobe for fluorescent detection of lead(II) ions with high sensitivity selectivity and tunable dynamic range, Chemical Communications, 2011, **47**(22): 6278

92 Dou Q, Sha M L, Fu H Y, *et al.* Molecular dynamics simulation of the interfacial structure of [C(n)mim][PF_6] adsorbed on a graphite surface: effects of temperature and alkyl chain length, Journal of Physics-Condensed Matter, 2011, **23**(17)

93 Wang Huabin, Wang Xinyan, Li Huabing, Zhang Xuehua, Zhang Yi, Hu Jun, Molecular Expansion of an Individual Coiled DNA on a Graphite Surface, LANGMUIR, 2011, **27**(6): 2405

94 Cai Jun, Xia XiaoBin, Xu XunJiang, *et al.* Monitoring system experiments on beam loss at SSRF injector, Science China-Physics Mechanics & Astronomy, 2011, **54**: S279

95 Zhang Donghua, Zhang Chen, Zhang Fuchun, *et al.* Hu Jun, MRT Letter: real time and in situ imaging the reversible evolution of ethanol vapor condensed on mica surface, Microscopy Research and Technique, 2011, **74**(6): 481

96 Zhang Xiaoyong, Li Jing, Zhu Ying, *et al.* Nanographene oxide labeling with ^{188}Re, Nuclear Science and Techniques, 2011, **22**(2): 99

97 Pan Dun, Wen Yangqin, Mi Lijuan, *et al.* Nanomaterials-based polymerase Chain reactions for dna detection, Current Organic Chemistry, 2011, **15**(4): 486

98 Zhang Qingzhi, Zhao Bin, Yan Juan, *et al.* Nanotube-based colorimetric probe for ultrasensitive detection of ataxia telangiectasia mutated protein, Analytical Chemistry, 2011, **83**(23): 9191

99 Zhang Meng, Gu Qiang. New linear accelerator (Linac) design based on C-band accelerating structures for SXFEL facility, Chinese physics C, 2011, **35**(11): 1066

100 Yang Qun, Deng Biao, Lu Weiwei, *et al.* Nondestructive imaging of elements distribution in biomedical samples by X-Ray fluorescence computed tomography, Spectroscopy and Spectral Analysis, 2011, **31**(10): 2753

101 Xue L. Observation of the antimatter helium-4 nucleus at the RHIC, Journal of Physics G-nuclear and Particle Physics, 2011, **38**(12)

102 Ren Yuqi, Chen Can, Chen Rongchang, *et al.* Optimization of image recording distances for quantitative X-ray in-line phase contrast imaging, Optics Express, 2011, **19**(5): 4170

103 Jin F, Chen J H, Huang H Z, *et al.* Parton transverse momentum distribution at the moment of hadronization at RHIC, Indian Journal of Physics, 2011, **85**(1): 161

104 Chen R C, Xie H L, Rigon L, *et al.* Phase retrieval in quantitative X-ray microtomography with a single sample-to-detector distance, Optics Letters, 2011, **36**(9): 1719

105 Zhang Peng, Li Haixia, Liu Yancheng, *et al.* Photochemical properties and reactions with biomolecules of 4 '-N-acetyl derivative of norfloxacin, Zeitschrift Fur Physikalische

Chemie-International Journal of Research in Physical Chemistry & Chemical Physics, 2011, **225**(8): 843

106 Tang Ruizhi, Zhang Peng, Li Haixia, *et al.* Photosensitized xanthone-based oxidation of guanine and its repair: A laser flash photolysis study, Journal of photochemistry and photobiology b-biology, 2011, **105**(2): 157

107 Li Jianbo, Shi Lingli, Wang Cheng, *et al.* Preliminary biological evaluation of ^{125}I-labeled anti-carbonic anhydrase IX monoclonal antibody in the mice bearing HT-29 tumors, Nuclear Medicine Communications, 2011, **32**(12): 1190

108 Yang Xuanxuan, Zhang Bowu, Liu Zhongying, *et al.* Preparation of the antifouling microfiltration membranes from poly(NN-dimethylacrylamide) grafted poly(vinylidene fluoride) (PVDF) powder, Journal of Materials Chemistry, 2011, 21(32): 11908

109 Kumar Sanjeev, Ma Y G, Zhang G Q, *et al.* Probing the density dependence of the symmetry energy via multifragmentation at subsaturation densities, Physical Review C, 2011, **84**(4)

110 Hu Wenbing, Peng Cheng, Lv Min, *et al.* Protein corona-mediated mitigation of cytotoxicity of graphene oxide, ACS Nano, 2011, **5**(5): 3693

111 Tang Ruizhi, Zhang Peng, Li Haixia, *et al.* Pulse radiolysis study of the reactions between phenothiazine and CCl_3OO center dot (OH)-O-center dot, Acta Physico-Chimica Sinica, 2011, **27**(8): 1975

112 Zhang Peng, Yao Side, Li Haixia, *et al.* Pulse radiolysis study on several fluoroquinolones, Radiation Physics and Chemistry, 2011, **80**(4): 548

113 Liu Zhonghua, Wang Jingyan, Li Yongping, *et al.* Quantized image patches co-occurrence matrix: A new statistical approach for texture classification using image patch exemplars, Third International Conference on Digital Image Processing (ICDIP 2011), 2011, 8009

114 Shi Lingli, Li Jianbo, Wang Cheng, *et al.* Quick and efficient F-18 labelling of peptides by "click chemistry", Journal of Labelled Compounds & Radiopharmaceuticals, 2011, **54**: S445

115 Chen Xuelian, Zhang Jianqi, Yi Zhiyong, *et al.* Radial structure of commercial styrene-co-butyl acrylate latex particles by means of synchrotron small-angle X-ray scattering under contrast-variation conditions, Journal of Coatings Technology and Research, 2011, **8**(4): 489

116 Zhao Yanning, Wang Mouhua, Tang Zhongfeng, *et al.* Radiation effects of UHMW-PE fibre on gel fraction and mechanical properties, Radiation Physics and Chemistry, 2011, **80**(2): 274

117 Tang Zhongfeng, Wang Mouhua, Zhao Yanning, *et al.* Radiation resistance evaluation of cross-linked polytetrafluoroethylene by the investigation of friction and wear behavior, Radiation Physics and Chemistry, 2011, **80**(3): 496

118 Xu Xiaoping, Zhang Yuanqing, Wang Xudong, Radiosynthesis biodistribution and micro-SPECT imaging study of dendrimer-avidin conjugate, Bioorganic & Medicinal Chemistry, 2011, **19**(5): 1643

119 He Zhoutong, Xia Huihao, Zhou Xingtai, *et al.* Raman study of correlation between defects and ferromagnetism in graphite, Journal of Physics D-Applied Physics, 2011, **44**(8)

120 Pei Hao, Wan Ying, Li Jiang, *et al.* Regenerable electrochemical immunological sensing at DNA nanostructure-decorated gold surfaces, Chemical communications, 2011, **47**(22): 6254

121 Zheng Liping, Zhu Zhiyuan, Li Yong, *et al.* Reply to "Comment on an improved critical angle equation for channeling", Nuclear Instruments & Methods in Physics Research Section B-Beam Interactions with Materials and Atoms, 2011, **269**(5): 557

122 Zheng Liping, Zhu Zhiyuan, Li Yong, *et al.* Reply to "Comment on isotopic mass effects for low-energy channeling in a silicon crystal", Radiation Effects and Defects in Solids, 2011, **166**(11): 870

123 Zheng Liping, Zhu Zhiyuan, Li Yong, *et al.* Reply to "comment on theoretical critical angels of ion channeling in carbon nanotubes", Nuclear Instruments & Methods in Physics Research Section B-Beam Interactions with Materials and Atoms, 2011, **269**(13): 1472

124 Wang Xiao, Yan Zhongbao, Du Hanwen, *et al.* Research on mechanical stability for third-generation light source, Science China-Physics Mechanics & Astronomy, 2011, **54**: S185

125 Sha Maolin, Niu Dongxiao, Dou Qiang, *et al.* Reversible tuning of the hydrophobic-hydrophilic transition of hydrophobic ionic liquids by means of an electric field, Soft matter, 2011, 7(9): 4228

126 Yi Xing, Leng Yongbin, Lai Longwei, *et al.* RF front-end for digital beam position monitor signal processor, NUCLEAR SCIENCE AND TECHNIQUES, 2011, 22(2): 65

127 Tian Feng, Tang Zhongfeng, Xu Hongjie, Wang Jie, Wu Guozhong, Li Xiuhong, SAXS studies on the structure behaviors of crosslinked PTFE irradiated by γ-ray, Polymers & Polymer Composites, 2011, **19**: 439

128 Li Jiang, Pei Hao, Zhu Bing, *et al.* Self-Assembled multivalent DNA nanostructures for noninvasive intracellular delivery of immunostimulatory cpg oligonucleotides, ACS Nano, 2011, **5**(11): 8783

129 Wang Jingyan, Li Yongping. Sequential linear neighborhood

propagation for semi-supervised protein function prediction, Journal of Bioinformatics and Computational Biology, 2011, **9**(6): 663

130 Li Shaoxin, Fang Deqing, Ma Yugang, *et al.* Shear viscosity to entropy density ratio in BUU transport model, Nuclear Science and Techniques, 2011, **22**(4): 235

131 Li S X, Fang D Q, Ma Y G, *et al.* Shear viscosity to entropy density ratio in the Boltzmann-Uehling-Uhlenbeck model, Physical Review C, 2011, **84**(2)

132 Yu Haibo, Liu Jianfei, Hou Hongtao, *et al.* Simulation of higher order modes and loss factor of a new type of 500-MHz single cell superconducting cavity at SSRF, Nuclear Science and Techniques, 2011, **22**(5): 257

133 Waheed Akram, Li Xiaolin, Tan Mingguang, *et al.* Size distribution and sources of trace metals in ultra-fine/fine/coarse airborne particles in the atmosphere of Shanghai, Aerosol Science and Technology, 2011, 45(2): 163

134 He Yongzhou, Zhou Qiaogen, Zhang Jidong. Sm_2Co_{17} magnet blocks for the in-vacuum undulators (IVU20) at the SSRF, Chinese Physics C, 2011, **35**(4): 392

135 Liu Guifeng, Zhao Hongwei, Liu Xiaohong, *et al.* solid-state reaction between p-benzoquinone and 44 '-biphenol: A thz time-domain spectroscopic study, Journal of Applied Spectroscopy, 2011, **78**(3): 318

136 Du Weitao, Song Li, Wang Yuzhu, *et al.* Studies of the super-smooth mirror roughness by grazing incidence X-ray scattering method, 2011 International Conference on Optical Instruments and Technology: Solid Sstate Lighting and Display Technologies Holography Speckle Pattern Interferometry and Micro/Nano Manufacturing and Metrology, 2011, 8202

137 Fu Haiying, Zhu Guanglai, Wu Guozhong, *et al.* Study of imidazolium ionic liquids: temperature-dependent fluorescence and molecular dynamics simulation, Chemical Research in Chinese Universities, 2011, **27**(4): 688

138 Li Xiaoyun, Li Xiuhong, Wang Yuzhu, Wang Jie, Study of microstructure in polyethylene terephthalate(PET) fiber using SAXS, Advanced Textile Materials PTS 1-3, 2011, **332-334**, 1171

139 Yang L F, Xu W, Zhang Q R, *et al.* Study of the ionization of hydrogen atoms in an intense circularly polarized laser field, Physica Scripta, 2011, T144

140 Wang L, Pan H, Guo X L, *et al.* Study on the mechanical instability of MICE coupling magnets, IEEE Transactions on Applied Superconductivity, 2011, **21**(3): 2363

141 Jiang Zhiqiang, Du Hanwen, Chen Chu, *et al.* Supporting and driving system for in-vacuum undulator, Nuclear Science and Techniques, 2011, **22**(1): 1

142 Li Zheng, Zhang Guoxin, Shen Hua, *et al.* Synthesis and cell uptake of a novel dualmodality Re-188-HGRGD (D) F-CdTe QDs probe, Talanta, 2011, **85**(2): 936

143 Zhu Hua, Huang Liliang, Zhang Yuanqing, *et al.* Synthesis of molecularly defined (L)-lactic acid oligomers and its tricarbonyl rhenium derivatives, Chinese Journal of Organic Chemistry, 2011, **31**(1): 87

144 Zhang Yujie, Hu Wenbing, Li Bo, *et al.* Synthesis of polymer-protected graphene by solvent-assisted thermal reduction process, Nanotechnology, 2011, **22**(34)

145 Zhang S, Zhu Y H, Ma G L, *et al.* System-size scan of dihadron azimuthal correlations in ultra-relativistic heavy ion collisions, Nuclear Physics A, 2011, **860**(1): 76

146 Huang Wei, Chen Shimou, Liu Yusheng, *et al.* The controlled synthesis of stable gold nanoparticles in quaternary ammonium ionic liquids by simple heating, Nanotechnology, 2011, **22**(2)

147 Zhou Pei, Tian Wendong, Ma Yugang, *et al.* The influence of multi-step sequential decay on isoscaling and fragment isospin distribution in gemini simulation, Chinese Physics Letters, 2011, **28**(6)

148 Liu Xiaohong, Liu Guifeng, Zhao Hongwei, *et al.* The quantitative monitoring of mechanochemical reaction between solid L-tartaric acid and sodium carbonate monohydrate by terahertz spectroscopy, Journal of Physics and Chemistry of Solids, 2011, **72**(11): 1245

149 Deng Haixiao, Lin Tangyu, Yan Jun, *et al.* Three- dimensional numerical investigations of the laser-beam interactions in an undulator, Chinese Physics C, 2011, **35**(3): 308

150 Zhang G Q, Ma Y G, Cao X G, *et al.* Unified description of nuclear stopping in central heavy-ion collisions from 10 A MeV to 1 2 A GeV, Physical Review C, 2011, 84(3)

151 Xu Wei, Tu Yusong, Wang Chunlei, *et al.* Water transport through T-shaped carbon nanotubes, Nuclear Science and Techniques, 2011, **22**(5): 307

152 Xu H, Yu X, Tai R., X-ray microscopy beamlines at ssrf - present status and future plan, 10th International Conference on X-ray Microscopy, 2011, **1365**: 52

153 Gao Yi, Shao Nan, Zhou Rulong, 10th international conference on x-ray microscopy $[CTi_7^{2+}]$: Heptacoordinate Carbon Motif?, Journal of Physical Chemistry Letters, 2012, **3**(16): 2264

154 Yan Han, Zhao Lei, Liu Shubin, *et al.* A beam position measurement system of fully digital signal processing at SSRF, Nuclear Science and Techniques, 2012, **23**(2): 75

155 Zhang Xiaoyong, Hu Wenbing, Li Jing, *et al.* A comparative study of cellular uptake and cytotoxicity of multi-walled

carbon nanotubes graphene oxide and nanodiamond, Toxicology Research, 2012, **1**(1): 62

156 Pei Hao, Li Jiang, Lv Min, *et al.* A graphene-based sensor array for high-precision and adaptive target identification with ensemble aptamers, Journal of the American Chemical Society, 2012, **134**(33): 13843

157 Ma Hongjuan, Yao Side, Li Jingye, *et al.* A mild method of amine-type adsorbents syntheses with emulsion graft polymerization of glycidyl methacrylate on polyethylene non-woven fabric by pre-irradiation, Radiation Physics and Chemistry, 2012, **81**(9): 1393

158 Zheng Xiaoxue, Wen Yanqin, Zhang Juan, *et al.* A nanoresonant gold-aptamer probe for rapid and sensitive detection of thrombin, Nuclear Science and Techniques, 2012, **23**(5): 317

159 Wang Cheng, Zhou Wei, Yu Junfeng, *et al.* A study of the radiosynthesis of fac-$[Re\text{-}^{188}(CO)_3(H_2O)_3]^+$ and its application in labeling 123-triazole analogs obtained by click chemistry, Nuclear Medicine Communications, 2012, **33**(1): 84

160 Ai Xiaobai. A suggestion based on the OPERA experimental apparatus, Physica Scripta, 2012, **85**(4)

161 Liu Xiyan, Liu Hanzhou, Ma Hongjuan, *et al.* Adsorption of the uranyl ions on an amidoxime-based polyethylene nonwoven fabric prepared by preirradiation-induced emulsion graft polymerization, Industrial & Engineering Chemistry Research, 2012, **51**(46): 15089

162 Wang Bin, Chen Nan, Wei Yingliang, *et al.* Akt signaling-associated metabolic effects of dietary gold nanoparticles in Drosophila, Scientific Reports, 2012, **2**

163 Zhou Yongnian, Zheng Lifang, Li Yongping. An improved genetic algorithm for mobile robotic path planning, Proceedings of the 2012 24th chinese control and decision conference (CCDC), 2012, 3255

164 Xu Zhongmin, Wang Naxiu. An optimized side-cooling scheme for a collimation mirror at the SSRF, Journal of Synchrotron Radiation, 2012, **19**: 428

165 Kang Cheng, Liu Yonghao, Li Deming. Analysis of output voltage on a planar insulating core transformer. Nuclear Science and Techniques, 2012, **23**(1): 15

166 Wan Rongzheng, Hu Jun, Fang Haiping. Asymmetric transportation induced by thermal noise at the nanoscale, Science China-Physics Mechanics & Astronomy, 2012, **55**(5): 751

167 Wang Juan, Qin Haiying, Liu Jiabin, *et al.* Atomic structure of polypyrrole-modified carbon-supported cobalt catalyst, Journal of Physical Chemistry C, 2012, **116**(38): 20225

168 Tian Jian, Beam energy dependence of event-by-event hadron ratio fluctuations from au plus au collisions at rhic, Strangeness in Quark Matter 2011, 2012, **5**(2): 503

169 Li Yong, Zhang Wei, Xu Zijian, *et al.* Bonding effect on channeling of C ions in a carbon nanotube, Nuclear Science and Techniques, 2012, **23**(1): 57

170 Shen Yue, Guo Shouwu, Hu Jun, *et al.* Charging of nanostructured and partially reduced graphene oxide sheets, Applied Physics Letters, 2012, **101**(18)

171 Liu Yancheng, Zhang Peng, Li Haixia, Wang Wenfeng, Ciprofloxacin Photosensitized Oxidation of 2'-Deoxyguanosine-5'-Monophosphate in Neutral Aqueous Solution, PHOTOCHEMISTRY AND PHOTOBIOLOGY, 2012, **88**(3): 639

172 Ma Guoliang, Wang Xinnian, Comparative study of hadron- and gamma-triggered azimuthal correlations in relativistic heavy-ion collisions, Acta physica polonica B, 2012, **43**(4): 697

173 Tian Guohui, Chen Yajie, Bao Hongliang, *et al.* Controlled synthesis of thorny anatase TiO_2 tubes for construction of Ag-AgBr/TiO_2 composites as highly efficient simulated solar-light photocatalyst, Journal of materials chemistry, 2012, **22**(5): 2081

174 Kumar Sanjeev, Ma Y G, Zhang G Q . Correlation and isospin dynamics of participant-spectator matter in neutron-rich colliding nuclei at 50 MeV/nucleon, Physical Review C, 2012, **86**(4)

175 Rakha Sobia Allah, Yu Guojun, Cao Jianqing. Correlation between diamond grain size and hydrogen incorporation in nanocrystalline diamond thin films, Journal of Experimental Nanoscience, 2012, **7**(4): 378

176 Guo X L, Wang L, Green M A . Coupled transient thermal and electromagnetic finite element analysis of quench in MICE coupling magnet, Cryogenics, 2012, **52**: 420

177 Wang Chunlei, Zhou Bo, Tu Yusong, *et al.* Critical dipole length for the wetting transition due to collective water-dipoles interactions, Scientific Reports, 2012, **2**

178 Qian J H, Han D D, Ma Y G. Criticality and continuity of explosive site percolation in random networks, EPL, 2012, **100**(4)

179 Li Jian, Sun Lihua, Xu Chunyan, *et al.* Crystal Structures of n-terminal domain of human hsp90 with atp analogues reveal the functional regulation of Hsp90, Progress in Biochemistry and Biophysics, 2012, **39**(10): 995

180 Bian Sha, Du Linwei, Gao Yuxi, *et al.*Crystallization in aggregates of calcium phosphate nanocrystals: A logistic model for kinetics of fractal structure development, Crystal Growth & Design, 2012, **12**(7): 3481

181 Alessandria F, Andreotti E, Ardito R, *et al.* CUORE crystal

validation runs: Results on radioactive contamination and extrapolation to CUORE background, Astroparticle Physics, 2012, **35**(12): 839

182 Liu Yanxia, Zhang Wei, Li Li, *et al.*Cyanobacterial peptides as a prototype for the design of potent beta-secretase inhibitors and the development of selective chemical probes for other aspartic proteases, Journal of Medicinal Chemistry, 2012, **55**(23): 10749

183 Zhu Ying, Zhang Xiaoyong, Zhu Jianhua, *et al.* Cytotoxicity of phenol red in toxicity assays for carbon nanoparticles, International Journal of Molecular Sciences, 2012, **13**(10): 12336

184 Chen Guanghua, Chen Jianfeng, Wan Tianmin. Database application research in real-time data access of accelerator control system, Nuclear Science and Techniques, 2012, 23**(5)**: 267

185 Zhang Xiaohui, Qi Yujin, Zhao Cuilan. Design and development of compact readout electronics with silicon photomultiplier array for a compact imaging detector, Chinese Physics C, 2012, **36**(10): 973

186 Lu Changwang, Liu Jianfei, Hou Hongtao, *et al.* Design and simulation of a new type of 500 MHz single-cell superconducting RF cavity, Chinese Physics C, 2012, **36**(5): 447

187 Wei Yelong, Liu Jianfei, Hou Hongtao, *et al.*Design of large aperture 500 MHz 5-cell superconducting cavity, Nuclear Science and Techniques, 2012, **23**(5): 257

188 Feng Chao, Zhang Meng, Lin GuoQiang, *et al.* Design study for the cascaded HGHG experiment based on the SDUV-FEL, Chinese science bulletin, 2012, **57**(26): 3423

189 Pei Hao, Li Fan, Wan Ying, *et al.* Designed diblock oligonucleotide for the synthesis of spatially isolated and highly hybridizable functionalization of dna-gold nanoparticle nanoconjugates, Journal of the American Chemical Society, 2012, **134**(29): 11876

190 Sheng Nan, Tu Yusong, Guo Pan, *et al.* Diffusing of an ammonia molecule in water in a very short time period, Journal of Hydrodynamics, 2012, **24**(6): 969

191 Zhou Guangzhao, Wang Yudan, Ren Yuqi, *et al.* Digital simulation for 3D reconstruction of coherent x-ray diffractive imaging, Acta Physica Sinica, 2012, **61**(1)

192 Wen Yanli, Pei Hao, Shen Ye, *et al.* DNA Nanostructure-based Interfacial engineering for PCR-free ultrasensitive electrochemical analysis of microRNA, Scientific Reports, 2012, **2**

193 Lv Min, Zhang Yujie, Liang Le, *et al.* Effect of graphene oxide on undifferentiated and retinoic acid-differentiated SH-SY5Y cells line, Nanoscale, 2012, **4**(13): 3861

194 Wu Chen, Ma Yugang, Kumar Sanjeev, *et al.* Effective nucleon mass and thermodynamics in the quark-meson coupling model, Physical Review C, 2012, **86**(6)

195 Chen Jiajia, Zhang Chen, Zhao Binyu, *et al.* Effects of nanoparticles on fluorescence enhancement of the complexes of dsDNA and SYBR Green I, Nuclear Science and Techniques, 2012, **23**(4): 247

196 Li Junzheng, Li Jianguo. Effects of solidification rate and temperature gradient on microstructure and crystal orientation of $Co_{32}Ni_{40}Al_{28}$ alloys, Materials letters, 2012, **68**: 40

197 Wang Yudan, Peng Guanyun, Tong Yajun, *et al.* Effects of some factors on X-ray spiral micro-computed tomography at synchrotron radiation, Acta Physica Sinica, 2012, **61**(5)

198 Zhou H, Peng X, Peth S, *et al.* Effects of vegetation restoration on soil aggregate microstructure quantified with synchrotron-based micro-computed tomography, Soil & Tillage Research, 2012, **124**: 17

199 Chen Xiliang, Chen Xin, Zhu Zhiyong. Electrical and optical properties of MWNTs/HDPE composites in terahertz region, Nuclear Science and Techniques, 2012, **23**(3): 156

200 Wen Yanli, Lin Meihua, Pei Hao, Lu Na, Fan Chunhai, Electrochemical-Based MicroRNA Sensors, Progress in Chemistry, 2012, **24**(9): 1656

201 Wang Shen, Tu Yusong, Wan Rongzheng, *et al.* Evaporation of tiny water aggregation on solid surfaces with different wetting properties, Journal of Physical Chemistry B, 2012, 116(47): 13863

202 Tian Jian. Event-by-event hadron ratio fluctuations from Au plus Au collisions at RHIC-STAR, Central European Journal of Physics, 2012, **10**(6): 1365

203 Zhu Ying, Li Wenxin, Zhang Yu, *et al.* Excessive sodium ions delivered into cells by nanodiamonds: implications for tumor therapy, Small, 2012, **8**(11): 1771

204 Cai X L, Xu W, Luo W, Yang L, *et al.* Experimental study for measuring the decay branching ratio for nuclear excitation by electron transition in Os-189, Nuclear Physics A, 2012, **874**: 1

205 Huang Lei, Huang Wei, Fu Hai-Ying, *et al.* Extraction of Ce^{3+} using CMPO-ionic liquid systems, Chinese Journal of Inorganic Chemistry, 2012, **28**(4): 669

206 Yang Qun, Deng Biao, Lv Weiwei, *et al.* Fast and accurate X-ray fluorescence computed tomography imaging with the ordered-subsets expectation maximization algorithm, Journal of Synchrotron Radiation, 2012, **19**: 210

207 Zhao Z T, Wang D, Chen J H, *et al.* First lasing of an echo-enabled harmonic generation free-electron laser, Nature Photonics, 2012, **6**(6): 360

208 Zhang Honglu, Chao Jie, Pan Dun, *et al.* Folding super-sized DNA origami with scaffold strands from long-range PCR,

Chemical Communications, 2012, **48**(51): 6405

209 Yang Li, Sheng Nan, Tu Yusong, *et al.* Friction force effects on vertical manipulation of nanoparticles, Nuclear Science and Techniques, 2012, **23**(3): 176

210 Feng Chao, Chen Jianhui, Zhao Zhentang. Generating stable attosecond x-ray pulse trains with a mode-locked seeded free-electron laser, Physical Review Special Topics-Accelerators and Beams, 2012, **15**(8)

211 Pan Dun, Mi Lijuan, Huang Qing, *et al.*Genetic analysis with nanoPCR, Integrative Biology, 2012, **4**(10): 1155

212 Zeng Dongdong, Luo Weijie, Li Jiang, *et al.* Gold nanoparticles-based nanoconjugates for enhanced enzyme cascade and glucose sensing, Analyst, 2012, **137**(19): 4435

213 Zhang Bowu, Wei Rongmao, Yu Ming, *et al.* Graft co-polymerization of maleic acid and vinyl acetate onto poly(vinylidene fluoride) powder by pre-irradiation technique, Nuclear Science and Techniques, 2012, **23**(2): 103

214 He Shijiang, Liu Keng-Ku, Su Shao, *et al.* Graphene-based high-efficiency surface-enhanced raman scattering-active platform for sensitive and multiplex dna detection, Analytical Chemistry, 2012, **84**(10): 4622

215 Ma Y G, Liu G H, Cai X Z, Fang D Q, Guo W, Shen W Q, Tian W D, Wang H W, Hard-photon flow and photon-photon correlation in intermediate-energy heavy-ion collisions, PHYSICAL REVIEW C, 2012, **85**(2)

216 Zhang YuJie, Geng MaKe, Zhang Huan, *et al.* High-conductivity graphene nanocomposite via facile covalent linkage of gold nanoparticles to graphene oxide, Chinese Science Bulletin, 2012, **57**(23): 3086

217 Yu Yang, Zhang BoWu, Yu Ming, *et al.* High-selective removal of ultra-low level mercury ions from aqueous solution using oligothymonucleic acid functionalized polyethylene film, Science China-Chemistry, 2012, **55**(10): 2202

218 Zhang Linjuan, Wang Jianqiang, Li Jiong, *et al.* High-T-c ferromagnetism in a Co-doped ZnO system dominated by the formation of a zinc-blende type Co-rich ZnCoO phase, Chemical Communications, 2012, **48**(1): 91

219 Lu Yanling, Liu Jinxi, Li Xiaoke, *et al.* Hot deformation behavior of Hastelly C_{276} superalloy, Transactions of Nonferrous Metals Society of China, 2012, **22**: S84

220 Li Huabing, Fang Haiping. Hysteresis and saturation of contact angle in electrowetting on a dielectric simulated by the lattice boltzmann method, Journal of a Dhesion Science and Technology, 2012, **26**: 1873

221 Yang Xinmei, Feng Shanglei, Zhou Xingtai, *et al.* Interaction between nuclear graphite and molten fluoride salts: A synchrotron radiation study of the substitution of graphitic hydrogen by fluoride ion, Journal of Physical Chemistry A, 2012, **116**(3): 985

222 Ren Jie, Huang JianMing, Zhang YuTian, *et al.* Investigate the nonuniformity of low-energy electron beam with large cross-sections, Science China-Technological Sciences, 2012, **55**(4): 997

223 Liu Huiqiang, Ren Yuqi, Zhou Guangzhao, *et al.* Investigation on the application of phase-attenuation duality to X-ray mixed contrast quantitative micro-tomography, Acta Physica Sinica, 2012, **61**: 7

224 Lu Qipeng, Li Yongjun, Peng Zhongqi. Kinematics analysis of six-bar parallel mechanism and its applications in synchrotron radiation beamline, Nuclear Instruments & Methods in Physics Research Section A-Accelerators Spectrometers Detectors and Associated Equipment, 2012, **674**: 8

225 Li Lanting, Wang Chao, Song Bo, *et al.* Kinetic parameters estimation in the polymerase chain reaction process using the genetic algorithm, Industrial & Engineering Chemistry Research, 2012, **51**(40): 13268

226 Zhou Jinming, Wang Jingxia, Huang Yu, *et al.* Large-area crack-free single-crystal photonic crystals via combined effects of polymerization-assisted assembly and flexible substrate, Npg asia Materials, 2012, **4**

227 Tang Ruizhi, Li Haixia, Liu Yancheng, *et al.* Laser flash photolysis study on electron transfer oxidation reaction of tryptophan or tyrosine with triplet state vitamin K-3, Acta Physico-Chimica Sinica, 2012, **28**(1): 213

228 Deng H X, Yan J, Wang D, *et al.* Laser-induced energy modulation in a dipole and potential applications for FEL (vol 622 pg 508 2010), Nuclear Instruments & Methods in Physics Research Section A-Accelerators Spectrometers Ddetectors and Aassociated Equipment, 2012, **664**(1): 48

229 Wang Peng, Wang Degao, Lin Jun, *et al.* Lattice defect-enhanced hydrogen production in nanostructured hematite-based photoelectrochemical device, ACS Applied Materials & Interfaces, 2012, **4**(4): 2295

230 Zhang Linjuan, Li Jiong, Du Yaping, *et al.* Lattice distortion and its role in the magnetic behavior of the Mn-doped ZnO system, New Journal of Physics, 2012, **14**

231 Wen Binghai, Li Huabing, Zhang Chaoying, *et al.* Lattice-type-dependent momentum-exchange method for moving boundaries, Physical Review E, 2012, **85**(1)

232 Li Lanting, Mi Lijuan, Hu Jun. Local and global sensitivity analysis of PCR kinetic model, Nuclear Science and Techniques, 2012, **23**(2): 124

233 Zhou Juan, Li Yongping, Low-resolution range data surface matching for 3D face verification, Automation Equipment and Systems PTS 1-4, 2012, **468-471**: 1957

234 Yang C, Zhang B, Wang J Z, Shi L Q, C *et al*. Microstructure and room temperature ferromagnetism of Cu-doped ZnO films, Nuclear Instruments & Methods in Physics Research Section B-Beam Interactions with Materials and Atoms, 2012, **283**: 24

235 Zhang Chuanfu, Wen Mou, Zeng JianRong, *et al*. Modeling the impact of the viaduct on particles dispersion from vehicle exhaust in street canyons, Science China- Technological Sciences, 2012, **55**(1): 48

236 Kang Seunggu, Li Hai, Tien Huynh, *et al*. Molecular mechanism of surface-assisted epitaxial self-assembly of amyloid-like peptides, ACS Nano, 2012, **6**(10): 9276

237 Xiu Peng, Tu Yusong, Tian Xingling, *et al*. Molecular wire of urea in carbon nanotube: a molecular dynamics study, Nanoscale, 2012, **4**(2): 652

238 Yan Juan, Su Shao, He Shijiang, *et al*. Nano rolling-circle amplification for enhanced sers hot spots in protein microarray analysis, Analytical Chemistry, 2012, **84**(21): 9139

239 Liu Qing, Jing Chao, Zheng Xiaoxue, *et al*. Nanoplasmonic detection of adenosine triphosphate by aptamer regulated self-catalytic growth of single gold nanoparticles, Chemical Communications, 2012, **48**(77): 9574

240 Li Wei. Non-photonic electron and charged hadron azimuthal correlation in p plus p collisions at root s=500 gev in star, Strangeness in Quark Matter 2011, 2012, **5**(2): 413

241 Song Bo. Cuniberti gianaurelio, sanvito stefano, fang haiping, Nucleobase adsorbed at graphene devices: Enhance bio-sensorics, Applied Physics Letters, 2012, **100**(6)

242 Cao X G, Cai X Z, Ma Y G, *et al.*, Nucleon-nucleon momentum-correlation function as a probe of the density distribution of valence neutrons in neutron-rich nuclei, Physical review C, 2012, 86(4):

243 Dai Jinhua, Deng Haixiao, Dai Zhimin, Numerical modeling of a high power terahertz source in Shanghai, Chinese Physics C, 2012, **36**(7): 648

244 Wang Xiao, Yan Zhongbao, Du Hanwen. Optimization analysis using orthogonal array designs for magnet girder assembly of SSRF, Nuclear Science and Techniques, 2012, **23**(1): 1

245 Zhang Guoqiang, Cao Xiguang, Fu Yao, *et al*. Origin of the finite nuclear spin and its effect in intermediate energy heavy ion collisions, Nuclear Science and Techniques, 2012, **23**(1): 61

246 Zhou Bo, Xiu Peng, Wang Chunlei, *et al*. Peptide friction in water nanofilm on mica surface, Chinese Physics B, 2012, **21**(2):

247 Tang Ruizhi, Zhang Peng, Li Haixia, *et al*. Photosensitized oxidation of tryptophan and tyrosine by aromatic ketones: A laser flash photolysis study, Science China-Chemistry, 2012, **55**(3): 386

248 Zhang Tong, Deng Haixiao, Chen Jianhui, *et al*.Polarization control proposal for Shanghai deep ultraviolet free electron laser, Nuclear Instruments & Methods in Physics Research Section A-Accelerators Spectrometers Detectors and Associated Equipment, 2012, **680**: 112

249 Wang Zihao, Ge Zhilei, Zheng Xiaoxue, *et al*. Polyvalent DNA-graphene nanosheets "click" conjugates, Nanoscale, 2012, **4**(2): 394

250 Wei Min, Chen Nan, Li Jiang, *et al*. Polyvalent Immunostimulatory nanoagents with self-assembled CpG oligonucleotide-conjugated gold nanoparticles, Angewandte Chemie-International Edition, 2012, **51**(5): 1202

251 Liu Hanzhou, Yu Ming, Deng Bo, *et al*. Pre-irradiation induced emulsion graft polymerization of acrylonitrile onto polyethylene nonwoven fabric, Radiation Physics and Chemistry, 2012, **81**(1): 93

252 Zhang Huifang, Liu Min, Yan Long, *et al*. Preparation and characterization of graphene nanoribbons, Nuclear Science and Techniques, 2012, **23**(3): 139

253 Shen Liguo, Bian Xiaokai, Lu Xiaofeng, *et al*. Preparation and characterization of ZnO/polyethersulfone (PES) hybrid membranes, Desalination, 2012, **293**: 21

254 Zhang Bowu, Zhang Yujie, Peng Cheng, *et al*. Preparation of polymer decorated graphene oxide by gamma-ray induced graft polymerization, Nanoscale, 2012, **4**(5): 1742

255 Yu Ming, Liu Hanzhou, Liu Xiyan, *et al*. Preparation of uranyl carbonate ions absorbent containing amidoxime groups via pre-irradiation induced grafting method, Abstracts of Papers of the American Chemical Society, 2012, **244**

256 Wang Jingyan, Li Yongping, Wang Quanquan, *et al*. Predicting membrane protein types by fusing different modes of pseudo amino acid composition, Computers in Biology and Medicine, 2012, **42**(5): 564

257 Xue L, Ma Y G, Chen J H, *et al*. Production of light (anti)nuclei (anti)hypertriton and di-Lambda in central Au plus Au collisions at energies available at the BNL relativistic heavy ion collider, Physical Review C, 2012, **85**(6)

258 Ren Xiuping, Zhou Bo, Wang Chunlei. Promoting effect of ethanol on dewetting transition in the confined region of melittin tetramer, Nuclear Science and Techniques, 2012, **23**(4): 252

259 Ma Mingwang, Wu Shengwei, Lin Jun, *et al*. Properties of ion track in polystyrene irradiated with high energy ^{56}Fe ions, Nuclear Instruments & Methods in Physics Research Section B-Beam Interactions With Materials and Atoms, 2012,

286: 233

260 Dai Jinhua, Deng Haixiao, Dai Zhimin. Proposal for an X-Ray free electron laser oscillator with intermediate energy electron beam, Physical Review Letters, 2012, **108**(3)

261 Dai Jinhua, Deng Haixiao, Dai Zhimin. Proposal for an X-Ray free electron laser oscillator with intermediate energy electron beam, Physical Review Special Topics- Accelerators and Beams, 2012, **15**(1)

262 Fu HaiYing, Xing ZhaoGuo, Cao XiYan, *et al.* Pulse radiolysis studies of functionally substituted imidazolium-based ionic liquids, Chinese Science Bulletin, 2012, **57**(21): 2752

263 Li Haixia, Liu Yanxheng, Tang Ruizhi, *et al.* Pulse radiolysis study on gatifloxacin - A fluoroquinolone antibiotic, Science China-Chemistry, 2012, **55**(7): 1358

264 Wang Lihua, Lu Xiaoming, Wei Xiangjun, *et al.* Quantitative Zn speciation in zinc-containing steelmaking wastes by X-ray absorption spectroscopy, Journal of Analytical Atomic Spectrometry, 2012, **27**(10): 1667

265 Wang Ping, Ge Zhilei, Pei Hao, *et al.* Quartz Crystal Microbalance Studies on Surface-Initiated DNA Hybridization Chain Reaction, Acta Chimica Sinica, 2012, **70**(20): 2127

266 Liu Heng, Zhou Yongnian, Jiang Zheng, *et al.* QXAFS system of the BL14W1 XAFS beamline at the Shanghai Synchrotron Radiation Facility, Journal of Synchrotron Radiation, 2012, **19**: 969

267 Xing Zhe, Wu Guozhong, Wang Mouhua. Radiation grafting of acrylonitrile to UHMWPE fiber for the preparation of uranium collection material, Abstracts of Papers of the American Chemical Society, 2012, 244

268 Cai Ren, Deng Bo, Jiang Haiqing, Yu Yang, *et al* Radiation induced graft polymerization of a fluorinated acrylate onto fabric, Radiation Physics and Chemistry, 2012, **81**(9): 1354

269 Zhang Bowu, Li Linfan, Wang Ziqiang, *et al* Radiation induced reduction: an effective and clean route to synthesize functionalized graphene, Journal of Materials Chemistry, 2012, **22**(16): 7775

270 Liu Weihua, Wang Mouhua, Xing Zhe, *et al.* Radiation-induced crosslinking of polyacrylonitrile fibers and the subsequent regulative effect on the preoxidation process, Radiation Physics and Chemistry, 2012, **81**(6): 622

271 Li Jianbo, Shi Lingli, Jia Lina, *et al*. Radiolabeling of RGD peptide and preliminary biological evaluation in mice bearing U87MG tumors, Bioorganic & Medicinal Chemistry, 2012, **20**(12): 3850

272 Zhou C L, Ma Y G, Fang D Q, *et al.* Ratio of shear viscosity to entropy density in multifragmentation of Au+Au, EPL, 2012, **98**(6)

273 Fan Guangwei, Fukuda Mitsunori, An Zhendong, *et al.* Reaction cross section studies of ^{12}C using the modified Glauber model in conjunction with nonlinear relativistic mean-field theory, Nuclear Science and Techniques, 2012, **23**(5): 312

274 Pei Hao, Liang Le, Yao Guangbao, *et al.* Reconfigurable three-dimensional DNA nanostructures for the construction of intracellular logic sensors, Angewandte Chemie- international Edition, 2012, **51**(36): 9020

275 Zhang Linjuan, Wang Jianqiang, Li Jiong, *et al.* Regulation of magnetic behavior and electronic configuration in Mn-doped ZnO nanorods through surface modifications, Chemistry of Materials, 2012, **24**(9): 1676

276 Wang Hua, Yan Shuai, Yan Fen, *et al*. Research on spatial coherence of undulator source in Shanghai synchrotron radiation facility, Acta Physica Sinica, 2012, **61**(14)

277 He Zhoutong, Yang Xinmei, Xia Huihao, *et al*. Role of defect electronic states in the ferromagnetism in graphite, Physical Review B, 2012, **85**(14)

278 Wang Jingyan, Li Yongping, Zhang Ying, *et al*. Semi- supervised protein function prediction via sequential linear neighborhood propagation, Bio-inspired Computing and Applications, 2012, **6840**: 435

279 Kumar Sanjeev, Ma Y G, Zhang G Q, *et al*. Sensitivity of neutron to proton ratio toward the high density behavior of the symmetry energy in heavy-ion collisions, Physical Review C, 2012, **85**(2)

280 Zhou Chenglong, Ma Yugang, Fang Deqing. Shear viscosity to entropy density ratio in au plus au central collisions, Plasma Science & Technology, 2012, **14**(7): 585

281 Lin Zuokang, Sun Guomin, Chen Jingen, *et al.* Simulation and optimization for a 30 MeV electron accelerator driven neutron source, Nuclear Science and Techniques, 2012, 23(5): 272

282 Cheng Cheng, Wang Changying, Huai Ping, *et al*. Structural and electronic properties of actinides fluorides: a density functional study, Atalante 2012 International Conference on Nuclear Chemistry for Sustainable Fuel Cycles, 2012, **7**: 460

283 Li Jian, Sun Lihua, Xu Chunyan, *et al*. Structure insights into mechanisms of ATP hydrolysis and the activation of human heat-shock protein 90, Acta Biochimica ET Biophysica Sinica, 2012, **44**(4): 300

284 Zhang Miao, Zhou Qiaogen. Study of the beam tune-shift effects for DEPU at SSRF, IEEE Transactions on Applied Superconductivity, 2012, **22**(3)

285 Chen Can, Tong Yajun, Xie Honglan, *et al*. Study of the focusing properties of Laue bent crystal by ray-tracing, Acta Physica Sinica, 2012, **61**(10)

286 Lu Yanling, Jiao Sihai, Zhou Xingtai, *et al*. Study on hot deformation behavior of TC4 titanium alloy, TMS 2012 141ST Annual Meeting & Exhibition-Supplemental Proceedings vol 1: Materials Processing and Interfaces, 2012, 841

287 Wang Xiao, Yan Zhong-bao, Du Han-wen. Suppression of ground vibration for SSRF Foundation, Vibration Structural Engineering and Measurement I PTS 1-3, 2012, **105-107:** 30

288 Yang HaiJun, Hou ZhengChi, Hu Jun. Surface Modification of Ultra-Flat Polydimethylsiloxane by UV-Grafted Poly (acrylic acid) Brushes, Journal of Applied Polymer Science, 2012, **123**(4): 2266

289 Tang Siwei, Yin Chongxian, Liu Dekang. Synchrotrons radiation stability measurement and improvement, Nuclear Science and Techniques, 2012, **23**(1): 7

290 Shi Lingli, Li Jianbo, Wang Cheng, *et al*. Synthesis of F-18-c(RGDfK) as Integrin alpha(v)beta(3) Targeted PET Tracer via Click Chemsitry with Cu(I) Catalyst Systems, Chemical Journal of Chinese Universities-Chinese, 2012, **33**(7): 1486

291 Ma C W, Pu J, Ma Y G, *et al*. Temperature determined by isobaric yield ratios in heavy-ion collisions, Physical Review C, 2012, **86**(5)

292 Leng Yongbin, Huang Guoqing, Zhang Manzhou, *et al*. The beam-based calibration of an X-ray pinhole camera at SSRF, Chinese Physics C, 2012, **36**(1): 80

293 Zhu Ying, Li Jing, Li Wenxin, *et al*. The biocompatibility of nanodiamonds and their application in drug delivery systems, Theranostics, 2012, 2(3): 302

294 Wang L, Sun S, Cao Y, Yin L X, *et al*. The cooling and safety design of a pair of binary leads for the MICE coupling magnets, IEEE Transactions on Applied Superconductivity, 2012, **22**(3)

295 Zhou Q, Zhang W , The Design of a Pair of Elliptically Polarized Undulators at SSRF, IEEE TRANSACTIONS ON APPLIED SUPERCONDUCTIVITY, 2012, **22**(3)

296 Liu Weihua, Wang Mouhua, Xing Zhe, Wu Guozhong, The free radical species in polyacrylonitrile fibers induced by gamma-radiation and their decay behaviors, Radiation Physics and Chemistry, 2012, **81**(7): 835

297 Mei Longwei, Cai Xiangzhou, Chen Jingen, *et al*. The investigation of thermal neutron scattering data of flibe, Proceedings of the 20th International Conference on Nuclear Engineering and the Asme 2012 Power Conference-2012 vol 1, 2012, 777

298 Zhang Lijuan, Wang Chunlei, Tai Renzhong, *et al*. The morphology and stability of nanoscopic gas states at water/solid interfaces, Chemphyschem, 2012, **13**(8): 2188

299 Liu Yiyong, Jiang Dikui, Wang Zhishan, *et al*. The operation of SSRF storage ring vacuum system, 18th International Vacuum Congress (IVC-18), 2012, **32**: 297

300 Li Xudong, Gu Qiang, Zhang Meng, *et al*. The QE numerical simulation of PEA semiconductor photocathode, Chinese Physics C, 2012, **36**(6): 531

301 Zhang Xingmin, Gao Mei, Gu Yueliang, *et al*. The structure-property investigation of bi1-xCexFeO$_3$ (x=0 0 05)-Li battery: In situ XRD and XANES studies, Journal of Physical Chemistry C, 2012, **116**(38): 20230

302 Zhang Haiou, Wang Zhishan. The vacuum system for SDUV FEL experiment facility, 18th International Vacuum Congress (IVC-18), 2012, **32**: 623

303 Wang Li, Wang Xiaoya, Shi Guosheng, *et al*. Thiacalixarene covalently functionalized multiwalled carbon nanotubes as chemically modified electrode material for detection of ultratrace Pb^{2+} ions, Analytical Chemistry, 2012, **84**(24): 10560

304 Cao Changqing, Wang Min. Treatment of municipal sewage sludge by electron beam irradiation, Nuclear Science and Techniques, 2012, **23**(1): 29

305 Zhang Jianbing, Deng Haixiao, Lin Xuling, *et al*. Tunable few-cycle coherent terahertz radiation with watt-level power from relativistic femtosecond electron beam, Nuclear Instruments & Methods in Physics Research Section A-accelerators Spectrometers Detectors and Associated Equipment, 2012, **693**: 23

306 Tan Juhua, Lin Dongdong, Pillai Saju, *et al*. Ultrasound effects on assembly of glucagon fibrils, Integrated Ferroelectrics, 2012, 136: 1

307 Kumar Sanjeev, Ma Y G. Understanding the symmetry energy using data from the ALADIN-2000 collaboration taken at the GSI large neutron detector, Physical Review C, 2012, **86**(5)

308 Shi Guosheng, Ding Yihong, Fang Haiping. Unexpectedly strong anion-p interactions on the graphene flakes, Journal of Computational Chemistry, 2012, **33**(14): 1328

309 Chen Shimou, Liu Yusheng, Fu Haiying, *et al.* Unravelling the role of the compressed gas on melting point of liquid confined in nanospace, Journal of Physical Chemistry Letters, 2012, **3**(8): 1052

310 Zhang Meng, Gu Duan, Gu Qiang, *et al.* Velocity bunching for the linac of Shanghai Deep UV FEL facility, Nuclear Science and Techniques, 2012, 23(3): 134

311 Ren Xiuping, Zhou Bo, Wang Chunlei. Water-induced ethanol dewetting transition, Journal of Chemical Physics, 2012, **137**(2)

312 Gao Yi, Zeng Xiao Cheng. Water-Promoted O_2 Dissociation on small-sized anionic gold clusters, ACS Catalysis, 2012, **2**(12): 2614

313 Dai Binbin, Wang Qian, Ma Jingyuan, *et al.* XAFS study of Cu^{2+} in aqueous solution of $CuBr_2$, Nuclear Science and Techniques, 2012, **23**(3): 129

314 Ao Lu, Chen Xiangru, Zhong Honggang, *et al.* Effect of stirring on the solidification structure and segregation of 60Si2MnA spring steel during continuous casting, TMS Annual Meeting, 2011(**3**): 589-597

315 Ayvazyan V, Baboi, N, Balandin, *et al.* FLASH II: A project update, FEL 2011-33rd International Free Electron Laser Conference, 2011, 247-250

316 Chen Can, Tong Yajun, Ren Yuqi, *et al.* Study on the optical properties of Laue bent crystal by ray-tracing, Guangxue Xuebao/Acta Optica Sinica, 2011, **31**(10): 1034002-1-1034002-9

317 Chen Jie, Ye Kairong, Leng Yongbin. Development of Shanghai Synchrotron Radiation Facility synchrotron radiation interferometer, Qiangjiguang Yu Lizishu/High Power Laser and Particle Beams, 2011, **23**(1): 179-184

318 Chen Xiangru, Sun Qingqing, Ao Lu, *et al.* Experimental simulation on the continuous casting solidified structure of S32205 duplex stainless steel, TMS Annual Meeting, 2011, **3**: 577-584

319 Chen Xiliang, Chen Xin, Li Dangsheng, *et al.* Dielectric properties of carbon-materials-filled composites characterized by terahertz time-domain spectroscopy, Advanced Materials Research, 2011, **295-297**, 1408-1413

320 Chien Chiachi, Zhang Guilin, Hwu Yeukuang, *et al.* Erratum to: Detecting small lung tumors in mouse models by refractive-index microradiology, Analytical and Bioanalytical Chemistry. 2011, 1

321 Gao A R, Lu N, Gao X L *et al.* Label-free DNA detection based on silicon nanowires, 2011 16th International Solid-State Sensors, Actuators and Microsystems Conference, TRANSDUCERS'11, 2011, 2271-2274

322 He Zifeng, Zhang Jinling, Liu Yonghao, *et al.* Characteristics of a symmetrical Cockcroft-Walton power supply of 50 Hz 12 MV50 mA, Review of Scientific Instruments, 2011, **82**(5)

323 He, Zifeng, Zhang Jinling, Liu Yonghao, *et al.* Erratum: Characteristics of a symmetrical Cockcroft-Walton power supply of 50 Hz 12 MV 50 mA (Review of Scientific Instruments (2011) 82 (055116)), Review of Scientific Instruments, 2011, **82**(8)

324 Hu Xiao, Zhou Qiaogen, Yin Lixin. The design of dual canted in-vacuum undulators at SSRF, IPAC 2011 - 2nd International Particle Accelerator Conference, 2011, 3287-3289

325 Li Lina, Huang Yuying. Health risk assessment of heavy metals in Shanghai urban parks, Proceedings-International Conference on Computer Distributed Control and Intelligent Environmental Monitoring, CDCIEM 2011, 2011, 1536-1539

326 Li R, Guo C L, Huang M M, *et al.* Operation status of SSRF power supplies and interlocks for top-up operation, IPAC 2011-2nd International Particle Accelerator Conference, 2011, 3349-3351

327 Ling, Xin Long, Tang, Zhong Feng(1,2), Huang, Shi Rong(3), Morphological changes of irradiated PMMA via Supercritical carbon dioxide treatments, Advanced Materials Research, 2011, **239-242**, 1510-1514

328 Okano Makoto, Yoshita Masahiro, Akiyama Hidefumi, *et al.* Coulomb-modulated gain spectra in current-injection T-shaped quantum-wire lasers, Physica Status Solidi (C) Current Topics in Solid State Physics, 2011, **8**(1): 20-23

329 Ren Yuqi, Zhou Guangzhao, Wang Yudan, *et al.* Study of multi-component sample using quantitative X-ray phase contrast imaging, Guangxue Xuebao/Acta Optica Sinica, 2011, **31**(8)

330 Sha Maolin, Niu Dongxiao, Dou Qiang, *et al.* Reversible tuning of the hydrophobic-hydrophilic transition of hydrophobic ionic liquids by means of an electric field, Soft Matter, 2011, **7**(9): 4228-4233

331 Shi Guosheng, Wang Zhigang, Zhao Jijun, *et al.* Adsorption of sodium ions and hydrated sodium ions on a hydrophobic graphite surface via cation-π interactions, Chinese Physics B, 2011, **20**(6)

332 Tao Shixing, Niu Jing, Chen Mingzhi, *et al.* Calibration of synchrotron radiation photon energy using crystal multiple diffraction, Guangxue Jingmi Gongcheng/Optics and Precision Engineering, 2011, **19**(5): 977-982

333 Togano Y, Motobayashi T, Aoi N, *et al.* Experimental investigation of the Stellar reaction $30S(p, \gamma)^{31}Cl$ via Coulomb dissociation, Journal of Physics: Conference Series, 2011, 312**(**SECTION 4)

334 Wang Chunlei, Li Jingye, Fang Haiping. Ordered water monolayer at room temperature, Rendiconti Lincei, 2011, **22**(SUPPL 1):S5-S16

335 Wang Xiao, Tian Feng, Zhang Yumei, *et al.* Microstructure and property changes of poly (ethylene terephthalate) fiber with moderate tenacity during heat treatment under constant-length conditions, Advanced Materials Research, 2011, **332-334**, 313-316

336 Wu Yanqing, Xue Chaofan, Chen Jiahua, *et al.* Designing a

pulse-resolved photon diagnostic system for Shanghai SXFEL, FEL 2011-33rd International Free Electron Laser Conference, 2011, 374-376

337 Zhang M Z, Hou J, Jiang B C, *et al.* Vertical beam size correction at the SSRF storage ring, IPAC 2011-2nd International Particle Accelerator Conference, 2011, 2043-2045

338 Zhang Manzhou, Li Haohu, Li Deming. Estimate of eddy current effects in APTRON, Qiangjiguang Yu Lizishu/High Power Laser and Particle Beams, 2011, **23(**5), 1357-1360

339 Zhang T, Zhao Z T, Wang D, *et al.* Conceptual design of a high brightness and fully coherent free electron laser in VUV regime, FEL 2011-33rd International Free Electron Laser Conference, 2011, 302-303

340 Zhao Z T, Chen S Y, Yu L H, *et al.* Shanghai soft X-ray free electron laser test facility, IPAC 2011-2nd International Particle Accelerator Conference, 2011, 3011-3013

341 Zhao Z T, Yin Y L, Li H H, *et al.* Progress towards top-up operation at SSRF, IPAC 2011 - 2nd International Particle Accelerator Conference, 2011, 3008-3010

342 Zheng Liping, Zhu Zhiyuan, Li Yong, *et al.* Reply to Comment on isotopic mass effects for low-energy channeling in a silicon crystal, Radiation Effects and Defects in Solids, 2011, **166**(11): 870-872

343 Zhu L F, Wang L S, Xie B P, *et al.* Inelastic x-ray scattering study on the single excitations of helium, Journal of Physics B: Atomic, Molecular and Optical Physics, 2011, 4**4**(2)

344 Antipov S, Jing C, Schoessow P, Kanareykin A, *et al.* Experimental observation of energy modulation in electron beams passing through terahertz dielectric wakefield structures, IPAC 2012 - International Particle Accelerator Conference 2012, 2012, 95-597

345 Chen Nian, He Yongzhou, Ren Fanglin, *et al.* Magnet measurement using 2D automatic rotation Helmholtz coils, Qiangjiguang Yu Lizishu/High Power Laser and Particle Beams, 2012, **4**(8): 941-1946

346 Deng Bo, Yang Xuanxuan, Li Linfan, *et al.* Antifouling microfiltration membranes from modified PVDF powder via radiation-induced graft polymerization technique, Harbin Gongye Daxue Xuebao/Journal of Harbin Institute of Technology, 2012, **44**(SUPPL2): 50-52

347 Deng H X, Yan J, Wang D, Dai Z M. Erratum: Laser-induced energy modulation in a dipole and potential applications for FEL (Nuclear Instruments and Methods in Physics Research, Section A: Accelerators, Spectrometers, Detectors and Associated Equipment (2010) 622 (508-511)), Nuclear Instruments and Methods in Physics Research, Section A: Accelerators, Spectrometers, Detectors and Associated Equipment, 2012, **6649**(1): 48

348 Feng C, Wang D, Zhao Z T, Study of the energy chirp effects on seeded FEL schemes at SDUV-FEL, IPAC 2012 - International Particle Accelerator Conference 2012, 2012, 1724-1726

349 Feng C, Zhang T, Chen J H, *et al.* Measurement of the local energy spread of electron beam at SDUV-FEL, IPAC 2012 - International Particle Accelerator Conference 2012, 2012, 143-2145

350 Feng C, Ding Y, Huang Z, *et al.* Two-color FEL schemes based on emittance-spoiler technique, FEL 2012 - 34th International Free Electron Laser Conference, 2012, 654-657

351 Gu Duan, Zhao Minghua. Beam alignment for SXFEL, Qiangjiguang Yu Lizishu/High Power Laser and Particle Beams, 2012, **24(**9): 2183-2186

352 He Xiaoan, Du Huabing, Li Chaoguang, *et al.* Scintillator's sensitivity calibration method in synchrotron radiation facility, Qiangjiguang Yu Lizishu/High Power Laser and Particle Beams, 2012, **24**(7): 1575-1578

353 He Y Z, Wang L, Zhou Q G. The research on magnetic properties of magnet for SSRF cryogenic permanent magnet undulator, IPAC 2012-International Particle Accelerator Conference 2012, 2012, 735-737

354 He Yongzhou, Zhou Qiaogen. Experiment research on Sm_2Co_{17} magnets for SSRF in-vacuum undulators, Qiangjiguang Yu Lizishu/High Power Laser and Particle Beams, 2012, **24**(9): 2187-2192

355 Huang T, Gao X, Pooke D, *et al.* A commercial HTS dipole magnet for x-ray magnetic circular dichroism (XMCD) experiments, IEEE Transactions on Applied Superconductivity, 2012, **22**(3)

356 Kang Cheng, Liu Yonghao, Huang Jianming, *et al.* Compensation of leakage flux on insulated core flat winding transformer, Qiangjiguang Yu Lizishu/High Power Laser and Particle Beams, 2012, **24(**7): 1595-1598

357 Li Xiaoheng, Chen Jingen, Cai Xiangzhou, *et al.* Criticality and burnup analysis of 2400 MW AHTR, Yuanzineng Kexue Jishu/Atomic Energy Science and Technology, 2012, **46**(SUPPL 1): 379-382

358 Lin Xuling, Zhou Feng, Zhang Jianbing, *et al.* High power wideband terahertz sources based on femtosecond facility, Hongwai yu Jiguang Gongcheng/Infrared and Laser Engineering, 2012, **41**(1): 116-118

359 Lin Zuokang, Zou Xin, Cao Yun, *et al.* Analysis of simulation for neutron target driven by 15 MeV electron beam, Yuanzineng Kexue Jishu/Atomic Energy Science and Technology, 2012, **46(**SUPPL 1): 505-509

360 Liu Jingwang, Hou Yan, Wang Jingyan, *et al.* Fusing iris and palmprint at image level for multi-biometrics verification,

Proceedings of SPIE - The International Society for Optical Engineering, 2012, **8350**

361 Liu Yafen, Mei Longwei, Cai Xiangzhou, *et al.* Calculation and analysis of DPA rate in core can and reactor vessel of molten salt reactor experiment, Yuanzineng Kexue Jishu/Atomic Energy Science and Technology, 2012, **46(**SUPPL 1): 459-463

362 Ma Guoliang, Wang Xinnian. Comparative study of hadron-and γ-triggered azimuthal correlations in relativistic heavy-ion collisions, Acta Physica Polonica B, 2012, **43**(4): 697-704

363 Ma Shihua, Wang Wenfeng, Chen Hua, *et al.* Identification of the (+) and (-)-ephedrine used by THz-TDS, Laser and Tera-Hertz Science and Technology, LTST 2012, 2012

364 Ma Xinpeng, Pei Guoxi, Liu Bo, *et al.* Digital monitoring for length variation of optical fibers in femtosecond timing and synchronization system of XFEL, Qiangjiguang Yu Lizishu/High Power Laser and Particle Beams, 2012, **24**(2), 297-300

365 Qi Yujin, Zhang Xiaohui, Zhao Cuilan, *et al.* Performance comparison of two compact multiplexed readouts with SensL's SPMArray4 for high-resolution detector module, IEEE Nuclear Science Symposium Conference Record, 2012, 455-457

366 Sheng Yinxiangzi, Liu Lixing, Xu Jiaqiang, *et al.* Radiation dose simulation and measurement plan for SSRF beam lines by using atom phantom, IPAC 2012 - International Particle Accelerator Conference 2012, 2012, 4008-4010

367 Tian S Q, Jiang B C, Zhang M Z, *et al.* Design and commissioning of the very low emittance optics in the SSRF storage ring, IPAC 2012 - International Particle Accelerator Conference 2012, 2012, 1647-1649

368 Tian S Q, Jiang B C, Zhang M Z, *et al.* Lattice design of the SSRF storage ring with super bend, IPAC 2012 - International Particle Accelerator Conference 2012, 2012, 1644-1646

369 Wang Xiao, Yan Zhongbao, Du Hanwen. Numerical analysis of vibration-attenuation effect of trenches in the engineering project of Shanghai free electron laser, Zhendong yu Chongji/Journal of Vibration and Shock, 2012, **31**(15): 190-194

370 Wu Yuting, Yang Hang, Zhao Hongwei, *et al.* Dielectric properties of DNA solution probed by terahertz time-domain spectroscopy, Laser and Tera-Hertz Science and Technology, LTST 2012, 2012

371 Yan Yingbing, Leng Yongbin, Lai Longwei, *et al.* Beam lifetime measurement using beam position monitor in SSRF, Qiangjiguang Yu Lizishu/High Power Laser and Particle Beams, 2012, **24(**1): 189-192

372 Yang Jianguo, Chen Shuangjian, Huang Nan, *et al.* Factors affecting deformation induced martensitic transformation of SUS304 stainless steel, Hanjie Xuebao/Transactions of the China Welding Institution, 2012, **33**(12): 89-92

373 Yang Li, Hu Junhui, Sheng Nan, *et al.* Capillary force in the particle-particle-substrate system, Applied Mechanics and Materials, 2012, **232**: 292-295

374 Zeng Peiying, Tang Xiaoyun, Yang Xuedong, *et al.* Design of Shenguang-II facility centralized control system, Qiangjiguang Yu Lizishu/High Power Laser and Particle Beams, 2012, **24**(11): 2595-2598

375 Zhang Guoqiang, Zhou Hu, He You, *et al.* Ring artifacts correction of computerized tomography image based on polar-coordinate transform, Guangxue Xuebao/Acta Optica Sinica, 2012, **32**(5)

376 Zhang Jianbing, Deng Haixiao, Lin Xuling, *et al.* Status of femtosecond accelerator based high power terahertz source at Shanghai, Laser and Tera-Hertz Science and Technology, LTST 2012, 2012

377 Zhang L Y, He J J, Xu S W, *et al.* Experimental study of the key astrophysical ^{18}Ne(α, p)21Na reaction, Proceedings of Science, 2012

378 Zhang M Z, Tian S Q, Jiang B C, *et al.* Study of a new injection scheme for the SSRF storage ring, IPAC 2012 - International Particle Accelerator Conference 2012, 2012, 685-687

379 Zhang Tong, Wang Dong, Zhao Zhentang, *et al.* Design of a wavelength continuously tunable ultraviolet coherent light source, IPAC 2012-International Particle Accelerator Conference 2012, 2012, 1727-1728

380 Zhu Haijun, Ding Jianguo, Zheng Lifang, *et al.* Remote control system of modulators in SDUV-FEL, Yuanzineng Kexue Jishu/Atomic Energy Science and Technology, 2012, **46**(12): 1508-1511

381 Zhu Jing, Wang Tongmin, Chen Zongning, *et al.* Real time imaging on dendrite morphology evolution during alloy solidification under electric field, IOP Conference Series: Materials Science and Engineering, 2012, **33**(1)

382 包良满, 贾彦彦, 雷前涛, 等. 大气颗粒物中轻元素的 PIGE 分析, 核技术, 2011, **34**(7): 494

383 曾建荣, 包良满, 龙时磊, 等. 结合 XANES 和 IC 技术测量大气颗粒物中硫的形态分布及其含量, 核技术, 2011, **34**(1): 65

384 陈灿, 佟亚军, 任玉琦, 等. 劳厄弯晶光学特性的光线追迹研究, 光学学报, 2011, **31**(10): 1034002

385 陈家华, 薛松, 卢启鹏, 等. 变包含角平面光栅单色器及其关键技术, 中国科学. 物理学, 力学, 天文学, 2011,

41(1): 6

386 陈杰, 叶恺容, 冷用斌. 上海光源同步辐射空间干涉仪研制, 强激光与粒子束, 2011, **23**(1): 179

387 陈鹏, 侯铮迟, 陆晓峰. 聚偏氟乙烯共辐射接枝N一乙烯基吡咯烷酮的红外光谱分析, 辐射研究与辐射工艺学报, 2011, **29**(3): 134

388 陈文豪, 陈敏, 肖体乔. 同步辐射中 FT-IR 谱仪入射光束角度偏移对光谱测量的影响, 核技术, 2011, **34**(1): 60

389 程坤, 赵明华, 顾强, 等. 基于 Poisson Superfish 和 General Particle Tracer 的高亮度高平均功率电子枪设计. 核技术, 2011, **34**(8): 581

390 崔巍, 张元庆, 许晓平, 等. 叶酸修饰 PAMAM 树状大分子的合成及 ^{188}Re 标记, 核技术, 2011, **34**(5): 386

391 丁喻, 漆玉金, 张雪竹, 等. 高性能影像处理平台构建及显微 CT 图像重建算法的并行实现, 核技术, 2011, **34**(8): 626

392 段雪非, 张满洲, 李浩虎. 上海质子治疗装置束流输运系统物理设计, 核技术, 2011, **34**(5): 381

393 范雪波, 林俊, 刘卫, 等. 大气颗粒物中碳官能团组分的NEXAFS分析, 核技术, 2011, **34**(10): 731

394 范雪波, 刘卫, 林俊, 等. 太仓大气细颗粒物的粒径分布及来源分析, 环境污染与防治, 2011, **33**(2): 35

395 范雪波, 刘卫, 王广华, 等. 杭州市大气颗粒物浓度及组分的粒径分布, 中国环境科学, 2011, **31**(1): 13

396 付海英, 邢兆国, 吴国忠. 芘在离子液体及常规溶剂中的激光闪光光解研究, 光谱学与光谱分析, 2011, **31**(5): 1344

397 顾俊俊, 邹杨, 魏向军, 等. BL14W1 光束线 XAFS 实验站极低浓度数据采集系统, 核技术, 2011, **34**(5): 341

398 黄国庆, 陈杰, 陈之初, 等. 上海光源 X 射线针孔相机控制系统设计, 核技术, 2011, **34**(9): 641

399 江家友, 陈志豪. 任意形状的脉冲信号发生器的研制, 核技术, 2011, **34**(4): 241

400 冷用斌, 易星, 赖龙伟, 等. 新型数字BPM信号处理器研制进展, 核技术, 2011, **34**(5): 326

401 李玖栋, 邓辉宇. 上海光源 PDM 全文检索系统的改进, 核技术, 2011, **34**(10): 721

402 李良, 侯铮迟, 陆晓峰, 等. 不同分子量聚醚砜超滤膜性能的研究(I)不同添加剂的影响, 膜科学与技术, 2011, **31**(6): 6

403 李潇, 张国欣, 周伟, 等. α-FeO(OH)纳米棒的制备、表征及光催化性能, 材料导报, 2011, **25**(6B): 88

404 李晓龙, 王灿, 顾月良, 等. 利用同步辐射 XRD 研究 $BiFeO_3$ 外延多铁薄膜的微结构, 中国科学. 物理学, 力学, 天文学, 2011, **41**(1): 12

405 刘慧, 汪冰, 王卓, 等. CdSe@ZnS 量子点在果蝇及其幼虫体内的分布, 核技术, 2011, **34**(6): 415

406 刘慧芳, 李瑞, 郭春龙. 可编程快脉冲电源的研制, 核技术, 2011, **34**(9): 710

407 刘建华, 刘京松, 谭菊花, 等. 高湿度环境下衬底表面对牛胰岛素聚集的影响, 科学通报, 2011, **56**(12): 956

408 刘静培, 李潇, 张岚, 等. 炔基修饰 Fe_3O_4 磁纳米粒子的合成及其 click"环加成反应, 四川大学学报. 自然科学版, 2011, **48**(5): 1137

409 刘石磊, 王丽, 徐中民, 等. 同步辐射双晶单色器平行度测量方法研究, 核技术, 2011, **34**(6): 411

410 刘伟华, 王谋华, 吴国忠. 辐射引发和热引发聚丙烯腈纤维的自由基研究, 波谱学杂志, 2011, **28**(4): 447

411 刘玉胜, 付海英, 唐忠锋, 等. 离子液体[EMIM][PF_6]负载纳米 SiO_x 表面的熔点及结构, 物理化学学报, 2011, **27**(7): 1725

412 刘忠英, 侯铮迟, 陆晓峰, 等. 不同分子量聚醚砜超滤膜性能的研究(II)有否无纺布支撑的影响, 膜科学与技术, 2011, **31**(6): 13

413 陆晓峰, 周保昌, 沈飞, 等. 厌氧膜生物反应器在食品废水处理中的应用研究, 膜科学与技术, 2011, **31**(3): 234

414 罗文, 徐望, 潘强岩, 等. 基于LabVIEW的X射线探测系统及其在激光康普顿散射实验中的应用, 核电子学与探测技术, 2011, **31**(7): 722

415 马春桃, 罗红心, 王劼, 宋丽, 斜入射法检测平面反射镜的面形误差, 激光与光电子学进展, 2011, **48**(7): 71201

416 戚英娜, 王谋华, 宋永才, 等. 聚碳硅烷纤维的辐照氧化联合热处理研究, 化工新型材料, 2011, **39**(10): 85

417 祁斌川, 朱海君, 丁建国. SDUV-FEL 真空联锁保护系统, 核技术, 2011, **34**(12): 885

418 钱江海, 韩定定, 马余刚. 开放式复杂航空网络系统的动力学演化, 物理学报, 2011, **60**(9): 98901

419 任玉琦, 周光照, 王玉丹, 等. 复合组分材料的 X 射线定量相衬成像研究, 光学学报, 2011, **31**(8): 834002

420 沈飞, 陈荣昌, 肖体乔. 基于 GPU 并行计算实现快速显微 CT 重构, 核技术, 2011, **34**(6): 401

421 宋健, 漆玉金, 赵翠兰. 一台便携式伽玛相机的数据采集系统设计, 核技术, 2011, **34**(11): 851

422 孙发力, 夏晓彬, 张志宏, 等. 用于测量放射性气溶胶 beta 射线的 Phoswich 探测器的蒙特卡罗模拟, 核技术, 2011, **34**(8): 594

423 孙福权, 傅远, 祝万钱. 压弯镜系统自重平衡多点调节方法的研究, 核技术, 2011, **349**(4): 246

424 孙凯, 陆晓峰, 周保昌, 等. 厌氧膜生物反应器(AnMBR)处理高浓度豆制品废水的研究, 膜科学与技术, 2011, **31**(4): 65

425 谭兴兴, 刘海岗, 郭智, 等. 基于上海光源扫描透射 X 射线显微术的相干衍射成像模拟, 光学学报, 2011, **31**(4): 236

426 唐睿智, 张鹏, 李海霞, 等. 脉冲辐解研究吩噻嗪与 CCl_3OOOH 的反应, 物理化学学报, 2011, **27**(8): 1975

427 陶世兴, 牛晶, 陈鸣之, 等. 利用晶体多重衍射进行同步辐射光子能量标定, 光学精密工程, 2011, **19**(5): 977
428 田丰, 唐忠锋, 李秀宏, 等. 同步 X 射线散射技术研究 γ 射线辐照后 PTFE 的结构变化, 核技术, 2011, **34**(7): 481
429 佟兴帆, 邓辉宇, 李志明. 上海光源产品管理系统及其全文检索子系统的改进, 核技术, 2011, **34**(7): 485
430 汪宝亮, 赵明华, 侯汨, 裴士伦, 张猛, S 波段双边对称耦合器的模拟设计, 核技术, 2011, **34**(12): 881
431 王成, 王妮, 张岚, 等. 点击化学在三羰基铼标记 2,2'-二吡啶甲基胺衍生物中的应用, 精细化工, 2011, **28**(12): 1244
432 王纳秀, 刘石磊, 徐中民, 等. SSRF 活动光子挡光器的模拟与实验结果比较, 核技术, 2011, 34(3): 165
433 王倩, 邹杨, 姜政, 等. 同步辐射 XANES 方法对 $FeCl_3$ 水溶液的研究, 中国科学. 物理学, 力学, 天文学, 2011, **41**(1): 17
434 魏勤, 漆玉金, 张雪竹. 小动物 X 射线显微 CT 的 MTF 曲线测量, 核电子学与探测技术, 2011, **31**(3): 293
435 熊亮, 殷重先, 刘鸣, 等. 数字化平均流强测量方法研究, 核技术, 2011, **34**(4): 251
436 许晓平, 张元庆, 沈玉梅. Avidin-dendrimer 对 Hela 细胞的靶向研究, 核技术, 2011, **34**(4): 293
437 薛超凡, 王勇, 吴衍青, 等. 软 X 射线光束线能量分辨率测量中气体压强对谱线的影响研究, 核技术, 2011, **34**(8): 561
438 闫芬, 张继超, 李爱国, 等. 基于同步辐射的快速扫描 X 射线微束荧光成像方法, 物理学报, 2011, **60**(9): 90702
439 杨光, 朱华, 沈玉梅. 新型聚乙二醇(PEG)-Cyclofenil 雌激素受体分子 beta 探针的合成, 有机化学, 2011, **31**(5): 715
440 杨桂森, 冷用斌, 袁任贤, 等. 基于逐圈位置频谱的束流不稳定性, 强激光与粒子束, 2011, **23**(8): 2187
441 杨明成, 钟磊, 朱德荣, 等. γ 射线辐射对 CF-PTFE/PA6 复合材料性能的影响, 复合材料学报, 2011, **28**(4): 7
442 杨群, 邓彪, 吕巍巍, 等. 利用荧光 CT 实现生物医学样品内元素分布的无损成像, 光谱学与光谱分析, 2011, **31**(10): 2753
443 杨璇璇, 邓波, 虞鸣, 等. 预辐射接枝丙烯酰胺改性 PVDF 粉体及其亲水性滤膜的制备, 辐射研究与辐射工艺学报, 2011, **29**(4): 209
444 于海生, 黄宇营, 魏向军, 等. 用掠入射 XAFS 方法研究 Ti/Ni/Ti 纳米薄膜的界面结构, 核技术, 2011, **34**(7): 489
445 苑洪铭, 李吉豪, 于洋, 等. PVDF 粉体预辐照接枝甲基丙烯酸缩水甘油酯制备锂离子二次电池隔膜研究, 辐射研究与辐射工艺学报, 2011, **29**(5): 266
446 张东华, 胡钧. 振动扫描极化力显微技术原位研究乙醇在云母表面的吸附行为, 核技术, 2011, **34**(4): 317
447 张国欣, 刘静培, 沈华, 等. 氨基功能化磁性 FeO(OH)纳米棒的制备研究, 功能材料, 2011, **42**(6): 1134
448 张俊强, 俞路阳, 殷重先, 等. 次谐波聚束器相位控制的算法改进, 强激光与粒子束, 2011, **23**(8): 2179
449 张满洲, 后接, 李浩虎, 等. 上海光源储存环线性模型校正, 原子核物理评论, 2011, **28**(3): 290
450 张满洲, 李浩虎, 李德明. 上海质子医疗装置的涡流效应, 强激光与粒子束, 2011, **23**(5): 1357
451 张伟, 周巧根, 王宏飞. 上海光源真空内波荡器性能的优化, 中国科学. 物理学, 力学, 天文学, 2011, **41**(1): 2
452 张莹, 李勇平, 敖新宇. 基于 OpenCV 的通用人脸检测模块设计, 计算机工程与科学, 2011, **33**(1): 97
453 郑俊义, 余笑寒, 刘敏, 等. 镍基合金受熔融氟化盐腐蚀的同步辐射 XRF 分析, 核技术, 2011, **34**(5): 336
454 周保昌, 陆晓峰, 卞晓锴, 等. 浸没式厌氧膜生物反应器的研发及其除污效能, 中国给水排水, 2011, **27**(15): 29
455 周晨, 陆晓峰, 侯铮迟, 等. 分光光度法和总有机碳法对超滤膜截留性能测定的比较, 膜科学与技术, 2011, **31**(5): 34
456 周光照, 佟亚军, 陈灿, 等. 相干 X 射线衍射成像的数字模拟研究, 物理学报, 2011, **60**(2): 28701
457 周虎, 彭新华, 张中彬, 等. 基于同步辐射微 CT 研究不同利用年限水稻土团聚体微结构特征, 农业工程学报, 2011, **27**(12): 343
458 周冉冉, 张祥志, 许子健, 等. 超分辨重建方法在 STXM 图像处理中的应用, 核技术, 2011, **34**(5): 321
459 朱华, 黄立梁, 张元庆, 等. L-乳酸齐聚物的制备及其三羰基铼衍生物的合成, 有机化学, 2011, **31**(1): 87
460 朱燕, 李晓林, 李玉兰, 等. 同位素稀释电感耦合等离子体质谱法分析降尘中铂族元素, 分析化学, 2011, **39**(5): 695
461 白凌志, 王廷栋, 刘月, 等. 掺杂 T 型半导体量子线的量子限域效应与有效库仑作用, 核技术, 2012, **35**(5): 390
462 卞晓锴, 施柳青, 于洋, 等. 粉体辐射接枝丙烯酸的聚偏氟乙烯超滤膜的制备, 膜科学与技术, 2012, **32**(2): 10
463 曾建荣, 龙时磊, 包良满, 等. 上海近海(洋山)海水主要成分及微量元素分析, 海洋环境科学, 2012, **31**(2): 186
464 曾沛颖, 汤晓云, 杨学东, 等. 神光Ⅱ激光装置集中控制系统设计, 强激光与粒子束, 2012, **24**(11): 2595
465 陈灿, 佟亚军, 谢红兰, 等. Laue 弯晶聚焦特性的光线追迹研究, 物理学报, 2012, **61**(10): 104102
466 戴建兴, 张焕琦, 李晴暖, 等. 铀化合物与不同氟化剂反应的高温热力学, 核技术, 2012, **35**(9): 704
467 狄兰兰, 谷鸣, 袁启兵, 等. 亚纳秒触发脉冲延时分配器设计, 核技术, 2012, **35**(1): 12
468 丁建国, 赵欢, 朱海君, 等. 上海同步辐射装置电源控制系统, 核技术, 2012, **35**(8): 573
469 董思民, 蒋志强, 杜涵文. 质子治疗装置大回转架支撑驱动系统的运动机理及分析, 核技术, 2012, **35**(3): 226

470 杜鹏, 米清茹, 周剑英, 等. 基于EPICS/MATLAB图像处理的光束位置测量系统, 核技术, 2012, **35**(10): 735

471 杜韦陶, 宋丽, 王玉柱, 等. 掠入射 X 射线散射法研究超光滑镜面粗糙度, 核技术, 2012, **35**(4): 255

472 谷端, 赵明华. 上海软 X 射线自由电子激光束流准直, 强激光与粒子束, 2012, **24**(9): 2183

473 何永周, 周巧根. 上海光源真空波荡器 Sm_2Co_{17} 永磁铁的实验研究, 强激光与粒子束, 2012, **24**(9): 2187

474 洪时金, 周巧根, 王宏飞. 高精度三维霍尔探头的标定, 核技术, 2012, **35**(3): 171

475 胡鹏飞, 李瑞, 胡志敏, 等. 开关型扫描磁铁电源的研制, 核技术, 2012, **35**(6): 438

476 黄辉, 黄跃峰, 李勇平, 等. EPICS 下基于 ARM 处理器的电机控制系统, 核技术, 2012, **35**(6) : 418

477 黄君艺, 陈敏, 佟亚军, 等. 上海光源红外束线中 CVD 金刚石窗的参数对红外透射率的影响, 核技术, 2012, **35**(3): 161

478 黄麟飞, 郁峰, 徐春艳, 等. 沼泽红假单胞菌砷(Ⅲ)S-腺苷甲基转移酶的初步晶体学分析, 核技术, 2012, **35**(5): 326

479 黄庆, 孙艳红, 王璐, 等. 针灸对帕金森小鼠模型运动机能调节的分子机制研究, 核技术, 2012, **35**(11): 877

480 黄亚, 张祥志, 祝江威, 等. CT 断层图像重建的新滤波函数, 核电子学与探测技术, 2012, **32**(12): 1388

481 蒋舸扬, 姜伯承, 方文定, 等. 一个基于 EPICS 框架的 EPU 前端反馈系统, 核技术, 2012, **35**(8): 568

482 康成, 刘永好, 黄建鸣, 等. 绝缘磁芯平面变压器的漏磁补偿, 强激光与粒子束, 2012, **24**(7): 1595

483 雷前涛, 刘江峰, 包良满, 等. 扫描质子微探针质子束刻写, 强激光与粒子束, 2012, **24**(7): 1603

484 李剑波, 沈华, 牛婷婷, 等. 抗 CA IX 单克隆抗体的 ^{99}Tcm 标记及其在荷瘤鼠体内显像, 核技术, 2012, **35**(7): 535

485 李健, 孙丽华, 徐春艳, 等. 热休克蛋白 90 的 N 端与 ATP 类似物的晶体结构揭示其功能调控, 生物化学与生物物理进展, 2012, **39**(10): 995

486 李静, 裴昊, 李凡, 王丽华, 等. 基于氧化石墨烯淬灭效应的 DNA 传感器特异性检测三聚氰胺, 核技术, 2012, **35**(5): 386

487 李兰婷, 米丽娟, 胡钧. PCR 理论模拟研究进展, 核技术, 2012, **35**(8): 635

488 李林, 张金金, 胡钧. 非接触调频模式 AFM 的发展及生物学应用, 核技术, 2012, **35**(6): 462

489 李荣, 王衡东, 王文峰, 等. 聚丙烯无纺布亲水性与血液相容性改性初步研究, 中国输血杂志, 2012, **25**(11): 1165

490 李瑞, 胡志敏, 胡鹏飞. 一种波形可编程扫描电源研制, 核技术, 2012, **35**(10): 728

491 李旭东, 陈丽萍, 顾强, 等. 锑钾铯光阴极制备系统, 核技术, 2012, **35**(7): 486

492 林维豪, 罗红心, 宋丽, 等. 同步辐射用光学元件面形绝对检测方法的研究, 光学学报, 2012, **32**(9): 912005

493 刘亨, 周永年, 顾颂琦, 等. IK220 计数卡在 XAFS 线站数据采集系统改造中的应用, 核技术, 2012, **35**(8): 561

494 刘慧芳, 胡志敏, 李瑞. 数字化 PWM 技术在电流传感器中的运用, 核电子学与探测技术, 2012, **32**(1): 123

495 刘慧强, 任玉琦, 周光照, 等. 相移吸收二元性算法用于 X 射线混合衬度定量显微 CT 的可行性研究, 物理学报, 2012, **61**(7): 78701

496 刘慧强, 王玉丹, 任玉琦, 等. 采用吸收修正 Bronnikov 算法的有机复合样品的 X 射线显微计算机层析研究, 光学学报, 2012, **32**(4): 320

497 刘锦溪, 陆燕玲, 李肖科, 等. C276 合金高温拉伸变形的本构方程, 塑性工程学报, 2012, **19**(5): 11

498 刘卫, 位楠楠, 王广华, 等. 碳同位素比技术定量估算城市大气 CO_2 的来源, 环境科学, 2012, **33**(4): 1041

499 刘晓庆, 刘波, 马新朋. 高精度中频数字鉴相器在 FPGA 上的实现, 核技术, 2012, **35**(5): 380

500 刘应都, 张国强, 王宏伟, 等. ^{3}He 正比计数器探测效率模拟及灵敏度刻度, 核技术, 2012, **35**(3): 175

501 刘月, 王廷栋, 白凌志, 等. T 型半导体量子线的动态屏蔽效应, 核技术, 2012, **35**(6): 467

502 刘中华, 边风刚, 李勇平, 等. 同步辐射散射图像中心定位算法研究, 核技术, 2012, **35**(9): 646

503 吕敏, 张欢, 诸颖, 等. 石墨烯氧化物抗菌效果的测定方法比较, 核技术, 2012, **35**(10): 785

504 牛冬校, 胡钧. 石墨烯与双链 DNA 分子复合结构电导性的 c-AFM 研究, 核技术, 2012, **35**(2): 141

505 牛晶, 汪启胜, 王玉, 等. SSRF 生物大分子晶体学光束线站多波长反常散射信号采集自动化系统, 核电子学与探测技术, 2012, **32**(1): 46

506 牛婷婷, 汪建军, 吴王锁, 等. 表面功能化 Fe_3O_4 的合成及其用于分离锶(II), 核化学与放射化学, 2012, **34**(3): 166

507 彭冠云, 江泽慧, 刘杏娥, 等. 木材、竹材密度的 CT 技术检测, 光谱学与光谱分析, 2012, **32**(7): 1935

508 沈轶, 胡钧. 单分子力谱测量方法及其在生物学中的应用, 核技术, 2012, **35**(1): 74

509 施玲丽, 李剑波, 王成, 等. 整合素 $\alpha_v\beta_3$ 靶向 PET 探针 ^{18}F-c(RGDfK)在 Cu(I)催化体系中的点击合成, 高等学校化学学报, 2012, **33**(7): 1486

510 史丹, 欧阳联华, 谷鸣. 上海质子治疗装置慢引出 RFKO 研究, 核技术, 2012, 35(3): 231

511 苏荣锋, 吴胜益, 许瑞年. 数字化电源控制器的 PWM 波同步, 核电子学与探测技术, 2012, **32**(8): 907

512 苏荣锋, 许瑞年, 黄毛毛. 基于 FPGA 生成 PWM 波的实现, 核技术, 2012, **35**(6): 423

513 汤宁, 李勇平, 王靖琰, 等. 多模式生物特征识别的身份验证系统, 计算机工程与设计, 2012, **33**(1): 317
514 唐睿智, 李海霞, 刘艳成, 等. 维生素 K_3 的激发三重态与色氨酸、酪氨酸电子转移氧化反应的激光闪光光解研究, 物理化学学报, 2012, **28**(1): 213
515 汪宝亮, 林国强, 顾强, 等. 上海光源直线加速器的弱流强运行, 核技术, 2012, **35**(6): 401
516 汪启胜, 黄胜, 孙波, 等. SSRF 生物大分子晶体学线站用户数据采集系统, 核技术, 2012, **35**(1): 5
517 汪全全, 王靖琰, 李勇平. 最大熵矢量量化及其在 TMS320DM642 上的实现, 数据采集与处理, 2012, **27**(6): 639
518 汪睿, 李文斌, 刘波, 等. HGHG 自由电子激光时间相干性研究, 核技术, 2012, **35**(4): 251
519 王存立, 赵玉彬, 张文志. 基于FPGA的DDS信号获取与PI反馈算法设计, 核技术, 2012, **35**(3): 236
520 王华, 闫帅, 闫芬, 等. 上海同步辐射装置波荡器光源空间相干性的研究, 物理学报, 2012, **61**(14): 144102
521 王华, 闫帅, 闫芬, 等. 超环面镜对同步辐射硬 X 光束空间相干性的影响, 核技术, 2012, **35**(8): 583
522 王丽, 徐中民, 王纳秀. 变形晶体X射线分光性能的数值模拟, 核技术, 2012, **35**(6): 413
523 王丽玮, 谷鸣, 袁启兵. 脉冲调制器稳定性监控中的数据采集与处理, 核技术, 2012, **35**(7): 543
524 王鹏, 汪德高, 彭程, 等. 用于光电化学水分解的高光氢转换效率 TiO_2 纳米棒阵列, 核技术, 2012, **35**(6): 472
525 王萍, 葛志磊, 裴昊, 等. 表面引发的DNA杂交链式反应的石英晶体微天平研究, 化学学报, 2012, **70**(20): 2127
526 王晓, 严中保, 杜涵文. 上海自由电子激光工程隔振沟减振数值分析, 振动与冲击, 2012, **31**(15): 190
527 王玉丹, 彭冠云, 佟亚军, 等. 影响同步辐射 X 射线螺旋显微 CT 的若干因素研究, 物理学报, 2012, **61**(5): 54205
528 闻艳丽, 林美华, 裴昊, 等. 基于电化学技术的microRNA生物传感器, 化学进展, 2012, **24**(9): 1656
529 熊文纲, 李文新, 王敏. 基于热堆的钍铀转换过程中 ^{232}U 生成的模拟计算, 核技术, 2012, **35**(5): 395
530 熊云, 冷用斌, 易星, 等. 上海光源 DCCT 系统置信度算法, 核技术, 2012, **35**(9): 651
531 熊云, 阎映炳, 冷用斌, 等. 恒流模式直流流强检测系统的优化, 核技术, 2012, **35**(2): 81
532 徐慧超, 周剑英, 龚培荣, 等. YAG 晶体在软 X 射线荧光靶探测器中的应用, 核技术, 2012, **35**(8): 587
533 徐望, 罗文, 黄勃松, 等. 能量连续可调 LCS 光源 SINAP-III, 原子核物理评论, 2012, **29**(3): 253
534 许新磊, 李健, 孙丽华, 等. 1.9A分辨率mu-crystallin蛋白晶体结构及其酮亚胺还原酶活性位点分析, 核技术, 2012, **35**(10): 721
535 阎映炳, 冷用斌, 赖龙伟, 等. 用束流位置监测器测量上海光源束流寿命, 强激光与粒子束, 2012, **24**(1): 189
536 晏宇, 陈永忠, 俞路阳. 基于 ARM 与 FPGA 的运动控制平台研究, 核技术, 2012, **35**(3): 166
537 姚剑, 耿彦红, 王广华, 等. 用碳稳定同位素估算大气细颗粒物中多环芳烃的来源, 核技术, 2012, **35**(4): 315
538 易星, 冷用斌, 赖龙伟, 等. 基于软件无线电的新型数字束流位置处理器, 核技术, 2012, **35**(5): 346
539 于海波, 刘建飞, 侯洪涛, 等. 三次谐波超导腔高次模抑制研究, 核技术, 2012, **35**(1): 1
540 于洋, 蒋海青, 李林繁, 等. 尼龙滤布共辐射接枝 N-异丙基丙烯酰胺研究, 辐射研究与辐射工艺学报, 2012, **30**(4): 193
541 俞毅, 吴立, 张青, 等. 上海光源空调系统湿度控制问题的分析与改进, 核技术, 2012, **35**(10): 741
542 张传福, 曾建荣, 文谋, 等. 高架桥对街道峡谷内大气颗粒物输运的影响, 环境科学研究, 2012, **25**(2): 159
543 张国强, 周虎, 和友, 等. 基于极坐标变换去除计算机层析图像环形伪影, 光学学报, 2012, **32**(5) : 534001
544 张俊强, 殷重先, 高永强, 等. FPGA 实现次谐波聚束器的幅相控制, 核技术, 2012, **35**(7): 499
545 张宁, 冷用斌, 陈之初, 等. 基于示波器嵌入式 IOC 技术的逐束团位置监测系统研制, 核技术, 2012, **35**(5): 337
546 张永立, 蒋建国, 龚培荣. 上海光源 XBPM 自动量程 I-V 转换器的研制, 核电子学与探测技术, 2012, **32**(6): 686
547 钟磊, 杨常桥, 唐忠锋, 等. 辐照交联聚四氟乙烯(XPTFE)在空气气氛下的热稳定性, 辐射研究与辐射工艺学报, 2012, **30**(6): 333
548 周光照, 王玉丹, 任玉琦, 等. 相干 X 射线衍射成像三维重建的数字模拟研究, 物理学报, 2012, **61**(1): 18701
549 周娟, 李勇平, 黄跃峰. 基于强度图和深度图的多模态人脸识别, 计算机工程与应用, 2012, **48**(25): 5
550 周永年, 张招红, 姜政, 等. EPICS 在 SSRF 液氮冷却单色器运动控制中的应用, 计算机工程与应用, 2012, **48**(8): 236
551 周志中, 胡守明, 王君, 等. 工频倍加型电子束辐照装置的调压控制, 核技术, 2012, **35**(2): 87
552 朱海君, 丁建国, 郑丽芳, 等. SDUV-FEL 调制器远程控制系统, 原子能科学技术, 2012, **46(**12): 1508
553 朱海君, 郭春龙, 丁建国, 等. SSRF 储存环 B 铁和 S 铁电源故障信息监控系统, 核技术, 2012, **35**(9): 641
554 朱海君, 刘亚娟, 袁启兵. 上海光源调制器远控系统的设计与实现, 核电子学与探测技术, 2012, **32**(6): 690
555 朱海君, 刘亚娟, 袁启兵. 基于EPICS的上海光源注入引出远控系统, 核技术, 2012, **35**(5): 342
556 祝江威, 许子健, 刘海岗, 等. 基于 X 射线相干衍射成像的元素分布成像, 核技术, 2012, **35**(4): 245
557 STAR 合作, Longitudinal and transverse spin asymmetries for inclusive jet production at mid-rapidity in polarized p+p

collisions at $\sqrt{S}$ =200 GeV, Physical Review D, 2012, **86(**3)

558 STAR 合作, Di-electron spectrum at mid-rapidity in p+p collisions at $\sqrt{S}$ =200 GeV, Physical Review C, 2012, **86**(2)

559 STAR 合作, Inclusive charged hadron elliptic flow in Au+Au collisions at $\sqrt{S_{NN}}$ =7.7–39 GeV, Physical Review C, 2012, **86**(5)

560 STAR 合作, Measurements of D^0 and D* production in p plus p collisions at $\sqrt{S_{NN}}$ =200 GeV, Physical Review D, 2012, **86**(7)

561 STAR 合作, Transverse single-spin asymmetry and cross section for π^0 and η mesons at large Feynman x in $p^{\uparrow}$ + p collisions at root $\sqrt{S}$ =200 GeV, Physical Review D, 2012, **86**(5)

562 STAR 合作, Directed Flow of Identified Particles in Au plus Au Collisions at $\sqrt{S_{NN}}$ =200 GeV at RHIC, Physical Review Letters, 2012, **108**(20)

563 STAR 合作, Strangeness Enhancement in Cu-Cu and Au-Au Collisions at $\sqrt{S_{NN}}$ =200 GeV, Physical Review Letters, 2012, **108**(6)

564 STAR 合作, System size and energy dependence of near-side dihadron correlations, Physical Review C, 2012, **85**(1)

565 STAR 合作, Identified Hadron Compositions in p+ p and Au+Au Collisions at High Transverse Momenta at $\sqrt{S_{NN}}$ =200 GeV, Physical Review Letters, 2012, **108**(6)

566 STAR 合作, Evolution of the differential transverse momentum correlation function with centrality in Au+ Au collisions at $\sqrt{S_{NN}}$ =200 GeV, Physical Review B, 2011, **704**(5): 467

567 STAR 合作, ρ^0 photoproduction in AuAu collisions at $\sqrt{S_{NN}}$ =62.4 GeV measured with the STAR detector, Physical Review C, 2012, **85**(1)

568 STAR 合作, Energy and system-size dependence of two- and four-particle μ^2 measurements in heavy-ion collisions at $\sqrt{S_{NN}}$ =62.4 and 200 GeV and their implications on flow fluctuations and nonflow, Physical Review C, 2012, **86**(1)

569 STAR 合作, Directed and elliptic flow of charged particles in Cu+Cu collisions at root $\sqrt{S_{NN}}$ =22.4 GeV, Physical Review C, 2012, **85**(1)

570 STAR 合作, Anomalous centrality evolution of two-particle angular correlations from Au-Au collisions at $\sqrt{S_{NN}}$ =62 and 200 GeV, Physical Review C, 2012, **86**(6)

571 STAR 合作, Observation of the antimatter helium-4 nucleus, Nature, 2011, **473**(7347): 353

572 STAR 合作, Experimental studies of di-jet survival and surface emission bias in Au plus Au collisions via angular correlations with respect to back-to-back leading hadrons, Physical Review C, 2011, **83**(6)

573 STAR 合作, High p_T nonphotonic electron production in p+ p collisions at $\sqrt{S}$ =200 GeV, Physical Review D, 2011, **83**(5)

574 STAR 合作, K^{*0} production in Cu plus Cu and Au + Au collisions at $\sqrt{S_{NN}}$ =62.4 GeV and 200 GeV, Physical Review C, 2011, **84(**3)

575 STAR 合作, Scaling properties at freeze-out in relativistic heavy-ion collisions, Physical Review C, 2011, **83**(3)

576 STAR 合作, Measurement of the Parity-Violating Longitudinal Single-Spin Asymmetry for $W^{\pm}$Boson Production in Polarized Proton-Proton Collisions at $\sqrt{S}$ =500 GeV, Physical Review Letters, 2011, **106**(6)

577 STAR 合作, Strange and multistrange particle production in Au +Au collisions at $\sqrt{S_{NN}}$ =62.4 GeV, Physical Review C, 2011, **83**(2)

578 STAR 合作, Pion femtoscopy in p + p collisions at $\sqrt{S_{NN}}$ =200 GeV, Physical Review C, 2011, **83**(6)

579 STAR 合作, CUORE crystal validation runs: Results on radioactive contamination and extrapolation to CUORE background, Astroparticle Physics, 2012, **35**(12): 839

附录 2

2010-2012 年度举办（承办）国际会议表

2011

No.	会议名称 Conference Name	日期 Dates	规模 Scale
1	Collaborative Computational Project No.4 Workshop：Lectures and Tutorials on Software for Macromolecular X-Ray Crystallography 2011 上海 CCP4 晶体学培训班	Mar.28-31	共 169 人: 国外专家 7 人,国内专家 162 人
2	2011 Workshop on Water at Interfaces 2011 界面水性质研讨会	May 27-28	共 95 人: 国外专家 6 人, 国内专家 89 人
3	The 33rd International Free Electron Laser Conference FEL 2011 第 33 届自由电子激光国际会议	Aug.22-26	共 350 人:国外专家 150 人, 国内专家 150 人
4	Fourth Internaitonal Partical Accelerator Conference -First Meeting of the IPAC.13 Scientific Programme Committee 第四届国际粒子加速器大会(IPAC'13)科学议程委员会(SPC)及大会组委会(OC)会议	Nov.21-23	共 30 人: 国外专家 24 人, 国内专家 6 人
5	The 18th Meeting of the Asian Committee for Future Accelerators 第 18 届未来加速器亚洲委员会 ACFA 上海会议	Nov.24	共 20 人: 国外专家 15 人, 国内专家 5 人

2012

No.	会议名称 Conference Name	日期 Dates	规模 Scale
1	DNA Nanotechnology Conference: from structure to function DNA 纳米技术：从结构到功能国际研讨会	Mar.16-19	共 40 人: 国外专家 10 人, 国内专家 30 人
2	International Review Meeting for the 2 MW TMSR Pre-Conceptual Design and the High Temperature FLiNaK Loop Technical Design 2MW 固态堆概念设计和 FLiNaK 高温熔盐回路工程方案国际评议会	July 11-13	约 40 人: 国外专家 8 人,: 国内专家 32 人
3	The 11th International Conference on X-ray Microscopy(XRM2012) 第十一届国际 X 射线显微会议	Aug.5-10	共 320 人: 国外专家 189 人,国内专家 111 人
4	7th International Conference on Mechanical Engineering Design of Synchrotron Radiation Equipment and Instrumentation (MEDSI2012) 第七届同步辐射装备和仪器机械工程设计国际会议	Oct.15-19	共 126 人: 国外专家 71 人, 国内专家 55 人
5	The 7th International Workshop on Medical Applications of Synchrotron Radiation (MASR2012) 第 7 届同步辐射(生物)医学应用国际研讨会	Oct.17-20	共 115 人: 国外专家 63 人, 国内专家 52 人
6	Thorium Energy Conference 2012 2012 年钍能源会议	Oct.29-Nov.1	约 200 人: 国外专家 40 人,国内专家 160 人
7	1st International Symposium on Advanced Synchrotron Techniques for Energy and Catalysis Applications 第一届先进同步辐射技术在能源和催化研究中的应用国际研讨会	Nov.12-14	约 50 人: 国外专家 9 人, 国内专家 41 人
8	The 3rd International workshop on nuclear dynamics in heavy-ion reactions (IWND2012) 2012 第三届国际重离子碰撞中核反应动力学研讨会	Dec.15-20	约 80 人: 国外专家 8 人, 国内专家 72 人

附录 3

2011–2012 年度国际合作协议

No.	协议名称	合作单位	国家	签署日期	有效期	我方签署人	对方签署人
1	Memorandum of Understanding of Collaborative Research between Shanghai Institute of Applied Physics CAS and Diamond Light Source Ltd.(DLS)	Diamond Light Source Ltd.(DLS)	England	2011.2.17	5 年	Zhao Zhentang Director of SINAP	Dr.Gerhard Materlik, Chief Executive officer
2	Memorandum between the National Institute of Radiological Sciences and the Shanghai Institute of Applied Physics	National Institute of Radiological Sciences, Japan	Japan	2011.5.31	5 年	Zhao Zhentang Director of SINAP	Yoshiharu Yonekura, President
3	MEMORANDUM OF UNDERSTANDING Between Shanghai Institute of Applied Physics, And Japan Synchrotron Radiation Research Institute And RIKEN Harima Institute	Japan Synchrotron Radiation Research Institute And RIKEN Harima Institute	Japan	2011.9.22	5 年	Zhao Zhentang Director of SINAP	SHIRAKAWA Tetsuhisa (President)ISHIKAWA Tetsuya (Director)
4	MEMORANDUM OF UNDERSTANDING Between Shanghai Institute of Applied Physics, And Canadian Light Source Inc.	Canadian Light Source Inc.	Canada	2012.4.10	长期	Zhao Zhentang Director of SINAP	Thomas Fllis(Director); Bery Lepage
5	MEMORANDUM OF UNDERSTANDING Between Shanghai Institute of Applied Physics, And COSYLAB Control System Laboratory	COSYLAB Control System Laboratory	Slovenia	2012.7.16	长期	Zhao Zhentang Director of SINAP	Mark Plesko (CEO)
6	MEMORANDUM OF UNDERSTANDING Between Shanghai Institute of Applied Physics, And State Committee of Science of the Ministry of Education and Science of RA (SCS of RA MES)	State Committee of Science of the Ministry of Education and Science of RA (SCS of RA MES)	Armenia	2012.11.7	长期	Zhao Zhentang Director of SINAP	S.Haroutiunian
7	MEMORANDUM OF UNDERSTANDING Between Shanghai Institute of Applied Physics(SINAP) and The Australian Nuclear Science and Technology Organisation(ANSTO)	The Australian Nuclear Science and Technology Organisation (ANSTO)	Australia	2012.12.10	5 年	Zhao Zhentang Director of SINAP	Adrian Paterson (chief Executive officer)
8	MEMORANDUM OF UNDERSTANDING Between Shanghai Institute of Applied Physics, And Brazilian Center for Research in Energy and Materials (CNPEM) legally responsible for managing Brazilian Synchrotron Light Lab (LNLS)	Brazilian Synchrotron Light Lab (LNLS)	Brazilian	2012.12.20	5 年	Zhao Zhentang Director of SINAP	Carlos Alberto Aragao de Carvalho Filho (Director)

附录 4

2011–2012 年专利申请、授权一览表

2011 申请专利

NO.	专利名称	申请号	审请日	类型	发明人
1	一种抗菌织物及其制备方法	201110004877.4	2011-1-11	发明	李景烨 黄庆 樊春海 张玉杰 赵金明 胡文兵 蒋海青 于洋 虞鸣 李林繁 邓波
2	一种 PVDF 接枝 NVP 的方法及由其制得的接枝共聚物	201110027380.4	2011-1-25	发明	侯铮迟 陈鹏
3	一种 ^{99m}Tc 配合物、其制备方法、中间体及其应用	201110040441.0	2011-2-18	发明	沈玉梅 张元庆 许晓平 孙艳红 杨光 崔巍 朱华
4	适用于太赫兹时域光谱测量的液体样品架及其方法	201110040716.0	2011-2-18	发明	赵红卫 吴胜伟 朱海云 张增艳 李晴暖 刘晓鸿 朱智勇
5	一种稳定双链 DNA 的方法及双链 DNA 稳定剂	201110040726.4	2011-2-18	发明	雷豪志 米丽娟 张益 陈佳佳 郭守武 胡钧
6	一种纳米金-单宁酸-氧化石墨烯纳米复合材料的制备方法	201110045170.8	2011-2-24	发明	张玉杰 张小勇 彭程 张欢 胡文兵 黄庆
7	自适应数字混频正交本振信号频率控制字的获取方法	201110071198.9	2011-3-23	发明	赖龙伟 冷用斌 韩扣兄
8	单个生物分子反应实时原位表征方法	201110069865.X	2011-3-22	发明	吴娜 李宾 胡钧
9	一种高分子接枝的氧化石墨烯及其制备方法	201110088928.6	2011-4-8	发明	李景烨 黄庆 张伯武 张玉杰 邓波 李林繁 彭程 虞鸣 胡文兵 吕敏
10	对功能分子进行 18F 标记的方法	201110152843.X	2011-6-8	发明	张岚 施玲丽 李剑波 王成 周伟
11	靶向分子受体检测方法、聚酰胺-氨衍生物及其制备方法	201110152831.7	2011-6-8	发明	孙艳红 张元庆 徐晓平 沈玉梅 林俊 郭智 王华 崔巍 杨光
12	同步辐射原位在线纤维纺丝设备	201110173600.4	2011-6-24	发明	李秀宏 边风刚 柳义 李志军 王玉柱 周平 王劼
13	一种还原氧化石墨烯及其制备方法	201110243292.8	2011-8-23	发明	李景烨 张伯武 黄庆 于洋 李林繁 邓波 虞鸣
14	接枝改性高分子材料及其制备方法和应用	201110255378.2	2011-8-22	发明	李景烨 李林繁 邓波 虞鸣
15	一种防烫伤纺织品及其制备方法	201110303495.1	2011-10-10	发明	李景烨 于洋 邓波 李林繁 虞鸣 蒋海青
16	预辐照 PVDF 接枝 NVP 的制备方法和所制得的共聚物	201110346202.8	2011-11-4	发明	侯铮迟 陈利芳 陆晓峰
17	一种碳纳米材料-棉纤维复合导电材料及其制备方法和用途	201110360286.0	2011-11-15	发明	邓波 张伯武 王自强 李林繁 虞鸣 蒋海青
18	一种改性超高分子量聚乙烯纤维及其制备方法	201110388139.4	2011-11-29	发明	王谋华 吴国忠 邢哲 刘伟华
19	一种改性高分子筛网及其制备方法和应用	201110451402.X	2011-12-27	发明	李景烨 邓波 于洋 蒋海青 李林繁 虞鸣
20	一种涉及 DNA 折纸的方法及其结构和应用	201110451573.2	2011-12-27	发明	吴娜 李宾 胡钧
21	一种杀灭肿瘤细胞的系统和方法	201110027344.8	2011-1-25	发明	张国欣 李潇 张岚

NO.	专利名称	申请号	审请日	类型	发明人
22	适用于太赫兹时域光谱测量的液体样品架	201120041905.5	2011-2-18	实用新型	赵红卫 吴胜伟 朱海云 张增艳 李晴暖 刘晓鸿 朱智勇
23	冷却式薄膜X射线衍射仪样品台及X射线衍射仪	201120471638.5	2011-11-23	实用新型	李小龙 何庆 顾月良
24	加热式薄膜X射线衍射仪样品台及X射线衍射仪	201120472297.3	2011-11-23	实用新型	顾月良 李小龙 何庆
25	电池测试装置	201120537974.5	2011-12-20	实用新型	文闻 高梅 顾月良 何庆 黎忠 周兴泰
26	纳米材料测试装置	201120538631.0	2011-12-20	实用新型	文闻 张兴民 高梅 杨铁营 何庆 周兴泰
27	外加电场测试台架及薄膜测试平台	201120559975.X	2011-12-28	实用新型	李晓龙 顾月良 何庆
28	远程温度监测系统	201120561521.6	2011-12-28	实用新型	马新朋 刘波

2012 申请专利

NO.	专利名称	申请号	审请日	类型	发明人
1	一种高温介质泵热屏蔽装置	201210510151.2	2012-12-3	发明	黎忠 傅远 黄建平 张健宇 林良程 毛文玉 王纳秀 王晓 李波 陆世瑞
2	熔盐电化学实验装置	201210003346.8	2012-1-6	发明	左勇 黄鹤 李晓云 王敏
3	一种高温熔盐同步辐射原位研究装置	201210014460.0	2012-1-17	发明	何上明 李爱国 闫帅
4	加热装置	201210034327.1	2012-2-15	发明	何上明 李爱国 闫帅
5	PVDF-G-PVP 接枝共聚物的制备方法及所得的接枝共聚物	201210151999.0	2012-5-15	发明	侯铮迟 秦强
6	一种采用碲化镉量子点清除帕金森模式细胞中产生的α-核突触蛋白的方法及其应用	201210586127.7	2012-12-28	发明	黄庆 陈楠 李晓明 魏敏 樊春海
7	一种远程监控系统	201210022017.8	2012-1-31	发明	胡纯 刘平
8	一种光强探测电离室	201210058796.7	2012-3-7	发明	边风刚 王劼 李秀宏
9	同步辐射红外显微镜的数值孔径匹配装置	201210096476.0	2012-4-1	发明	佟亚军 陈敏 吉特
10	一种对化合物进行[^{18}F]标记的方法	201210103511.7	2012-4-10	发明	张岚 贾丽娜 李剑波 施玲丽
11	一种利用物理磨损 AFM 探针操纵 DNA 分子的方法及其探针	201210112726.5	2012-4-17	发明	段娜 张益 胡钧
12	实现单色器与谱学显微镜通信的接口系统和方法	201210163250.8	2012-5-22	发明	刘平 王勇 郑丽芳
13	液体样品池	201210163281.3	2012-5-23	发明	赵红卫 张建兵 武余亭
14	核用电缆无卤阻燃绝缘料、电缆绝缘层，制备方法和应用	201210356203.5	2012-9-20	发明	张聪 李景烨 李林繁
15	无卤无红磷阻燃热收缩材料、热收缩管，制备方法和应用	201210356195.4	2012-9-20	发明	张聪 李景烨 李林繁
16	电子射线源产生装置及产生低剂量率电子射线的方法	201210348278.9	2012-9-18	发明	何子锋 朱希恺 翟光延
17	一种基于 DNA 折纸的生物分子亲和常熟测定方法	201210391472.5	2012-10-15	发明	樊友杰 李宾 吴娜

NO.	专利名称	申请号	审请日	类型	发明人
18	使用波带片将柱面波线光源聚焦为点光斑的方法	201210391151.5	2012-10-15	发明	毛成文 闫帅 闫芬
19	波荡器及波荡器的制造方法	201210413719.9	2012-10-25	发明	张正臣 许皆平 李炜
20	电子射线源产生装置及产生低剂量率电子射线的方法	201210425491.5	2012-10-30	发明	李景烨 李林繁 王敏
21	高温熔盐泵轴密封装置	201210437444.2	2012-11-6	发明	黎忠 傅远 谢雷东
22	电子射线源产生装置及产生低剂量率电子射线的方法	201210556558.9	2012-12-19	发明	何子锋 朱希恺 翟光延 黄建鸣 李林繁 李景烨 盛康龙 张宇田 李德明 张海荣
23	一种光电流数据获取系统	201210022016.3	2012-1-31	发明	胡纯 刘平
24	一种光束线设备的数据处理系统	201210041198.9	2012-2-22	发明	周永年
25	一种多通道电路不对称性的校准方法	201210044556.1	2012-2-24	发明	易星 冷用斌
26	一种用于高频加速结构的次谐波聚束器	201210049188.X	2012-2-28	发明	赵振堂 赵明华 张猛
27	一种光束线同步光位置在线诊断系统	201210051741.3	2012-3-1	发明	胡纯 张招红
28	氢扩散渗透特性测量装置	201210036886.6	2012-2-17	发明	吴胜伟 刘卫 曾友石 钱渊 朱海云 张东勋 王广华 姚剑
29	偕胺肟基螯合聚丙烯腈纤维及其制备方法和应用	201210048187.3	2012-2-28	发明	吴国忠 王谋华 张文礼 刘伟华 邢哲 叶泽文 何亚星
30	一种基于四叉树与邻域搜索相结合的分形图像压缩方法	201210065874.6	2012-3-13	发明	祁斌川 丁建国
31	低能段 X 射线的高次谐波抑制装置	201210074150.8	2012-3-20	发明	魏向军 傅远 李丽娜
32	用于掠入射 XAFS 方法的样品台	201210074161.6	2012-3-20	发明	魏向军 李丽娜 于海生
33	一种脉冲宽度调制同步方法	201210091724.2	2012-3-31	发明	许瑞年
34	一种控制系统环境的虚拟架构	201210096769.9	2012-4-1	发明	沈立人 万天敏
35	一种基于单色器快速扫描控制系统的数据采集方法	201210098360.0	2012-4-5	发明	顾颂琦 黄宇营 姜政
36	一种压弯机构运动控制系统	201210098300.9	2012-4-6	发明	张招红 胡纯 米清茹
37	一种基于 EPICS 的四刀狭缝控制系统及其控制方法	201210111385.X	2012-4-16	发明	刘平 张招红 胡纯
38	一种加速器控制系统的实时数据库集群架构及其建立方法	201210163219.4	2012-5-22	发明	陈广花 陈建锋 万天敏
39	多维调整平台	201210174581.1	2012-5-30	发明	姜政 李丽娜 黄宇营
40	一种基于腔式 BPM 的加速器束团长度测量方法	201210195628.2	2012-6-13	发明	袁任贤 俞路阳 周伟民
41	一种纳米金复合物及其制备和应用	201210241611.6	2012-7-12	发明	樊春海 裴昊 黄庆
42	一种基于荧光共振能量转移的超分辨成像方法	201210288305.8	2012-8-14	发明	樊春海 黄庆 程亚 陈建芳 邓素辉 梁乐
43	核用电缆无卤阻燃护套料、电缆护套，制备方法和应用	201210352803.4	2012-9-20	发明	张聪 李景烨 李林繁
44	一种水性的聚四氟乙烯材料及其制备方法和用途	201210356207.3	2012-9-20	发明	吴国忠 杨常桥 钟磊
45	一种高温超导跑道线圈阵列型波荡器	201210427935.9	2012-10-31	发明	张正臣 许皆平 李炜
46	熔盐样品制备装置、制得的熔盐样品及其制备、析晶方法	201210425507.2	2012-10-30	发明	耿俊霞 张国欣 李晴暖

NO.	专利名称	申请号	审请日	类型	发明人
47	一种基于 DNA 三维纳米结构探针的电化学 miRNA 检测方法	201210445958.2	2012-11-9	发明	樊春海 闻艳丽 林美华
48	一种二硼化镁超导波荡器	201210488830.4	2012-11-27	发明	张正臣 许皆平 李炜 崔剑 李明 江勇
49	波荡器	201210495631.6	2012-11-28	发明	张正臣 许皆平 李炜 崔剑 李明 江勇
50	一种杂合纳米结构构建方法	201210495672.5	2012-11-28	发明	汪颖 张益 胡钧
51	一种多价免疫刺激纳米制剂及其制备方法和应用	201210586959.9	2012-12-31	发明	黄庆 陈楠 魏敏 裴洁 李凡 孙艳红 李晓明 樊春海
52	一种海水提铀用螯合纤维吸附剂及其制备方法	201210076705.2	2012-3-21	发明	王谋华 吴国忠 邢哲
53	一种物理关系数据库系统的建设方法	201210099858.9	2012-4-6	发明	敖新宇 胡纯 米清茹
54	一种管式高温熔盐同步辐射原位研究装置	201220023954.0	2012-1-18	实用新型	何上明 李爱国 闫帅
55	准直激光器调整架	201220021293.8	2012-1-17	实用新型	陈杰 俞路阳 袁任贤
56	涡轮流量计的涡轮组件	201220037832.7	2012-2-6	实用新型	张慧民
57	一种调整平台倾斜角度的装置	201220037417.1	2012-2-6	实用新型	谷鸣 王锐萍 陈嵘
58	一种样品架	201220039006.6	2012-2-7	实用新型	张继超 李爱国 余笑寒
59	一种移门驱动装置,及其双移门和防护移门	201220042301.7	2012-2-9	实用新型	杨东 朱卫华 乌振亮 黄国正 苏东
60	一种低感叠层母排	201220049270.8	2012-2-15	实用新型	郭春龙 李瑞
61	一种五相步进电机驱动器	201220049291.X	2012-2-15	实用新型	黄跃峰
62	燃料电池催化剂测试装置	201220051163.9	2012-2-16	实用新型	王娟 何燕 刘嘉斌 秦海英 李爱国 余笑寒
63	一种步进脉冲信号分配装置	201220055917.8	2012-2-20	实用新型	谷鸣 袁启兵 王锐萍
64	一种磁铁线圈支撑结构	201220055919.7	2012-2-20	实用新型	谷鸣 欧阳联华 陈嵘
65	一种液氮自动填充装置	201220056839.3	2012-2-21	实用新型	刘科 黄胜 孙波 何建华
66	一种电子枪快脉冲传输装置	201220056838.9	2012-2-21	实用新型	林国强
67	一种遮挡杂散X光和直通X光的装置	201220058907.X	2012-2-22	实用新型	杨科 洪执华 闫帅
68	一种分布式集中控制系统	201220058911.6	2012-2-22	实用新型	缪海峰 沈立人 丁建国 蒋舸扬 陈键锋 万天敏
69	一种步进电机信号电缆	201220062375.7	2012-2-24	实用新型	郑丽芳 王星
70	一种钢铅夹心板	201220066560.3	2012-2-27	实用新型	杨东 刘小栋 朱卫华
71	一种用于功率变换器的配对模块组件	201220070253.2	2012-2-28	实用新型	郭春龙 沈天健 李瑞

NO.	专利名称	申请号	审请日	类型	发明人
72	氢扩散渗透特性测量装置	201220053326.7	2012-2-17	实用新型	吴胜伟 刘卫 曾友石 钱渊 朱海云 张东勋 王广华 姚剑
73	一种光强探测电离室	201220084235.X	2012-3-7	实用新型	边风刚 王劼 李秀宏 王玉柱 田丰 周平
74	一种 X 射线强度衰减器	201220091275.7	2012-3-12	实用新型	黄胜 汪启胜 张敏 何建华
75	一种光束线站设备的保护系统	201220095892.4	2012-3-14	实用新型	朱周侠 龚培荣 张永立 徐慧超 周剑英 蒋建国 施学兰
76	一种控制系统开发环境架构	201220093903.5	2012-3-13	实用新型	米清茹 郑丽芳
77	一种用于三相电加热器的加热管	201220106923.1	2012-3-20	实用新型	袁平均 李文静 张琴
78	一种三相电加热器	201220106888.3	2012-3-20	实用新型	袁平均 李文静 张琴 吴立
79	一种电子束次谐波聚散器	201220123901.6	2012-3-28	实用新型	赵振堂 赵明华 钟少鹏
80	一种快连锁控制器	201220146348.8	2012-3-31	实用新型	蒋舸扬 陈建锋 刘亚娟
81	一种棚屋内同步辐射人身安全防护系统	201220138764.3	2012-4-1	实用新型	龚培荣 朱周侠 徐慧超
82	一种控制系统网络架构	201220143366.0	2012-4-6	实用新型	蔡浩军 沈立人 陈建锋
83	一种十字丝扫描探测器	201220153457.2	2012-4-12	实用新型	周剑英 黎忠 龚培荣
84	辐射防护棚屋的离线辐射泄漏测试装置	201220165867.9	2012-4-18	实用新型	朱卫华 苏东 杨东
85	一种低温液氮远距离输送管道	201220165870.0	2012-4-18	实用新型	苏东 朱卫华 郑永培
86	一种电流电压转化器	201220164110.8	2012-4-17	实用新型	张永立 蒋建国 龚培荣
87	一种荧光靶探测器	201220198995.3	2012-5-3	实用新型	徐慧超 周剑英 龚培荣 刘昕 张永立 蒋建国 朱周侠
88	组合式辐射防护棚屋	201220235837.0	2012-5-22	实用新型	朱卫华 杨东 黄正国
89	箱式电源的状态监控系统	201220235808.4	2012-5-22	实用新型	吴盈锋 胡纯
90	液体样品池	201220238306.7	2012-5-23	实用新型	赵红卫 张建兵 武余亭
91	紧凑型双向兼用条带激励电极	201220260246.9	2012-6-4	实用新型	袁任贤 俞路阳 周伟民
92	液体样品池	201220417598.0	2012-8-21	实用新型	赵红卫 杨航 张建兵
93	一种抑制信号振铃的滤波器	201220524955.3	2012-10-12	实用新型	周伟民 冷用斌 叶恺容
94	高温熔盐泵轴密封装置	201220581425.2	2012-11-6	实用新型	黎忠 傅远 谢雷东

NO.	专利名称	申请号	审请日	类型	发明人
95	一种高温介质泵热屏蔽装置	201220656612.2	2012-12-3	实用新型	黎忠 傅远 黄建平 张健宇 林良程 毛文玉 王纳秀 王晓 李波 陆世瑞
96	熔盐电化学实验装置	201220005014.9	2012-1-6	实用新型	左勇 黄鹤 李晓云 王敏
97	防护罩	201220023955.5	2012-1-18	实用新型	金林 金江
98	冷却水管的老化模拟装置	201220021294.2	2012-1-17	实用新型	封自强
99	自动配气系统	201220021527.9	2012-1-17	实用新型	高倩 黄宇营 姜政
100	数据采集系统	201220027693.X	2012-1-20	实用新型	颂琦 黄宇营 姜政 魏向军 邹杨 李丽娜 高倩 张硕 李炯 王建强
101	一种两相步进电机驱动器	201220049290.5	2012-2-15	实用新型	贾文红
102	用于荧光 XAFS 测试的数据采集系统	201220076905.3	2012-3-2	实用新型	高倩 姜政 魏向军 李丽娜 李炯 顾颂琦 张硕 黄宇营
103	用于液氮传输支线的预冷装置	201220093587.1	2012-3-13	实用新型	苏东 朱卫华 杨建萍
104	一种用于液氮输送系统的控制装置	201220131192.6	2012-3-31	实用新型	苏东 熊芳 朱卫华

2011 专利授权

NO.	专利名称	申请号	授权日	类型	发明人
1	一种产氢储氢一体化方法和装置	ZL200510111758.3	2011-6-15	发明	张立娟 胡钧 方海平 樊春海 张益 沈广霞
2	采用裸云母作为蛋白质晶体生长基底的方法	ZL200610025545.3	2011-6-1	发明	唐琳 孙丽华 徐春艳 胡钧 何建华
3	血管活性肠肽类似物及其放射性标记物，以及它们的制备方法	ZL200610027652.X	2011-4-20	发明	尹端沚 程登峰 汪勇先 张岚
4	微流控阵列蛋白质芯片及其使用方法	ZL200610117234.X	2011-7-27	发明	宋世平 樊春海 颜娟
5	一种低拷贝生化反应的方法	ZL200710036291.X	2011-6-15	发明	周化岚 张益 胡钧
6	一种采用茎环结构检测探针的电化学 DNA 检测方法及其试剂盒	ZL200710046090.8	2011-8-3	发明	樊春海 刘刚
7	β-榄香烯氨基酸衍生物及其合成方法和用途	ZL200710181826.2	2011-6-1	发明	沈玉梅 任云峰 成康民 孙艳红 刘贵锋 王谋华
8	一种检测 DNA 的 i-motif 构象的光学方法	ZL200710048136.X	2011-6-15	发明	刘兴奋 王丽华 樊春海
9	富勒醇在美容护肤品中的应用	ZL200710172972.9	2011-7-27	发明	刘瑞丽 蔡小青 李文新
10	一种苯磺酰胺类化合物及其中间体，及其制备方法和应用	ZL200810037644.2	2011-6-1	发明	张岚 武明星 郭飞虎 施玲丽 汪勇先 尹端沚
11	一种苯磺酰胺类羟基衍生物及其中间体及其制备方法和应用	ZL200810037632.X	2011-4-20	发明	张岚 武明星 郭飞虎 施玲丽 汪勇先 尹端沚
12	利用 THz-TDs 鉴别不同旋光性的麻黄碱	ZL200810040557.2	2011-6-15	发明	马士华 刘桂锋 吉特 宋西玉 张鹏 王文锋
13	一种非水溶性单体的水相接枝聚合方法	ZL200810040814.2	2011-7-27	发明	李景烨 邓波 谢雷东 虞鸣 李林繁 吉玉玲 杨璇璇
14	一种聚乙烯亚胺修饰的碳纳米管及其复合物、制备方法及用途	ZL200810201238.5	2011-6-15	发明	于伯章 马继飞 黄庆
15	一种电化学发光系统	ZL200810203100.9	2011-1-26	发明	宋世平 樊春海
16	甲基丙烯酸酯嵌段聚合物及其复合物及它们的制备方法和用途	ZL200910053908.8	2011-2-16	发明	于伯章
17	DNA 分子的微/纳米图形的构建方法	ZL200710041865.2	2011-1-26	发明	王化斌 胡钧 张益 孙洁林 王鹏
18	电化学生物传感器	ZL201020190473.X	2011-1-26	实用新型	孟伟丽 宋世平 姜智能 顾睿风 朱欣华 苏岩 樊春海
19	适用于太赫兹时域光谱测量的液体样品架	ZL201120041905.5	2011-11-16	实用新型	赵红卫 吴胜伟 朱海云 张增艳 李晴暖 刘晓鸿 朱智勇

2012 专利授权

NO.	专利名称	申请号	授权日	类型	发明人
1	一种具有周期性纳米结构的高分子膜的制备方法及所用模板	ZL200910049959.3	2012-2-22	发明	李景烨 黄庆 邓波 于 洋 吕敏
2	一种标记胆汁酸衍生物及其参照化合物、制备方法和应用	ZL200910051767.6	2012-10-3	发明	沈玉梅 黄立梁 朱华 张春春
3	甲基丙烯酸酯聚合物及其复合物及它们的制备方法和用途	ZL200910053907.3	2012-8-15	发明	于伯章
4	一种***Tc 配合物、其制备方法、中间体及其应用	ZL200910195514.6	2012-10-3	发明	沈玉梅 张元庆 孙艳红 许晓平
5	一种用γ射线辐照使聚丙烯腈改性的方法	ZL200910200308.X	2012-1-4	发明	王谋华 吴国忠 刘伟华
6	一种用电子束辐照使聚丙烯腈纤维改性的方法	ZL201010108710.8	2012-5-30	发明	王谋华 吴国忠 刘伟华
7	一种 DNA 三维纳米结构探针的电化学检测方法	ZL201010119941.9	2012-4-25	发明	樊春海 裴昊
8	一种磁固相分离剂及其制备方法	ZL201010118153.8	2012-8-15	发明	张国欣 王妮 张岚 刘静培 李潇 沈华
9	炔基修饰磁纳米粒子模块、氨基酸类化合物修饰的磁纳米粒子，及制备方法和用途	ZL201010115570.7	2012-10-3	发明	张岚 刘静培 张国欣 李潇
10	一种提高碳纳米管网络导电性的方法	ZL201010172009.2	2012-1-4	发明	周广颖 闫隆
11	一种快速 X 射线荧光 CT 方法	ZL201010171983.7	2012-7-4	发明	邓彪 杨群 谢红兰 杜国浩 肖体乔
12	一种纳米硅线/纳米银复合材料的制备方法	ZL201010187582.0	2012-8-15	发明	黄庆 樊春海 吕敏 苏邵
13	自动化滤膜通量评价装置和方法	ZL201010263877.1	2012-10-3	发明	李景烨 邓波 魏永波 周保昌 虞鸣
14	一种单层石墨烯的制备方法	ZL201010515366.4	2012-8-15	发明	张玉杰 张欢 胡文兵 樊春海 黄庆
15	一种抗菌织物及其制备方法	ZL201110004877.4	2012-10-10	发明	李景烨 黄庆 樊春海 张玉杰 赵金明 胡文兵 蒋海青 于洋 虞鸣 李林繁 邓波
16	一种 PVDF 接枝 NVP 的方法及由其制得的接枝共聚物	ZL201110027380.4	2012-11-28	发明	侯铮迟 陈鹏
17	一种基于智能卡的人脸识别系统及其方法	ZL00910196047.9	2012--5-2	发明	敖新宇 李勇平 鲍强
18	冷却式薄膜X射线衍射仪样品台及X射线衍射仪	ZL201120471638.5	2012-7-11	实用新型	李小龙 何庆 顾月良
19	加热式薄膜X射线衍射仪样品台及X射线衍射仪	ZL201120472297.3	2012-7-11	实用新型	顾月良 李小龙 何庆
20	电池测试装置	ZL201120537974.5	2012-8-15	实用新型	文闻 高梅 顾月良 何庆 黎忠 周兴泰
21	纳米材料测试装置	ZL201120538631.0	2012-8-15	实用新型	文闻 张兴民 高梅 杨铁营 何庆 周兴泰
22	一种管式高温熔盐同步辐射原位研究装置	ZL201220023954.0	2012-10-3	实用新型	何上明 李爱国 闫帅
23	准直激光器调整架	ZL201220021293.8	2012-10-3	实用新型	陈杰 俞路阳 袁任贤

NO.	专利名称	申请号	授权日	类型	发明人
24	涡轮流量计的涡轮组件	ZL201220037832.7	2012-10-10	实用新型	张慧民
25	一种调整平台倾斜角度的装置	ZL201220037417.1	2012-10-10	实用新型	谷鸣 王锐萍 陈嵘
26	一种样品架	ZL201220039006.6	2012-10-3	实用新型	张继超 李爱国 余笑寒
27	一种移门驱动装置,及其双移门和防护移门	ZL201220042301.7	2012-10-10	实用新型	杨东 朱卫华 乌振亮 黄国正 苏东
28	一种低感叠层母排	ZL201220049270.8	2012-10-3	实用新型	郭春龙 李瑞
29	一种五相步进电机驱动器	ZL201220049291.X	2012-10-10	实用新型	黄跃峰
30	燃料电池催化剂测试装置	ZL201220051163.9	2012-10-10	实用新型	王娟 何燕 刘嘉斌 秦海英 李爱国 余笑寒
31	一种步进脉冲信号分配装置	ZL201220055917.8	2012-10-10	实用新型	谷鸣 袁启兵 王锐萍
32	一种磁铁线圈支撑结构	ZL201220055919.7	2012-10-10	实用新型	谷鸣 欧阳联华 陈嵘
33	一种液氮自动填充装置	ZL201220056839.3	2012-10-10	实用新型	刘科 黄胜 孙波 何建华
34	一种电子枪快脉冲传输装置	ZL201220056838.9	2012-10-10	实用新型	林国强
35	一种遮挡杂散 X 光和直通 X 光的装置	ZL201220058907.X	2012-10-3	实用新型	杨科 洪执华 闫帅
36	一种分布式集中控制系统	ZL201220058911.6	2012-10-10	实用新型	缪海峰 沈立人 丁建国 蒋舸扬 陈键锋 万天敏
37	一种步进电机信号电缆	ZL201220062375.7	2012-10-10	实用新型	郑丽芳 王星
38	一种钢铅夹心板	ZL201220066560.3	2012-10-10	实用新型	杨东 刘小栋 朱卫华
39	一种用于功率变换器的配对模块组件	ZL201220070253.2	2012-10-10	实用新型	郭春龙 沈天健 李瑞
40	氢扩散渗透特性测量装置	ZL201220053326.7	2012-10-3	实用新型	吴胜伟 刘卫 曾友石 钱渊 朱海云 张东勋 王广华 姚剑
41	一种光强探测电离室	ZL201220084235.X	2012-10-10	实用新型	边风刚 王劼 李秀宏 王玉柱 田丰 周平
42	一种 X 射线强度衰减器	ZL201220091275.7	2012-10-10	实用新型	黄胜 汪启胜 张敏 何建华
43	一种光束线站设备的保护系统	ZL201220095892.4	2012-10-10	实用新型	朱周侠 龚培荣 张永立 徐慧超 周剑英 蒋建国 施学兰
44	一种控制系统开发环境架构	ZL201220093903.5	2012-10-10	实用新型	米清茹 郑丽芳
45	一种用于三相电加热器的加热管	ZL201220106923.1	2012-11-28	实用新型	袁平均 李文静 张琴
46	一种三相电加热器	ZL201220106888.3	2012-10-10	实用新型	袁平均 李文静 张琴 吴立

NO.	专利名称	申请号	授权日	类型	发明人
47	一种电子束次谐波聚散器	ZL201220123901.6	2012-11-28	实用新型	赵振堂 赵明华 钟少鹏
48	一种快连锁控制器	ZL201220146348.8	2012-11-28	实用新型	蒋舸扬 陈建锋 刘亚娟
49	一种棚屋内同步辐射人身安全防护系统	ZL201220138764.3	2012-11-28	实用新型	龚培荣 朱周侠 徐慧超
50	一种十字丝扫描探测器	ZL201220153457.2	2012-11-28	实用新型	周剑英 黎忠 龚培荣
51	辐射防护棚屋的离线辐射泄漏测试装置	ZL201220165867.9	2012-11-28	实用新型	朱卫华 苏东 杨东
52	一种电流电压转化器	ZL201220164110.8	2012-11-28	实用新型	张永立 蒋建国 龚培荣
53	外加电场测试台架及薄膜测试平台	ZL201120559975.X	2012-10-3	实用新型	李晓龙 顾月良 何庆
54	远程温度监测系统	ZL201120561521.6	2012-10-3	实用新型	马新朋 刘波
55	防护罩	ZL201220023955.5	2012-10-10	实用新型	金林 金江
56	冷却水管的老化模拟装置	ZL201220021294.2	2012-10-3	实用新型	封自强
57	自动配气系统	ZL201220021527.9	2012-10-3	实用新型	高倩 黄宇营 姜政
58	数据采集系统	ZL201220027693.X	2012-10-10	实用新型	顾颂琦 黄宇营 姜政 魏向军 邹杨 李丽娜 高倩 张硕 李炯 王建强
59	一种两相步进电机驱动器	ZL201220049290.5	2012-10-3	实用新型	贾文红
60	用于荧光XAFS测试的数据采集系统	ZL201220076905.3	2012-10-10	实用新型	高倩 姜政 魏向军 李丽娜 李炯 顾颂琦 张硕 黄宇营
61	用于液氮传输支线的预冷装置	ZL201220093587.1	2012-10-10	实用新型	苏东 朱卫华 杨建萍
62	一种用于液氮输送系统的控制装置	ZL201220131192.6	2012-11-28	实用新型	苏东 熊芳 朱卫华
63	熔盐电化学实验装置	ZL201220005014.9	2012-10-3	实用新型	左勇 黄鹤 李晓云 王敏

附录 5

2011–2012 上海应用物理所博士、硕士学位授予一览表

2011

No.	学位	学生	专业	导师	论文题目	研究方向
1	博士	张东华	粒子物理与原子核物理	胡钧	乙醇气体诱导云母表面液滴去润湿作用机制研究	物理生物学
2	博士	WAHEED AKRAM	粒子物理与原子核物理	李晓林	上海大气超细/细/粗颗粒物特征和源查证	核分析技术在环境科学中的应用
3	博士	吴可非	粒子物理与原子核物理	方海平	水填充窄的碳纳米管的理论和模拟研究	物理与生物的交叉
4	博士	张福春	粒子物理与原子核物理	胡钧	纳米操纵辅助下的多肽自组装	多肽自组装
5	博士	李静	无机化学	李文新	纳米金刚石作为药物载体的研究	纳米材料生物效应
6	博士	侯洪涛	侯洪涛	刘建飞	500MHz 单 cell 超导高频腔测试技术研究	超导高频腔技术研究
7	博士	范功涛	粒子物理与原子核物理	马余刚	在近库仑位垒能区利用轻核与重核的弹性散射精确测量 ^{3}He 和 ^{4}He 的电极化率	粒子物理与原子核物理
8	博士	李勇	粒子物理与原子核物理	朱志远	荷能粒子在碳纳米管中传输机制的模拟研究	粒子束与碳纳米结构相互作用
9	博士	万莹	无机化学	樊春海	电化学生物传感器在分子诊断中的应用研究	电化学生物传感器
10	博士	叶鸣	无机化学	胡钧	若干生物分子与纳米水层间相互作用研究	物理生物学
11	博士	张小勇	无机化学	朱智勇	三种碳纳米材料的生物效应研究	纳米生物效应
12	博士	张馨允	无机化学	姚思德	铂系纳米合金催化剂辐射法制备研究	多元纳米复合材料辐射法制备研究
13	博士	朱长锋	无机化学	樊春海	基于功能 DNA 的纳米机器与生物传感器	生物传感器与分子机器
14	博士	王会军	核技术及应用	许皆平	超导多极扭摆器设计研究	超导插入件技术
15	博士	贺周同	粒子物理与原子核物理	周兴泰	碳离子注入石墨的磁性研究	凝聚态物理
16	博士	李薇	粒子物理与原子核物理	马余刚	相对论重离子碰撞(RHIC)实验中非光电子与带电强子的方位角关联及双强子方位角关联模拟的研究	高能核物理实验与唯象理论
17	博士	孙小艳	粒子物理与原子核物理	马余刚	丰中子核的中子皮厚度探针与 22Mg 双质子发射现象研究	中低能重离子反应
18	博士	薛超凡	核技术及应用	邰仁忠	上海光源软 X 射线谱学显微光束线站的能量分辨率研究	同步辐射光束线站
19	博士	阳丽	粒子物理与原子核物理	方海平	纳米尺度下颗粒之间相互作用的理论研究	计算物理
20	博士	杨利峰	粒子物理与原子核物理	徐望	强激光与原子相互作用的非微扰理论研究	强激光与物质相互作用研究
21	博士	周光照	核技术及应用	肖体乔	相干 X 射线衍射成像中影响相位重建精度的若干因素研究	X 射线成像光学
22	博士	窦强	无机化学	吴国忠	离子液体在受限空间内的结构及动力学研究	表面物理化学、分子模拟
23	博士	胡文兵	无机化学	樊春海	石墨烯氧化物的生物学效应及应用	纳米生物和纳米医药

2011

No.	学位	学生	专业	导师	论文题目	研究方向
24	博士	黄卫	无机化学	吴国忠	离子液体辐射稳定性研究及其中金纳米粒子的制备	离子液体、辐射化学
25	博士	温燕勤	无机化学	樊春海	基于石墨烯纳米探针和功能化 DNA 分子机器的生物传感器	生物传感器和分子机器
26	博士	杨璇璇	无机化学	李景烨	辐射接枝极性单体制备 PVDF 功能性滤膜的研究	高分子材料辐射改性
27	博士	张鹏	无机化学	王文锋	诺氟沙星及其衍生物的光化学性质与光敏损伤研究	快速反应动力学
28	博士	张元庆	无机化学	黄庆	基于树枝形分子的纳米显像试剂和载药研究	分子显像和放射性药物
29	博士	朱华	无机化学	黄庆	Cyclofenil 分子探针的制备及其在 ER 受体显像中的应用研究	分子显像及放射性药物
30	博士	蒋志强	核技术及应用	赵振堂	上海光源真空波荡器机械驱动系统分析与优化	机械设计分析与优化
31	博士	梁平	核技术及应用	李勇平	嵌入式离子迁移谱的研究与实现	信号处理，核电子学与探测技术
32	博士	罗文	核技术及应用	徐望	激光康普顿 X/γ 光源的实验研究及蒙特卡罗模拟	激光康普顿散射，核电子学与探测技术
33	博士	任玉琦	核技术及应用	肖体乔	X 射线定量相衬成像中高精度相位恢复研究	X 射线成像光学
34	博士	唐思巍	核技术及应用	刘德康	束测光斑位置反馈系统研究	加速器技术与应用
35	博士	陶世兴	核技术及应用	何建华	同步辐射 X 射线光束线及单色器性能测试研究	同步辐射光束线站
36	博士	田丰	核技术及应用	徐洪杰	聚烯烃类热塑性塑料材料辐照效应的 X 射线小角散射研究	同步辐射技术应用
37	博士	闫芬	核技术及应用	余笑寒	基于 EPICS 的同步辐射微探针实验站控制和数据采集系统	同步辐射光束线站运动控制和数据采集
38	博士	张伟	核技术及应用	周巧根	新型螺旋型波荡器的物理研究	插入件物理及技术
39	硕士	孙培建	粒子物理与原子核物理	朱志远	一维系统角分辨光电子谱的理论研究	光电子谱学的理论研究
40	硕士	耿马可	无机化学	黄庆	纳米金-碳纳米材料复合物的制备及应用研究	纳米材料的制备及生物学效应
41	硕士	范雪波	粒子物理与原子核物理	刘卫	灰霾天大气颗粒物组分的粒径特征	大气科学
42	硕士	谭兴兴	光学工程	郜仁忠	软 X 射线 SXDM 成像方法	相干衍射成像
43	硕士	王倩	粒子物理与原子核物理	徐洪杰	基于同步辐射 XAFS 方法的金属离子溶液的研究	同步辐射技术应用
44	硕士	于海生	核技术及应用	黄宇营	上海光源 BL14W1 线站掠入射 XAFS 方法的实现及应用研究	X 射线技术及应用
45	硕士	郑俊义	核技术及应用	余笑寒	利用同步辐射 X 射线分析技术研究镍基合金在熔融氟化物中的腐蚀	同步辐射分析方法及应用
46	硕士	蔡仁	无机化学	李景烨	辐射接枝法制备超疏水棉织物及其性能研究	功能纤维研究
47	硕士	陈鹏	无机化学	侯铮迟	PVDF 共辐射接枝亲水性单体 NVP 的研究	PVDF 共辐射接枝改性
48	硕士	崔巍	无机化学	黄庆	两种载药大分子的合成与初步生物学评价	分子显像及放射性药物

2011

No.	学位	学生	专业	导师	论文题目	研究方向
49	硕士	耿彦红	无机化学	刘卫	大气颗粒物中离子和多环芳烃的来源分析	大气颗粒物中污染物来源解析
50	硕士	李良	无机化学	陆晓峰	分子量分布对聚醚砜超滤膜性能的影响	超滤膜的研制与应用
51	硕士	李潇	无机化学	张岚	特征形貌磁纳米粒生物学行为及应用研究	药物载体的制备及生物学评价
52	硕士	刘晓鸿	无机化学	赵红卫	固态反应的太赫兹时域光谱研究	太赫兹技术应用研究
53	硕士	刘亚辉	无机化学	何建华	电磁场对溶液状态下的胰岛素的结构的影响研究	生物大分子 晶体学
54	硕士	罗仕海	无机化学	黎忠	锂离子电池正极材料铁酸铋的制备及构效关系研究	锂离子电池正极材料
55	硕士	戚英娜	无机化学	吴国忠	聚碳硅烷纤维经辐射氧化-热交联处理制备高性能碳化硅纤维	高分子材料的辐射改性
56	硕士	杨光	无机化学	沈玉梅	基于 cyclofenil 的 ER-β 分子探针的合成与研究	合成化学，放射化学
57	硕士	苑洪铭	无机化学	李景烨	辐射接枝改性锂电池隔膜的制备与性能研究	锂离子电池隔膜
58	硕士	张惠芳	无机化学	周兴泰	石墨烯纳米带的制备及其场发射性能研究	石墨烯纳米带的制备及其场发射性质的研究
59	硕士	郑小雪	无机化学	樊春海	基于类葡萄糖氧化酶催化活性金纳米颗粒的 DNA 传感器研究	生物传感器和分子机器
60	硕士	周冉冉	无机化学	郜仁忠	超分辨重建方法在 STXM 图像处理中的应用	软 X 射线谱学显微数据处理方法的研究
61	硕士	刘石磊	光学工程	王纳秀	同步辐射双晶单色器平行度测量方法研究	精密光学检测
62	硕士	马春桃	光学工程	王劼	斜入射法检测平面反射镜面形的研究	精密光学检测技术
63	硕士	沈飞	光学工程	肖体乔	基于 GPU 并行计算实现快速显微 CT 重构	成像光学
64	硕士	孙福权	光学工程	薛松	压弯镜系统重力补偿方法的研究	精密机械设计和 CAE 分析
65	硕士	殷波	电磁场与微波技术	刘建飞	500 MHz 多路功率合成器及固态功率放大器研制	低温超导高频腔技术
66	硕士	袁刚	电磁场与微波技术	周兴泰	氧化铟纳米线的低温合成与性质研究	纳米材料
67	硕士	程坤	信号与信息处理	赵明华	高精度高平均功率电子枪设计研究	高精度高平均功率电子枪的设计仿真
68	硕士	丁喻	信号与信息处理	漆玉金	基于 CPU-GPU 异构集群的显微 CT 图像重建及三维可视化技术研究	医学图像处理
69	硕士	顾俊俊	信号与信息处理	徐洪杰	BL14W1 XAFS 光束线实验站极低浓度数据采集系统	信号与信息处理
70	硕士	厉娜	信号与信息处理	赵明华	直线加速器老炼自动控制系统研制	直线加速器自动控制
71	硕士	孙发力	信号与信息处理	夏晓彬	放射性 β 气溶胶探测器的数值模拟与探测系统设计	基于射线探测技术的信号与信息处理
72	硕士	汤宁	信号与信息处理	李勇平	生物特征识别技术在光束线站安全管理上的应用	嵌入式系统和生物特征识别
73	硕士	熊亮	信号与信息处理	王晓	数字化平均流强测量算法研究	加速器控制与束流信号处理

2011

No.	学位	学生	专业	导师	论文题目	研究方向
74	硕士	徐玮	信号与信息处理	万荣正	T 形管水流分析	T 形碳纳米管水流分析
75	硕士	杨桂森	信号与信息处理	冷用斌	加速器逐束团数据采集与处理技术研究	束流测量与控制
76	硕士	张莹	信号与信息处理	李勇平	低分辨率人脸识别系统的研究	生物特征识别
77	硕士	段雪非	核技术及应用	李浩虎	上海质子治疗装置高能输运系统的物理设计	加速器技术及应用
78	硕士	江家友	核技术及应用	陈志豪	任意形状脉冲信号发生器的研制	加速器技术
79	硕士	李玖栋	信号与信息处理	邓辉宇	上海光源 PDM 系统架构的实施及应用	信息检索与人工智能
80	硕士	牛晶	信号与信息处理	唐琳	SSRF 生物大分子晶体学光束线站多波长反常散射信号采集自动化系统	光束线控制方向
81	硕士	宋健	信号与信息处理	漆玉金	MicroSPECT 数据获取系统的设计与开发	多通道数据采集

2012

No.	学位	学生	专业	导师	论文题目	研究方向
1	博士	周波	粒子物理与原子核物理	方海平	云母表面上乙醇、多肽和水的结构与动力学的理论研究	界面分子的结构与特性
2	博士	李兰婷	无机化学	胡钧	聚合酶链式反应数学模型的构建及应用	计算生物学
3	博士	谢牧云	无机化学	胡钧	不同环境因子对纳米水层中多肽分子自组装行为的影响	纳米生物学
4	博士	于海波	核技术及应用	刘建飞	500 MHz 超导高频腔高次模吸收器前期研究	低温超导高频技术
5	博士	常睿	核技术及应用	邰仁忠	软 X 射线谱学实验方法及其在电池材料研究上的应用	同步辐射及其应用
6	博士	陈灿	粒子物理与原子核物理	肖体乔	劳厄弯晶光学特性的光线追迹研究	X 射线光学
7	博士	樊广伟	粒子物理与原子核物理	徐望	精确测量 ^{8}Li 的反应截面并利用修正的 Glauber 模型提取 8Li 的核密度分布	粒子物理与原子核物理
8	博士	李林	粒子物理与原子核物理	胡钧	溶液中的非接触调频模式原子力显微镜的搭建及其高分辨成像研究	仪器设计、纳米科学
9	博士	牛冬校	粒子物理与原子核物理	胡钧	于 c-AFM 技术的 DNA 分子与其它纳米材料电导性研究	生物物理及材料科学多学科交叉
10	博士	任杰	粒子物理与原子核物理	李德明	低能电子加速器的设计与建造	电子帘加速器的设计
11	博士	沈轶	粒子物理与原子核物理	胡钧	平行大通量单分子磁力谱方法构建与生物学应用	单分子单细胞纳米生物学与相关技术
12	博士	张传福	粒子物理与原子核物理	李燕	大气颗粒物在城市街道峡谷中的输运行为研究	基于核技术的分子环境科学研究
13	博士	张国强	粒子物理与原子核物理	马余刚	中能核反应的核物质状态方程以及核子类马赫发射现象研究	粒子物理与原子核物理
14	博士	周培	粒子物理与原子核物理	马余刚	Al-23 质子发射机制的实验探索及多步级联衰变对同位旋标度律影响的理论研究	中能重离子碰撞
15	博士	卞晓锴	无机化学	陆晓峰	PVDF-g-PAA 超滤膜的制备及功能化研究	膜分离技术
16	博士	段娜	无机化学	胡钧	纳米缲纵中机械力诱导的 DNA 损伤和突变研究	机械力诱导 DNA 突变
17	博士	李健	无机化学	何建华	Hsp90 的 ATP 水解机制及基于片段的 Hsp90 抑制剂研究与膜蛋白 PR 的结晶	膜蛋白及复合物的晶体生长
18	博士	施玲丽	无机化学	汪勇先	基于 Click 反应的 ^{18}F 标记多肽方法研究	放射性药物
19	博士	陈杰	核技术及应用	叶恺容	干涉仪测量电子储存环束流截面的研究	束流诊断技术
20	博士	周娟	核技术及应用	李勇平	基于三维点云及多模态人脸融合识别研究	生物特征识别
21	博士	张宁	核技术及应用	冷用斌	基于宽带虚拟仪器的嵌入式 EPICS IOC 在束流诊断中的应用研究	加速器束流震荡
22	博士	易星	核技术及应用	冷用斌	加速器束流信号调理及高速采集技术研究	高速数据采集及信号处理
23	博士	杨群	核技术及应用	徐洪杰	快速低剂量 X 射线荧光 CT 及其生物医学应用研究	X 射线荧光成像
24	博士	王玉丹	核技术及应用	肖体乔	同步辐射 X 射线显微 CT 用于材料定量分析的方法学研究	同步辐射 X 射线成像及 CT
25	博士	王靖琰	核技术及应用	李勇平	机器学习方法学创新研究及其在 SSRF 生物医学数据理解中的应用	机器学习，生物信息学，医学成像

2012

No.	学位	学生	专业	导师	论文题目	研究方向
26	博士	刘慧强	核技术及应用	肖体乔	硬 X 射线相衬显微 CT 及其混合样品成分的定量研究	X 射线成像及显微 CT
27	博士	李旭东	核技术及应用	赵明华	电子枪中光阴极制备，清洗及性能研究	光阴极材料制备、测试
28	博士	赖龙伟	技术及应用	用斌	FPGA 在数字 BPM 信号处理器中的应用	基于 FPGA 信号处理
29	博士	康成	核技术及应用	李德明	一种新型绝缘磁芯平面变压器的研究	大功率高压直流电源的研究
30	博士	方文程	核技术及应用	赵振堂	用于紧凑型自由电子激光 C 波段高梯度加速结构研究	加速器物理及微波技术
31	博士	张伯武	无机化学	李景烨	辐射化学法制备纳米碳及其复合材料的研究	高分子辐射化学
32	博士	于洋	无机化学	李景烨	辐射接枝法制备功能型纺织品的研究	高分子材料改性
33	博士	许晓平	无机化学	黄庆	基于树状大分子 SPECT 造影剂和载药研究	放射性药物
34	博士	闻艳丽	无机化学	樊春海	基于 DNA 纳米结构的电化学生物传感器研究	电化学生物传感器
35	博士	王鹏	无机化学	樊春海	纳米结构 TiO_2 和 α-Fe_2O_3 薄膜电极的制备及其光电化学水分解应用	纳米材料的光电转换
36	博士	王成	无机化学	黄庆	点击化学在放射性药物合成中的应用研究	放射性药物
37	博士	裴昊	无机化学	樊春海	基于 DNA 的功能化纳米材料的设计及其在生物诊断中的应用	DNA 纳米技术
38	博士	吕敏	无机化学	黄庆	硅纳米线@纳米银复合材料和石墨烯氧化物的生物效应	纳米材料的生物学效应
39	博士	刘伟华	无机化学	吴国忠	聚丙烯腈纤维的辐射交联及对预氧化的影响	高分子材料辐射改性
40	博士	李剑波	无机化学	漆玉金	靶向 CA IX 特异性分子影像探针的研究	放射性药物
41	博士	何世江	无机化学	樊春海	基于石墨烯的生物传感器的构建及应用	生物传感器
42	博士	薛亮	粒子物理与原子核物理	马余刚	反物质氦 4 原子核的实验观测及其产生机制研究	高能重离子反应
43	博士	钱江海	粒子物理与原子核物理	马余刚	复杂网络中标度律和爆炸性渗流的研究	复杂网络
44	硕士	李绍歆	粒子物理与原子核物理	方德清	BUU 模型研究中能重离子核反应的粘滞系数与熵密度比	中能重离子核反应
45	硕士	白凌志	粒子物理与原子核物理	怀平	非电中性半导体量子线的光谱学理论研究	半导体光谱学
46	硕士	祝江威	核技术及应用	邰仁忠	双能相干衍射成像元素分析方法研究	相干 X 射线衍射显微成像方向
47	硕士	张国强	信号与信息处理	肖体乔	CT 成像中环形伪影的去除算法研究	数字图像处理、CT 图像环形伪影校正
48	硕士	王存立	信号与信息处理	张文志	质子治疗加速器高频低电平反馈控制算法设计	高频低电平控制技术
49	硕士	苏荣锋	信号与信息处理	许瑞年	基于 FPGA 生成 PWM 波的研究	数字化电源的 PWM 控制
50	硕士	邵伟涛	核技术及应用	陈建锋	熔盐堆 HTS 实验回路加热器系统辨识及智能控制	熔盐堆 HTS 实验回路控制系统建模与控制仿真
51	硕士	刘慧芳	信号与信息处理	李瑞	数字化电流传感器优化研究	信号与信息处理

2012

No.	学位	学生	专业	导师	论文题目	研究方向
52	硕士	刘亨	信号与信息处理	姜政	SSRF-XAFS 实验站快速扫描(QXAFS)系统的研究	束线检测与控制
53	硕士	黄亚	核技术及应用	邰仁忠	CT 重建滤波函数的改进及重建软件的实现	数字图像处理
54	硕士	胡鹏飞	信号与信息处理	李德明	开关型扫描磁铁电源的研制	开关电源
55	硕士	杜鹏	信号与信息处理	黎忠	高精度光学式同步辐射 X 射线光斑测量系统	基于射线探测技术的信号与信息处理
56	硕士	戴彬彬	核技术及应用	徐洪杰	基于 XAFS 方法的 Cu^{2+}溶液配位研究及金属基离子液体发光研究	同步辐射 XAFS 方法对物质结构的研究
57	硕士	周志中	信号与信息处理	胡守明	800 keV/30 mA 工频倍加型电子加速器控制系统研制	应用加速器控制
58	硕士	张晓慧	信号与信息处理	漆玉金	基于 SiPM 阵列的新型伽玛相机读出电路研究	SPECT/CT 成像系统研究
59	硕士	晏宇	信号与信息处理	陈永忠	基于ARM和FPGA的束流截面测量平台研究	嵌入式应用
60	硕士	熊云	信号与信息处理	冷用斌	上海光源直流流强监测系统的优化	数据采集以及数字信号处理
61	硕士	王丽玮	信号与信息处理	谷鸣	基于 FPGA 的脉冲调制器幅度稳定性监控研究	加速器物理技术
62	硕士	史丹	信号与信息处理	欧阳联华	上海医用质子治疗加速器 RFKO 横向激励慢引出研究	上海质子治疗装置慢引出
63	硕士	祁斌川	信号与信息处理	丁建国	SDUV-FEL 实验装置真空联锁保护系统	加速器控制
64	硕士	刘晓庆	信号与信息处理	刘波	自由电子激光同步系统中鉴相系统研究	自由电子激光飞秒同步系统
65	硕士	黄辉	信号与信息处理	李勇平	EPICS 下基于 ARM 处理器的电机控制系统	运动控制系统
66	硕士	熊文纲	核技术及应用	王敏	热堆中钍铀燃料循环燃耗分析	核燃料循环
67	硕士	韦业龙	电磁场与微波技术	刘建飞	强流大孔径 500 MHz 5-cell 超导高频腔的设计	超导高频技术的研究
68	硕士	陆昌旺	电磁场与微波技术	刘建飞	新型 500 MHz 单 cell 超导高频腔的仿真设计	超导高频技术
69	硕士	董思民	电磁场与微波技术	杜涵文	质子治疗装置大回转机架(Gantry)支撑驱动系统	机械设计方向
70	硕士	王丽	光学工程	王纳秀	变形晶体分光性能表征方法的研究	同步辐射光束线技术
71	硕士	汪睿	光学工程	王东	高增益高次谐波放大自由电子激光时间相干性研究	自由电子激光相干性研究
72	硕士	黄君艺	光学工程	陈敏	上海光源红外光束线设计及性能分析	光束线设计
73	硕士	洪时金	光学工程	周巧根	高精度霍尔探头标定方法的研究	插入件技术
74	硕士	杜韦陶	光学工程	王劼	X 射线散射法测量超光滑表面方法研究	光学元件加工及检测
75	硕士	许新磊	生物物理学	何建华	CRYM 结构及其酶活分析以及 LsrK 表达纯化	蛋白质晶体学
76	硕士	李静	生物物理学	樊春海	基于氧化石墨烯和生物芯片的新型生物传感器的研究	纳米生物传感器
77	硕士	雷豪志	生物物理学	张益	利用氧化石墨烯抑制核酸酶切割核酸的研究	纳米生物学

2012

No.	学位	学生	专业	导师	论文题目	研究方向
78	硕士	黄麟飞	生物物理学	唐琳	ArsM 酶的初步晶体学分析及结合铁元素的光谱学检测	生物大分子晶体学
79	硕士	王子豪	无机化学	黄庆	石墨烯的化学功能化及应用	纳米材料合成
80	硕士	唐睿智	无机化学	王文锋	酮类光敏剂对生物分子的光敏损伤及其保护研究	光化学和光生物学
81	硕士	陈佳佳	无机化学	胡钧	纳米材料对聚合酶链式反应及双链 DNA 荧光检测的影响研究	纳米生物学
82	硕士	吴丽	信号与信息处理	赵明华	相空间重建方法及算法的研究	束团横向相空间重建方法与算法研究
83	硕士	刘月	粒子物理与原子核物理	怀平	低维半导体中载流子的动态屏蔽效应	半导体光谱学
84	硕士	戴进华	粒子物理与原子核物理	戴志敏	自由电子激光振荡器的物理研究	自由电子激光方向